i

Geomagnetic Impulses and the Electrical Conductivity of the Lower Mantle

by

Douglas Norman Stewart

Submitted in accordance with the requirements for the

degree of Doctor of Philosophy

The University of Leeds, Department of Earth Sciences, December, 1991

The candidate confirms that the work submitted is his own and that appropriate

credit has been given where reference has been made to the work of others.

Abstract

This thesis is an investigation of the changes in the magnetic field as measured at the surface of the Earth on the time–scale of months to decades. In particular the phenomena of geomagnetic "impulses" or "jerks" are investigated. Vigorous discussion has surrounded these phenomena since they were first suggested to have been of global scale, of short duration and originating within the core (Courtillot *et al*, 1978), primarily because of their implications for lower mantle conductivity. A major point of discussion has been whether they were of internal or external origin, and to what extent external fields determine their apparent time–scale.

A large quantity of monthly means of the geomagnetic field is analysed here to investigate the contribution from external and induced fields. A model of the disturbance fields on the time–scale of months and years is derived. Using the aa geomagnetic index to represent the temporal dependence, the spatial morphology is found to be primarily dipolar aligned with the Earth's main dipole. This model allows a better representation of the core field to be obtained. Seasonal fluctuations in the field are also quantified. The results are found to be consistent with an insulating mantle down to about $600km$ and a conductivity of about $0.1Sm^{-1}$ to $1Sm^{-1}$ below that.

A new method is developed to analyse the time–dependence of the improved representation of the core–field and is applied to a large set of geomagnetic annual means. This method determines the periods of time for which the field, as measured at different locations, can be represented by a quadratic time–dependence. Such a representation is found to be valid typically for 10 years at a time and valid for 93% of the data. Dates at which the changes from one quadratic time–dependence to another occur are found, to a certain extent, to be globally synchronous. Particular dates when this occurs are found to be 1970, 1978 and 1983, the latter events being similar in character to the 1970 jerk, and are thought to arise from impulses in the third time–derivative of the core field.

Spherical harmonic models of the main field with a quadratic time–dependence are then derived for epochs 1965.5, 1974.5, 1981.5 and 1986.5 using the technique of stochastic inversion. These models are then used to map the changes in secular acceleration associated with the 1970, 1978 and 1983 jerks. The global extent of the 1978 and 1983 jerks have not previously been investigated. The 1983 jerk is found to be much weaker

than the others and the 1978 jerk appears anti–correlated with the 1970 jerk.

The role of electromagnetic coupling between the core and mantle is considered in the presence of a thin conducting layer at the base of the mantle. Time–dependent torques are computed for the period 1900 to 1980 and found to correlate closely with the torque required to explain the decade fluctuations in the length of day. If electro-magnetic coupling is solely responsible for the decade fluctuations then this implies the conductance of the layer must be $\sim 7 \times 10^8 S$. Various other pieces of evidence relating to lower mantle conductivity are also discussed.

Contents

List of Tables

List of Figures

List of Abbreviations

GFA1	Gubbins (1983)
GFA2	Gubbins (1984)
GFA3	Gubbins & Bloxham (1985)
KBM	Kent, Briden & Mardia (1983)

AVDF91	Preferred average disturbance field model of Chapter 3
BJ1	Time–dependent field model used in Chapter 6
BJ2	Time–dependent field model of Bloxham & Jackson (1990)
CMB	Core–mantle boundary
GDS	Geomagnetic deep sounding
IAGA	International Association of Geomagnetism and Aeronomy
IGRF	International geomagnetic reference field
L1, L2	Thin layer models of Chapter 7.
LOD	Length of day
MF	Main field
ML	Maximum likelihood
OPRA	Optimal piecewise regression algorithm
PAIC	Partial Akaike information criterion
PCA	Principal components analysis
PRA	Piecewise regression algorithm
PR19xx, PO19xx	Stable secular acceleration models (referred to epoch 19xx)
r.m.s	Root mean square
RVIF	Relative virtual impulse frequency
SA	Secular acceleration
SH	Spherical harmonic
SHA	Spherical harmonic analysis
SI	Stochastic inversion
SSAD	Stable secular acceleration date
SV	Secular variation
VI	Virtual impulse
VIE	Virtual impulse epoch
w.r.t	With respect to

Acknowledgements

Over the 3 years or so spent researching for and preparing this thesis I have been greatly assisted by many. First and foremost I would like to say a special thank you to my supervisor Kathy Whaler for initiating this project, being a great source of ideas and encouragement, giving concrete support when difficulties arose and providing much constructive criticism during the preparation of this thesis.

I would also like to thank Dave Gubbins who has shown an active interest in this project since he came to Leeds and in particular with his help in verifying the computation of the torque integrals in Chapter 6. Also at Leeds I would like to thank Keke Zhang, Robert Davis and Ken Hutcheson for their encouragement and discussions on a plethora of topics. A special thank you also to Nick Barber, geomagnetic graphics guru at Leeds without whom the graphical content of this thesis wouldn't be half of what it is and also to Stuart Borthwick, computer officer at Leeds, for his endless patience and help. Thanks also to John Kent in the Department of Statistics at Leeds for several useful discussions regarding the work for Chapter 4 and also for useful comments on a late draft of that chapter.

Away from Leeds I would particularily like to thank Fritz Busse for his collaboration in the work on the electromagnetic coupling problem, and for making me feel so welcome during my stay in Bayreuth. I would also like to thank Wolfram Hirsching and his family for being so friendly and hospitable during my stay in Germany. Thanks also to Johannes Wicht for his help with some of the algebra for Chapter 6 and Wolfram Hirsching for many lengthy and useful discussions.

Special thanks are due to Bob Parker for supervising me during my time at the Institute of Geophysics and Planetary Physics at La Jolla, and for providing such an interesting problem to work on while there. I am also indebted to him for providing his "plotxy" program with which most of the diagrams in this thesis have been prepared. I can't pass over the subject of La Jolla without saying a special thanks to my diving buddies Maya, Jerry and Garnet (and family) who made my visit so memorable. I would also like to thank George Backus for his interest in the project and useful discussions.

Around Britain I would like to thank Dave Barraclough and Dave Kerridge of the British Geological survey in Edinburgh for providing data and useful information, as well

Dedication

To my Parents.

Chapter 1

Introduction

1.1 The Earth's magnetic field

1.1.1 The origin of the geomagnetic field

William Gilbert (1600) hypothesised that the Earth behaves in a manner akin to a large permanent magnet which was the first "modern" explanation for the north–seeking behaviour of compasses. However in 1635 Gellibrand noted that the direction of the magnetic field changed significantly over a period of decades. These changes amount to a maximum of around 1% of the field per year which has a typical flux density of magnitude $50000nT$ at the Earth's surface. It is now generally accepted that for the most part this *geomagnetic* field originates within a liquid shell (the *outer core*), consisting largely of liquid iron, lying (approximately) between a radius of $1217 \pm 10km$ and $3485 \pm 2km$ (Melchior, 1986). This conclusion has largely been reached through the elimination of alternative hypotheses and the reader is referred to Parkinson (1983) for a review of these. Beneath this liquid lies a solid *inner core* which will not be of direct interest in the present work, and references to "the core" will relate to the liquid outer core. In order to reconcile the geologically inferred age of the Earth with the time it would take for the field to decay, were the liquid static, it is now widely accepted that the magnetic field must undergo a self–regeneration process known as dynamo action. Dynamo theory is the subject of intensive research today and many fundamental questions remain unanswered; for example the strength of the magnetic

field within the core (since we can only observe part of the field at the Earth's surface), the source of energy for the fluid flow and the magnetic diffusion timescale for the core. For background on dynamo theory see for example Parkinson (1983), Jacobs (1987b), Parker (1979) or Melchior (1986).

In addition to the core motions, a number of other phenomena contribute to the observed field. The permanent magnetisation of the crust gives rise to a field with a density of a few hundred nT and is a significant source of error in determining the core field accurately. The interaction of the core field with plasma and ionised gas in the Earth's near–space environment creates a time varying flow of electric currents external to the solid Earth, with which are associated time varying magnetic fields ("external fields") (see eg. Chapman & Bartels, 1940; Matsushita & Campbell, 1967; Jacobs, 1989, 1991). These originate in two main regions: the *ionosphere*, a region of diffuse and partially ionised gas extending from altitudes of approximately $100km$ to $500km$ and the *magnetosphere*, a volume of space in which the Earth's main field is largely confined due to the pressure of the solar wind. The time–dependence of these external fields also gives rise to currents (and hence magnetic fields) induced in the crust and *mantle*, which lies between the crust and core.

The study of the geomagnetic field plays a key role in our understanding of core dynamics. The study of the changing magnetic field has, for example, yielded reliable estimates of the pattern of flow at the top of the core (eg. Bloxham & Jackson 1991a; Gire & LeMouël, 1990; Whaler & Clarke, 1988; Whaler, 1990; Voorhies, 1986). Although the long period variations such as geomagnetic reversals and the steady decay of the dipole field since Roman times are of interest in themselves, it is the changes in the field on timescales from 1 to 100 years, commonly known in geomagnetism as the *secular variation* (SV), which are most relevant when analysing the historical data (as opposed to archæomagnetic and palæomagnetic data) from this and earlier centuries (eg. Bloxham & Jackson, 1989; Barraclough *et al*, 1978; Langel *et al*, 1986; Gubbins, 1984). Note that the term secular variation is also commonly used to refer more specifically to the first derivative of the field with respect to time. In recent years it has been recognised that significant and global variations in the field on timescales of less than a year or two have occurred, these being known in the literature as geomagnetic "jerks" (Malin *et al*, 1983)

or "impulses" (Courtillot *et al*, 1978). These form a central theme of this thesis and will be reviewed in §1.2.

1.1.2 The mantle and the geomagnetic field

As the atmosphere is effectively an insulator the magnetic field can be represented as the gradient of a scalar potential at the Earth's surface (Kellog, 1953). If the field is to be represented at the core surface, which is clearly desirable for investigating the physics of the core, then the surface representation of the field must be *downward continued*. If the crust and mantle can be considered to be electrical insulators then this is straightforward and only the effect of our distance from the source, known as *geometrical attenuation*, need be taken into account (eg. Jacobs, 1987b). As a first approximation this is reasonable and is widely used in geomagnetism. Although the effects of mantle conductivity are probably relatively small for a static core field the effect is thought to be more significant for the secular variation of the field and higher time derivatives (Benton & Whaler, 1983). The apparent lack of secular variation over the Pacific Ocean for example may stand as evidence of this if the conductivity of the mantle under the Pacific is high. This highlights a fundamental problem — the conductivity of the mantle is a very poorly known function, even if assumed to be a function of radius alone, and hence the geomagnetic field can be considered as the output from an unknown filter with an unknown input. Figure 1.1 illustrates this situation. Reproduced from Ducruix *et al* (1980), this shows estimated radial conductivity profiles from a number of authors and illustrates how these estimates vary by up to 4 orders of magnitude below a depth of $1000km$. At shallower depths there is in general greater agreement as a result of the applicability of "top down" methods such as geomagnetic deep sounding and magnetotellurics (for the crust and lithosphere). These methods have placed an approximate upper bound on upper mantle conductivity of $1Sm^{-1}$ above $700km$ or so (see for example Parkinson & Hutton, 1989).

1.1.3 Observing the geomagnetic field

The magnetic field at the Earth's surface is very weak and requires sensitive instrumentation to measure it accurately (see eg. Jacobs (1987a) for a review of instrumentation).

Due to the timescales of motions in the core, the determination of the core field and its changes requires regular and consistent measurements to be made over extended periods of time. To facilitate this, a number of permanent magnetic observatories have been established and now number approximately 170. Unfortunately, however, about 75% of these lie in the northern hemisphere with a particular concentration in Europe which causes difficulties when analysing the global field (see eg. Langel, 1987). In addition to observatory data, measurements are obtained from repeat stations which are reoccupied intermittently, land, marine and aeromagnetic surveys, as well as magnetic
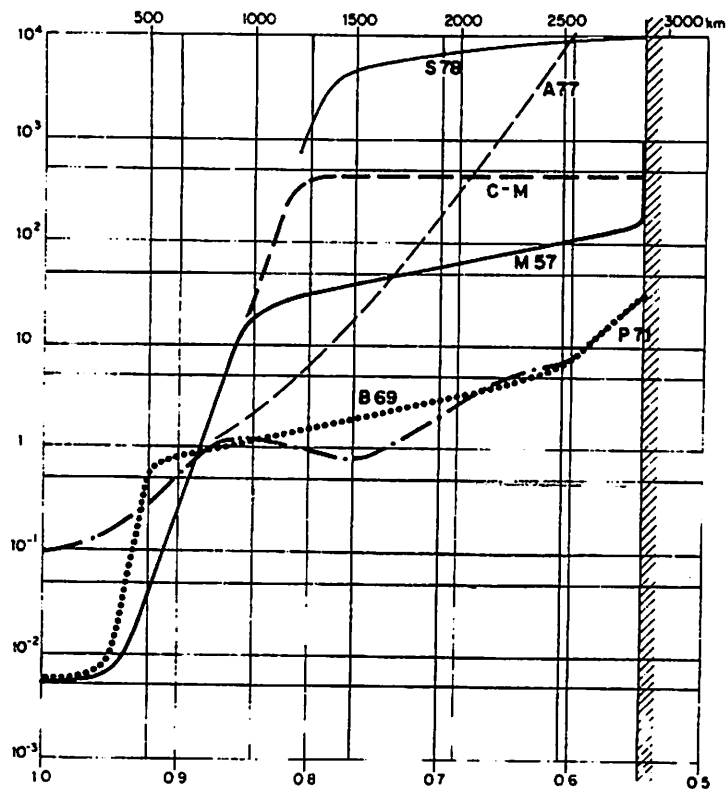
Figure 1.1: Diagram from Ducruix *et al* (1980) showing conductivity profiles from the works of McDonald (1957) (M57), Banks (1969) (B69), the Cantwell–McDonald model (see Banks, 1972) (C–M), Alldredge (1977b) (A77), and Stacey *et al* (1978) (S78). The upper horizontal scale gives the depth in *km* while the lower scale gives the radius in units of Earth radii. The vertical axis gives the conductivity in units of Sm^{-1}.

measurements made on satellites. These latter data provide the best global coverage by far. The satellite Magsat for example has allowed a significant improvement in mapping of the core field and has led to over 400 related publications (Langel *et al*, 1991). However, until such satellites become more regular or have a longer lifetime, observatory data will continue to provide the most consistent measurements for the determination of the time–dependence of the geomagnetic field. Temporal homogeneity of data is crucial here and so only observatory data will be used. The magnetic field, being a vector (**B**) requires 3 linearly independent measurements to determine it fully. The combination most commonly measured in geomagnetism has been declination (D), horizontal intensity (H), inclination (I) and also total intensity (F). To ease further analysis these are often converted to intensities in the directions of local north (X), east (Y) and vertically down (Z) in a geodetic coordinate system. Modern proton precession magnetometers allow these latter three components to be measured directly. Observations of the magnetic field are of course subject to instrumental and observational error as well as being susceptible to environmental noise (primarily man made), although in general geomagnetic observatories are located so as to minimise this. The problem is such that even averages of the field over periods of months and years (monthly and annual means) can be subject to errors of several nT. In this thesis these will be assumed to be random with zero mean and a Gaussian (normal) distribution for the components X, Y and Z. The discrepancy between the geodetic coordinate system (with respect to which X, Y and Z are measured) and the geocentric coordinate system (in which the Earth is assumed spherical) will be neglected throughout this thesis.

1.2   Geomagnetic jerks

Courtillot & LeMouël (1976a, b), in an investigation of the solar cycle related fluctuations in the geomagnetic field, removed a trend consisting of a polynomial (in time) from time–series of monthly and annual geomagnetic means and found global coherence among the residuals from different observatories. They attributed this coherent and systematic fluctuation to an external magnetic field with a dipolar morphology together with the induced field one would expect assuming simple induction models for the mantle. They

found, however, that some of their induction results were inconsistent and that there was a loss of residual coherence in the late 1960s. Courtillot, Ducruix & LeMouël (1978) extended this work and noted that this departure from the parabolic trend far exceeded the typical amplitude of the external field fluctuations and the noise in the data within the space of a year or two. They concluded that this represented a true feature of the SV originating in the core. Noting its rapidity, internal origin and geographically wide extent, they recognised that its observability at the Earth's surface had important implications for the conductivity of the mantle. They suggested this departure could be well approximated by a sudden change in the *secular acceleration* (SA) (second time derivative of the geomagnetic field) and used the term "secular variation impulse" loosely to describe the event. They also noted that similar events seem to have occurred around 1840 and 1910 and that such events seem to correlate with minima in the rotation rate of the Earth.

The topic of "secular variation impulses" had been discussed in the geomagnetic literature previously by Weber & Roberts (1951) and Walker & O'Dea (1952) although these only arose as an artifact of a data reduction exercise rather than as examples of a physical phenomenon. However Runcorn (1955), McDonald (1957) and Cox & Doell (1964) proposed that such impulses imply that the conductivity of the mantle must therefore be quite low. Alldredge (1975) pointed out that most of these impulses correlate with the solar cycle and are therefore unlikely to be associated with the core field. The phenomenon highlighted by Courtillot *et al* (1978) was much greater in amplitude and different in character to these earlier "secular variation impulses" and led to a significant amount of research. Malin *et al* (1983) later coined the term geomagnetic "jerk" by analogy with its usage for the rate of change of mechanical acceleration (Schot, 1978), and this term has come to be used the most widely in the geomagnetic literature. The terms jerk, geomagnetic jerk, impulse and geomagnetic impulse will be used (to a certain extent) synonymously throughout this thesis to refer to such phenomena. Where something more specific is intended this will be made clear. The investigation and discussion of jerks falls into several main areas which will now be reviewed in detail.

1.2.1 At what dates have jerks occurred?

The late 1960s event has been identified as occurring at 1967 (Courtillot *et al*, 1978), at 1969 (Golovkov *et al* (1989), McLeod (1989a,b), Courtillot & LeMouël (1984)) and 1970 (Kerridge & Barraclough (1985)). Gubbins & Tomlinson (1986) and Whaler (1987) found a later emergence time (1971/72) in the Australian region. These disparities in emergence time may, to a certain extent, be due to the poor temporal resolution arising from the filtering techniques found to be necessary when dealing with monthly means (Courtillot & LeMouël (1976a), Gubbins & Tomlinson (1986), Gavoret *et al* (1986)) and the use of annual means, particularily when these are pretreated by filters (eg. Malin *et al* (1983), Whaler (1987), Golovkov *et al* (1989)). However theoretical considerations (Backus, 1983) suggest that impulsive fields of differing spatial length scale will be propagated through a conducting mantle at different rates which could lead to variations in the emergence times at different locations for a jerk. The investigation described here has concentrated primarily on the latter part of this century.

Several authors (Gavoret *et al*, 1986; Gubbins & Tomlinson, 1986; Langel *et al*, 1986; McLeod, 1989a) have suggested that another jerk may have occurred around 1978, while it has recently been reported that there were sudden changes in secular variation in 1983/84 in Southern Africa (Kotzé *et al*, 1991) and South Georgia (Dowson *et al*, 1988). The reality and global extent of these latter events has not previously been investigated and will be examined in this thesis. Note that although Nevanlinna & Sucksdorff (1981) have reported a "secular variation impulse" in 1978, they found this to be an impulse in the first time derivative and of external origin and it is wholly different in character to the jerks under discussion here. Jerks occurring earlier this century have also been reported; the dates 1840 and 1910 were originally highlighted by Courtillot *et al* (1978), while Courtillot & LeMouël (1984) suggest that a jerk occurred in 1913. McLeod (1989b) found 1925 and 1940 to be dates of prominent jerks while Golovkov *et al* (1989) found 1937, 1947 and 1958 as heralding significant jerks. Kerridge & Barraclough (1985) found an apparent jerk in 1949 which they showed to be an artifact arising from the poor distribution of geomagnetic observatories and found only one significant jerk (at 1970) in the period 1931 to 1971.

1.2.2 The internal nature of jerks

Malin & Hodder (1982) demonstrated using spherical harmonic analysis (SHA) that the mean squared value of the jerk field (change in SA) at 1970 was primarily of internal origin while McLeod (1989a, b) has also shown that the 1969 jerk was of internal origin and worldwide in extent. Gubbins & Tomlinson (1986) systematically removed changes in the field of external origin and still found jerks apparent in the resulting time–series, assumed to be of purely internal origin. Gavoret *et al* (1986) also carried out a careful analysis of monthly means and were able to establish the internal nature of several jerks. Whaler (1987) noted that quantitative analysis of the 1969/70 jerk is hampered by rapid changes in the field, possibly of external origin, while Backus & Hough (1985) found the effect of sunspot related field variations to be critical in characterising the 1970 jerk. Alldredge (1984) challenged the findings of Malin & Hodder (1982) and claimed that SHA does not demonstrate conclusively the internal origin of the 1970 jerk, although he makes the same error of using Lowes' (1966) formula for the mean square value of the internal field for quantifying the external field as do Malin & Hodder (1982). This error works in favour of the argument of Malin & Hodder (1982) and against that of Alldredge (1984).

1.2.3 The characteristic time–scale of jerks

Perhaps the most remarkable and controversial aspect of jerks is the apparent rapidity with which they become manifest at the Earth's surface. The recognition of changes in the core field on the time–scale of a year or so contradicts some previous estimates of mantle conductivity which in general imply that variations of the core field on the time–scale of less than about 4 years or so are severely attenuated by transition through the mantle (eg. Currie, 1967, 1968; Alldredge, 1977b). Alldredge (1975) had earlier rightly pointed out that most impulses (of the Walker & O'Dea (1952) kind) were most likely due to external sources but Alldredge (1984) vociferously argued that, although (perhaps) of internal origin, the 1970 "impulse" was in fact a pseudo–periodic variation with its apparent rapidity arising from mixing with more rapid variations of external origin. However Alldredge's argument only works if the SV after the jerk is the negative

of the SV before the jerk, thus forming a "V" or inverted "V" shape when plotted. Nevertheless, Gubbins & Tomlinson (1986) asserted that within the resolving power of their data (6-18 months) the 1970/1971 jerk was "instantaneous" while even the heavily filtered data of Gavoret *et al* (1986) shows the duration of the emergence of the 1969 event to take no more than 2 years. Both these studies took careful account of the effects of external fields.

1.2.4 Related topics

Two other important issues that have arisen in relation to jerks are their relationship to changes in the length of day and their implications for mantle conductivity. Correlations between Earth rotation and geomagnetic parameters show wide disagreement, even to the extent of whether geomagnetic variations lead (LeMouël *et al*, 1981; Gire & LeMouël, 1986) those of Earth rotation, lag behind (Backus, 1983) or even both (Mörner, 1989)! Correlations that have been suggested in relation to jerks include a direct correlation between jerks of 1840, 1910 and 1970 and minima in the Earth's rotation rate (Courtillot *et al*, 1978) or a common link between the 1969 event and the 1956 "elbow" in Morrison's (1979) length of day data (Backus, 1983). This question is tied to the issues of core–mantle coupling and the time taken for the geomagnetic field to propagate from the core–mantle boundary to the Earth's surface and will be addressed in more detail in Chapters 6 and 7. The issue of mantle conductivity gained new stimulus with the recognition of the internal nature and short characteristic time–scale of the 1970 jerk and this topic will be discussed in Chapter 7 also.

1.3 Outline of this thesis

The aim of this thesis is to investigate the spatial and temporal nature of jerk phenomena, as observed at the Earth's surface, and to consider their implications under the hypothesis that they are the result of a third order impulse in the geomagnetic field at the core–mantle boundary.

The question of the internal or external origin of geomagnetic jerks is tackled by first investigating (in Chapter 2) to what extent phenomena external to the Earth contribute

to the observed magnetic field. To achieve this time–series of observatory monthly means are analysed. It is shown how geomagnetic data can be adjusted for the major effect of such external fields and the associated induced field, thus removing "signal" which is often treated as merely a source of random error in analyses of the core field. In Chapter 3 the global morphology of these external field variations is investigated and their implications for the conductivity of the mantle discussed. This results in a model which permits time–averaged data from any site to be adjusted for the effects of external fields. A more accurate representation of the time–dependent core field can therefore be produced.

One of the observations which has led workers to speculate that jerk phenomena consist of third order impulses in the core-field is the apparent simplicity of the typical time–signature of SV at many observatories. The SV appears to change linearly for many years, undergo a sudden change and then continue linearly for several more years. This corresponds to a quadratic time–dependence for the main field. One of the main criticisms levelled against such investigations has been the imposition of the date at which such transitions occur. In Chapter 4 the question of how well the main field can be represented by a quadratic time-dependence is addressed. A new method is developed which reveals objectively the periods of time for which such a representation is valid and is applied to an extensive data set of observatory annual means.

The results of this analysis are then discussed in the context of geomagnetic jerks in Chapter 5. It is shown that the dates at which the magnetic field at different locations changes from one quadratic time–dependence to another are, to a large extent, globally synchronous. Therefore at certain epochs between such dates it seems reasonable to consider the geomagnetic field to be in a period of stable secular acceleration. For these epochs, the analysis of Chapter 4 provides estimates of the quadratic time–dependence of each component of the field at a number of observatories. These are used in Chapter 5 to derive time–dependent models of the geomagnetic field for these epochs, by the application of the method of *stochastic inversion* (see eg. Bloxham *et al*, 1989). This yields reliable models of geomagnetic jerks at 1970, 1978 and 1983 which are discussed and compared. These dates will be quoted consistently throughout the thesis for brevity but are not meant to imply exact knowledge of the dates jerks occurred.

Chapter 6 examines the viability of electromagnetic coupling as a mechanism for the transfer of angular momentum between the core and the mantle and considers correlations between geomagnetic parameters and the length of day. A model for the conductivity of the mantle consisting of a thin layer of finite conductivity at the base of the mantle is assumed and the magnitude of conductance required to explain changes in the length of day is assessed. Some aspects of geomagnetic observations and geomagnetic jerks in particular, and their implications for the conductivity of the mantle are discussed in Chapter 7. Results are summarised, conclusions are drawn and possibilities for future work highlighted in Chapter 8.

Chapter 2

Solar related phenomena of the geomagnetic field

2.1 Introduction

The Sun is known to emit a continuous stream of charged particles known as the solar wind, which is subject to sporadic intensification as a result of solar activity. It is the interaction of the solar wind with the Earth's core field that gives rise to the transient and irregular fluctuations in the geomagnetic field observed at the Earth's surface known as disturbance phenomena (eg. Chapman & Bartels, 1940). The timescale of these phenomena is primarily of the order of seconds to hours. Although disturbances are always present to some extent, more systematic disturbance to the field occurs during geomagnetic storms which are the result of bouts of particularly intense solar activity. Such storms typically last a few days. The fluctuation of these external fields induces currents in the Earth, with which are associated time–varying *induced fields* (Banks, 1969; Parkinson & Hutton, 1989). As mentioned in Chapter 1, the assumption that monthly and annual geomagnetic means are free from such solar related effects is overly optimistic. In particular, as the disturbance phenomena are aperiodic, simple time–averaging of the field is unlikely to eliminate the effects of disturbance phenomena. If an investigation of the core field and its secular variation (SV) is intended, then an accurate separation of the external and induced fields from the core field is essential. There exist

two fundamental obstacles to this task. Firstly, although it is possible, in theory at least, to use the classical method of spherical harmonic analysis (SHA) to effect an internal/external spatial separation of the field, this method fails to distinguish between the core field and the induced fields, which requires some further criterion. Secondly, the application of techniques such as high or low pass filtering is only appropriate where the different phenomena are distinct in the frequency domain. Until relatively recently it was thought that for the geomagnetic field such a distinction could be made, with the existence of a cutoff period of approximately 4 years (Currie, 1967), below which rapid core variations are unable to penetrate the full thickness of the mantle, due to its electrical screening properties. The recognition of the rapid SV apparently originating within the core (Courtillot, Ducruix & LeMouël, 1978, Malin, Hodder & Barraclough, 1983, Gavoret et al 1986) has led to the idea that the timescale of the observed core field extends to periods shorter than this cutoff. The long period modulation of solar activity, together with seasonal effects, leads to the modulation of the external and (therefore) the induced fields on time scales of up to a decade or so. For example, Courtillot & LeMouël (1976a) found spectral peaks at 11, 5.5 and 3.7 years period associated with the solar cycle and its harmonics. It is clear, then, that there is a significant overlap of the timescales of the core field on the one hand and the external and induced fields on the other. This has led to controversy and discussion in the literature as to the internal or external nature of geomagnetic jerks (Alldredge, 1984).

Attempting to identify the external field variations, Alldredge, Stearns & Sugiura (1979) performed SHA on observatory annual means. They found the external dipole strength to vary (qualitatively) with the sunspot number and various geomagnetic activity *indices* (Mayaud, 1980). They were, however, unable to distinguish the induced potential because of the large internal contribution from the core. In a more thorough and extensive study, Yukutake & Cain (1979) also performed SHA. The variation of the external dipole strength was found to correlate (quantitatively) with geomagnetic indices on the timescale of several years, but comparison with the sunspot number time–series revealed only a qualitative, partial correlation. They then attempted to separate the long period induced component associated with the solar cycle by performing Fourier analyses of their time–series of 1st degree internal zonal harmonics (see eg. Langel,

1987). However this presumes the frequency distinction between internal and external phenomena discussed earlier and also that the solar cycle is an exactly periodic phenomenon which is in fact not the case as Harwood & Malin (1977) point out. SHA is affected by the additional problem that by its nature it can only distinguish the internal and external parts of a global *model* of the field which relies on good global data coverage, as well as the choice of truncation level, for its accuracy (Langel, 1987). It cannot be applied to time–series of geomagnetic data recorded at single locations such as magnetic observatories. Harwood & Malin (1977) detrended time–series of observatory annual means with low degree polynomials of time and numerical filters and modelled what was left as a function of sunspot number and its derivatives. Having done this for 81 observatories they performed SHA yielding estimates of the external (inducing) and internal (induced) 1st degree zonal harmonics. Filtering and detrending in this way (see also Alldredge, 1976), however, may unwittingly remove some variation of the external field or alternatively fail to remove some rapid variations of the core field thus compromising any determination of the induced field.

This chapter quantifies the extent to which the geomagnetic field, on the time scale of months and years, is affected by the solar related phenomena, including the induced fields, and attempts to find a practical way of removing these effects. This is achieved through the analysis of geomagnetic monthly means from a number of observatories. The method adopted has had to be somewhat unconventional due to the perceived shortcomings of more traditional methods as described above. The alternative strategy which is adopted here is to make prior assumptions about the time dependence of the external and induced fields (described in section 2.3) and to model series of geomagnetic monthly means in the time domain. The estimated external and induced fields may then be subtracted from the observed field and what is left considered as a "best" estimate of the time–varying core field. Much of the work reported in this chapter is also reported by Stewart & Whaler (1992).

2.2 Data selection and validation

The source of data for this study was the National Geophysical Data Centre (1987) NGDC01 optical disc data base. This includes a file of monthly means based on all day measurements from more than 197 observatories worldwide. However, for the purposes of this study an important criterion in data selection was the length and continuity of time series with northward (X), eastward (Y) and downward (Z) components either available or recoverable (for example from declination (D), horizontal intensity (H) and Z). An arbitrary length criterion applied was to retain those observatories for which time series of 12 years or more were available, such that for each component at least 90% of the data were present. This initial selection process yielded 46 observatories with a total of 1565 observatory years of monthly means. The lengths of individual time–series are given in Table 2.1. The shortest of these is 12 years (Tbilisi, Republic of Georgia) and the longest 84 years (Sitka, USA). Clearly, more digitised monthly means may be available and certainly more monthly means are available in observatory year books, but a full compilation of such data would be a major task in itself. In the case of Bangui, however, data for 1972/1 to 1978/12 and 1980/7 to 1981/12 were added from a published compilation (Godivier, 1982). These digitised monthly means of X, Y and Z have been submitted to the World Data Centre WDDC–C1 (Edinburgh).

After this initial selection process, time series were subjected to a careful validation procedure. Firstly all time–series were automatically checked for extreme outliers, by finding any data lying more than 6σ from a locally fitted quadratic of time where σ is the r.m.s. residual to such a parabola. In addition, time–series were visually inspected for any outlying data clearly resulting from transcription or keying errors (for example when a minus sign had obviously been omitted). Such data were rejected if they could not be corrected with confidence.

Having maximised the length and continuity of time–series it was recognised that in some instances corrections would have to be made for changes in instrumental baseline. The first method consisted of a cross–validation of the monthly means with the annual means data set lodged with the World Data Centres. It was found, by forming annual means from the monthly means and comparing these against the annual means obtained

from WDDC-C1, that for some observatories at certain epochs the two data sets failed to agree. Discussions with WDDC-C1 (D. R. Barraclough, personal communication, 1990) revealed that instrumental changes that occurred at Eskdalemuir at various epochs can account for such differences at that observatory. It therefore seems likely that corrections to allow for known instrumental changes have been applied to the annual means data set in some cases but not to the monthly means data set. Numerical comparison of the two data sets reconstructs these instrumental changes which can then be applied to the monthly means data set. This comparison was performed for the 46 selected observatories and in the majority of cases the two data sets were found to agree to within ± 1nT. However, at a number of observatories, changes in baseline were discovered and were applied to the monthly means.

It seemed likely that some time–series would still contain undetected changes in base level and so all time–series were carefully visually inspected. Where such a change was suspected the difference was estimated by a least squares fit of quadratics before and after the epoch at which it occurred and taking the difference of the constant terms. This was then used to correct for the base level change.

An inspection of the geographical distribution of the selected observatories revealed certain areas with very poor coverage. This might have inhibited the interpretation of the results, so short time–series from 13 observatories in key locations were also included (marked by an asterisk in Table 2.1). Special attention was paid to the continuity of these time–series and to the validation of these data by the methods described above. The list of observatories with lengths of time–series is given, together with summarised baseline correction information, in Table 2.1. (As the geographical distribution of observatories is of more relevance in Chapter 3, this is shown in Figure 3.1.)

Table 2.1: IAGA code, geomagnetic latitude and longitude in degrees, name of observatory, length of time series (in years) and information concerning baseline corrections applied. "Short" (see §2.2) time series are marked by an asterisk (*).

Key to baseline corrections:

o: outlier removed;

cc: corrections determined from comparison with annual means followed by the number of corrections applied to each component;

d: drift correction found from comparison with annual means;

fc: further baseline corrections applied (numerically determined) followed by the number of corrections applied to each component.

MBC	79.49	259.24	Mould Bay	24	
CBB	76.91	298.03	Cambridge Bay	13	
BLC	73.79	318.52	Baker Lake	35	cc:4x, 3y, 2z, fc:1x,1y
LRV	69.80	72.28	Leirvogur	24	
BRW	69.14	243.36	Barrow	22	o
FCC	68.63	325.68	Fort Churchill	22	
GWC	66.35	350.00	Great Whale River	20	
CMO	65.02	258.73	College	37	
SOD	63.71	120.91	Sodankyla	70	
DIK*	63.15	162.35	Dikson	6	
LER	62.18	89.75	Lerwick	60	cc:1x,2y,2z, d:z, fc:1z
MEA	61.96	303.57	Meanook	54	fc:2y,1x (undetermined)
TIK*	60.80	192.65	Tixie	2	
SIT	60.29	277.66	Sitka	84	cc:5x,5y,5z, fc:1x,1z
ESK	58.09	84.21	Eskdalemuir	75	cc:1x,2y,2z, d:x,z
STJ	58.09	23.32	St. John's	18	
NUR	57.65	113.65	Nurmijarvi	30	
LNN	56.08	118.44	Voyeykova	13	cc:1x,1y,1z, fc:1x,1y,1z
RSV	55.55	99.74	Rude Skov	23	
NEW	55.21	302.40	Newport	20	
AGN	54.83	349.31	Agincourt	38	
VIC	54.38	295.27	Victoria	22	
HAD	54.24	80.40	Hartland	29	fc:1z
WIT	53.81	92.49	Witteveen	47	1983/84: sign of D is wrong in source file.
ABN	53.63	84.66	Abinger	31	
DOU	53.42	90.66	Dourbes	36	fc:2z
YAK*	51.34	195.23	Yakutsk	2	
CLH	49.86	352.63	Cheltenham	56	cc:2x,2z, fc:2z
FRD	49.32	352.02	Fredericksburg	30	cc:1z
BOU	49.00	318.72	Boulder	19	
LVV	47.78	107.16	L'Vov	14	
AQU	42.54	94.37	L'Aquila	22	
IRT	41.10	175.96	Patrony	12	
TUC	40.47	314.29	Tucson	77	cc:4x,4y,4z, d:z, fc:2z
TFS	36.55	123.48	Tbilisi	12	o, fc:1x,1z
MMB	34.44	210.03	Memambetsu	29	
SJG	29.54	5.06	San Juan	58	cc:2x,1y,1z, fc:1x,1y,1z
VQS	29.29	5.79	Vieques	22	cc:1x,1z, d:x, fc:1y
KAK	26.45	207.60	Kakioka	29	
HON	21.42	268.30	Honolulu	79	cc:3x,3y,3z

Table 2.1 continued...

KNY	20.94	199.69	Kanoya	29	
SSH*	20.12	190.88	Sheshan	2	
LNP*	14.02	191.13	Lunping	5	
ABG	9.51	145.27	Alibag	51	cc:1x,1y,1z
AAE	5.16	110.84	Addis Ababa	13	o
BNG	4.48	90.20	Bangui	19	
GUA	4.41	214.61	Guam	27	
MUT*	3.40	191.42	Muntinlupa	10	
HUA*	-.88	355.52	Huancayo	4	
PPT*	-15.08	284.39	Pamatai	3	
API*	-15.67	261.90	Apia	2	
PMG*	-18.15	219.64	Port Moresby	9	
NMP*	-18.63	106.78	Nampula	3	
PIL*	-20.54	6.25	Pilar	4	
TRW*	-32.09	4.67	Trelew	4	
HER	-33.68	82.40	Hermanus	40	
WAT	-41.43	187.65	Watheroo	41	cc:3x,1z, d:x,z
AIA	-54.10	4.63	Argentine Islands	27	
SPA	-78.80	0.00	South Pole	13	o

2.3 Method: a time–series model

2.3.1 Accounting for the core field and its variation

An attempt to model a time–series of geomagnetic data must necessarily take some account of the field from the core as this is the dominant contribution to the observed field. In addition if these time–series span several years, the SV of the core field cannot be ignored. The details of the SV, however, cannot be prescribed and it is markedly different both in rate and orientation at different geographic locations. For this investigation, where the requirement was to model the secular trend whilst simultaneously modelling other much more rapid variations of external origin, a cubic polynomial in time was felt to be an adequate representation for the time–dependent core field. Low degree polynomials in time are recognised as remaining valid for at least a few years (Barraclough et al, 1975; Barraclough et al, 1978). However, over time spans of much more than a decade the cubic polynomial may break down as an adequate representation of time changes. This problem is returned to in §2.3.5.
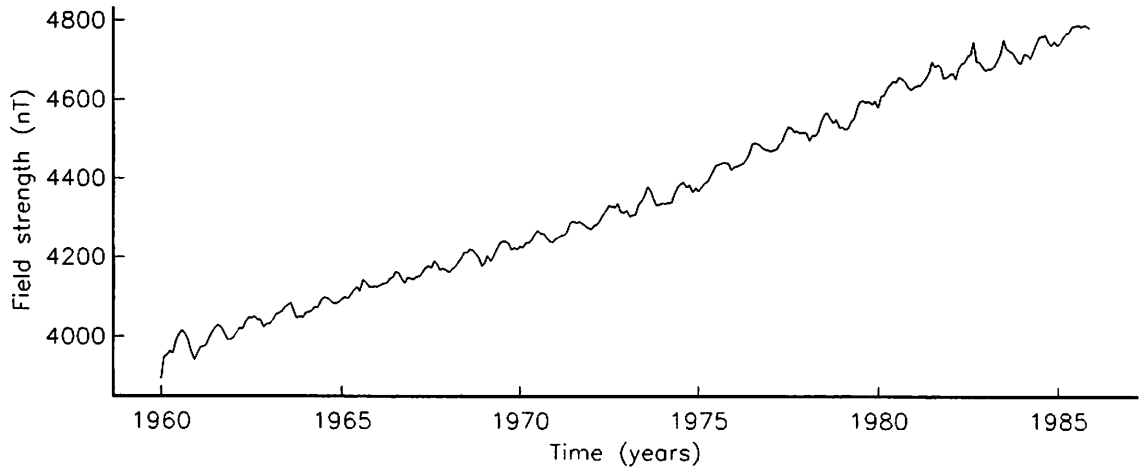
Figure 2.1: North (X) component of the geomagnetic field at Baker Lake (Canada) showing the annual variation

2.3.2 Seasonal effects.

Two of the clearest peaks in spectral analyses of the geomagnetic record occur at the 1 year and 6 month periodicities (Courtillot & LeMouël, 1976a). Although the annual variation is present at most observatories (Malin & Isikara, 1976), at some locations the phenomenon is especially pronounced as in Figure 2.1 which shows the X component of the field at Baker Lake in Canada. Such seasonal fluctuations are clearly a significant feature of the geomagnetic field and must be accounted for in modelling time–series of monthly means. The induced response to these fluctuations is expected to be at the same frequency (Parkinson & Hutton, 1989). Therefore both sine and cosine functions of 12 and 6 month periods were included to account for the annual and biannual (or semi-annual as it is sometimes known) variations, this being equivalent to including both phase and amplitude as free parameters. Annual and biannual variations are thought to arise partly from seasonal fluctuations in the amplitude of the (quiet time) regular daily variation S_q (Campbell, 1982). As S_q is modulated by the solar cycle (Campbell & Matsushita, 1982), the annual and biannual variations are solar cycle dependent also (Campbell, 1980). However this effect will be supposed to be averaged out over the time periods considered here, which are maximised to obtain the best estimates possible for the effect of the disturbance fields.

2.3.3 Disturbance fields

As discussed in the introduction to this chapter, it is suspected that part of the observed field on the time–scale of months and years is the result of disturbance phenomena and it is this which will be referred to as the "average disturbance field", **D**. The most significant feature of the instantaneous field associated with disturbance phenomena is the dipolar field of the magnetospheric ring current which can be dramatically enhanced during geomagnetic storms (Chapman & Bartels, 1940). Due to its (temporally) asymetric form this storm time field is likely to contribute significantly to **D**. In addition to the planetary characteristics of the average disturbance field, more localised effects may exist. In particular, the average intensification of the auroral electrojets during periods of increased geomagnetic activity, as evidenced by the close correlation between the electrojet index AE and other geomagnetic indices (Gavoret et al, 1986), may result in additional disturbance to the average field at auroral latitudes. Further, the bombardment of the ionosphere by charged particles from the magnetosphere leads to increased ionisation and an enhancement of the regular daily variation (which contributes to all day means (Gavoret et al, 1986; Campbell, 1987)) in auroral regions during disturbed periods (W.H.Campbell, personal communication, 1990). To summarise, significant variation in the average disturbance field in different regions is to be expected. Despite variations in intensity and orientation however, it is hypothesised that on the timescale of months and years such disturbance variations will correlate very closely with the average level of geomagnetic activity.

As a result of the irregular nature of the disturbance phenomena no clear spectral peak can be associated with the external disturbance field and consequently they contribute to the spectral continuum (Currie, 1966; Banks, 1969). This does not, however, preclude the existence of an induced response to this continuum, and indeed Banks (1969) quantifies such a response. As the time–scale of disturbance phenomena is of the order of a few days at most it is further hypothesised that geomagnetic data averaged over a period of a month or greater will reflect the cumulative effect of both the external and induced fields, with no associated phase difference on these timescales. As the frequency content of induced fields reflects that of the inducing field (Parkinson & Hutton,

1989), it is supposed that the average induced disturbance field will also correlate with the average level of geomagnetic activity.

The time–series of monthly means of the aa geomagnetic index was adopted to represent the overall level of global geomagnetic activity. (The reader is referred to Mayaud (1980) for a full treatise on geomagnetic indices.) Based on measurements of the range of variation of the field within three hour intervals, this index characterises geomagnetic activity at mid–latitudes on a time–scale several orders of magnitude too short to be associated with the core. One possible objection to the aa index is that it is derived from observations at only two observatories: Hartland (which succeeded Abinger and Greenwich) in the UK and Canberra (which succeeded Toolangi and Melbourne) in Australia. It might therefore be suspected that it may give a rather biased representation of the level of geomagnetic activity. However, statistical comparison with the am index, which is based on a global network of mid–latitude observatories, reveals an extremely close correlation on the time–scale of months to years (Mayaud, 1980). It therefore seems unlikely that the aa index is biased. The Dst index, which was specifically designed to monitor the intensity of magnetospheric ring current, would be inappropriate here. Firstly, it is suspected that it may be contaminated by short term secular variation of the core field due to poor determination of an appropriate base level (eg. Ducruix et al, 1980; Langel & Estes, 1985) and, secondly, it is only available back to 1957. As the Sun is the ultimate cause of disturbance phenomena one might expect a correlation to exist between the sunspot number and geomagnetic activity. However, although a qualitative correlation does exist, it is little more than this (see Figure 2.2). Even over a whole solar cycle, there is a distinct difference in character between the variation of the number of sunspots and the level of geomagnetic activity, in particular the well known double peak in geomagnetic activity in each solar cycle (Yukutake & Cain, 1979). Finally, it is worth noting that on the timescale of months to years, a strong correlation exists between the aa, Ap, AE and Dst geomagnetic indices, with the exception of the Dst index at certain epochs presumably for the reason mentioned above.

The great advantage of the aa index over all others is the great time span for which it is available (1868 to the present), which is important here. As the aa index is scaled in nT, a linear correlation with the average disturbance field is to expected. However,
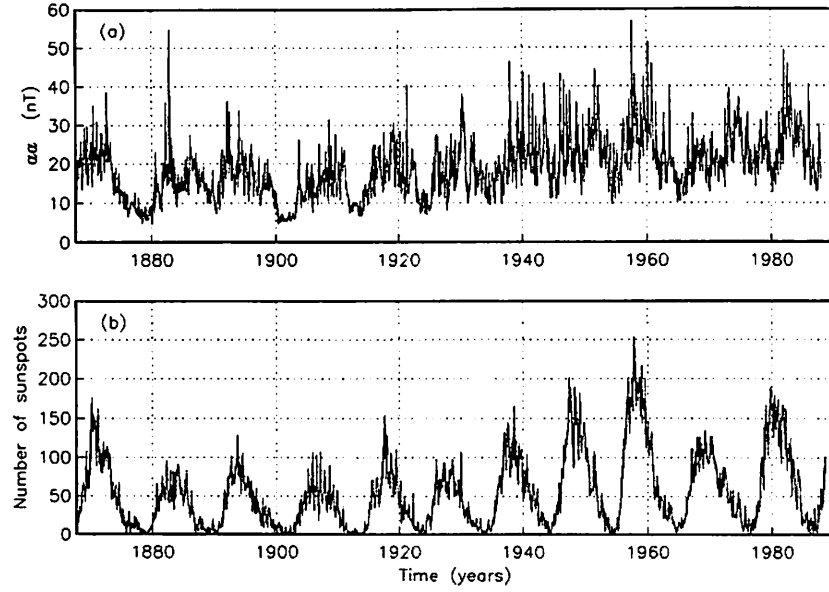
Figure 2.2: Plot showing monthly means of the aa index (a) and sunspot number (b) from 1868 to 1987. Note the qualitative correlation in long term behaviour.

as the intensity and orientation of the average disturbance field depends on geographical location, a "relative amplitude of disturbance" parameter α_i must be included for each time–series analysed. This was multiplied by the aa time–series to represent the disturbance field. Consequently the α_i parameters are dimensionless and will have an order of magnitude of 1.

2.3.4   Form of the model.

Taking the discussions of §2.3.1 to §2.3.3 into consideration, the functional form chosen for the model was

$$u_i(t_j) = \alpha_i aa(t_j) + \beta_{i1} \sin(\frac{2\pi t_j}{12}) + \beta_{i2} \cos(\frac{2\pi t_j}{12}) + \beta_{i3} \cos(\frac{2\pi t_j}{6}) + \beta_{i4} \sin(\frac{2\pi t_j}{6})$$
$$+ \sum_{k=0}^{3} \gamma_{ik}(t_j - \bar{t})^k$$

where t_j is the time expressed in months.

$u_i(t_j)$ represents the field value of time series i (monthly means) centred on time t_j.

α_i is the (constant w.r.t. time) relative amplitude of disturbance to this component and

$aa(t_j)$ the monthly mean of the aa index centred on t_j while the $\beta_{ik}, k = 1, \ldots, 4$, are the amplitudes of the sine and cosine terms of the annual and biannual variations (again assumed constant w.r.t. time).

$\bar{t}$ is the mean epoch for the data to which the model is fitted.

The $\gamma_{ik}, k = 0, \ldots, 3$, define the cubic polynomial included to model the secular variation.

This gave a total of nine parameters to be determined.

2.3.5   Parameter estimation and errors

For each time–series, all 9 parameters were simultaneously determined by an undamped least squares fit. The eigenvalue–eigenvector structure of the normal equations matrices for the problem were examined from which it was concluded that damping did not provide any significant improvement. The square root of diagonal elements of the covariance matrix were taken as standard errors for parameters, correlation between parameters being neglected.

The length of time–series used to estimate model parameters was limited to 133 months as it was felt that a cubic model could not, in general, be expected to emulate the secular variation for much longer than this. As most of the time–series were significantly longer than this limit, model estimates were determined from a "sliding window" of data from the time–series. The method is illustrated in Figure 2.3. For a long time–series of n data $u_j, j = 1, \ldots, n$, the fit was to the subset of data $u_k, \ldots, u_{k+132}$ where k ranged progressively from 1 to $n - 132$. At each stage the model parameters (eg. α_{ik}) were determined and assigned to epoch t_{k+66}. The means of all these estimates were then calculated and taken as a best estimate of the parameters. Parameter errors were estimated as the mean of the standard errors or the standard deviation of the means, whichever was the greater. For the 13 "short" time–series, error estimates were doubled as an arbitrary recognition of the relatively few data on which they were based. To ensure the reliability of the parameters, the time series $\alpha_{ik}, k = 1, \ldots, n - 132$ were plotted together with the root mean square residual (r.m.s.r.) for each inversion (Figure 2.3 (a) and (b)). Where strong peaks in the r.m.s.r. were present (for example in Figure 2.3(a) prior to 1930) the appropriate sections of the original data series were examined. This
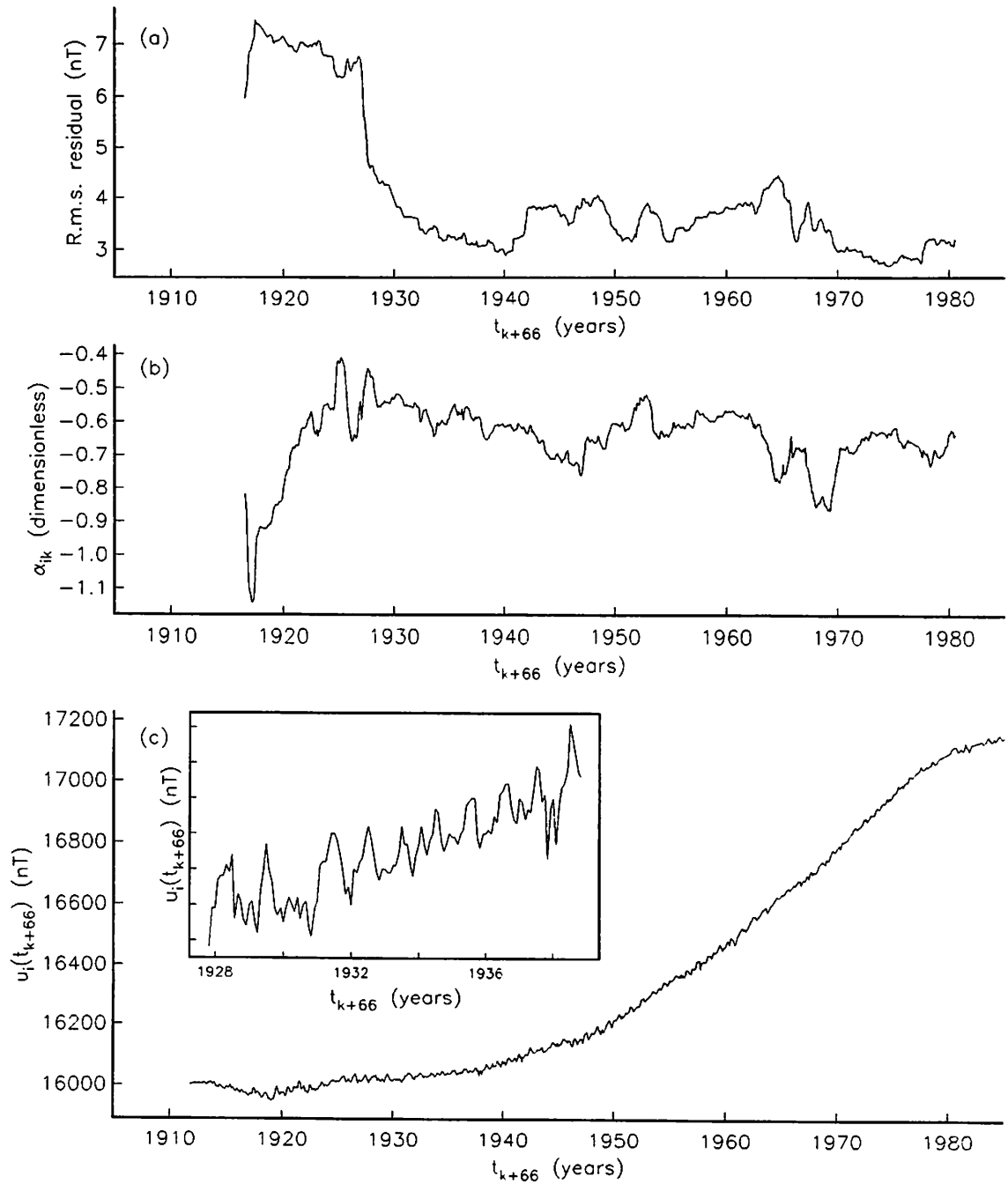
Figure 2.3: Illustration of the "sliding window" method described in the text, here for the northward (X) component at Eskdalemuir. A 133 month section of the data series in (c) is enlarged, the inversion of each window yields an estimate, α_{ik}, of α_i. As the window traverses the data series, the series of parameter estimates α_{ik} (b) is produced. The misfit for each inversion (a) can be used as a guide to parameter reliability.

usually revealed that the increased r.m.s.r. was associated with undetected changes in the base level or particularily rapid secular variation for which the cubic model was inappropriate. In such cases the corresponding model parameters were omitted from the calculation of means described above.

Stationarity of parameter estimates

In taking the mean of the parameter estimates from each window there is an implicit assumption that the "true" parameters are constant with respect to time. Due to the overlap of "windows", i.e. data being shared by adjacent estimates, no formal statistical method was available to assess this. One method used to investigate this however was to plot the parameter estimates from each window to see if they stray systematically beyond their mean by more than the estimated error for the mean. This is illustrated in Figure 2.4.

It might also be expected that $\sigma_{\bar{\alpha}_i} < \bar{\sigma}_{\alpha_i}$ would be true for the majority of α_{ik} series, that is, the standard deviation of the α_{ik} should not exceed the mean standard
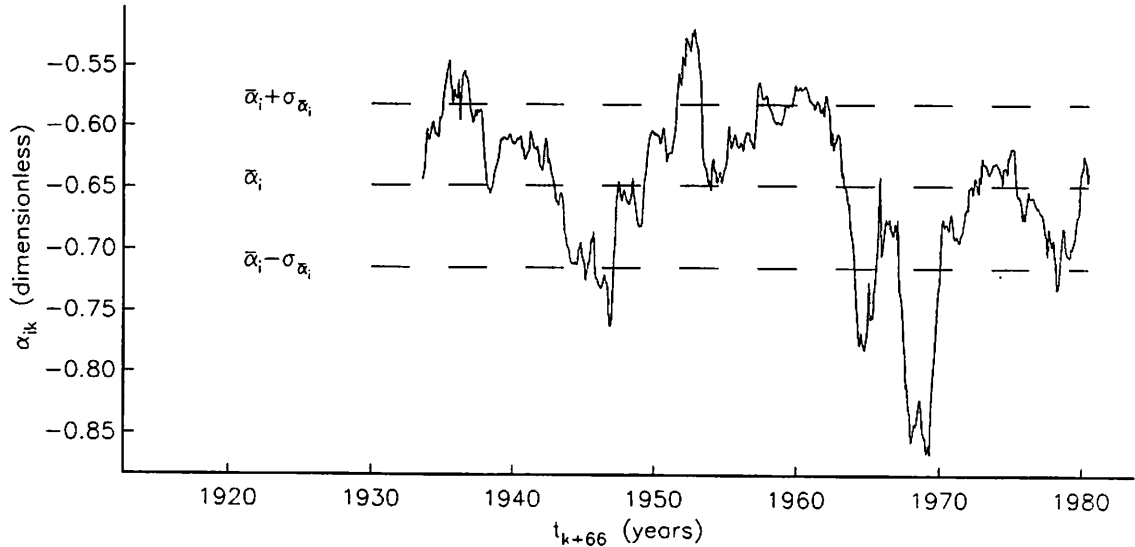
Figure 2.4: Illustration of the stationarity of the relative disturbance amplitude estimate determined from each "window" over the full length of the time-series for the X component at Eskdalemuir. Dashed lines show the mean ± the estimated error and the solid curve shows the estimate from each window.

Table 2.2: Percentages showing distribution of the individual determinations of α_{ik} relative to their mean $\overline{\alpha}_i$ for 9 time–series.

IAGA code	Component	$1\sigma_{\overline{\alpha}_i} < |\alpha_{ik} - \overline{\alpha}_i| < 2\sigma_{\overline{\alpha}_i}$	$|\alpha_{ik} - \overline{\alpha}_i| > 2\sigma_{\overline{\alpha}_i}$
CLH	X	38.57%	1.79%
CLH	Y	51.81%	0.00%
ESK	X	26.09%	6.44%
ESK	Y	31.27%	4.65%
ESK	Z	34.69%	3.25%
SOD	X	40.95%	0.00%
SOD	Y	17.76%	10.38%
SOD	Z	28.95%	6.72%
HON	Y	33.48%	3.67%
HON	Z	30.11%	4.84%

error. This provided an additional method of assessing the reliability of the results. Of the 138 long time series analysed, 76 gave results for which $\sigma_{\overline{\alpha}_i} < \overline{\sigma}_{\alpha_i}$ and so for these the α_i can be considered constant and that $\overline{\alpha}_i \pm \overline{\sigma}_{\alpha_i}$ is a good estimate of the relative disturbance parameter. Of the remainder, 55 satisfied the less strict condition $\sigma_{\overline{\alpha}_i} < 2\overline{\sigma}_{\alpha_i}$ leaving 7 for which $\sigma_{\overline{\alpha}_i} \geq 2\overline{\sigma}_{\alpha_i}$. If the α_{ik} were distributed normally about $\overline{\alpha}_i$ with standard deviation $\sigma_{\overline{\alpha}_i}$ one would expect $\sigma_{\overline{\alpha}_i} < |\alpha_{ik} - \overline{\alpha}_i| < 2\sigma_{\overline{\alpha}_i}$ in the case of 27% of α_{ik} and $|\alpha_{ik} - \overline{\alpha}_i| > 2\sigma_{\overline{\alpha}_i}$ for less than 5% of the α_{ik}. The distribution of the α_{ik} was investigated for a small sample of α_{ik} series, most of which had failed the strictest stationarity criterion. These are presented in Table 2.2 and appear to verify the constancy of the α.

2.4 Results

2.4.1 Disturbance field results

The full results for the relative amplitude of disturbance are presented in Table 2.3.

2.4.2 Annual and biannual variations

Results for the annual and biannual periodic variations are presented in Tables 2.4 and 2.5. Only the results for the "long" time series are presented as the others were not felt to have been meaningfully determined. Results for β_1 to β_4 are presented as

Table 2.3: Relative disturbance amplitudes α for each component at 59 observatories , which are labelled by their IAGA code (see Table 2.1) and arranged in order of decreasing magnetic latitude. Observatories marked with an asterisk are those for which only short time series were available. Auroral observatories are marked by (a).

IAGA code	X	Y	Z
MBC	-0.142±0.129	-0.164±0.122	0.744±0.186
CBB	-0.146±0.201	-0.029±0.105	1.237±0.145
BLC(a)	-0.600±0.151	-0.189±0.086	1.194±0.213
LRV(a)	-1.096±0.111	0.587±0.178	0.827±0.135
BRW(a)	-0.729±0.215	-0.579±0.098	1.196±0.203
FCC(a)	-1.205±0.152	-0.117±0.115	1.373±0.183
GWC(a)	-1.142±0.216	0.067±0.126	0.985±0.163
CMO(a)	-1.260±0.108	-0.699±0.062	0.491±0.119
SOD(a)	-1.155±0.154	0.307±0.035	0.445±0.135
DIK*(a)	-0.867±0.360	0.096±0.140	0.850±0.430
LER(a)	-0.711±0.059	0.301±0.032	0.144±0.085
MEA(a)	-1.174±0.100	-0.447±0.127	0.249±0.109
TIK*(a)	-1.209±0.510	0.056±0.340	-0.022±0.530
SIT(a)	-0.836±0.113	-0.353±0.068	0.249±0.164
ESK	-0.649±0.066	0.215±0.039	0.349±0.085
STJ	-0.692±0.127	0.051±0.137	0.360±0.107
NUR	-0.738±0.108	0.295±0.067	0.362±0.069
LNN	-0.794±0.068	0.239±0.037	0.226±0.083
RSV	-0.650±0.134	0.347±0.066	0.297±0.076
NEW	-0.787±0.068	-0.191±0.075	0.414±0.065
AGN	-0.651±0.099	-0.043±0.087	0.447±0.133
VIC	-0.839±0.079	-0.204±0.039	0.337±0.122
HAD	-0.692±0.055	0.276±0.044	0.345±0.057
WIT	-0.739±0.077	0.267±0.045	0.468±0.075
ABN	-0.638±0.048	0.213±0.023	0.387±0.078
DOU	-0.780±0.082	0.266±0.094	0.586±0.130
YAK*	-0.728±0.128	0.080±0.128	0.047±0.220
CLH	-0.772±0.066	-0.044±0.124	0.341±0.103
FRD	-0.936±0.100	0.087±0.031	0.512±0.102
BOU	-0.928±0.072	-0.166±0.039	0.457±0.051
LVV	-0.861±0.081	0.320±0.038	0.573±0.156
AQU	-0.909±0.076	0.372±0.028	0.387±0.064
IRT	-1.244±0.076	-0.060±0.031	0.392±0.088
TUC	-0.982±0.105	-0.169±0.032	0.306±0.133
TFS	-1.203±0.074	0.198±0.045	0.377±0.085
MMB	-1.206±0.072	-0.233±0.031	0.325±0.040
SJG	-1.008±0.089	0.063±0.085	0.331±0.160
VQS	-1.159±0.150	-0.162±0.099	0.244±0.256
KAK	-1.296±0.076	-0.197±0.023	0.298±0.035
HON	-1.266±0.076	-0.290±0.039	0.238±0.072
KNY	-1.350±0.095	-0.148±0.018	0.245±0.034
SSH*	-1.866±0.230	0.040±0.090	0.227±0.210
LNP*	-1.636±0.120	-0.036±0.080	0.083±0.060
ABG	-1.264±0.169	0.242±0.067	0.232±0.158
AAE	-1.348±0.110	0.263±0.087	0.061±0.056
BNG	-1.336±0.123	0.039±0.177	0.132±0.070
GUA	-1.331±0.093	-0.215±0.040	0.122±0.098
MUT*	-2.040±0.306	-0.294±0.170	-0.255±0.110
HUA*	-1.032±0.180	0.024±0.110	-0.010±0.080
PPT*	-1.506±0.160	-0.278±0.050	-0.180±0.300
API*	-1.320±0.260	-0.335±0.240	-0.022±0.110
PMG*	-1.340±0.140	-0.202±0.050	-0.544±0.190
NMP*	-1.047±0.226	0.461±0.140	-0.076±0.190
PIL*	-1.519±0.300	0.058±0.070	0.157±0.260
TRW*	-1.389±0.220	-0.092±0.200	-0.319±0.240
HER	-1.178±0.074	0.369±0.037	-0.366±0.091
WAT	-1.214±0.086	0.011±0.033	-0.171±0.081
AIA	-1.033±0.124	-0.075±0.046	-0.284±0.074
SPA	-0.161±0.183	1.151±0.172	-0.934±0.521

Table 2.4: Estimated amplitudes and phases, with estimated errors, of the annual variation. Amplitudes are in nT and phases are in degrees ($°$). Observatories are in order of decreasing geomagnetic latitude (θ_g). Geomagnetic longitude (ϕ_g) is also given (see §2.5).

IAGA			X component		Y component		Z component	
code	θ_g	ϕ_g	Amplitude	Phase	Amplitude	Phase	Amplitude	Phase
MBC	79	259	8.0± 1.0	64±6	2.4± 1.2	67±22	18.1± 1.4	-88±4
CBB	76	298	21.4± 1.8	88±4	2.4± 0.9	101±19	13.2± 1.3	-88±5
BLC	73	318	15.6± 1.2	84±4	1.0± 0.6	61±33	4.2± 1.5	-127±20
LRV	69	72	2.0± 0.8	5±39	1.3± 0.6	119±23	0.4± 0.9	142±122
BRW	69	243	16.1± 2.8	77±6	4.8± 0.9	79±9	3.8± 1.7	-146±26
FCC	68	325	9.0± 1.2	62±7	1.5± 0.7	19±26	6.6± 1.5	117±14
GWC	66	350	4.2± 1.6	17±22	1.6± 1.1	44±39	8.5± 1.3	95±7
CMO	65	258	9.7± 1.1	73±8	1.6± 0.5	57±20	2.7± 0.9	74±16
SOD	63	120	1.9± 0.7	40±22	1.5± 0.3	-104±11	0.6± 1.1	-52±106
LER	62	89	3.4± 0.6	59±8	1.2± 0.3	-107±16	4.4± 0.9	-99±9
MEA	61	303	5.1± 1.2	63±13	0.7± 0.4	34±30	1.3± 0.8	-110±30
SIT	60	277	5.1± 0.8	64±7	1.0± 0.4	68±18	0.9± 0.7	62±42
ESK	58	84	5.1± 0.7	62±7	1.0± 0.3	-108±17	3.8± 0.7	-94±9
STJ	58	23	7.0± 1.0	74±7	2.0± 0.8	25±24	3.1± 0.8	-72±14
NUR	57	113	4.5± 0.5	77±5	2.1± 0.3	-96±7	3.2± 0.6	-103±9
LNN	56	118	4.6± 0.6	78±7	1.6± 0.3	-115±11	3.6± 0.8	-114±11
RSV	55	99	4.5± 0.4	62±5	1.2± 0.3	-101±12	3.2± 0.6	-111±9
NEW	55	302	5.4± 0.5	69±5	1.2± 0.3	91±12	0.3± 0.5	-153±95
AGN	54	349	7.9± 1.0	89±6	0.7± 0.6	27±51	2.5± 1.4	-108±29
VIC	54	295	5.1± 0.7	71±7	1.4± 0.5	70±13	0.3± 0.5	37±111
HAD	54	80	5.1± 0.4	62±4	0.7± 0.2	-104±16	3.3± 0.4	-114±7
WIT	53	92	5.4± 0.5	63±5	0.8± 0.3	-128±18	3.1± 0.6	-105±9
ABN	53	84	5.0± 0.6	66±5	1.0± 0.2	-95±11	3.6± 0.6	-98±9
DOU	53	90	4.0± 0.5	31±7	1.4± 0.3	-165±12	5.2± 1.1	-116±11
CLH	49	352	5.6± 0.7	61±7	0.8± 0.3	113±18	2.1± 1.5	0±45
FRD	49	352	6.1± 0.6	64±5	0.3± 0.2	137±43	0.9± 0.5	113±29
BOU	49	318	5.2± 0.6	66±6	0.7± 0.3	91±24	1.1± 0.4	152±21
LVV	47	107	5.1± 0.7	84±7	0.9± 0.3	-134±20	1.2± 1.4	-81±63
AQU	42	94	4.4± 0.6	54±7	0.1± 0.2	159±81	1.8± 0.7	-87±14
IRT	41	175	4.4± 0.7	71±8	0.4± 0.3	16±37	0.4± 0.8	72±103
TUC	40	314	4.7± 0.8	59±11	0.4± 0.3	99±38	1.7± 0.6	110±20
TFS	36	123	5.1± 0.7	79±6	0.4± 0.4	98±58	2.7± 0.8	-92±14
MMB	34	210	3.6± 0.6	49±8	0.9± 0.2	-60±11	0.9± 0.3	-111±19
SJG	29	5	4.3± 0.9	75±10	0.7± 0.3	94±24	3.6± 1.0	75±14
VQS	29	5	3.1± 1.0	53±17	0.6± 0.4	-61±40	3.3± 1.6	87±24
KAK	26	207	3.3± 0.6	47±10	1.2± 0.1	-60±6	1.0± 0.2	-174±15
HON	21	268	2.4± 0.7	36±15	0.3± 0.2	-163±41	3.2± 0.6	85±8
KNY	20	199	3.3± 0.6	42±10	0.8± 0.1	-51±9	0.7± 0.2	173±22
ABG	9	145	4.1± 2.2	68±22	0.4± 0.5	4±79	5.4± 2.5	79±11
AAE	5	110	1.1± 1.0	76±47	2.1± 0.8	95±19	1.1± 0.5	82±24
BNG	4	90	0.9± 1.0	91±54	1.0± 1.2	179±68	1.7± 0.5	95±17
GUA	4	214	1.2± 0.7	35±33	1.2± 0.3	-91±13	4.4± 0.5	81±5
HER	-33	82	3.8± 0.7	-128±10	0.5± 0.2	22±25	0.3± 0.4	-172±83
WAT	-41	187	5.7± 0.8	-92±11	1.6± 0.3	77±9	3.5± 0.7	137±11
AIA	-54	4	2.9± 0.7	-98±15	2.6± 0.3	-95±5	2.4± 0.6	-117±12
SPA	-78	0	13.4± 1.6	-93±6	7.4± 1.5	83±10	17.3± 4.3	-87±12

Table 2.5: Estimated amplitudes and phases, with estimated errors, of the biannual variation. Amplitudes are in nT and phases are in degrees (°). Observatories are in order of decreasing geomagnetic latitude (θ_g). Geomagnetic longitude (ϕ_g) is also given (see §2.5).

IAGA code	θ_g	ϕ_g	X component		Y component		Z component	
			Amplitude	Phase	Amplitude	Phase	Amplitude	Phase
MBC	79	259	2.6± 0.9	-175±22	0.2± 0.9	-158±224	5.7± 1.5	86±12
CBB	76	298	6.6± 1.8	-107±13	0.9± 0.9	-103±53	8.1± 1.3	88±7
BLC	73	318	4.5± 1.2	-116±13	0.7± 0.6	-137±51	6.8± 1.6	87±11
LRV	69	72	4.9± 0.9	-84±9	2.0± 0.5	107±13	3.4± 0.9	140±15
BRW	69	243	6.8± 1.8	-108±13	1.3± 0.9	-86±34	5.6± 1.8	109±16
FCC	68	325	5.4± 1.2	-102±11	1.3± 0.7	-56±28	5.1± 1.3	135±14
GWC	66	350	5.2± 1.7	-97±16	0.4± 0.9	52±132	2.8± 1.1	159±25
CMO	65	258	6.8± 1.2	-95±7	2.1± 0.5	-73±10	1.5± 0.7	172±31
SOD	63	120	5.4± 1.1	-78±7	1.3± 0.3	105±13	1.6± 1.1	167±42
LER	62	89	3.7± 0.7	-86±7	1.2± 0.3	113±13	0.9± 0.8	254±51
MEA	61	303	4.3± 0.9	-87±9	1.2± 0.5	-49±22	0.7± 0.7	147±61
SIT	60	277	3.8± 0.6	-101±8	1.5± 0.5	-75±12	0.9± 0.7	204±48
ESK	58	84	2.7± 0.6	-97±9	0.9± 0.3	114±15	0.8± 0.8	265±47
STJ	58	23	3.6± 1.0	-107±13	1.0± 0.8	121±46	0.5± 0.7	182±92
NUR	57	113	2.4± 0.6	-87±10	0.2± 0.3	175±79	1.0± 0.6	271±31
LNN	56	118	2.0± 0.6	-89±15	0.3± 0.3	162±72	1.4± 0.8	301±28
RSV	55	99	2.2± 0.4	-96±10	0.3± 0.3	-129±52	1.2± 0.6	268±23
NEW	55	302	3.6± 0.5	-101±6	0.8± 0.3	-59±19	0.8± 0.4	198±34
AGN	54	349	5.0± 1.0	-106±10	0.7± 0.7	-77±48	2.0± 1.3	132±37
VIC	54	295	3.2± 1.1	-111±10	0.7± 0.4	-76±23	0.7± 0.5	181±49
HAD	54	80	1.8± 0.4	-100±12	0.4± 0.2	148±28	1.1± 0.4	266±20
WIT	53	92	2.1± 0.6	-91±12	0.4± 0.2	170±42	1.0± 0.6	281±29
ABN	53	84	2.9± 0.5	-94±7	0.9± 0.2	118±13	0.4± 0.5	183±89
DOU	53	90	1.7± 0.5	-98±14	0.3± 0.3	143±65	1.8± 1.1	286±31
CLH	49	352	3.4± 0.5	-102±7	0.4± 0.3	-43±42	0.6± 0.8	152±81
FRD	49	352	3.0± 0.6	-102±10	0.5± 0.2	-55±24	1.1± 0.5	206±25
BOU	49	318	2.9± 0.6	-101±10	0.6± 0.3	-4±30	1.1± 0.4	207±20
LVV	47	107	1.6± 0.8	-97±23	0.3± 0.3	-144±71	2.1± 1.4	254±35
AQU	42	94	1.2± 0.6	-102±24	0.7± 0.2	-103±15	0.7± 0.5	305±37
IRT	41	175	1.3± 0.7	-94±27	0.5± 0.3	130±32	0.2± 0.8	279±183
TUC	40	314	2.6± 0.8	-92±13	0.8± 0.3	-42±18	1.4± 0.6	190±27
TFS	36	123	0.3± 0.7	-97±102	0.5± 0.4	159±49	0.4± 0.7	7±99
MMB	34	210	1.7± 0.7	-104±17	0.5± 0.2	94±21	0.3± 0.3	166±70
SJG	29	5	3.1± 0.9	-72±14	0.6± 0.3	-85±26	2.1± 1.0	204±30
VQS	29	5	1.7± 1.1	-90±31	0.3± 0.4	39±82	1.8± 1.4	187±52
KAK	26	207	1.7± 0.7	-86±18	0.4± 0.1	109±20	0.5± 0.2	185±33
HON	21	268	2.0± 0.7	-55±18	0.3± 0.2	34±53	1.8± 0.5	224±15
KNY	20	199	1.6± 0.7	-81±20	0.3± 0.2	112±25	0.5± 0.2	204±30
ABG	9	145	1.3± 1.6	-136±69	0.4± 0.6	79±72	1.2± 1.0	198±57
AAE	5	110	2.9± 0.9	37±18	1.5± 0.7	152±29	0.7± 0.4	177±40
BNG	4	90	1.3± 0.9	-55±38	0.5± 1.3	89±123	0.4± 0.5	105±63
GUA	4	214	1.8± 0.7	-33±23	0.7± 0.3	72±22	1.9± 0.5	231±14
HER	-33	82	2.7± 0.6	-25±14	0.4± 0.2	-139±35	1.0± 0.5	65±26
WAT	-41	187	2.5± 0.8	-39±18	0.7± 0.3	-176±26	2.2± 0.6	4±19
AIA	-54	4	2.2± 0.6	-43±15	0.9± 0.3	-23±19	2.2± 0.5	-19±15
SPA	-78	0	1.1± 1.4	-6±79	2.0± 1.3	171±43	5.6± 3.9	-24±43

amplitude A and phase ϵ which were found by equating coefficients in

$$A\sin(\omega t - \epsilon) = a_1\sin(\omega t) + a_2\cos(\omega t) \tag{2.1}$$

where t is time in months, ω is $2\pi/12$ or $2\pi/6$ and $(a_1, a_2) = (\beta_1, \beta_2)$ or (β_4, β_3) accordingly. Calculation of the estimated variances of A and ϵ was facilitated by the approximation

$$\begin{aligned} Var(\phi(x_1, \ldots, x_n)) &\approx (\frac{\partial\phi}{\partial x_1})^2 Var(x_1) + \ldots + (\frac{\partial\phi}{\partial x_n})^2 Var(x_n) \\ &+ 2\sum_{i,j,i\neq j}(\frac{\partial\phi}{\partial x_i}\frac{\partial\phi}{\partial x_j})Covar(x_i, x_j) \end{aligned} \tag{2.2}$$

(Hald, 1952, p118), where ϕ is a "well behaved" function of random variables $x_1, \ldots, x_n$. The covariance term was, in this instance, assumed zero. A linearised MacLaurin series of $\tan^{-1}$ was used as a further approximation in the calculation of the phase variance.

2.5 Discussion

2.5.1 The disturbance fields

The relative disturbance amplitudes presented in Table 2.3 are shown in Figure 2.5. Results for the X and Z components are plotted against $\cos(\theta_g)$ and $\sin(\theta_g)$ respectively, where θ_g is the geomagnetic latitude. The linear relationships apparent in Figure 2.5 therefore reveal that the disturbance variations are broadly consistent with a dipole field aligned with, but of opposite polarity to, the Earth's main field. This is in agreement with previous workers' findings of an average external field which is dipolar (eg. Yukutake & Cain, 1979; Langel & Estes, 1985), thought to be associated with the magnetospheric ring current. This also lends further credence to the assumption of a tilted dipolar morphology usually made in magnetotelluric studies (eg. Schultz & Larsen, 1987). The other significant feature in Figure 2.5 is the enhanced disturbance amplitudes in auroral latitudes which are generally defined as $60°$ to $75°$ absolute corrected geomagnetic latitude (Mayaud, 1980). This is the definition adopted here, except (tilted centred dipole) geomagnetic latitude is used (Matsushita & Campbell, 1967, p1329). This approximation is felt to be negligible considering the magnitude of the parameter errors.
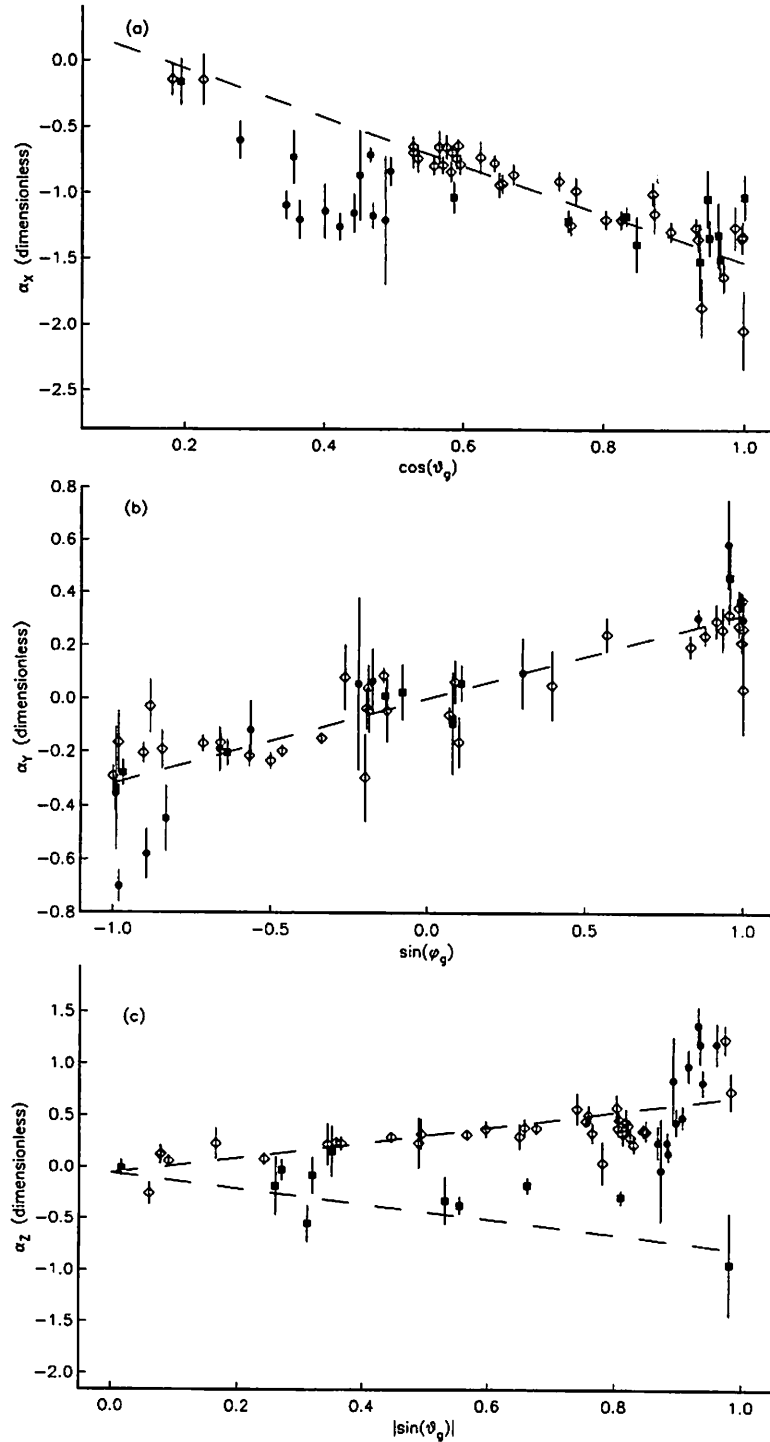
Figure 2.5: α values versus (a) $\cos(\theta_g)$ for X component; (b) $\sin(\phi_g)$ for Y component; (c) $|\sin(\theta_g)|$ for Z component, where θ_g and ϕ_g are the geomagnetic latitude and longitude respectively (see §2.5). All error bars are ± 1 estimated error. $\diamond$ represents non–auroral, northern hemisphere observatories, $\bullet$ northern hemisphere auroral observatories and $\blacksquare$ southern hemisphere observatories (all non–auroral). Dashed line is best fit (weighted by errors) to non–auroral observatories.

Table 2.6: Extract of the full results (given in Table 2.3) for the disturbance field, arranged to illustrate regional coherence of the field (see §2.5). θ_g and ϕ_g are the geomagnetic latitude and longitude respectively (as defined in §2.5). Errors given are 1 estimated error as defined in §2.3.5.

British Isles					
IAGA code	θ_g	ϕ_g	α_X	α_Y	α_Z
LER	62.18	89.75	-0.711 ± 0.059	0.301 ± 0.032	0.144 ± 0.085
ESK	58.09	84.21	-0.649 ± 0.066	0.215 ± 0.039	0.349 ± 0.085
HAD	54.24	80.40	-0.692 ± 0.055	0.276 ± 0.044	0.345 ± 0.057
ABN	53.63	84.66	-0.638 ± 0.048	0.213 ± 0.023	0.387 ± 0.078
Japan					
IAGA code	θ_g	ϕ_g	α_X	α_Y	α_Z
MMB	34.44	210.03	-1.206 ± 0.072	-0.233 ± 0.031	0.325 ± 0.040
KAK	26.45	207.60	-1.296 ± 0.076	-0.197 ± 0.023	0.298 ± 0.035
KNY	20.93	199.69	-1.350 ± 0.095	-0.148 ± 0.018	0.245 ± 0.034
Western Canada and Alaska					
IAGA code	θ_g	ϕ_g	α_X	α_Y	α_Z
BRW	69.14	243.36	-0.729 ± 0.215	-0.579 ± 0.098	1.196 ± 0.203
CMO	65.02	258.73	-1.260 ± 0.108	-0.699 ± 0.062	0.491 ± 0.119
MEA	61.96	303.57	-1.174 ± 0.100	-0.447 ± 0.127	0.249 ± 0.109
SIT	60.29	277.66	-0.836 ± 0.113	-0.353 ± 0.068	0.249 ± 0.164
VIC	54.38	295.27	-0.839 ± 0.079	-0.204 ± 0.039	0.337 ± 0.122

The only auroral observatories in this study lie in the northern hemisphere, however. At these latitudes the X component receives an additional negative disturbance. To the Z component, an additional positive disturbance occurs in latitudes north of the central auroral band ($68°$ to $71°$) and a negative disturbance to the south of this band. This is consistent with a mean westward localised electric current above the Earth and so is clearly associated with enhancement of the auroral electrojets during periods of magnetic disturbance. As can be seen from Figure 2.5(b), the results for Y clearly depend largely on the sine of geomagnetic longitude. This is due to the tilt of the geomagnetic coordinate system with respect to the geographic coordinate system in which X and Y are measured. This was confirmed by rotation of the X and Y components into the geomagnetic coordinate system which reduced the azimuthal component close to zero in most cases.

Closer examination of a selection of the results, in Table 2.6, reveals that the 4 observatories in the British Isles have a high degree of consistency. For the X component

the α values are not significantly different at the 1σ level and for those for Y are not significantly different at 2σ. However for the Z component at Lerwick the α value is significantly lower presumably as a result of its proximity to the southern fringes of the auroral zone where the effect of the auroral electrojets on the Z component is likely to be most negative. The results for the 3 Japanese observatories also show regional consistency. In particular, note that although these observatories are spread over almost 15° of geomagnetic latitude the α values for the X component differ little more than 1 standard error although they decrease monotonically in magnitude away from the geomagnetic equator. They are also significantly higher than those in the British Isles, as expected, due to their much lower geomagnetic latitude. The results for Y are all consistently negative due to their location in the western geomagnetic hemisphere. As 4 of the 5 observatories from western Canada and Alaska fall within the auroral zone there is significant scatter in the results. Notice the particularly high disturbance to the Y component at Barrow and College presumably due to the particularly large declination of the field at these locations.

2.5.2 Annual and biannual variations

The amplitudes of the annual variation in the X component (Figure 2.6), typically a few nT, are suggestive of a degree 2 zonal spherical harmonic (see eg. Langel, 1987), though this will be quantified in Chapter 3. A very pronounced enhancement of the annual variation occurs in auroral latitudes, with amplitudes of up to 15 to 20nT being present. The phases appear to be remarkably well determined considering the small amplitude of the phenomenon. They imply that in the northern hemisphere the maximum enhancement of the X component occurs around May/June at low latitudes and later than this at higher latitudes. This is in agreement with the results of Campbell (1980).

The amplitudes of the biannual variation, shown in Figure 2.7, are about half that of the annual and are also subject to great enhancement at high geomagnetic latitudes. Most of the phases are more tightly clustered than for the annual variation in this case around −100° and imply maximum enhancement to the X at the winter and summer solstices. The phase for the southern hemisphere is about −10° to −30° though the scatter here is quite large.
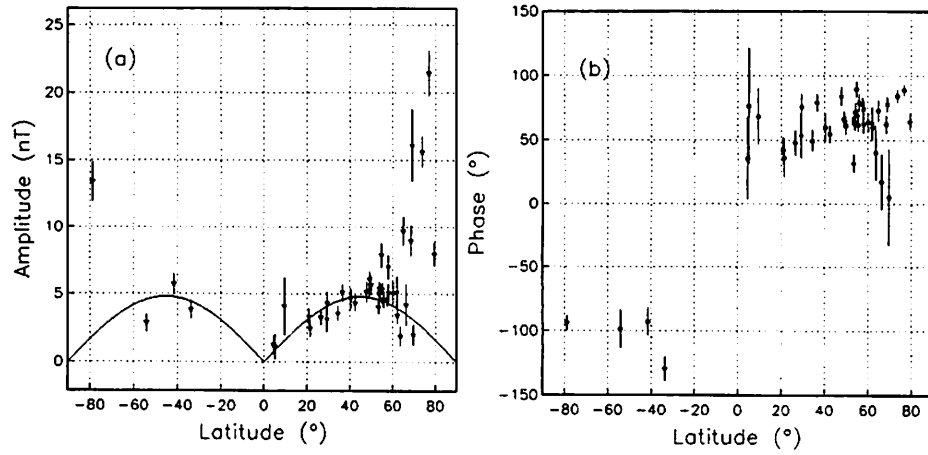
Figure 2.6: Amplitudes (a) and phases (b) of the annual variation in the X component against geomagnetic latitude (defined in §2.5). Error bars indicate ± one estimated error (see §2.3.5). The curve superimposed on the amplitudes shows the best fitting (by eye) 2nd degree zonal spherical harmonic aligned with the Earth's tilted dipole.
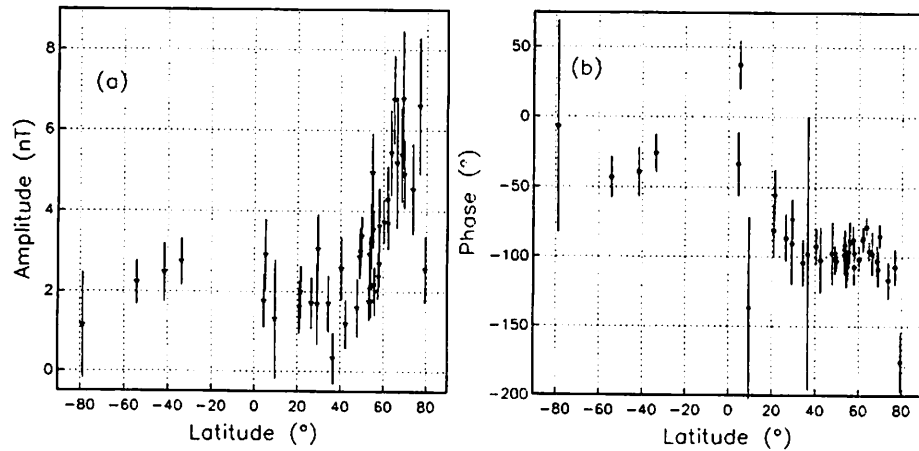
Figure 2.7: Amplitudes (a) and phases (b) of the biannual variation in the X component of the field against geomagnetic latitude (as defined in §2.5). Error bars indicate ± one estimated error (see §2.3.5).
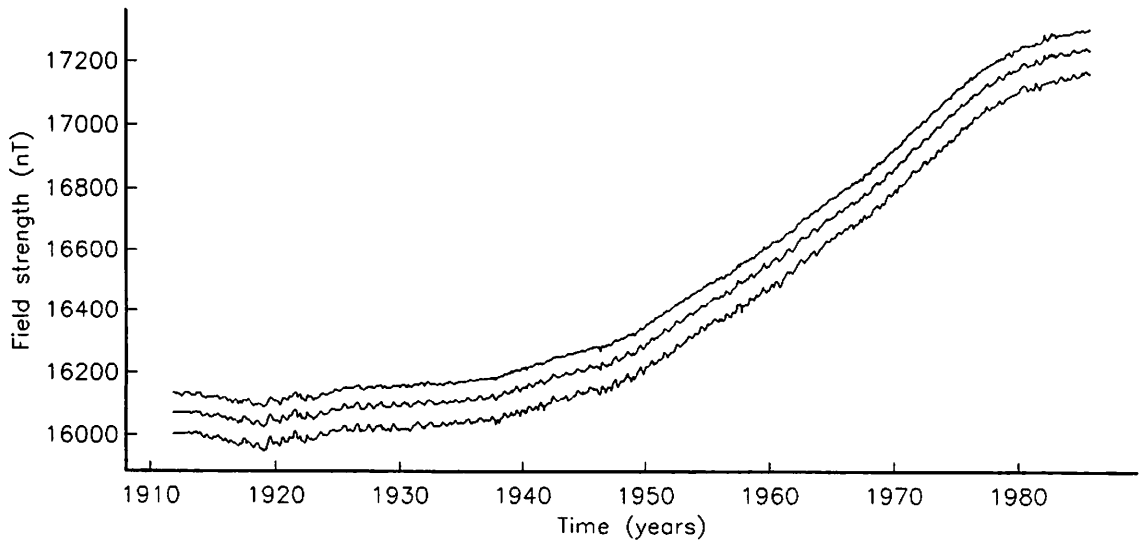
Figure 2.8: X component at Eskdalemuir. Lowest curve is "raw" monthly means. Middle curve is after removal of disturbance effects (see §2.6). Upper curve is after removal of annual and biannual variations in addition to disturbance effects. Curves offset for clarity. Scale applies absolutely to lowest curve.

2.6   The core field revealed

As discussed in the introduction, the stimulus for the work in this Chapter was the need to obtain a more accurate representation of the changes with time of the magnetic field originating within the core. The relative amplitude of disturbance estimate for a given component at an observatory may be used to rescale the aa time–series to give a time–series of the average disturbance field for that component. This can then be subtracted from the original observatory monthly or annual means time–series to yield a better representation of the core field and hence its secular variation.

Some examples of this are presented in figures 2.8 to 2.10. Figure 2.8 presents time series of monthly means of the X component at Eskdalemuir and Figure 2.9 shows the three point smoothed first differences of these as a representation of $\dot{X}$. A clear reduction in month–to–month variation occurs on removal of the disturbance field (from r.m.s. $= 4.41 nT$/month to $3.40 nT$/month) and a further reduction (to $2.62 nT$/month) occurs on removal of annual and biannual variations defined by the β parameters obtained from the analysis.
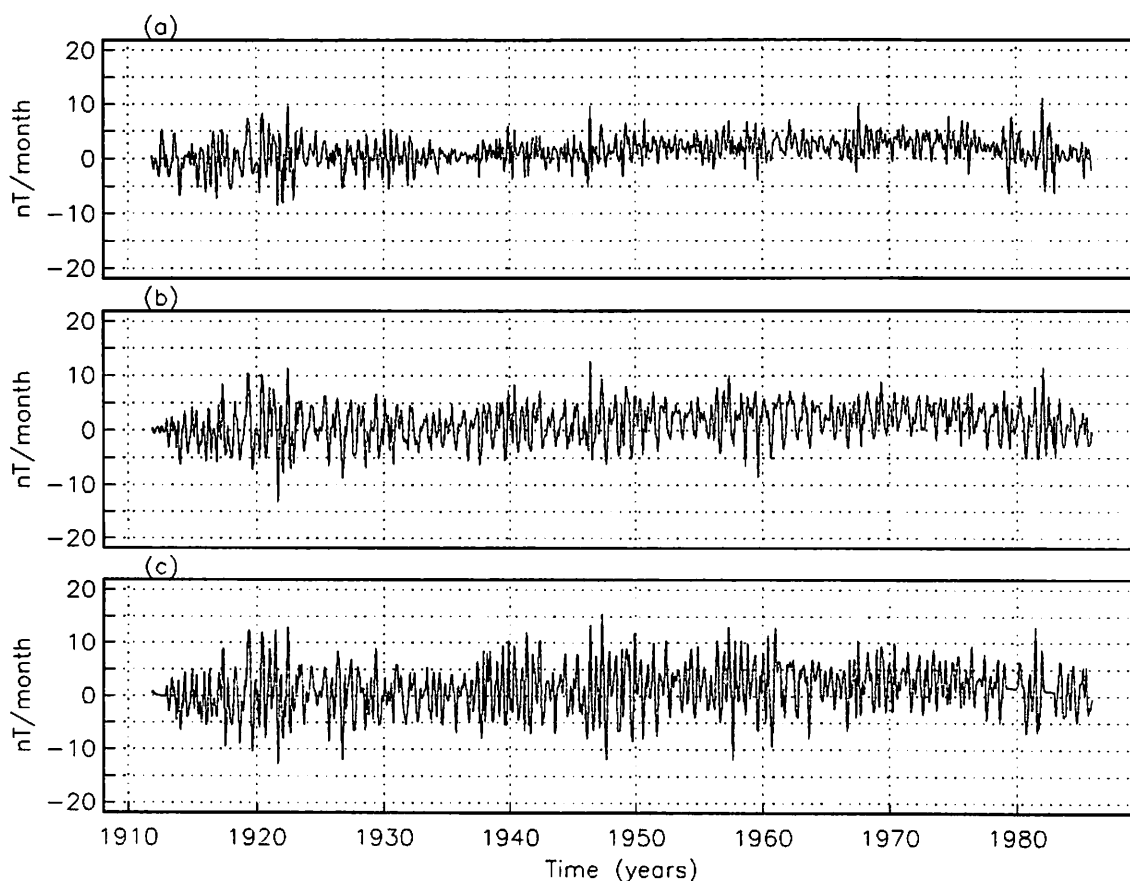
Figure 2.9: (c) $\dot{X}$ component at Eskdalemuir obtained by first differenc-
ing and three point smoothing has been applied to represent the first time
derivative. (b) is (c) with disturbance effects removed as described in § 2.6.
(a) is (b) but with annual and biannual variations also removed.

One feature that is particularly apparent in the Figure 2.9(b) is the modulation of

the amplitude of the annual variation by the solar cycle. The annual variation appears to

reach a maximum in 1927, 1938, 1949 and 1960 corresponding to approximate maxima in

the sunspot number time–series of Figure 2.2. However, the expected maximum in 1971

does not occur, which is surprising. As most of the time–series analysed are longer than

1 solar cycle (approximately 11 years) the annual and biannual amplitudes determined

here are believed to represent an average amplitude over a "typical" solar cycle, although

no solar cycle appears to be typical (Figure 2.2). It would be possible and worthwhile

to try and account for this in a future analysis.

Figure 2.10 shows first differences of annual means of the X component at 4 widely
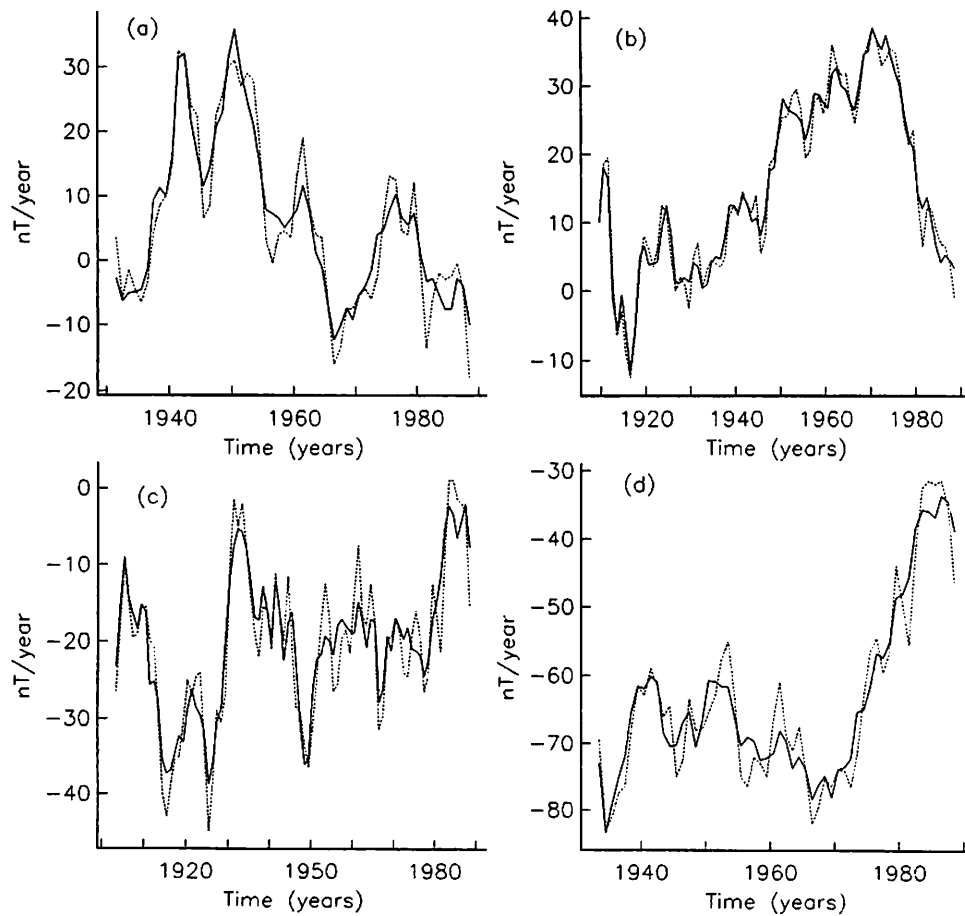
Figure 2.10: Representation of secular variation by $\dot{X}_i = X_{i+1} - X_{i-1}$. Dashed line is from 'raw' annual means. Solid line is after removal of the effect of disturbance phenomena as described in the text. (a) $\dot{X}$ component at Kakioka (KAK), Japan. (b) $\dot{X}$ component at Eskdalemuir (ESK), UK. (c) $\dot{X}$ component at Honolulu (HON), USA. (d) $\dot{X}$ component at Hermanus (HER) , South Africa.

spaced observatories. It can be seen from these that the removal of disturbance effects (using α values and annual means of the aa index) significantly reduces the year–to–year fluctuations in field values, and clarifies the character of the underlying trends which are concluded to be associated with the core. In particular, sudden changes in trend are apparent around 1970 at Eskdalemuir and Hermanus, this being the well documented jerk of 1969/70 to be investigated in Chapters 4 and 5. At Honolulu, a jerk is apparent in the late 1970s, a phenomenon noted in the $\dot{Y}$ component at European observatories by Gavoret et al (1986). This event is also apparent in the $\dot{X}$ component at Kakioka

(Japan) together with a jerk in the late 1960s. Before removal of the disturbance effect both these events are harder to discern.

2.7 Conclusions

In this chapter, estimates of the amplitude of the average disturbance field, relative to the aa geomagnetic index, have been derived for the X, Y and Z components of the field at 59 observatories. For most observatories, preliminary analysis suggests that a tilted dipole may be an adequate representation for the external and induced fields. This provides a practical solution, for these observatories, to the problem of removing both the external and induced field variations from observatory data as far back as 1868. The method can be applied equally to monthly means or any longer average of the field, such as annual means, as required. A more quantitative analysis of the spatial morphology of the disturbance and seasonal phenomena will be conducted in Chapter 3 and will allow the method to be applied to other observatories.

Some examples have shown, firstly, that apparent secular variation on the time–scale of months is significantly reduced on removal of disturbance, annual and biannual effects. Secondly, when disturbance effects are removed from observatory annual means, the complexity in plots of secular variation obtained from first differences, is significantly reduced. The fact that the effects of external and induced fields are not removed simply by using annual means is of importance not only to the interpretation of secular variation at individual observatories, but also on a regional scale. It could also have important consequences for field modelling (discussed in Chapter 4). The linear relationship between the activity index and the observed field, together with the fact that the average activity index is non–zero, implies that in addition to variations of the average disturbance field, the very long term average disturbance field is also quantified (ie. the effect of the ring current during apparently quiet times). This could, for example, be used to constrain the base level of the Dst index (Mayaud, 1980). The results of this study have shown that special consideration will have to made in dealing with observatories in auroral latitudes, as these can be particularly affected by external disturbance fields.

Estimates of the amplitudes and phases of the annual and biannual variations at each

observatory are an interesting by–product of this investigation. The annual variation appears to be dominated by a degree 2 zonal spherical harmonic though this will be clarified in Chapter 3. The results appear to be well determined enough to make an attempt at their further separation into external and induced components worthwhile.

Chapter 3

Spatial analysis of the external and induced fields

3.1 Introduction

The results of the investigation of the disturbance, annual and biannual phenomena will now be analysed using the technique of *spherical harmonic analysis* (SHA) (see eg. Langel, 1987; Barraclough, 1978) which will allow their spatial morphology to be quantified and clarified. The development of a spherical harmonic *model* of the disturbance phenomena will allow geomagnetic annual and monthly means from any location at any time back to 1868 to be corrected for these external field effects, giving a better representation of the core field and its changes (see Chapter 5). The analysis also allows a separation of the disturbance and seasonal variations into parts of external and internal origin. It will be assumed that any contribution to these from the core field is negligible. The implications of this for the conductivity of the mantle will be considered also.

3.2 Spherical harmonic analysis

It is reasonable to assume that the current density in the region where observatory measurements are made is negligible and hence the field can be represented as the gradient of a scalar potential

$$B = -\nabla \Phi \tag{3.1}$$

(eg. Langel, 1987; Parkinson, 1983). In the absence of monopoles, B is divergence free and so Φ is a solution of Laplace's equation. In the following a spherical Earth is assumed throughout, heights of observatories above sea level being neglected. The potential will be assumed to be seperable into a time–dependent amplitude function $A(t)$ and a time–independent dimensionless potential $\tilde{\Phi}(r, \theta, \phi)$. In the usual spherical polar coordinate system, (see eg. Jackson, 1975), $\tilde{\Phi}$ can be represented as an expansion in spherical harmonics so that

$$\Phi(r, \theta, \phi, t) = A(t)\tilde{\Phi}(r, \theta, \phi) = A(t)r_s \sum_{n=1}^{\infty} \sum_{m=0}^{n} \left\{ [g_n^{m_i} \cos(m\phi) + h_n^{m_i} \sin(m\phi)] \left(\frac{r_s}{r}\right)^{n+1} \right.$$
$$\left. + [g_n^{m_e} \cos(m\phi) + h_n^{m_e} \sin(m\phi)] \left(\frac{r}{r_s}\right)^{n} \right\} P_n^m(\theta) \tag{3.2}$$

where r_s is the radius of the Earth, P_n^m are Schmidt quasi–normalised associated Legendre functions of degree n and order m and i and e denote sources internal and external to the Earth respectively. In practise the expansion in harmonic degree n is usually truncated at some finite degree N to obtain estimates of the coefficients.

In Chapter 2 it was assumed that at a given location the relative amplitude of the annual, biannual and disturbance variations are fixed with respect to time, which is identical to assuming that the average spatial morphology of these magnetic fields is fixed over timescales greater than their own characteristic timescale. Therefore using the appropriate temporal basis function from Chapter 2 as $A(t)$ and denoting the corresponding *relative* amplitude parameters by $\tilde{X}$, $\tilde{Y}$ or $\tilde{Z}$ (for components X, Y and Z respectively) the disturbance or seasonal fluctuation at a given location and time can be given as

$$X(r, \theta, \phi, t) = A(t)\tilde{X} = A(t)\left(\frac{1}{r}\frac{\partial \tilde{\Phi}}{\partial \theta}\right) \tag{3.3}$$

$$Y(r, \theta, \phi, t) = A(t)\tilde{Y} = A(t)\left(-\frac{1}{r \sin\theta}\frac{\partial \tilde{\Phi}}{\partial \phi}\right) \tag{3.4}$$

$$Z(r, \theta, \phi, t) = A(t)\tilde{Z} = A(t)\left(\frac{\partial \tilde{\Phi}}{\partial r}\right). \tag{3.5}$$

These *equations of condition* can be solved using the empirical values of $\tilde{X}$, $\tilde{Y}$ and $\tilde{Z}$ obtained in Chapter 2 to give truncated spherical harmonic models of the fields.

The method of solution employed here was a (damped) weighted least squares fit of a truncated series of the coefficients to the data, the vector of estimated spherical harmonic coefficients being given by

$$\hat{m} = (G^T C_e^{-1} G + \lambda I)^{-1} G^T C_e^{-1} d \qquad (3.6)$$

where G is the equations of condition matrix, d the vector of data (relative amplitudes) and λ the damping constant. The estimated parameter variances derived in Chapter 2 were used as diagonal elements of the data covariance matrix C_e and the off-diagonal elements assumed zero.

The relative amplitudes of the disturbance field for all 59 observatories analysed in Chapter 2 were used as data for SHA. The locations of the observatories, the vast majority of which lie in the northern hemisphere, are shown in Figure 3.1. It has been noted already that the annual and biannual variations appear particularily enhanced in auroral latitudes (refer to §2.5.2). As such intense and localised features cannot be adequately represented by a low degree spherical harmonic expansion, as will be necessary here due to the relatively small number of data available, results from observatories with an absolute geomagnetic latitude of greater than 60° were omitted from the SHA for the annual and biannual variations. This was to allow the global character of these phenomena to be revealed more accurately. Also, none of the results from any observatories with "short" time series (see §2.2) were used as they were felt to be of too poor quality. This left 31 observatories providing data for the SHA of annual and biannual variations.

3.3 Results

3.3.1 Average disturbance field model.

The geometry of the field models in this and subsequent sections will be summarised using the terminology of Lowes (1974), in which the mean square value of the field due to harmonic degree n is referred to as the "power" of the field for that degree. Hence a spatial power spectrum may be defined in the obvious way. For fields of internal origin the power R_n is then defined as

$$R_n = (n+1) \sum_{m=0}^{n} ((g_n^{m_i})^2 + (h_n^{m_i})^2) \qquad (3.7)$$
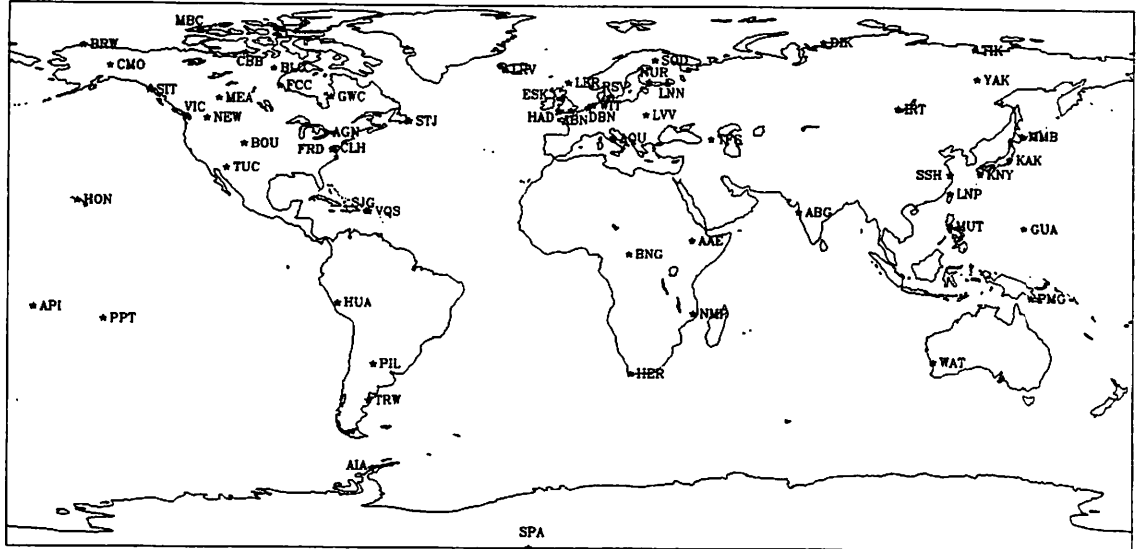
Figure 3.1: Distribution of observatories from which monthly geomagnetic means were analysed. Star indicates observatory location and the IAGA code of the observatory is shown close by. Projection is cylindrical equidistant with latitude from 90° south to 85° north.

(Lowes, 1966). However, it is important to note that for fields of *external* origin the equivalent formula is

$$R_n = n \sum_{m=0}^{n} ((g_n^{m_e})^2 + (h_n^{m_e})^2) \tag{3.8}$$

Lowes's (1966) formula does seem to be misused in this respect, eg. Malin & Hodder (1982), Alldredge (1984), McLeod (1989a).

Spherical harmonic analyses were initially performed in both a geographic reference frame and a geomagnetic reference frame (as defined in §2.5). The power spectra are effectively the same for models derived in the two reference frames, with no significant differences beyond one standard error (Tables 3.1 and 3.2). The power of the external field is more than six times that of the internal field and 99% of the power due to external sources comes from the degree 1 harmonics (Table 3.2). The misfit, $\hat{\sigma}$ is defined by

$$\hat{\sigma}^2 = \frac{\mathbf{d}^T \mathbf{C}_e^{-1} \mathbf{d} - \lambda \hat{\mathbf{m}}^T \mathbf{G}^T \mathbf{C}_e^{-1} \mathbf{d}}{n_d - Tr(\mathbf{R})} \tag{3.9}$$

where n_d is the number of data and $Tr(\mathbf{R})$ the trace of the resolution matrix $\mathbf{R}$ (see eg. Bloxham, Gubbins & Jackson, 1989). In the case of $\lambda = 0$, $Tr(\mathbf{R})$ is simply equal to the number of spherical harmonic coefficients. For models of maximum degree 3 (30

Table 3.1: Statistics of SHA for degree 3 disturbance field model, $\lambda = 0$, geomagnetic reference frame.

Misfit = 2.362		
Power spectrum		
n	External	Internal
1	1.275±0.078	0.189±0.021
2	0.005±0.004	0.009±0.004
3	0.004±0.002	0.004±0.002
Total	1.285±0.078	0.203±0.022

Table 3.2: Statistics of SHA for degree 3 disturbance field model, $\lambda = 0$, geographic reference frame.

Misfit = 2.449		
Power spectrum		
n	External	Internal
1	1.240±0.077	0.180±0.021
2	0.003±0.003	0.007±0.004
3	0.005±0.002	0.004±0.002
Total	1.249±0.079	0.190±0.021

Table 3.3: Statistics of SHA for degree 4 disturbance field model, $\lambda = 0$, geographic reference frame.

Misfit = 2.230		
Power spectrum		
n	External	Internal
1	1.389±0.120	0.229±0.050
2	0.122±0.040	0.156±0.041
3	0.130±0.031	0.182±0.035
4	0.107±0.015	0.078±0.012
Total	1.749±0.131	0.644±0.074

Table 3.4: Statistics of SHA for degree 4 disturbance field model, $\lambda = 15.0$, geographic reference frame.

Misfit = 2.224		
Power spectrum		
n	External	Internal
1	1.309±0.111	0.215±0.042
2	0.086±0.031	0.109±0.031
3	0.093±0.025	0.132±0.028
4	0.083±0.013	0.058±0.010
Total	1.571±0.119	0.513±0.060

parameters), little difference between the fits in the two reference frames could be found (Table 3.1 and 3.2), the geomagnetic frame giving a slightly lower misfit but a higher total power.

Having obtained a model estimate, any datum resulting in an absolute weighted residual more than 3 times the misfit was rejected and the model estimate rederived, the process being repeated until no more data were rejected. The data excluded for the model in Table 3.1 were CMO X, LRV X, MEA X, SOD Y and FCC X where the first three letters are the IAGA code of the observatory and the last letter the component excluded. Similarily, the data excluded for the model in Table 3.2 were CMO X, CMO Y, LRV X and MEA X. All these outliers were most likely due to auroral enhancement of the disturbance phenomena (see Figure 3.1). Table 3.3 shows the results of a degree 4 truncation with no damping and it is clear that increasing truncation level allowed power into the higher harmonics. The introduction of damping (Table 3.4) did not appear to

eliminate power from the higher harmonics preferentially and indeed convergence (by raising the truncation level) could not be achieved for any level of damping, with power spectra ultimately being "flattened out". This suggests that a more sophisticated method such as *stochastic inversion* (see Gubbins, 1983; Gubbins, 1984; Gubbins & Bloxham, 1985) might be more appropriate. However it is not clear how the present problem could be formulated within such a framework given the multiple and ill-defined source regions with which the external fields are associated. Overall, the solutions have a rather high misfit suggesting the standard errors may be underestimated by about 30%, or due to spatial features (eg. auroral enhancement) beyond the resolving power of these models.

The preferred model for the relative amplitude of the average disturbance field is of degree 3 in a geographic reference frame with no damping (Table 3.2), which when used in conjunction with the *aa* index as a temporal basis function, will be denoted model AVDF91. The spherical harmonic coefficients of this model are presented in Table 3.5. The relative disturbance amplitudes predicted from this model are plotted for each component in Figure 3.2. The half width of the 95% confidence region for the predictions, $t_{0.975}\sqrt{\mathbf{x}^T\mathbf{V}\mathbf{x}}$ (see eg. Wonnacott & Wonnacott 1981, p443), is plotted in Figure 3.3. $\mathbf{x}$ is the equation of condition relating the model vector to the predicted datum for each position and $t_{0.975}$ is the value of the Student's t distribution (Kendall & Stuart, 1961) for a lower tail of 97.5% on 143 degrees of freedom. The covariance matrix $\mathbf{V}$ for this model is given by

$$\mathbf{V} = \hat{\sigma}^2(\mathbf{G}^T\mathbf{C}_e^{-1}\mathbf{G})^{-1}. \tag{3.10}$$

Figure 3.3 shows that for all components the model is poorly constrained in the Southern hemisphere and over the oceans (especially for Z) as is to be expected from the distribution of observatories used. On the other hand, the confidence region is particularily tight over North America, Europe and Japan where most of the observatories are located.
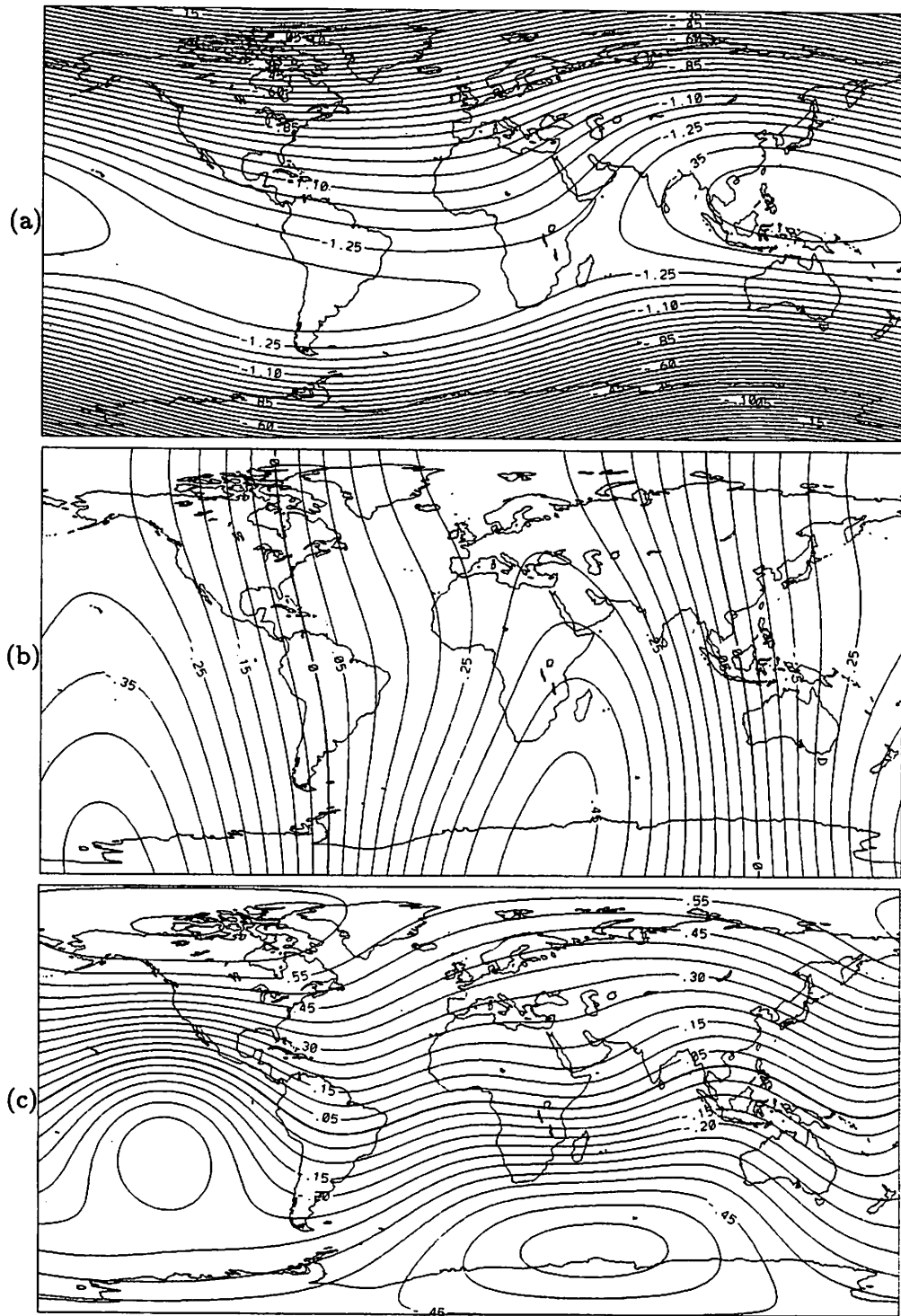
Figure 3.2: Relative amplitude of the average disturbance field for (a) the X component (b) the Y component and (c) the Z component, from field model AVDF91. Cylindrical equidistant projection. Latitude goes from 90° south to 90° north. Contour intervals are all 0.05.
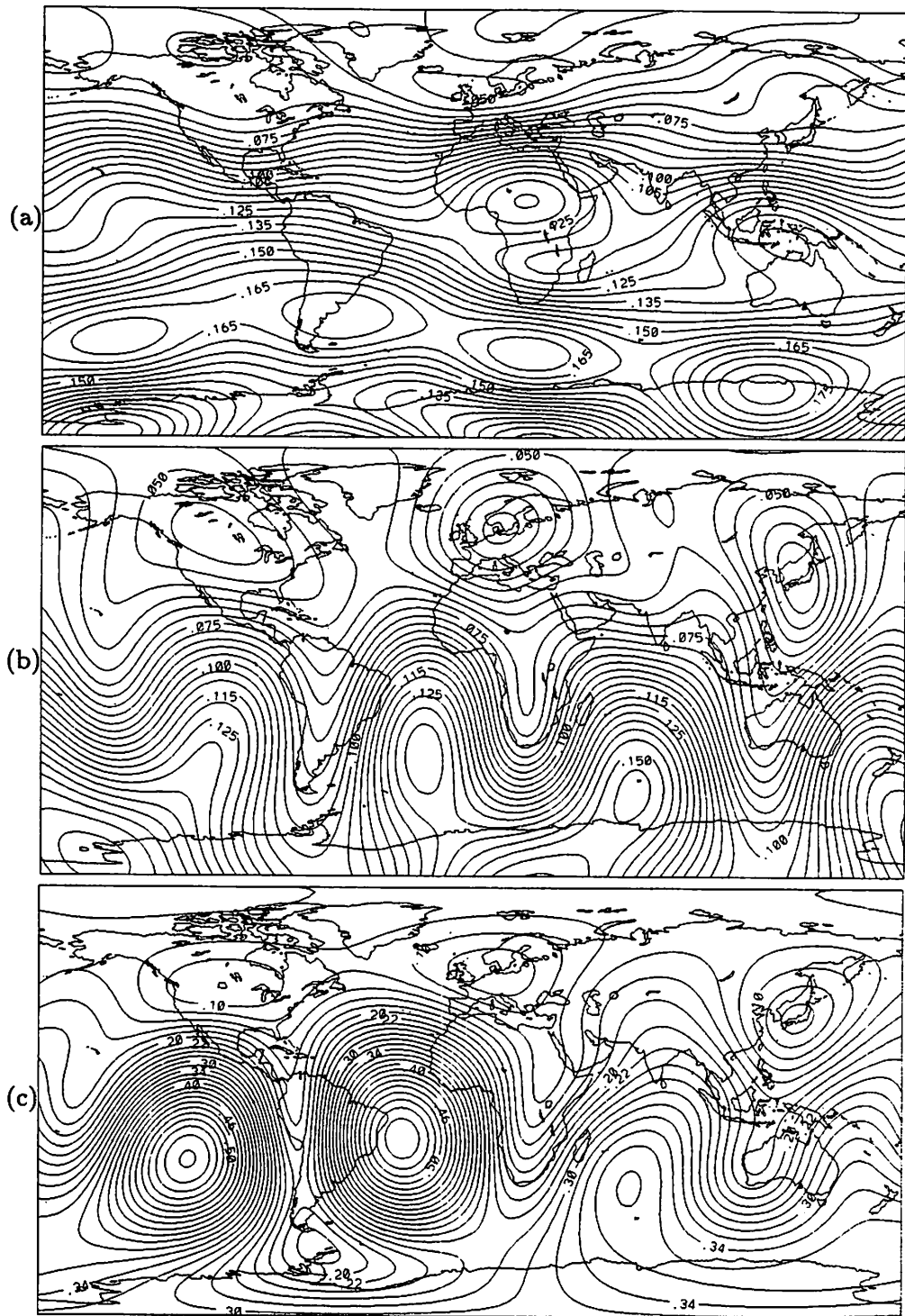
Figure 3.3: Confidence region half width for the relative amplitude of the average disturbance field for (a) the X component (b) the Y component and (c) the Z component, from field model AVDF91. Cylindrical equidistant projection. Latitude goes from 90° south to 90° north. Contour intervals are 0.005 for X and Y and 0.02 for Z.

Table 3.5: Spherical harmonic coefficients of the preferred average relative disturbance field model AVDF91. Standard errors quoted are square roots of the diagonal elements of the covariance matrix V (equation (3.10)). Note the coefficients are dimensionless, unlike a more conventional spherical harmonic model.

Spherical harmonic model AVDF91			
External		Internal	
g_1^{0e}	1.0844 ± 0.0356	g_1^{0i}	0.2837 ± 0.0243
g_1^{1e}	0.0995 ± 0.0365	g_1^{1i}	0.0458 ± 0.0343
h_1^{1e}	-0.2325 ± 0.0279	h_1^{1i}	-0.0862 ± 0.0250
g_2^{0e}	-0.0066 ± 0.0256	g_2^{0i}	-0.0284 ± 0.0215
g_2^{1e}	-0.0299 ± 0.0240	g_2^{1i}	-0.0271 ± 0.0223
h_2^{1e}	0.0209 ± 0.0223	h_2^{1i}	0.0156 ± 0.0193
g_2^{2e}	0.0208 ± 0.0278	g_2^{2i}	-0.0016 ± 0.0264
h_2^{2e}	-0.0073 ± 0.0349	h_2^{2i}	0.0216 ± 0.0335
g_3^{0e}	0.0259 ± 0.0181	g_3^{0i}	0.0198 ± 0.0159
g_3^{1e}	-0.0183 ± 0.0151	g_3^{1i}	0.0119 ± 0.0138
h_3^{1e}	-0.0232 ± 0.0156	h_3^{1i}	0.0092 ± 0.0139
g_3^{2e}	-0.0018 ± 0.0159	g_3^{2i}	-0.0009 ± 0.0150
h_3^{2e}	0.0019 ± 0.0194	h_3^{2i}	-0.0062 ± 0.0184
g_3^{3e}	-0.0111 ± 0.0157	g_3^{3i}	0.0157 ± 0.0151
h_3^{3e}	0.0123 ± 0.0162	h_3^{3i}	-0.0017 ± 0.0156

3.3.2 The annual and biannual variations.

With the pruned data set for the annual and biannual analyses, only degree 3 models were produced. In this instance, damping was found to be beneficial. The *trade-off curves* for the damped SHA of β_1–β_4 are shown in Figure 3.4. It is clear from these that in most cases the provision of damping gives a significant reduction in model complexity for a marginal degradation in the fit to the data, particularily in the case of β_2. The damping parameters chosen for the inversions for the β_1, β_2, β_3 and β_4 were 0.25, 0.5, 0.3 and 0.2 respectively which gave misfits of 1.316, 1.608, 0.767 and 0.354. The amplitude coefficients of the annual and biannual variations and associated errors were calculated using equations (2.1) and (2.2). It is apparent from the amplitude power spectra in Table 3.6 that the annual variation (for mid–latitudes) is dominated by the degree 2 harmonics (though note the large standard error). However for the biannual variation, degree 1 harmonics account for 34% of the total power, degree 2, 41% and degree 3, 26%. The amplitudes of the annual and biannual variations are plotted in Figures 3.5 and 3.6 respectively for each of the field components X, Y and Z.

3.4 Discussion

3.4.1 Disturbance phenomena

It has been established that the morphology of the disturbance phenemena is almost entirely accounted for by degree 1 spherical harmonics. Modelling in a tilted coordinate system was found to offer little advantage over the standard geographic frame. However with a tilted dipole pole position of 76.9°N and 293.1° E the field of model AVDF91 is clearly aligned with the Earth's main field. This is in agreement with the results found by Yukutake & Cain (1979) who applied SHA to filtered time–series of observatory annual means. (The corresponding pole position for the International Geomagnetic Reference Field (IGRF) at 1980 (Barraclough, 1981) is 78.8°N and 289.2° E (for degree one coefficients).) Yukutake & Cain (1979) were unable to draw conclusions regarding the higher order harmonics as they did not feel their data set was sufficiently accurate. In the present work, a larger data set has been used, and the problem of separation from

Table 3.6: Power spectra of the amplitudes of the annual and biannual variations, with standard errors. Units are $(nT)^2$.

Annual		
n	External	Internal
1	0.96±0.87	0.60±0.28
2	26.66±18.19	3.86±1.88
3	3.18±0.61	2.88±0.39
Total	30.79±18.22	7.34±1.94

Biannual		
n	External	Internal
1	4.02±2.00	1.16±0.41
2	4.62±1.53	1.61±0.32
3	1.80±0.30	2.11±0.28
Total	10.46±2.55	4.87±0.59
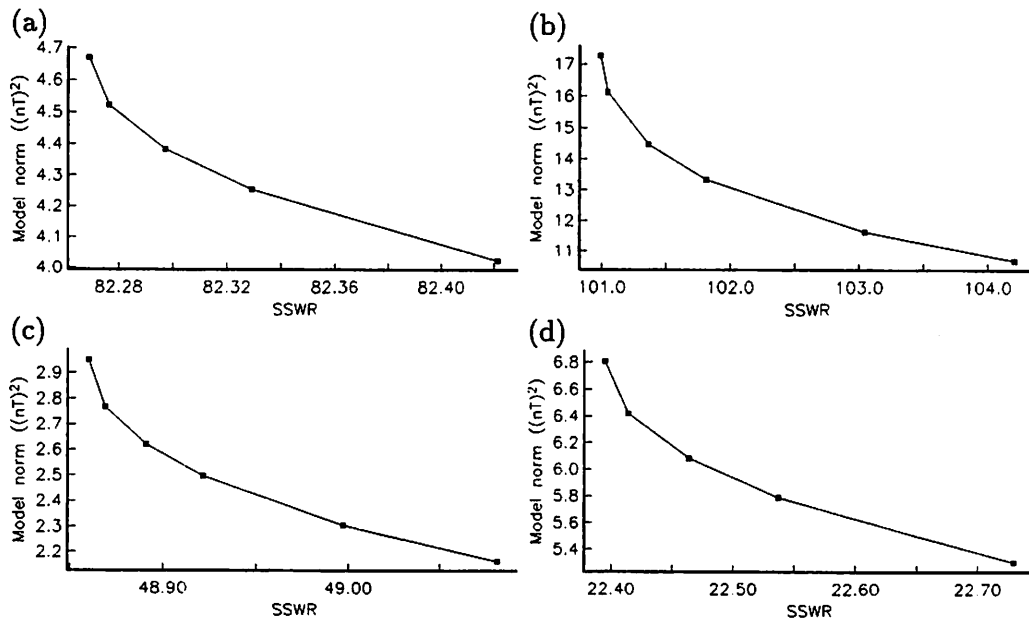
Figure 3.4: Trade–off curves for SHA of β_1–β_4, (a)–(d) respectively, showing reduction in *model norm* $\dot{m}.\dot{m}$ (and hence model complexity) at the expense of increased sum of squared weighted residuals (SSWR). Points, running from left to right are for damping values of (a) 0.0, 0.1, 0.2, 0.3, 0.5, (b) 0.0, 0.1, 0.3, 0.5, 1.0, 1.5, (c) 0.0, 0.1, 0.2, 0.3, 0.5, 0.7, (d) 0.0, 0.1, 0.2, 0.3, 0.5.
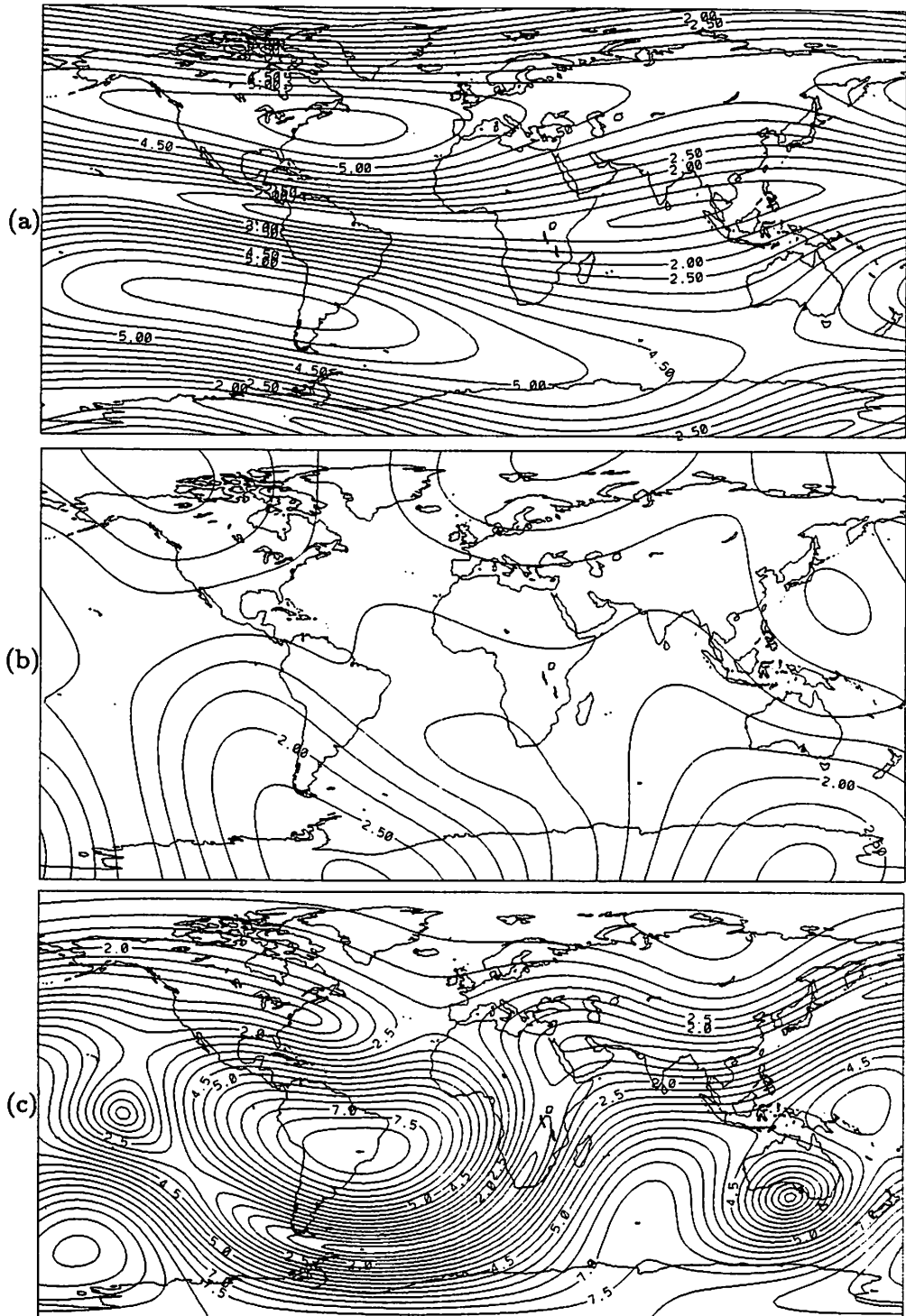
Figure 3.5: Amplitudes of the annual variation in (a) the X component, (b) the Y component and (c) the Z component. Contour intervals are all $0.5nT$. Cylindrical equidistant projection.
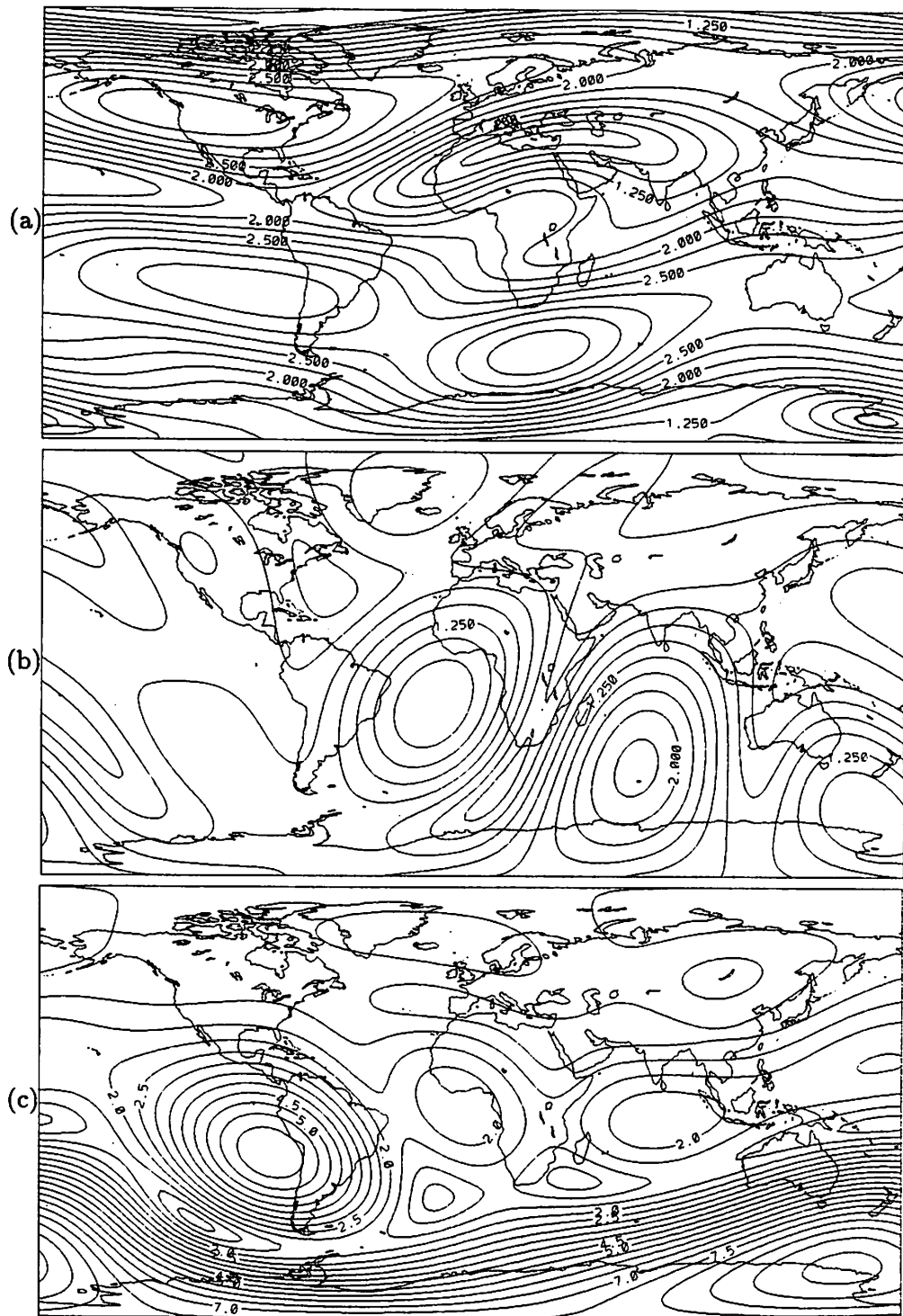
Figure 3.6: Amplitude the biannual variation for (a) the X component, (b) the Y component and (c) the Z component. Contour intervals are $0.25nT$ for (a) and (b), $0.5nT$ for (c). Cylindrical equidistant projection.

the core field has been dealt with deterministically rather than by the use of filtering techniques. It is therefore felt that the conclusion that there is insignificant energy in the higher harmonics is justified.

3.4.2 Annual and biannual variations

The morphology of the annual variation has been found here to be dominated by degree 2 spherical harmonics which agrees with the earlier findings of Malin & Isikara (1976). Since their analysis was based on values of the field measured at local midnight, they therefore concluded that the annual variation was not associated with ionospheric dynamo activity, attributing it instead to a seasonal shift in the position of the magnetospheric ring current as a consequence of the inclination of the Earth's rotational axis with respect to the solar–ecliptic. However, Campbell (1982, 1989) found significant annual and biannual variations in the amplitude of S_q and so the ionospheric dynamo cannot be entirely ruled out. Runcorn & Winch (in Barraclough et al (1992)) performed SHA of the annual variation for 1964-1965 (a solar minimum period) and determined an internal field higher than could be explained by induction in the Earth. They were led to the conclusion that there is a significant contribution from an oceanic dynamo effect primarily because of an apparent correlation between the associated current function and the world's oceans (Figure 4, Barraclough et al, 1992). However it has been pointed out (S. R. C. Malin, personal communication, 1991) that anomalously high internal spherical harmonic coefficents can arise if due account is not taken of the very large annual variation in high latitudes.

The significant power in the degree 1 harmonics of the biannual variation determined here points to the magnetospheric ring current as being partly responsible, but only by association, and the physical mechanisms governing both the annual and biannual variations cannot be determined from the spatial morphology alone. Banks (1969) also found, from a limited data set, that a P_1^0 harmonic is an adequate spatial description of the biannual variation, and therefore concluded that the magnetospheric ring current is responsible. Campbell's (1982) Figure 4 is suggestive of P_1^0 geometry for biannual modulation of S_q and so this cannot be ruled out as a source of the biannual variation found here. Currie (1966), who gives a comprehensive discussion of both the annual

and biannual variations, and Banks (1969) both concluded that the annual and biannual variations were the consequence of different mechanisms. What is clear from the results presented here is that the global distribution of the biannual variation is described by both P_1^0 and P_2^0 harmonics in approximately equal measure.

3.5 Response of the upper Earth to the external fields

Schuster (1889) investigated the global morphology of the daily variation of the Earth's magnetic field during magnetically quiet times. He recognised that part of the observed variation is due to the induced magnetic response of the Earth to the external fields as a consequence of its weakly conducting nature. Chapman (1919) followed Schuster's line of investigation, now known as geomagnetic deep sounding (GDS), and agreed with Schuster's conclusion that the conductivity must increase with depth. The response is characterised by *response functions*; for example $Q_n^m = p_n^{m_i}/p_n^{m_e}$, the ratio of internal and external coefficients in a spherical harmonic separation of the field and the *inductive length scale $C = -(i/\omega)E_\phi/B_\theta$* where $i = \sqrt{-1}$, E_ϕ, B_θ are horizontal, orthogonal components of the time-varying electric and magnetic fields of frequency ω. The former of these will be used here. Note that since Q is a ratio, the use of the coefficients of the dimensionless potential $\tilde{\Phi}$ defined earlier is fully justified in determining the response. Assuming the Earth has a spherically symetric conductivity profile, C and Q are related by

$$C = \frac{r_s(n - (n+1)Q)}{n(n+1)(1+Q)},$$ (3.11)

where r_s is the Earth's radius (see eg. Schultz & Larsen (1987); Parkinson & Hutton (1989)). This can be related to the *transfer function* of magnetotellurics for a 1–D layered Earth model using the projection of Weidelt (1972) (Schultz & Larsen (1987)).

3.5.1 Empirical response estimates

In the SHA of α, β_1, β_2, β_3 and β_4, the square roots of the diagonal elements of the covariance matrix were taken as estimated standard errors for the spherical harmonic coefficients. For β_1 to β_4 the SH coefficients were converted to phase and amplitude and errors propagated as described in §2.4.2.

For the disturbance model AVDF91, the only response estimates to be significantly non–zero at the 95% level (also non–zero at the 99% level), were for harmonic coefficients g_1^0, g_1^1, and h_1^1 and were, respectively, 0.261 ± 0.024, 0.461 ± 0.384, 0.371 ± 0.116. No phase estimates for the disturbance phenomena have been obtained in the present work as it was implicitly assumed (in §2.3.3) that any phase lag would be on the time–scale of the disturbance phenomena themselves and therefore not resolvable by monthly means.

Although the problem of inferring a conductivity distribution from a finite set of response data is non–unique, if certain simple models of the conductivity are adopted then the parameters of such models can be determined uniquely. Two such profiles, which have been widely used in GDS, are the *superconducting sphere* and the *uniformly conducting sphere* models. The former is just a limiting case of the latter. The latter model assumes the Earth is an insulator down to a radius r_0 and has uniform conductivity σ_0 below that. For an angular frequency of $\omega = \frac{2\pi}{T}$, (where T is the period), the response Q_n^m for harmonic degree n and order m is given by (eg. Parkinson & Hutton, 1989; Parkinson, 1983),

$$Q_n^m = -\frac{n J_{n+\frac{3}{2}}(r_0 k)}{(n+1) J_{n-\frac{1}{2}}(r_0 k)} \left(\frac{r_0}{r_s}\right)^{2n+1} \tag{3.12}$$

where r_s is the radius of the Earth. In the following let $z_0 = r_s - r_0$ denote the depth. The *propagation constant* is $k = \sqrt{-i\omega\mu\sigma_0}$, where μ is the permeability, taken to be that of free space ($4\pi \times 10^{-7} H m^{-1}$). J_n is a Bessel function of the first kind (eg. Arfken, 1985). Since the response for this model depends only on degree n, but not on azimuthal order m, the weighted mean (0.287) for harmonic degree 1 will be considered in the following. As the primary phenomena contributing to the average disturbance field are geomagnetic storms, and the main and recovery phases have typical timescales of the order of 0.5 to 10 days, representative frequencies will be taken as 365cycles/year (c/yr) and 18.25c/yr. The response of the uniform sphere model to a degree 1 harmonic at these frequencies is shown in Figure 3.7. For the higher frequency, and for depths ranging from 400km to 900km, conductivities ranging from $0.011 S m^{-1}$ to $0.171 S m^{-1}$ are required to explain the observed response modulus. For the lower frequency the corresponding range is $0.215 S m^{-1}$ to $3.410 S m^{-1}$. Jady (1975), following an analysis of geomagnetic storm data, concluded that mantle conductivity rises sharply between 500km and 600km to
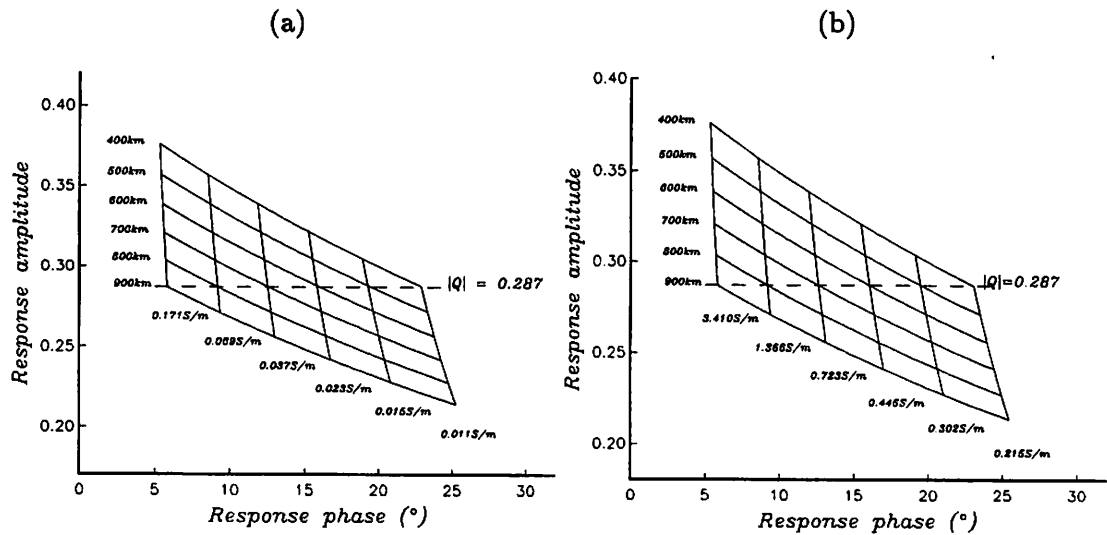
Figure 3.7: Nomograms showing dependence of response on depth and conductivity for an inducing field of spherical harmonic degree 1. These are for the uniform sphere model (see §3.5.1). (a) Frequency of 365c/yr; (b) Frequency of 18.25c/yr. Observed response modulii are indicated by a dashed line.

$1Sm^{-1}$ and stays reasonably constant to at least 1200km. Representing such a profile by a uniform sphere model with $\sigma_0 = 1Sm^{-1}$ and $z_0 = 600km$, the results obtained here are consistent with those of Jady for 18.25c/yr, but a lower conductivity (by an order of magnitude) is sufficient to explain the higher frequency. If the depth of the uniform sphere were between $700km$ and $800km$ there would be closer agreement with the results of Jady (1975). The reality of a sharp increase in conductivity near 600km has also gained further support from Jady et al (1983), though they estimate the rise to occur between 650km and 700km to only $0.1Sm^{-1}$. This is in closer agreement with the results found here for 365c/yr, which is probably more typical of most storms.

Of the response estimates for the annual and biannual variations, presented in Table 3.7, most have very wide margins of error — particularily those for the phase. For the annual variation the best determined response amplitude is for g_2^0, (the dominant harmonic of the phenomenon), and is surprisingly low though in reasonable agreement with the value of 0.046 ± 0.007 found by Banks (1969). However the phase for this harmonic is poorly determined. Figure 3.8 shows the theoretical response of the uniform

Table 3.7: Response estimates for the annual and biannual variations. Errors given were estimated as described in §3.5.1

Annual			Biannual		
Harmonic	Modulus	Phase (°)	Harmonic	Modulus	Phase (°)
g_1^0	0.506±0.251	299±49	g_1^0	0.329±0.029	87±14
g_1^1	0.334±0.256	289±128	g_1^1	0.377±0.197	53±65
h_1^1	0.856±0.565	198±59	h_1^1	0.556±0.115	199±29
g_2^0	0.062±0.006	47±81	g_2^0	0.242±0.028	180±37
g_2^1	0.263±0.063	152±46	g_2^1	1.017±0.344	137±35
h_2^1	0.520±0.227	149±55	h_2^1	1.933±1.178	170±52
g_2^2	0.911±0.362	185±39	g_2^2	0.528±0.220	191±45
h_2^2	1.066±0.522	188±38	h_2^2	0.929±1.067	40±68
g_3^0	2.028±2.443	101±90	g_3^0	1.500±0.595	74±24
g_3^1	0.810±0.306	183±32	g_3^1	0.623±0.155	172±19
h_3^1	1.054±0.409	39±25	h_3^1	1.798±0.814	45±19
g_3^2	0.652±0.234	177±39	g_3^2	0.352±0.119	222±51
h_3^2	0.761±0.292	204±32	h_3^2	0.331±0.176	49±70
g_3^3	0.652±0.236	207±31	g_3^3	1.284±1.126	129±70
h_3^3	0.831±0.367	196±38	h_3^3	6.449±21.593	158±170

sphere model for a degree 2 harmonic of the annual variation. For z_0 in the 600km to 700km depth range, the observed response requires a conductivity of about $0.8Sm^{-1}$, in broad agreement with the results for the disturbance field. The phase is too poorly determined to be of help in determining the depth and conductivity independently.

Of the biannual response estimates only those for g_1^0 and g_2^0 are well enough determined to be interpretable. However the observed response for g_1^0 would require, for example, a conductivity of at least $5Sm^{-1}$ below a depth of 400km if the uniform sphere model is to be accepted, and the g_2^0 response at least $1Sm^{-1}$ below 400km. These are both much higher than estimates from the disturbance and annual variations. The phase for g_2^0 is incompatible with the uniform sphere model. The phase for g_1^0, although apparently better determined than for other harmonics requires a much lower conductivity than that allowed by the observed reponse modulus. In the above, only a particular range of depths has been considered. The lack of good phase estimates has meant that
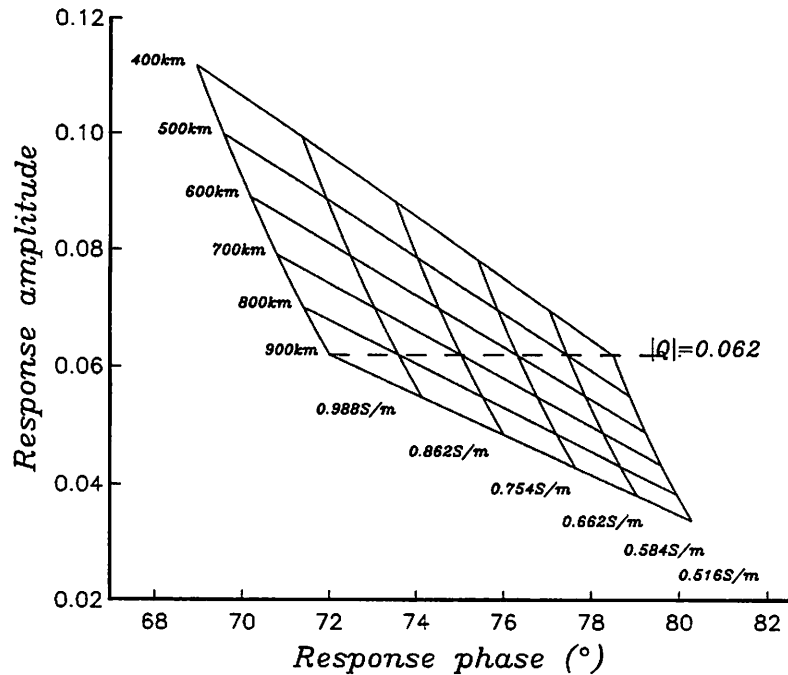
Figure 3.8: Nomogram of the response of the uniform sphere model to the g_2^0 harmonic of the annual variation. Dashed line indicates the modulus of the observed response.

conductivity could only be determined if a particular depth was assumed.

3.5.2 Theoretical limitations — an example from magnetotellurics.

The inherent non–uniqueness of determing an arbitrary conductivity distribution from a finite set of data (even if these were free of observational error), was well illustrated by the COPROD study (Jones, 1980) in which the same magnetotelluric data set was given to a number of investigators to invert for a 1–dimensional conductivity distribution. Although there were wide variations in the conductivities and thicknesses of conducting layers, there was broad agreement on the conductance. Response estimates at a finite set of frequencies cannot even place finite, non–zero upper bounds on the conductivity at a fixed depth z (Weidelt, 1985). However, Oldenburg (1983) constructed bounds on conductivity *averages* over finite depth ranges using a linear approximation to the non–linear problem. Weidelt (1985) showed that formal bounds can be placed on the conductance functional

$$S = \int_0^H \sigma(z)dz \qquad (3.13)$$

where H is a finite depth and σ is the conductivity which is a function of depth alone. For the single frequency case, Weidelt also considered the conductance extremisation problem in the presence of prior conductivity bounds.

In the following, Weidelt's (1985) results concerning the extremisation of S for the single frequency case without prior conductivity bounds (other than $\sigma \geq 0$), is confirmed by an independent method. In equation (3.13), S may be considered as a functional acting on the vector space of pairs (H, σ) where $H \in \mathcal{R}$ and $\sigma \in C^1[0, H]$, the set of continuously differentiable functions on the closed interval $[0, H]$. This vector space may be equipped with an appropriate norm (Smith, 1974, p153). The electric field in an infinite half space in which conductivity is a function of depth alone is governed by the equation

$$E'' = i\omega\mu_0\sigma(z)E \qquad (3.14)$$

where $'$ denotes differentiation with respect to z. Only a single frequency ω is considered here. By substituting $Y = \frac{E'}{E}$, equation (3.14) reduces to

$$Y^2 + Y' = i\omega\mu_0\sigma \qquad (3.15)$$

which is simply the Ricatti equation (Ince, 1956, p294). Note that $-\frac{1}{Y(z=0)} = C$, the magnetotelluric response function (Weidelt, 1985). Writing $Y = g - ih$ in equation (3.15) and considering real and imaginary parts shows that the physical contraint $\sigma \in \mathcal{R}$ is equivalent to

$$g' + g^2 - h^2 = 0 \qquad (3.16)$$

and

$$\sigma = -\frac{1}{\omega\mu_0}[h' + 2gh] \qquad (3.17)$$

Integration of (3.17) leads to the alternative expression

$$S = -\frac{1}{\omega\mu_0}\left[h(H) - h(0) + 2\int_0^H ghdz\right] \qquad (3.18)$$

The inequalities

$$g \leq 0, h \leq 0 \tag{3.19}$$

(since $\Re(C), \Im(C) \geq 0$ (Weidelt, 1972)), with (3.16) imply therefore that $h = -(g'+g^2)^{\frac{1}{2}}$.

Consideration of the extremisation of S as a calculus of variations problem (eg. Smith, 1974) leads to the natural boundary condition

$$g(H) = 0 \tag{3.20}$$

and the requirement that (gh) must satisfy the Euler–Lagrange equation (Smith, 1974)

$$\frac{\partial}{\partial z}\frac{\partial(gh)}{\partial g'} - \frac{\partial(gh)}{\partial g} = 0 \tag{3.21}$$

After some algebra this leads to

$$g'' = -\frac{2(g')^2}{g} - 12gg' - 8g^3, g \neq 0 \tag{3.22}$$

Substituting $h = -(g' + g^2)^{\frac{1}{2}}$ and hence $h' = -\frac{1}{2}(g' + g^2)^{-\frac{1}{2}}(g'' + 2gg')$ into (3.17) leads to

$$\sigma = \frac{1}{\omega\mu_0}\left[\frac{g'' + 6gg' + 4g^3}{2h}\right] \tag{3.23}$$

Substitution using (3.16) and (3.22) reduces (3.23) to the simpler form

$$\sigma = \frac{1}{\omega\mu_0|g|}\left[h\left(g^2 + h^2\right)\right] \tag{3.24}$$

Therefore in light of (3.19) and the fact that $\sigma \geq 0$, the only physically tenable conductivity profile that leads to an extreme value of the conductance functional S is $\sigma = 0$, except at the boundaries $z = 0$ and $z = H$. Thus to yield a non–zero extremum of S, σ must have a delta function at $z = 0$ and/or $z = H$ which is (qualitatively) the result found using non–linear programming by Weidelt (1985)

3.6 Conclusions

The spatial analysis of this chapter has shown that the estimates of magnetic fluctuations associated with both seasonal and disturbance phenomena found in Chapter 2 can be separated further into parts of internal and external origin. It has also been shown that the internal part is, on the whole, consistent with the existence of currents induced in the weakly conducting Earth by the external fields. The problem of inferring the

conductivity of the Earth from such observations has been discussed. It has been shown that, adopting the uniform conducting sphere model at a depth of 600km to 700km, the mantle must have a conductivity of the order 0.1Sm^{-1} to 1Sm^{-1} as found by other workers. The results for the biannual variation seem to be inconsistent with such a model but are likely to be less reliable due to its smaller amplitude. An analysis of the biannual variation using daily values could yield interesting and improved results.

The confirmation that the results of Chapter 2 embody the induced fields as well as the external inducing fields supports the assertion of §2.6 that the major part of the time–varying non–core field can be removed. The spherical harmonic model AVDF91 developed in this chapter allows such a correction to be made to data from any observatory. This eliminates a significant time–varying part of the field, which is often treated as a random error in geomagnetic annual means, thus allowing a more accurate investigation of the SV of the core field. In particular, rapid variations on the time scale of a few years, such as jerks, should be clarified.

Chapter 4

A new method for secular variation analysis

4.1 Introduction

Models of the main geomagnetic field are used for purposes such as the removal of background fields in the preparation of local and regional magnetic surveys. To reduce such models to the correct epoch, they are often extrapolated in time using models of constant secular variation (SV) with reasonable success. In some instances this linear extrapolation of the field can be a good approximation for as long as ten years (eg. Malin & Clark, 1974). Walker & O'Dea (1952) approximated the time-dependent main field at individual locations by series of straight line segments for data reduction purposes and introduced the use of the term "impulse" in the geomagnetic context. However this use of the term must not be confused with its use in the context of geomagnetic jerks. For the estimation of SV in the analysis of repeat station measurements or in the preparation of navigational charts, the assumption of constant SV at a particular site is also sometimes made (eg. Simmons, 1986; Dowson et al, 1988). The SV at many locations, such as Eskdalemuir in Scotland illustrated in Figure 4.1, shows a remarkably simple long term behaviour. The SV for the ith year is approximated by

$$\dot{u}_i = (u_{i+1} - u_{i-1})/2 \tag{4.1}$$

where the u_i are equally spaced annual means. It is clear from such plots that constant
SV is, in fact a fairly poor approximation to secular changes in the field, and that linear
SV is more appropriate over long periods. The assumption of linear SV has been found
to significantly improve the accuracy of extrapolated models of SV (Malin, 1969; Malin
& Clark, 1974).

Of more direct relevance here is the fact that investigations of geomagnetic jerks usu-
ally assume a period of constant geomagnetic secular acceleration (SA) before and after
the jerk epoch; equivalently a linear dependence of SV or a quadratic time–dependence
for the main field. The accurate determination of the coefficients of such a quadratic is
important in the investigation of mantle filter theory (in particular Backus (1983) and
Backus et al (1987)), as several years "post–jerk" the quadratic represents the asymp-
totic response of the mantle filter to a third order impulse (impulse in the third time
derivative). In a number of investigations of jerks, the transition dates between one lin-
ear SV segment and the next have been imposed, usually the same at each observatory
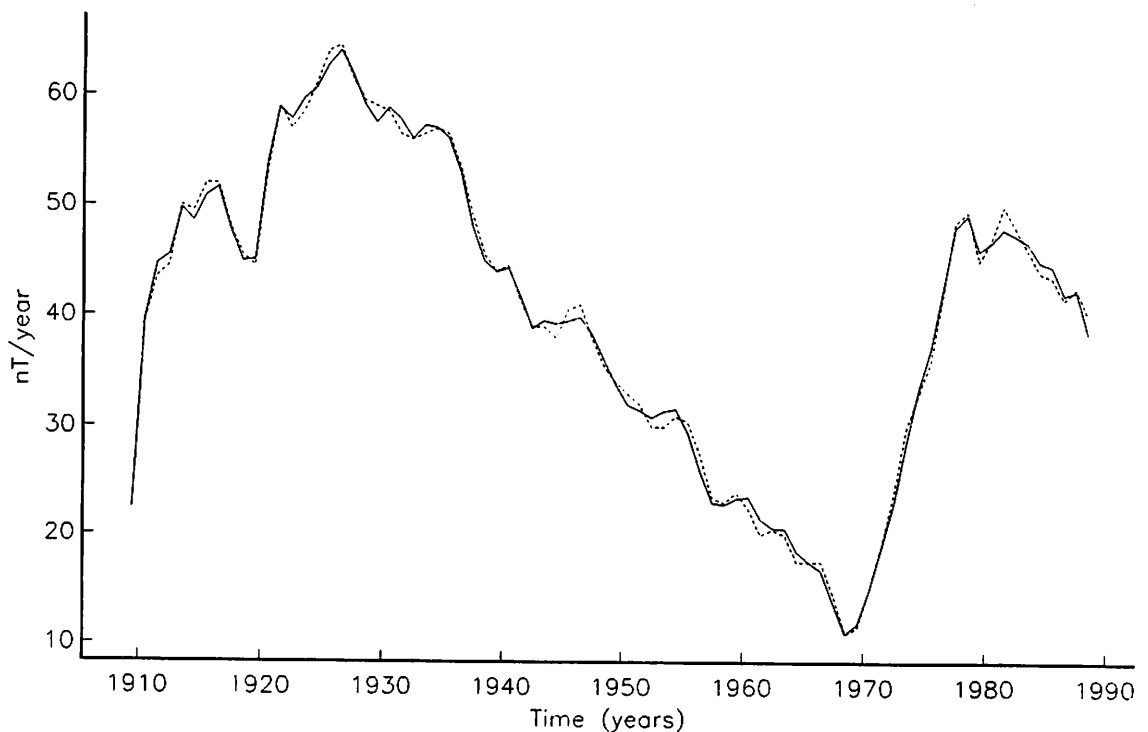
Figure 4.1: First derivative, approximated as in equation (4.1), of the Y
component at Eskdalemuir, Scotland.

and in each field component making the analysis subjective. Malin, Hodder and Barraclough (1983) assumed a jerk epoch of 1970, while LeMouël, Ducruix & Duyen (1982) determined the date between 1967 and 1972 which gave the least r.m.s. residual, (1969), to straight lines fitted by least squares to first differences of annual means. The latter method, however, ignores the correlation between succesive first differences and can give rise to spurious results, particularly in the case of relatively short time–series. Such methods were criticised for being too subjective by Alldredge (1979). In a more recent analysis Golovkov *et al* (1989) also assigned jerk epochs as the dates at which arbitrarily fitted linear SV approximations intersect. The method developed here on the other hand makes no assumptions about when and for how long the SV behaves linearly. The method determines objectively the periods of time during which the development of the main field can be reasonably well approximated by a quadratic time–dependence. The hypothesis that most geomagnetic time–series can be well approximated by a piecewise quadratic function (not necessarily continuous) will be investigated. This will be referred to as the "linear SV" hypothesis. Note that the analysis is performed for *individual observatories*; no assertion is being made, at this stage, about the global synchronicity or otherwise of sudden changes in slope of the SV. This issue will be dealt with in Chapter 5. However if there are particular epochs when a global jerk occurred then this analysis should reveal it objectively but in no way impose it. In the context of geomagnetic jerks and mantle filter theory, the quadratic segments need not and should not then be constrained to be continuous at the date when the first derivatives are equal (Backus *et al*, 1987). The quadratic segments are only representations of the asymptotic behaviour of the field before and after the jerk. The actual behaviour of the field during the transition is not specified. The rest of this chapter is devoted to the development of the method and its application to geomagnetic annual means. The interpretation of the results in the context of geomagnetic jerks is left until Chapter 5.

4.2 Optimal piecewise regression algorithm

The method I develop here is based on an algorithm developed by Kent, Briden and Mardia (1983) (hereafter referred to as KBM). Their algorithm was developed to partition a

sequence of 3 component vector data in $\mathcal{R}^3$ into an "optimal" spanning set of linear *segments*, a segment being a sub–sequence of points. (The algorithm also determined *planar chunks* which are not of interest here.) Their method assesses the statistical strength of each possible segment using principal components analysis (PCA) (eg. Murtagh & Heck, 1987; Preisendorfer, 1988; Jackson, 1991). The basis of PCA is the determination of the *sum of squares and cross products matrix* for a set of realisations of a set of random variables. The eigenvectors of this matrix are called the *principal components*. The corresponding eigenvalues are used to assess how well determined each component is. In the case of a set of 3 component vector data which all lie, or nearly lie, on a straight line one eigenvalue will be much larger than the others and the corresponding eigenvector will give the direction of the best fitting line. The smaller the other eigenvalues, the better the first principal component (or linearity) is determined. KBM's algorithm considers each possible segment and uses PCA to assess the strength of linearity among these data. Having assessed the strength of each segment their algorithm creates an optimal partition of the given series into a set of spanning segments. The partitioning algorithm used here is closely analogous to KBM's and details will be outlined in §4.2.3. The partition is optimal in the sense of giving an adequate fit to the data with the fewest well determined parameters. However it is not always the case that the parameters of enough segments are statistically well determined, in which case the resulting model does not span the whole time–series. The advantage of the KBM algorithm is its objective choice of segments which depends only on the assumed level of noise in the data, that is, the way in which one defines "adequate fit". However KBM go on to show how this decision can be made semi–objectively through the use of information criteria.

The method of KBM, developed primarily for the analysis of palæomagnetic data, was applied to the analysis of SV data by Whaler (1987). Applying the KBM algorithm to smoothed first differences of geomagnetic biennial means (those of Malin & Hodder (1982)), for the period 1962–1976, Whaler was successful in demonstrating that at several observatories a bilinear model for the SV, with a transition date around 1969, is an adequate representation. However Whaler also concluded that at many observatories the bilinear model is too simple, possibly due to contamination of the biennial means by external fields for which no account was made in the analysis. There are however,

drawbacks in the direct application of this algorithm to SV data. Firstly, the algorithm assumes independence of successive data points, which is not the case with SV estimates based on first differences (or biennial means for that matter). This is a problem of which Whaler was well aware, but which cannot be obviously overcome in PCA. Taking account of this correlation by use of the appropriate covariance matrix in linear regression leads identically to the first derivative of a quadratic model fitted to the undifferenced data. Secondly PCA only determines inter–relationships between, in this context, the 3 magnetic components and does not elucidate any time–dependence. Hence the algorithm only determines the "direction" of the changes in SV and not the magnitude of the change from one datum to the next. One could attempt to overcome this by including the time variable in the analysis but this variable is effectively perfectly known whereas the field components are subject to significant observational error. Appropriate weighting of the spatial and temporal variables to reflect this fact was found to result in the sum of squares and cross–products matrix becoming grossly ill–conditioned. To study jerks, Golovkov *et al* (1989) plotted "polarograms" (SV of one field component against another) which is similar to PCA although their method was entirely graphical rather than statistical.

Therefore, in analysing the linear SV hypothesis, it is more appropriate to investigate the quadratic time dependence directly. I therefore develop an algorithm analogous to that of KBM but based on regression analysis rather than PCA. Although Whaler (1987) saw some attraction in the simultaneous analysis of all three components, I choose to analyse each component separately. In this way there is no assumption made that changes in the SV should occur simultaneously in all components. In the context of geomagnetic jerks this allows for varying emergence times of jerks, as seen in different field components, as could occur as a result of the differential propagation of field harmonics through the mantle (Backus, 1983).

4.2.1 Formulation

Consider a series of geomagnetic annual means for some field component $\{u_i\}$, $i = 1, \ldots, N$. The subset $I_k = \{u_i\}, i = \alpha_k, \ldots, \beta_k$ will be termed a *segment* after the terminology of KBM. Let $n_k = \beta_k - \alpha_k + 1$ and t_i be the central epoch for annual mean u_i. Define a model for segment I_k by

$$u_i = a_k((t_i - \bar{t}_k)^2 - \bar{t}_k^2) + b_k(t_i - \bar{t}_k) + c_k + e_i \tag{4.2}$$

where e_i is the error term (assumed Gaussian with mean 0 and equal variance for a given observatory's field component), a_k, b_k and c_k are model parameters to be determined, $\bar{t}_k$ is the mean epoch for the segment and $\bar{t}_k^2$ is the mean square deviation of epochs from the mean. The parameters a_k, b_k and c_k can then be estimated by least squares:

$$\hat{\mathbf{m}} = (\mathbf{G}^T\mathbf{G})^{-1}\mathbf{G}^T\mathbf{d}$$

where $\hat{\mathbf{m}} = (c_k, b_k, a_k)^T$ and $\mathbf{d} = (u_{\alpha_k}, \ldots, u_{\beta_k})^T$. $\mathbf{G}$ is the equations of condition matrix with ith row

$$(\quad 1 \quad (t_i - \bar{t}_k) \quad ((t_i - \bar{t}_k)^2 - \bar{t}_k^2) \quad)$$

By defining the quadratic model and equations of condition in this way it is ensured that the normal equations matrix $(\mathbf{G}^T\mathbf{G})^{-1}$ is diagonal (provided the u_i are equally spaced in time), i.e. the parameter estimates are independent. The estimated data variance is defined by $\hat{\sigma}_k^2 = \frac{\mathbf{d}^T\mathbf{d} - \hat{\mathbf{m}}^T\mathbf{G}^T\mathbf{d}}{n_k - 3}$ (since 3 parameters are determined). The quantity $(n_k - 3)\frac{\hat{\sigma}_k^2}{\sigma^2}$ is then distributed as χ^2 with $n_k - 3$ degrees of freedom where σ is the standard deviation of the data which must be specified _a priori_. The quadratic defined by $\hat{\mathbf{m}}$ will be termed a _model segment_.

4.2.2 Segment confidence regions

To assess the "strength" with which a particular model segment is determined, note that $\hat{a}_k$, $\hat{b}_k$ and $\hat{c}_k$ are independent random variables. Assuming the null hypothesis $H_0 : \hat{\mathbf{m}} = 0$, $\frac{\hat{a}_k}{\delta a_k}$, $\frac{\hat{b}_k}{\delta b_k}$ and $\frac{\hat{c}_k}{\delta c_k}$ all have Student's t–distributions on $n_k - 3$ degrees of freedom, where

$$\begin{pmatrix} \delta c_k^2 & 0 & 0 \\ 0 & \delta b_k^2 & 0 \\ 0 & 0 & \delta a_k^2 \end{pmatrix} = \hat{\sigma}^2(\mathbf{G}^T\mathbf{G})^{-1} \tag{4.3}$$

(Montgomery & Peck 1982).

Now define $q_1 = (\frac{\hat{a}_k}{\delta a_k})^2$, $q_2 = (\frac{\hat{b}_k}{\delta b_k})^2$. It follows that the better the curvature and linearity are determined (corresponding to SA and SV respectively), the larger q_1 and q_2 will be; when they are less well determined $q_1, q_2 \to 0$. However, as the SV is a more

dominant effect than the SA, $\hat{b}_k$ will be better determined than $\hat{a}_k$. Thus q_2 will tend to dominate q_1. To curcumvent this problem, define a balanced, joint measure of the confidence placed in the curvature and linearity estimates by

$$q = \frac{q_1 q_2}{q_1 + q_2}.$$

The tighter the joint confidence region for $\hat{a}_k$ and $\hat{b}_k$, the larger q will be.

4.2.3 Piecewise regression algorithm

The algorithm to select the best piecewise quadratic model of the time–series is now developed in a manner analogous to that of KBM.

- For each segment $I_k = \{u_i\}, i = \alpha_k, \ldots, \beta_k$, fit a model segment by least squares as described above, where $\alpha_k = 1, \ldots, N - n_m + 1$ and $\beta k = \alpha_k + n_m - 1, \ldots, N$. n_m is the minimum permitted length of segment (see below).

- Reject any segment for which $(n_k - 3)\frac{\hat{\sigma}_k}{\sigma} > \chi^2_{0.95, n_k - 3}$. That is, reject any segment which has an unexpectedly high misfit (at the 95% confidence level) (Wonnacott & Wonnacott, 1981, p455).

- Reject any segment if $n_k \leq n_m = 5$. This is purely arbitrary but such short segments are too poorly determined to be of use.

- Rank all remaining segments in order of decreasing q, i.e. the best determined segments are placed first.

- Now work through this ordered list, rejecting any segment which overlaps unacceptably with any segment higher up the list (see below).

The result of this algorithm is a partition of the time–series into a set of segments (possibly spanning), which are well determined and fit the data adequately. The extent to which consecutive segments should be allowed to overlap one another requires a subjective choice. As nothing is assumed about the behaviour of the field between quadratic segments, allowance must be made for data in this transition period to be parameterised by either segment or both, if this is statistically acceptable. Here, the segments were allowed to overlap by up to 3 points. In practise, this was found to partially overcome the

problem of misassignment of points to longer (and therefore stronger) model segments encountered by KBM.

The complete model for the time–series consists of the set of accepted model segments. Clearly it is unacceptable to have points parameterised in two distinct ways where segments overlap. To clarify this apparent anomaly, the transition date from one model segment to another was defined as the date at which the first derivatives of the model segments were equal. Data before this date were parameterised by the first segment and data after this segment were parameterised by the second.

The output from the piecewise regression algorithm (PRA) is the best determined piecewise quadratic model which fits the data to a statistically acceptable level. Unlike the method of B–splines which requires the specification of the number of knots for example, this algorithm does not require the pre–specification of the transition dates or the number of segments. What the algorithm does require however, is an *a priori* value for the σ^2, the data variance. The smaller σ is the closer the model will have to follow the data — fewer and shorter segments will be acceptable. As $\sigma \to \infty$, longer, and ultimately fewer, segments will be acceptable.

4.2.4 Information criteria and optimisation

A range of values of σ thus implies a *family* of models within which there will be a model which is in some sense *optimal*. Akaike (1973) extended the maximum likelihood principle within an information theoretic framework by defining an information criterion based on the Kullback–Leibler discrepancy. (See for example Linhart & Zucchini, 1986, for background on discrepancies and model selection criteria.) Akaike defined the criterion

$$-2 \sum_{i=1}^{n} \log(g_{\hat{\theta}_i}) + 2p$$

where n is the number of data, p is the number of model parameters and $g_{\hat{\theta}_i}$ is the likelihood of the ith datum (which has been maximised by the model estimate $\hat{\theta}_i$). This essentially characterises a trade–off between quality of fit to the data and number of parameters in the model. An optimal model will result in a minimum value for this criterion.

KBM define a modified version of the Akaike criterion. They define a *Partial Akaike Information Criterion* or PAIC, which has the same form as the criterion which Linhart & Zucchini (1986) simply refer to as the Akaike Information Criterion:

$$-\frac{1}{n}\sum_{i=1}^{n}\log(g_{\hat{\theta}_i}) + \frac{p}{n}$$

Not all models in the family will parameterise the same number of points; for example for some value of σ only one short segment may be acceptable. This obviously affects the number of points contributing to the joint log–likelihood function. Division by n simply compensates for this so that a fair comparison between models can be made. Thus, under the assumption that the residuals are normally distributed, the form of the PAIC here is

$$-\frac{1}{N'}\sum_{i=1}^{N'}\log(\frac{1}{\hat{\sigma}\sqrt{2\pi}}\exp\left\{-\frac{(u_i - \hat{u}_i)^2}{2\hat{\sigma}^2}\right\}) + \frac{M}{N'}$$

$$= -\frac{1}{N'}\left[-N'\log(\hat{\sigma}\sqrt{2\pi}) - \frac{(N' - M)}{2}\right] + \frac{M}{N'} \tag{4.4}$$

where M is the total number of model parameters (equal to 3 times the number of accepted segments), N' is the total number of data which lie on accepted segments, $\hat{u}_i$ is the model estimate of the ith datum and $\hat{\sigma}^2$ is the total r.m.s. residual between the model segments and the data. Note that in calculating $\hat{\sigma}^2$, data jointly parameterised by overlapping segments were assigned to one segment or the other dependent on whether their central epoch came before or after the date at which the first derivatives of the model segments w.r.t. t were equal. The *essential* part of the criterion is therefore

$$\log(2\pi\hat{\sigma}^2) + \frac{M}{N'} + 1 \tag{4.5}$$

as linear scaling of the criterion does not affect its behaviour.

Clearly, in general a model can fit a data set perfectly given enough parameters, which could occur for large σ, thus sending the PAIC trivially to $-\infty$; conversely a model with a single parameter (ie. a mean value) will give a fit to the data which may be unacceptably poor. Neither of these extreme cases is particularily useful. Between these will lie an optimal model for some value of σ, which will in theory coincide with a local minimum or plateau of the PAIC when plotted against σ. For each prior value of σ specified, the PRA will, in general, yield a different set of accepted segments (model).
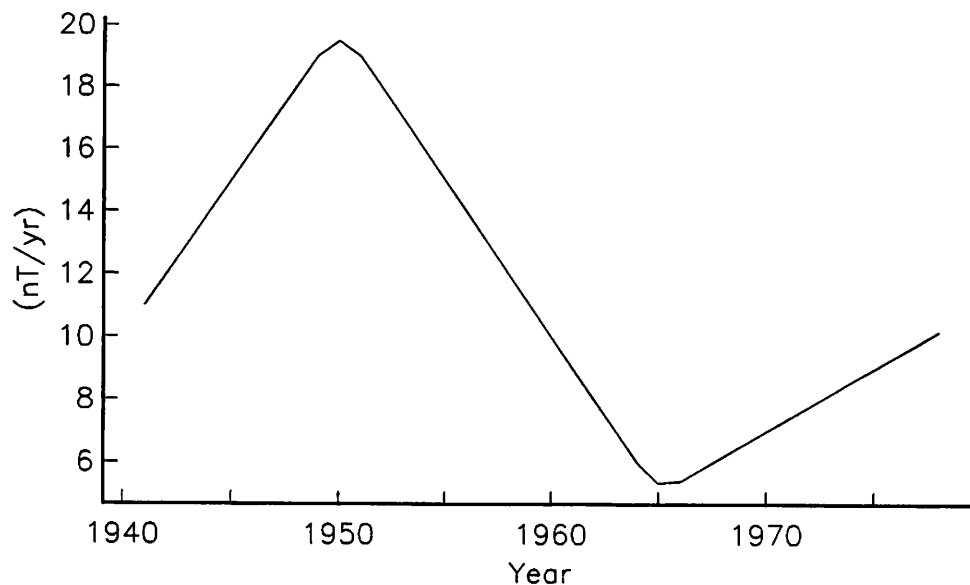
Figure 4.2: The synthetic model analysed using the OPRA algorithm before the addition of Gaussian noise.

Starting with an initial value σ_p^2 for the data variance, one may specify the *a priori* data variance as $\sigma^2 = (\rho\sigma_p)^2$. The space of acceptable models may be investigated by varying the controlling parameter ρ which KBM term the "excess standard deviation". Using the PAIC as a guide, an optimal piecewise quadratic model can hopefully be found. For $\rho < 1$ the implication is that the initial value for the data variance is too large. Values of $\rho > 1$ imply that either the initial value is too small or that there is some misspecification in the model; that is, the true model differs from the quadratic assumed. This procedure will be referred to as the optimal piecewise regression algorithm (OPRA).

4.3 Application to synthetic data

The OPRA algorithm was tested on synthetic data. The synthetics were generated from models consisting of various numbers of quadratic segments, with different curvatures and constrained to be continuous at the transition dates, and with various amplitudes of Gaussian errors added. An example synthetic based on a three segment model and with no noise added is shown in Figure 4.2. This and all subsequent segment plots will show the *first time derivative* of the segments, synthetics and (in §4.4) data, as this makes

the performance of the PRA clearer, and no relevant information is lost. Again the SV is approximated as in equation (4.1). The application of OPRA to this synthetic model (with Gaussian noise of r.m.s. amplitude $2nT$ added) is illustrated in Figure 4.3. For the lowest value of the excess standard deviation, ρ (0.3), only short, well determined segments are accepted, giving a poor representation of the series (Figures 4.3(a) and (d)). As the value of ρ is increased the PAIC increases sharply. This was in general found to correspond to a rapid increase in the number of acceptable segments. This then gave the algorithm the freedom to choose the strongest (and usually longest) segments possible. As ρ was subsequently increased segments which provided a poorer fit to the data but were better determined became acceptable, while shorter segments were rejected as being too poorly determined. Thus the number of parameters required to model the time–series in general decreased but the misfit increased. For a range of values of ρ centred around 1.0 the structure determined was stable and consequently there is a plateau in the PAIC (Figure 4.3(e)). The segments yielded by the PRA for $\rho = 1.0$ give a satisfactory and optimal fit to the time–series (Figure 4.3(b)). For $\rho = 2.7$, well beyond the optimal value, a long segment offering a poor fit to the data is accepted by the algorithm. There is then only scope for one other short segment to be accepted and so the overall fit to the data is poor. Having established that the algorithm was performing as expected, the next step was to apply the algorithm to geomagnetic data.

4.4 Geomagnetic data analysis

4.4.1 Selection and validation of data

The data for the analysis in this chapter consist of time–series of observatory annual means. The particular data set used was obtained from WDDC–C1 this being the most up to date and exhaustive compilation of annual means available. This was then separated by observatory. Many observatories had to be ignored as they did not have sufficiently continuous data for the application of OPRA. Gaps of a few years at the very most were deemed acceptable; longer gaps would have given rise to increasingly erroneous results. In the case of an observatory closing and moving to a nearby site, the data from the two sites were combined to form a single time–series. If a known
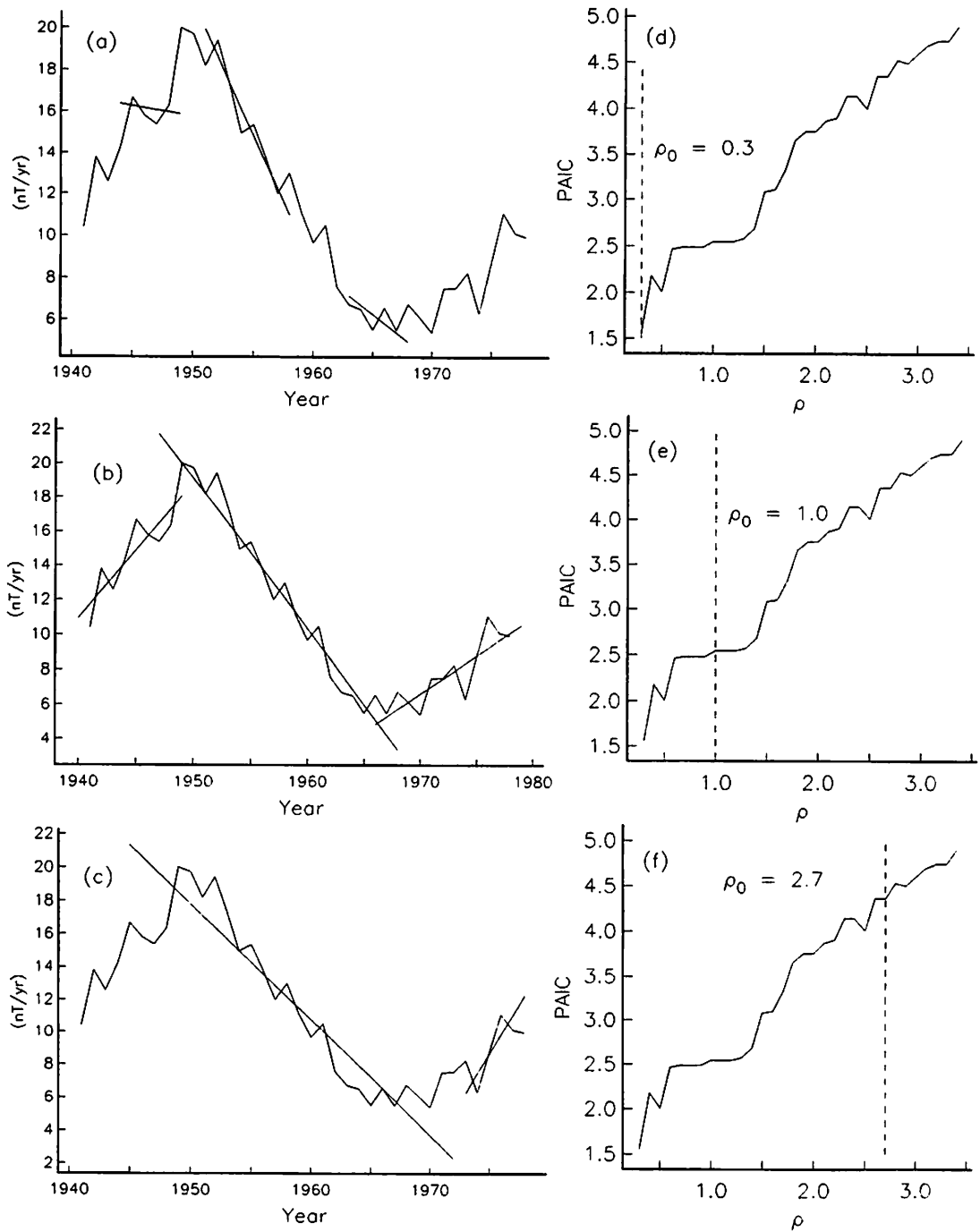
Figure 4.3: Model segments determined by the PRA for the indicated values of ρ. Plots (a)–(c) show the synthetic data (plus Gaussian noise of r.m.s. $2nT$) with model segments determined. Plots (d)–(f) show the corresponding values of ρ_0. Note the plateau centred on $\rho_0=1.0$ in (e)

site change correction was available then this was applied so as to reduce the time–series to the most recent site. Of the 119 observatories finally used, including composite observatories, only 26 had any gaps in their time series. Of the total of 37 gaps, 20, 10, 3, 3 and 1 were of length 1, 2, 3, 4 and 5 years repectively. No attempt was made to interpolate across these gaps as OPRA could still be applied, although slight non–orthogonality of the covariance matrix (4.3) arises. Table 4.1 details the 89 single site observatories and Table 4.2 the 30 composite sites. Once collated, each component of all observatory records was plotted to aid detection of baseline changes, obvious keying errors etc. In addition, approximations to the first derivatives of all time–series were calculated (using equation (4.1)) and then plotted, as these tended to reveal "glitches" more readily than plots of the main field. The few that were found were:

- Almeria (ALM), Z, 1986.5 omitted as suspect.

- Barrow (BRW), Z, Pre 1963.5, poor baseline control, 1974.5 removed as suspect.

- Changchun (CNH), Y, constant SV extrapolation to estimate jump of $+73$nT at 1979.5

- Hatizyo (HTY) – Simosato site differences unknown; values of old site extrapolated by constant SV to estimate: $X : -412nT$, $Y : -860nT$, $Z : -1301nT$

- Lerwick (LER), Z, 1934.5 jump in Z estimated as $+100nT$; since re–estimated by the BGS as $+144nT$.

- Wingst (WNG), X, 1989.5 value appeared as 19039 in the BGS file. As preceeding years were 18065 and 18053 this was assumed to be a keying error and taken as 18039.

The time–spans for each time–series are indicated in Tables 4.1 and 4.2. A total of 5766 vector annual means were analysed, with about one third of these being from European observatories.

4.4.2 Correction for the effects of external fields

As the annual means consist of averages over all hours of all days, they are affected by the average disturbance field in the same way as the monthly means analysed in Chapter 2.

As it was the intention to investigate the variation of the core field, it was necessary to remove as much of the disturbance and associated induced fields as possible. To achieve this, the method described in Chapter 3 was applied, using the disturbance field model AVDF91 in conjunction with the time–series of annual means of the aa index. For auroral observatories also analysed in Chapter 2 the actual relative amplitudes determined were used rather than the AVDF91 model prediction. I believe this removes the major part of the contribution to annual means from external sources and the associated induced fields. As discussed in Chapter 3 there may be some residual contribution from the S_q current systems, but this is neglected. The resulting annual means are considered to consist solely of core field, crustal anomaly and error.

4.4.3 Prior values for the standard deviation

In section §4.2.4 it was described how the OPRA analysis requires some initial estimate, σ_p, of the standard deviation of the data. The excess standard deviation, ρ, is then varied until an optimal model is found at $\rho = \rho_0$ say. The implied prior value of the standard deviation of the data is then $\sigma = \rho_0 \sigma_p$. The actual starting value σ_p is therefore irrelevant though clearly some reasonable value must be chosen and a sufficient range of values of ρ explored to cover the full family of possible models. Values of $\rho_0 \sigma_p$ finally chosen for each time–series analysed are given in Table 4.3.

Table 4.1: Details of the 89 single site geomagnetic observatories used in the analysis (see §4.4.1). The period given is the period from which data were‛ used. Locations of the observatories appear in Figure 5.7

IAGA code	Observatory name	Latitude	Longitude	Period
AAA	Alma Ata	43.25	76.92	1963–1988
AAE	Addis Ababa	9.03	38.76	1958–1989
AIA	Argentine Islands	-65.25	295.74	1957–1984
ALE	Alert	82.50	297.50	1961–1988
ALM	Almeria	36.85	357.54	1955–1989
ANN	Annamalainagar	11.37	79.68	1957–1988
API	Apia	-13.81	188.23	1905–1989
AQU	L Aquila	42.38	13.32	1960–1989
ASH	Vannovskaya	37.95	58.11	1959–1989
BEL	Belsk	51.84	20.79	1960–1989
BJI	Beijing	40.04	116.18	1957–1988
BJN	Bear Island	74.50	19.23	1951–1990
BLC	Baker Lake	64.33	263.97	1951–1989
BNG	Bangui	4.44	18.57	1955–1988
BRW	Barrow	71.38	203.72	1963–1989
CCS	Cape Chelyuskin	77.72	104.28	1951–1989
CMO	College	64.85	212.17	1959–1989
COI	Coimbra	40.21	351.58	1867–1989
CPA	Cha Pa	22.35	103.83	1955–1980
CWE	Cape Wellen	66.16	190.16	1955–1989
DIK	Dixon Island	73.50	80.42	1949–1989
DOB	Dombas	62.08	9.10	1952–1989
DOU	Dourbes	50.10	4.59	1955–1988
EBR	Ebro	40.82	0.49	1951–1980
ESK	Eskdalemuir	55.32	356.80	1908–1989
FUQ	Fuquene	5.47	286.26	1954–1982
FUR	Furstenfeldbruck	48.17	11.28	1939–1989
GCK	Grocka	44.63	20.77	1958–1989
GUA	Guam	13.58	144.87	1957–1989
GZH	Guangzhou	23.09	113.34	1958–1988
HLP	Hel	54.61	18.82	1955–1989
HRB	Hurbanovo	47.87	18.19	1950–1989
HUA	Huancayo	-12.05	284.66	1922–1988
ISK	Istanbul-kandilli	41.06	29.06	1947–1977
KAK	Kakioka	36.23	140.19	1930–1989
KGL	Port-aux-francais	-49.35	70.20	1957–1987
KNY	Kanoya	31.42	130.88	1958–1989
KNZ	Kanozan	35.25	139.96	1961–1988
KOD	Kodaikanal	10.23	77.46	1951–1988
LER	Lerwick	60.13	358.82	1923–1989
LGR	Logrono	42.46	357.49	1957–1976
LMM	Maputo	-25.92	32.58	1957–1987
LOV	Lovo	59.35	17.83	1929–1989

Table 4.1: Continued...

IAGA code	Observatory name	Latitude	Longitude	Period
LQA	La Quiaca	-22.11	294.42	1942-1976
LRV	Leirvogur	64.18	338.30	1957-1989
LUA	Luanda Belas	-8.92	13.17	1957-1985
LVV	Lvov	49.90	23.75	1957-1989
LZH	Lanzhou	36.09	103.85	1959-1988
MAW	Mawson	-67.61	62.88	1955-1987
MBO	M Bour	14.39	343.04	1952-1988
MCQ	Macquarie Island	-54.50	158.95	1951-1988
MEA	Meanook	54.62	246.67	1916-1989
MIR	Mirny	-66.55	93.02	1956-1988
MMB	Memambetsu	43.91	144.19	1952-1989
MNK	Pleshenitzi	54.50	27.88	1961-1988
MOS	Krasnaya Pakhra	55.48	37.31	1946-1989
MUT	Muntinlupa	14.38	121.01	1951-1988
NSM	Nagycenk	47.63	16.72	1961-1989
NUR	Nurmijarvi	60.51	24.66	1953-1989
NVL	Novolazarevskaya	-70.77	11.83	1961-1987
ODE	Odessa	46.43	30.77	1948-1989
PAG	Panagyurishte	42.51	24.18	1948-1983
PET	Paratunka	52.90	158.43	1969-1988
PIL	Pilar	-31.67	296.12	1905-1988
PMG	Port Moresby	-9.41	147.15	1959-1988
PPT	Pamatai	-17.57	210.43	1968-1988
QUE	Quetta	30.19	66.95	1953-1989
RES	Resolute Bay	74.70	265.10	1954-1989
RSV	Rude Skov	55.84	12.46	1907-1980
SBA	Scott Base	-77.85	166.78	1964-1989
SUA	Surlari	44.68	26.25	1950-1989
TAM	Tamanrasset	22.79	5.53	1952-1981
TEN	Canarias	28.48	343.74	1959-1988
TFS	Dusheti (Tbilisi)	42.09	44.71	1938-1989
THL	Thule	76.53	291.11	1956-1988
THY	Tihany	46.90	17.89	1955-1989
TIK	Tixie Bay	71.58	129.00	1944-1989
TRD	Trivandrum	8.52	77.00	1957-1989
TRO	Tromso	69.66	18.95	1931-1990
TUC	Tucson	32.25	249.17	1910-1987
VAL	Valentia	51.93	349.75	1899-1989
VIC	Victoria	48.52	236.58	1956-1989
VLA	Gornotayezhnaya	43.68	132.17	1958-1988
VOS	Vostok	-78.45	106.87	1958-1989
VSS	Vassouras	-22.40	316.35	1915-1988
WHN	Wuhan	30.53	114.56	1959-1988
WNG	Wingst	53.74	9.07	1940-1989
YAK	Yakutsk	62.02	129.72	1948-1987
YSS	Yuzhno Sakhalinsk	46.95	142.72	1950-1989

Table 4.2: Details of the 30 composite geomagnetic observatories analysed. Distance is the great circle distance from the previous site (see §4.4.1). The period given is the period from which data were used. Locations of the observatories appear in Figure 5.7

IAGA code	Observatory name	Latitude	Longitude	Period	Dist. (km)
ABG	Alibag	18.64	72.87	1904–1989	29
	Colaba (Bombay)			1868–1903	
ARS	Arti	56.43	58.57	1972–1989	157
	Vysokaya Dubrava			1932–1972	29
	Sverdlovsk (Yekaterinburg)			1887–1931	
CAN	Canberra	-35.31	149.36	1979–1988	427
	Toolangi			1922–1978	54
	Melbourne			1915–1921	
CLF	Chambon-la-forêt	48.02	2.26	1935–1988	90
	Val Joyeux			1901–1935	34
	Parc St.Maur			1883–1900	
CNH	Changchun (Helong)	43.83	125.30	1979–1988	25
	Changchun			1957–1978	
EYR	Eyrewell	-43.42	172.35	1978–1989	42
	Amberley			1929–1977	43
	Christchurch			1902–1928	
FRD	Fredericksburg	38.21	282.63	1956–1989	74
	Cheltenham			1901–1955	
GDH	Godhavn	69.24	306.48	1976–1989	2
	Godhavn			1927–1975	
GNA	Gnangara	-31.78	115.95	1959–1988	163
	Watheroo			1919–1958	
HAD	Hartland	50.99	355.52	1957–1989	286
	Abinger			1925–1956	42
	Greenwich			1900–1924	
HER	Hermanus	-34.42	19.23	1941–1989	87
	Cape Town			1932–1940	
HIS	Heiss Island	80.62	58.05	1959–1989	101
	Tikhaya Bay			1951–1957	
HON	Honolulu	21.32	201.94	1961–1989	10
	Honolulu			1947–1960	4
	Honolulu			1902–1946	
HTY	Hatizyo	33.12	139.80	1979–1989	362
	Simosato			1954–1977	
IRT	Patrony	52.27	104.27	1959–1989	43
	Zuy			1915–1958	27
	Irkutsk			1887–1914	
KIV	Dymer	50.72	30.30	1963–1989	0
	Kiev			1958–1963	
LNN	Voyeykovo (Leningrad)	59.95	30.70	1947–1988	31
	Slutsk			1877–1946	28
	St. Petersburg			1869–1877	
MGD	Stekolnyy (Magadan)	60.12	151.02	1966–1989	267
	Srednikan			1936–1965	
MLT	Misallat	29.51	30.89	1960–1986	57
	Helwan			1903–1959	
MMK	Loparskoye	68.25	33.08	1961–1985	77
	Murmansk			1958–1960	

Table 4.2: Continued...

NGK	Niemegk	52.07	12.68	1932–1989	43
	Seddin			1908–1931	12
	Potsdam			1890–1907	
SIT	Sitka	57.05	224.66	1940–1989	2
	Sitka			1902–1939	
SJG	San Juan	18.38	293.88	1965–1989	30
	San Juan			1926–1964	75
	Vieques			1903–1925	
SNA	Sanae	-70.30	357.63	1980–1989	1
	Sanae			1971–1979	9
	Sanae			1962–1970	23
	Norway Station			1960–1961	
SOD	Sodankyla	67.47	26.60	1946–1989	0
	Sodankyla			1914–1945	
SPT	San Pablo de Los Montes	39.60	355.65	1981–1988	41
	Toledo			1947–1980	
SSH	Zo–Se (Sheshan)	31.10	121.19	1932–1988	28
	Lukiaping			1908–1932	39
	Zi–Ka–Wei			1875–1908	
TKT	Yangi–Bazar	41.33	69.30	1964–1989	36
	Keles			1937–1963	
WIK	Wien-Kobenzl	48.26	16.32	1955–1989	9
	Wien–Auhof			1929–1954	
WIT	Witteveen	52.81	6.67	1938–1987	128
	De Bilt			1899–1937	5
	Utrecht			1891–1898	

4.4.4 Results

In general, KBM found their PAIC to increase monotonically with increasing ρ usually with some kind of inflection or plateau, as for the synthetic data shown in Figure 4.3. Used in conjunction with the PRA applied to geomagnetic data, I have found the PAIC to behave in a similar manner. For example, in Figure 4.5(e), there is a plateau in the PAIC curve from $\rho = 0.5$ to $\rho = 0.8$ following an initial, rapid increase.

This corresponds to the range in ρ values for which the maximum number of segments are acceptable (prior to partitioning) (Figure 4.4), thus giving the optimisation stage of the algorithm maximum freedom. Such plateaux or inflections centred on some value $\rho = \rho_0$ indicate a model or sub–family of models which is stable with respect to ρ. That is, the *structure* (set of accepted model segments) determined by the PRA does not change significantly for minor deviations of ρ from ρ_0.

Figures 4.5 to 4.7 show the models determined for a selection of components at

various observatories. As with the synthetic data, first time derivatives of the model segments are plotted against first differences of the data for clarity. In some cases, the plateaux in the PAIC are not so well defined as one would hope, as in Figure 4.5(d) for example, but in general a reasonable set of segments could be found near a "notch" or sharp change in gradient. The number of acceptable segments prior to partitioning was also found to be a useful guide in choosing ρ (see Figure 4.4). In Figures 4.5 to 4.7, subplots (d)-(f) show the PAIC plots used as a guide to the selection of the optimal value ρ_0 of the excess standard deviation. Sub-figures (a)-(c) show the first time derivatives of the resulting model segments compared to first differences of the data.

In general the model segments were found to correspond to what one might "pick by eye", and for the optimal value of ρ the set of accepted segments spans the time–series analysed. The model segments highlight some interesting features in the plots 4.5 to 4.7. In particular note the sudden change in SV trend at around 1970 in Figure 4.5(a)–(c), Figure 4.6(a)–(c) and Figure 4.7(a)–(c). Similar changes occur around 1978 in Figure 4.5(a) and (c), Figure 4.6(a)–(c) and Figure 4.7(a) and (b). Two sudden changes around 1978–1980 in Figure 4.7(c) are not properly resolved by the analysis. Changes are also apparent around 1983 in Figure 4.5(c) and Figure 4.7(b). The main characteristic of all these changes is that they appear to be complete within about 1 or 2 years.

Average lengths of segments, over all observatories, were 11.5, 10.3 and 10.3 years for the X, Y, and Z components respectively. In the case of some of the time–series analysed certain periods are not adequately represented by any segment. In such cases there is in
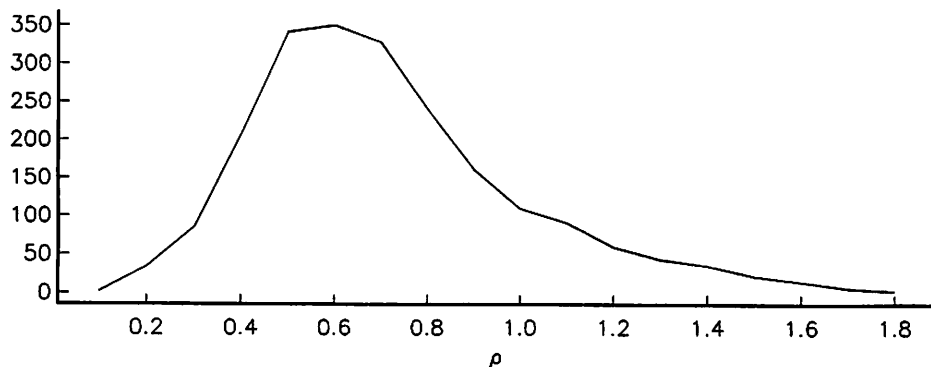
Figure 4.4: Number of acceptable segments generated for each value of ρ prior to partitioning, for the X component at Bangui.
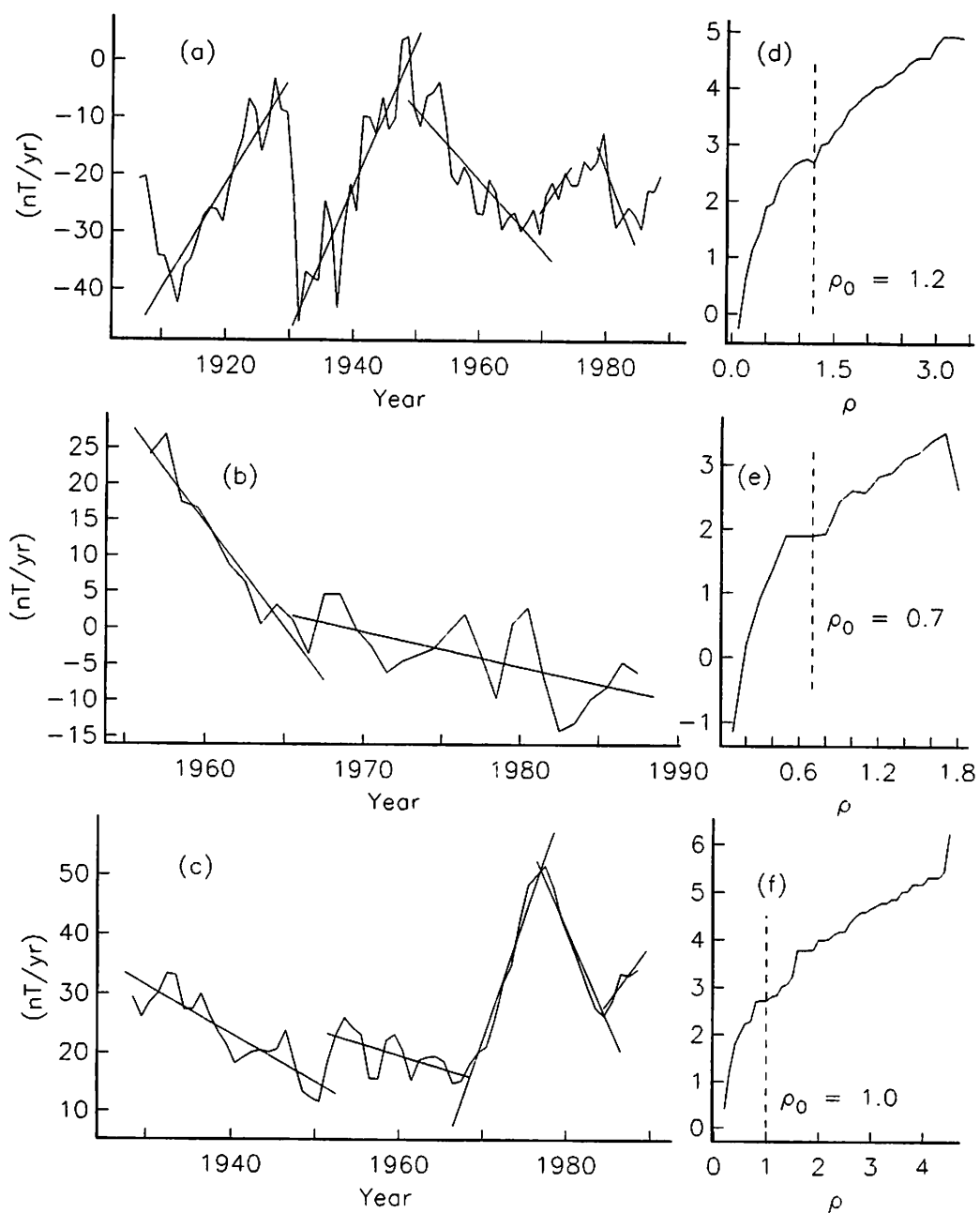
Figure 4.5: Plots (a)-(c) show the first differences of the X component at (a) Apia, south Pacific, (b) Bangui, central Africa and (c) Godhavn, Greenland with first derivative of optimal models. (d)-(f) show the corresponding plots of Partial Akaike Information Criterion (PAIC) against excess standard deviation ρ.
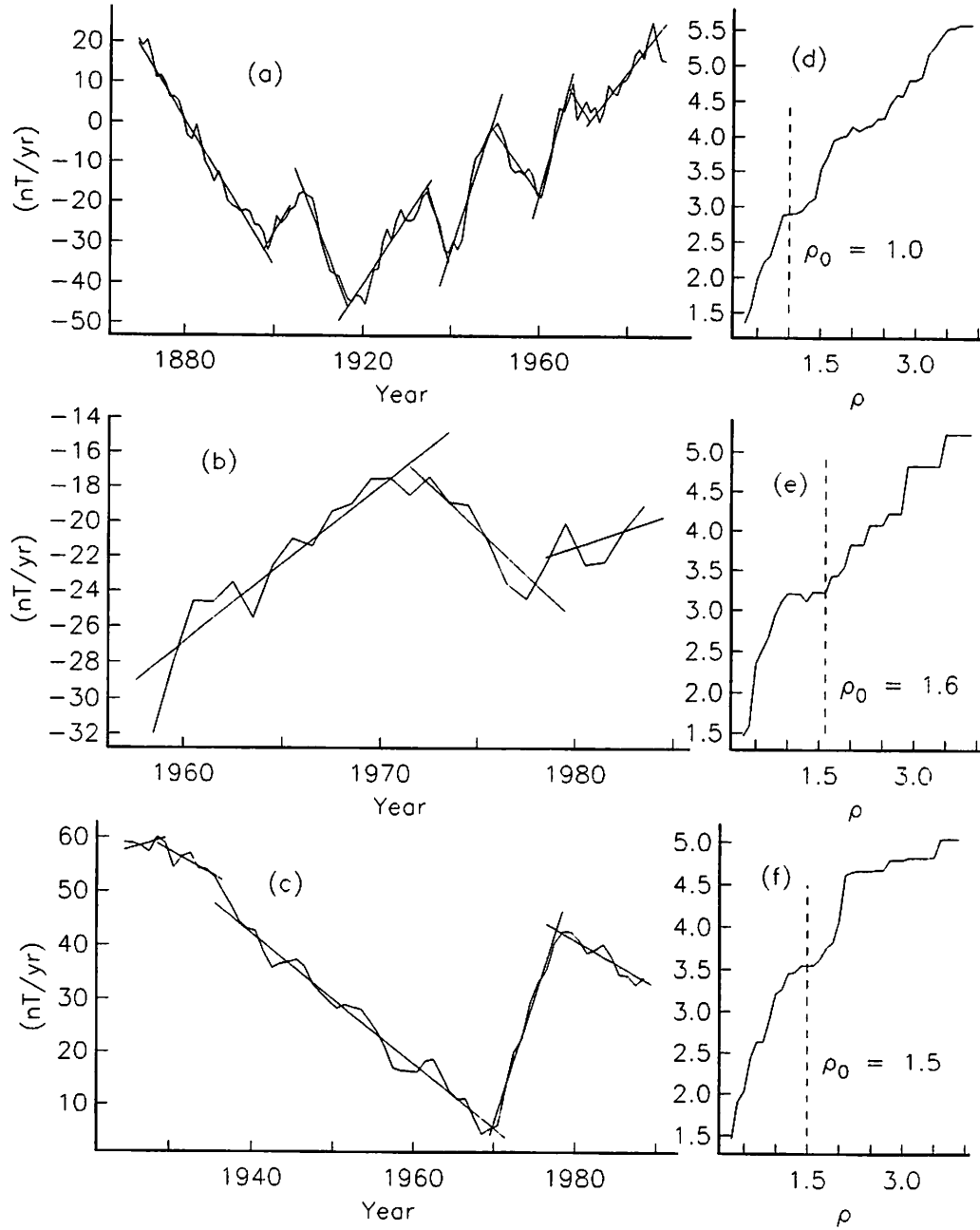
Figure 4.6: Plots are as for Figure 4.5 but this time for the Y component, for observatories (a) Alibag, southern India (b) Argentine Islands, Antarctica and (c) Lerwick, Europe. (d)–(f) as per Figure 4.5.
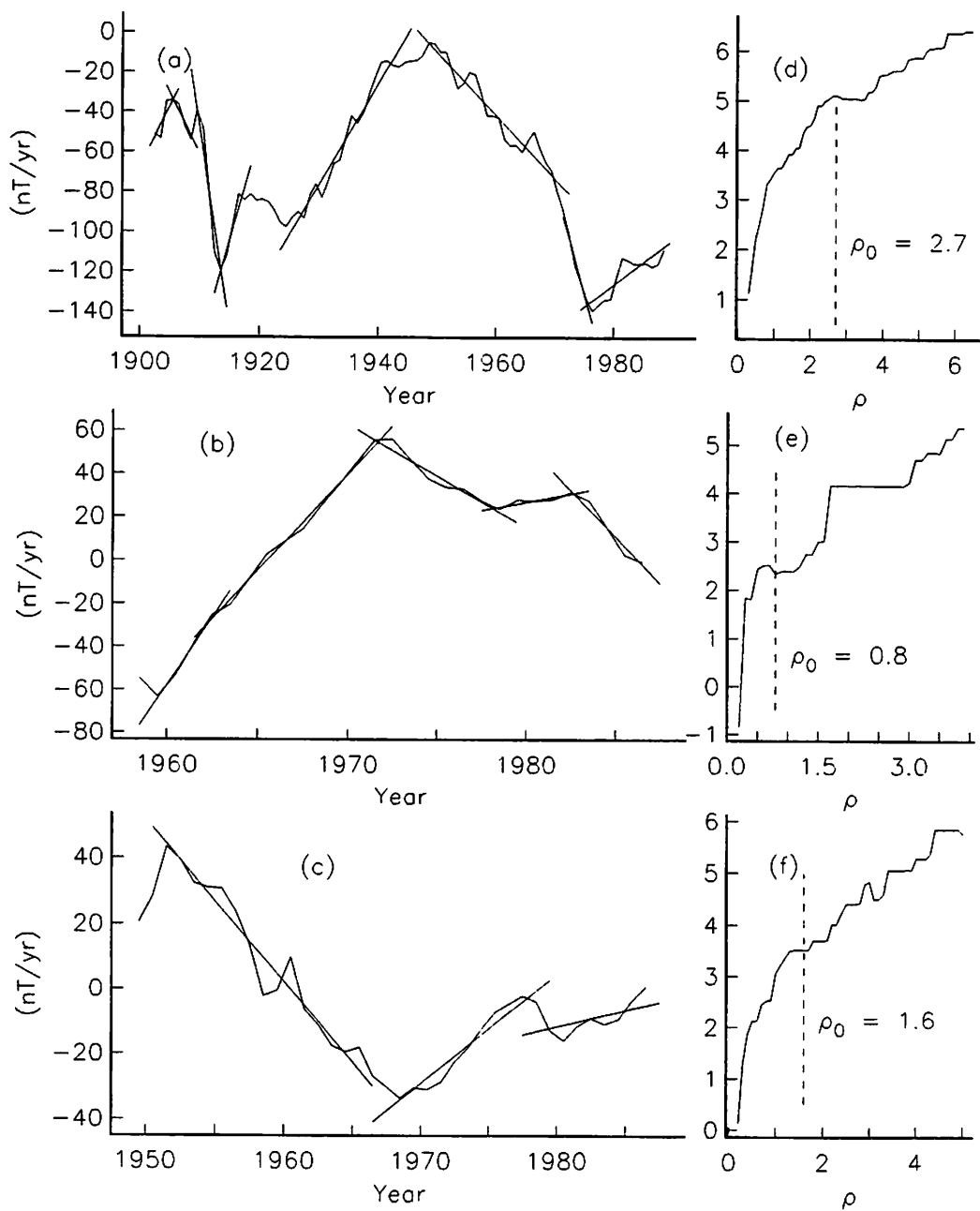
Figure 4.7: Plots are as for Figure 4.5 but this time for the Z component, for observatories (a) Fredericksburg, eastern United States, (b) Kerguelen Island, Indian Ocean and (c) Yakutsk, Siberia. (d)-(f) as per Figure 4.5.

effect a "missing segment" which is too short to be resolved by the PRA, ie. less than six data points long, or a quadratic time–dependence is inadequate for representing this period. Examples of this are in the X component at Apia (Figure 4.5(a)), in which data from 1975–1977 and 1985–1989 are not modelled by any segment, and the Z component at Fredericksburg (from Figure 4.7(a)) from 1919 to 1922. In some instances, although two segments may abut or even overlap, there is still clearly a "missing segment" or else the SV (at the resolution of annual means) is discontinuous. An example of such a situation arises at Apia in the X component from 1929 to 1930 (Figure 4.5(a)). Changing the last criterion in the PRA (the permitted segment overlap) might clarify such transitions but would greatly increase computational expense and lead to permitted models of useless complexity.

The use of composite site observatories could give rise to spurious changes in the character of SV due to regional variations in SV or local induction anomalies. If this were so then a correlation between segment transition dates and dates of site changes would arise. For the 30 composite observatories, there were 135 component-site changes (3 for each of the 45 site changes). These were checked to see whether segment transition dates, or the beginning or end of segments in the cases where there was no overlap, occurred within a fixed period before or after the site change. The number of components for which this occurred were 7, 24, and 32 for periods of 0.5, 1 and 2 years either side of the base change. Adopting the typical time scale of $\sim$ 10 years between SV transitions mentioned above and assuming uniformly distributed and uncorrelated occurrence of site changes and SV changes, the expected occurrence rates are approximately 13, 27 and 54 respectively. This supports the contention that the analysis has not been unduly affected by the site changes used here. Such an investigation was not conducted for baseline changes at single sites catalogued in, and applied from, the BGS annual means data set on the assumption that these would be less prone to error than site change corrections.

Table 4.3: Implied standard deviation of the data, $(\rho_0\sigma_p)$, and r.m.s. residual, $\hat{\sigma}$, for each component at the observatories analysed. (See §4.4.3 and §4.4.5 respectively.) Units are all nT.

IAGA code	$(\rho_0\sigma_p)$ X	Y	Z	$\hat{\sigma}$ X	Y	Z	IAGA code	$(\rho_0\sigma_p)$ X	Y	Z	$\hat{\sigma}$ X	Y	Z
AAA	11.0	5.0	4.0	7.4	3.5	2.6	LQA	13.0	5.5	10.5	11.1	3.0	6.8
AAE	7.8	7.3	6.5	4.3	7.1	4.9	LRV	4.6	3.1	3.6	3.4	1.7	3.2
ABG	12.0	5.0	13.0	10.1	4.1	13.0	LUA	10.0	3.0	20.2	7.4	1.8	18.9
AIA	8.0	3.5	6.2	6.2	1.9	5.4	LVV	2.7	2.7	8.1	2.3	1.6	6.2
ALE	10.0	5.0	22.5	5.9	2.7	12.6	LZH	10.0	3.0	10.0	6.7	1.8	6.6
ALM	3.5	3.9	4.9	2.7	5.1	5.9	MAW	7.0	6.0	18.0	4.9	5.1	15.0
ANN	5.0	11.0	15.0	3.4	7.4	12.8	MBO	11.0	5.0	13.5	6.1	4.9	10.4
API	12.0	4.0	12.0	6.3	2.4	10.2	MCQ	8.5	7.5	5.0	7.0	5.9	4.8
AQU	5.4	1.9	4.6	4.0	1.2	5.1	MEA	13.7	8.2	13.4	12.2	6.6	9.5
ARS	9.0	5.0	6.0	9.0	4.5	5.8	MGD	4.0	3.5	10.0	3.8	2.0	10.2
ASH	9.0	10.0	6.0	9.1	11.5	3.6	MIR	13.0	8.5	22.5	12.7	6.2	18.7
BEL	3.0	2.7	4.9	3.1	2.2	2.4	MLT	12.0	6.5	21.0	10.5	7.3	17.2
BJI	10.0	4.0	6.0	6.5	2.0	4.0	MMB	2.5	1.2	2.0	1.9	0.8	2.3
BJN	9.5	7.5	10.0	9.2	5.3	6.0	MMK	3.0	5.0	8.0	3.0	3.6	4.8
BLC	13.5	9.4	13.5	8.4	6.0	7.6	MNK	2.5	3.9	3.5	2.1	3.0	3.6
BNG	7.0	7.0	10.5	5.3	5.1	7.9	MOS	6.0	4.5	3.5	6.3	3.8	3.3
BRW	3.7	5.9	8.8	2.4	4.9	3.5	MUT	10.0	11.0	15.0	8.1	7.7	13.2
CAN	5.0	4.0	4.0	4.0	3.1	3.3	NGK	4.2	3.6	6.0	3.1	2.6	5.1
CCS	4.0	10.0	11.5	3.3	8.6	11.6	NSM	6.5	4.5	3.5	6.2	4.3	2.3
CLF	7.5	4.5	6.0	8.0	3.5	3.2	NUR	5.3	2.1	3.0	4.3	1.7	2.5
CMO	4.7	3.2	3.8	4.3	2.9	2.6	NVL	11.5	7.0	21.8	5.5	6.9	23.5
CNH	7.0	5.0	5.5	4.5	4.3	5.8	ODE	4.0	1.8	2.8	4.1	1.7	3.0
COI	7.0	3.0	5.6	6.9	2.7	5.2	PAG	4.0	2.2	6.3	2.0	1.7	6.1
CPA	15.0	7.5	19.0	15.9	5.0	21.9	PET	5.0	5.5	3.5	3.6	2.2	2.1
CWE	5.0	7.5	6.5	4.7	6.6	5.6	PIL	8.0	4.5	12.0	7.6	3.4	8.6
DIK	6.5	7.0	6.0	5.3	5.5	4.4	PMG	4.0	2.5	10.0	3.0	1.6	7.9
DOB	4.0	3.0	7.0	3.2	3.0	4.8	PPT	4.0	2.5	4.5	2.3	1.8	2.4
DOU	4.0	2.4	3.5	2.6	1.6	2.6	QUE	15.0	5.0	14.0	16.4	3.2	11.5
EBR	7.0	4.5	8.4	6.0	4.5	6.0	RES	3.5	5.0	7.0	3.0	3.5	7.4
ESK	4.1	2.1	4.2	4.1	1.9	3.5	RSV	4.0	2.8	3.3	3.0	2.3	3.2
EYR	5.0	2.5	6.0	4.7	1.9	6.1	SBA	11.0	6.0	15.0	9.9	5.1	14.9
FRD	6.0	3.8	9.5	5.1	2.8	8.2	SIT	3.1	2.2	5.2	2.2	1.8	4.5
FUQ	4.5	7.5	7.5	5.3	7.3	6.8	SJG	8.1	2.8	8.8	6.4	1.8	8.7
FUR	6.5	2.4	3.5	6.4	2.2	2.9	SNA	20.0	19.5	15.0	16.5	19.6	12.4
GCK	4.0	1.5	7.7	2.6	1.0	6.2	SOD	7.1	4.2	6.6	5.7	3.9	4.7
GDH	5.0	4.5	14.5	3.8	3.4	13.1	SPT	2.5	2.1	6.3	2.3	2.1	5.4
GNA	5.0	5.0	5.0	3.9	3.1	5.1	SSH	10.0	5.5	9.0	7.7	4.9	8.5
GUA	5.3	2.2	2.8	2.9	1.4	2.0	SUA	5.0	3.3	7.0	4.7	3.3	7.2
GZH	7.0	7.5	25.0	6.9	5.8	14.3	TAM	12.0	6.0	18.0	7.6	3.9	6.7
HAD	3.9	2.8	3.4	3.8	2.4	2.4	TEN	12.0	6.5	21.0	13.3	5.8	22.5
HER	6.3	4.9	3.8	4.4	4.5	2.5	TFS	4.2	2.0	7.0	2.3	1.8	7.1
HIS	7.5	12.5	15.0	7.0	9.1	10.9	THL	2.5	3.0	5.5	1.6	1.9	4.4
HLP	5.5	3.9	3.5	4.1	2.2	3.7	THY	4.5	4.5	7.0	4.6	4.1	5.8
HON	3.9	1.9	5.4	2.6	1.4	3.4	TIK	4.0	3.5	15.0	3.4	3.2	12.1
HRB	10.0	2.5	8.0	5.5	2.3	15.6	TKT	4.0	2.0	10.0	2.3	1.9	6.2
HTY	8.0	7.5	7.5	6.4	7.1	5.1	TRD	8.0	6.0	10.0	4.5	5.4	7.0
HUA	5.0	4.5	6.0	4.5	2.4	5.2	TRO	5.0	3.5	15.0	3.8	1.8	14.0
IRT	8.0	3.5	12.0	7.5	3.2	11.4	TUC	7.2	2.4	6.1	4.4	1.4	4.1
ISK	7.0	5.5	10.0	6.2	5.9	8.8	VAL	3.5	3.6	9.8	3.0	2.9	8.8
KAK	6.5	1.8	5.9	4.1	1.0	4.3	VIC	4.2	4.5	4.9	2.6	2.3	4.9
KGL	6.0	4.0	4.0	5.4	3.3	7.6	VLA	12.0	3.5	10.0	13.6	2.0	6.8
KIV	5.0	2.1	4.9	3.6	2.0	2.8	VOS	19.0	7.5	27.0	14.9	5.7	23.0
KNY	6.8	1.1	2.7	3.5	0.8	1.2	VSS	7.0	3.5	7.5	6.2	3.3	3.6
KNZ	6.0	2.0	5.0	4.0	0.9	3.8	WHN	13.0	3.5	8.0	7.3	2.5	7.8
KOD	5.0	3.5	5.0	4.2	3.6	4.4	WIK	3.5	2.1	5.6	3.1	2.1	4.8
LER	4.8	3.3	5.8	3.7	2.6	3.5	WIT	4.3	1.8	2.0	3.3	1.5	2.1
LGR	5.0	3.0	3.5	2.5	2.4	1.8	WNG	4.5	1.5	3.5	3.4	1.1	2.7
LMM	10.0	3.5	3.0	3.9	2.6	2.2	YAK	6.5	4.5	8.0	2.7	4.5	5.8
LNN	8.1	3.3	7.2	6.9	2.5	5.4	YSS	8.0	6.0	6.0	5.3	5.4	4.4
LOV	3.5	3.3	5.6	3.1	3.2	3.6							

4.4.5 Analysis of residuals

The models did not always span each time–series: certain epochs were not modelled by any segment. Hence not all data points were parameterised. Those points jointly parameterised by two segments were assigned to one segment as described in §4.2.4. Therefore, after the elimination of a handful of outliers from a few poor quality observatories, there were 5467, 5442 and 5195 residuals for the X, Y and Z components, respectively. R.m.s residuals for each component at each observatory are given in Table 4.3 for comparison with the implied prior value ($\rho_0 \sigma_p$) for the standard deviation of the data given to the PRA to yield the optimal model. It appears that in most cases the differences are marginal. Figures 4.8(a)–(c) show the normalised residuals to the segments determined by the OPRA analysis of the geomagnetic data. Normalisation was achieved by dividing residuals by the r.m.s. residual for each component at each observatory. It appears at first from these plots that there is little doubt as to their Gaussian distribution, thus confirming that the piecewise quadratic model is an adequate representation of the time–varying core field. Figures 4.8(d)–(f) show the normalised residuals of the same models to the annual means prior to correction for disturbance fields. Again the residuals appear to be normally distributed. Figures 4.9(a)–(c) show the unnormalised residuals to the corrected annual means while Figures 4.9(d)–(f) show the unnormalised residuals but for the uncorrected annual means. The r.m.s. residuals to the corrected X, Y and Z components were $6.1nT$, $3.6nT$ and $7.6nT$ respectively, while those for the uncorrected annual means were $10.7nT$, $6.7nT$ and $10.5nT$. Thus removal of disturbance fields has achieved a 50 to 70 percent reduction in the variance of residuals. The residuals to the uncorrected X, Y and Z components were found to have mean offsets of $-21.0nT$, $2.0nT$ and $4.8nT$.

Figures 4.9(a)–(c) show that the distribution of the unnormalised residuals of the corrected annual means are consistently more peaked than a normal distribution. This may well be due to the large number of European observatories in the dataset (37 out of 119) which tend to be of higher quality. The residuals for non-European observatories were found to have a r.m.s. typically 50–80% larger than European ones which would tend to centralise the distributions of unnormalised residuals. It is interesting to note
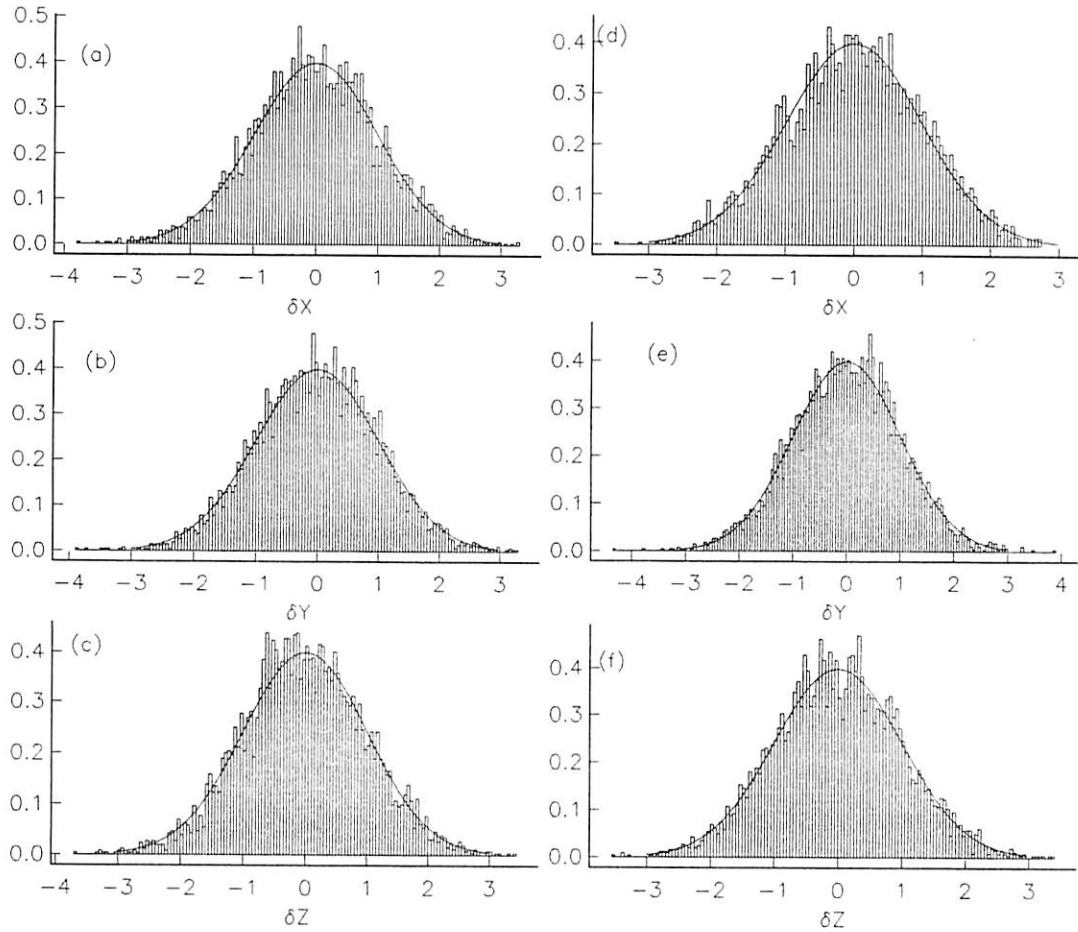
Figure 4.8: Plot of distribution of normalised residuals to piecewise quadratic models. (a)–(c) are residuals to annual means corrected for disturbance fields for the X, Y and Z components respectively. (d)–(f) are residuals to uncorrected annual means. Residuals from each observatory were normalised by the r.m.s residual at that observatory for the relevent component. A standard normal distribution is overplotted for comparison.

from these figures, however, that the Cauchy distribution appears to offer a far better fit to the sample distributions than the Gaussian distribution which is normally assumed in geomagnetism. A possible cause of this could be that errors in cartesian components derived from angular (polar) coordinates with uniform errors have a Cauchy distribution (Hald, 1952). Bearing in mind that most geomagnetic data are not measured in X, Y and Z cartesian components but as some combination of angular and intensity data, this could explain the apparent Cauchy distribution of the residuals. A uniform distribution of angular errors seems rather implausible however; what is more likely (J. T. Kent,
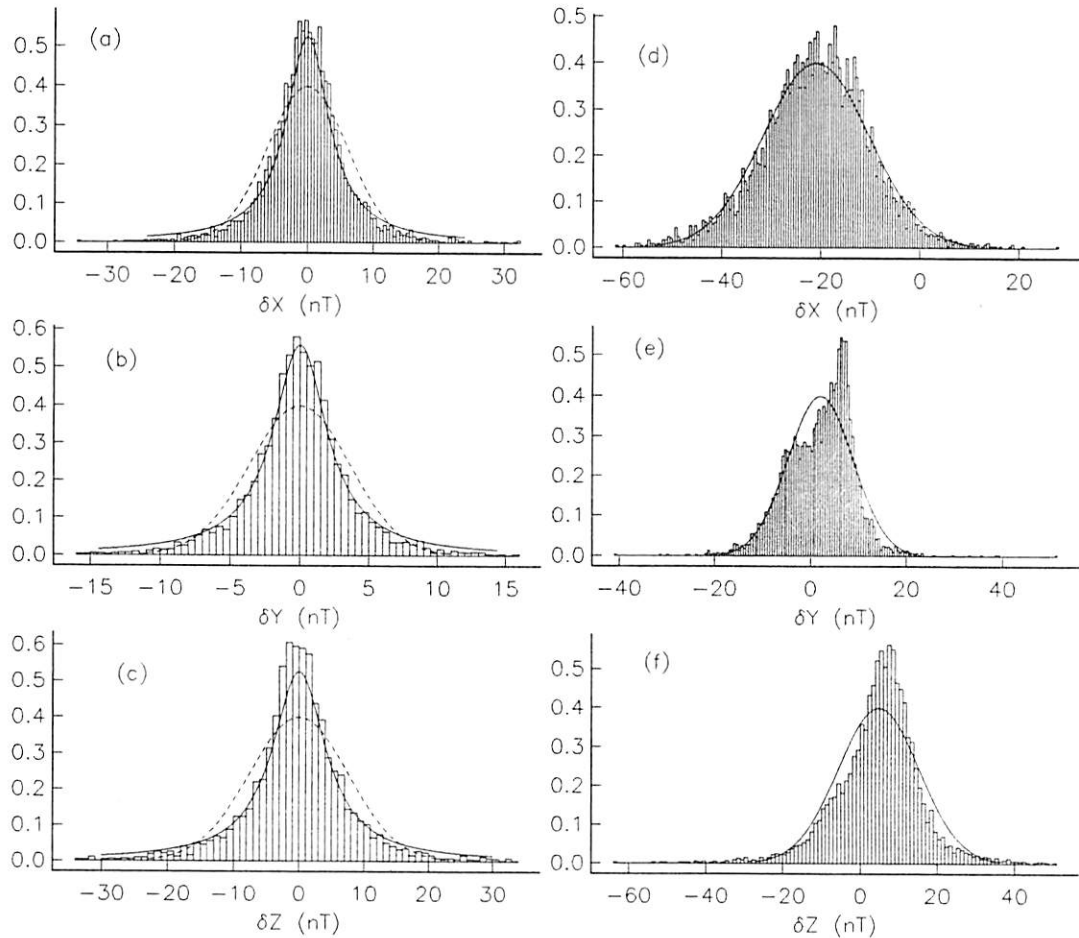
Figure 4.9: Plot of distribution of unnormalised residuals to piecewise quadratic models. (a)–(c) are residuals to annual means corrected for disturbance fields for the X, Y and Z components respectively. (d)–(f) are residuals to uncorrected annual means. In (a)–(c) dashed curves show the best fitting Gaussian distributions and solid curves show the best fitting (by eye) Cauchy distributions (see text). In (d)–(f) solid curve is best fitting Gaussian distribution.

personal communication, 1991) is that the distribution is a combination of Gaussian and Cauchy distributions. If this is the case, then it may be advisable to use the components of the data that were originally measured, rather than transforming to cartesian components as is often done when deriving geomagnetic field models (eg Benton *et al*, 1987). In the determination of geomagnetic main field models, the use of D, H, I and F leads to a non–linear inverse problem (eg. Bloxham *et al*, 1989) which requires an iterative solution. The alternative — a maximum liklihood (ML) solution based on the

Cauchy distribution — would also require an iterative solution, as the ML estimator of the median (which must be used because the sample mean is an inconsistent estimator of the population mean) cannot be obtained explicitly (Kendall & Stuart, 1961). This point warrants further investigation in its own right. This would require a separate analysis of data measured in X, Y and Z from that measured in D, H and Z though it is not always clear from published catalogues which are which.

The distributions of the unnormalised residuals for the uncorrected annual means show distinct abnormality, are offset from zero and have larger variance due to the effects of the external fields. In particular those for the Y and Z components show strong positive skewing. The fact that abnormality is apparent in the unnormalised residuals but not in the normalised is significant — the r.m.s. residuals computed from annual means uncorrected for external fields over-estimate the true standard deviations. When such biased estimates are used to achieve the normalisation of the residuals from the different observatories, the true asymmetric nature of the residuals (as in Figure 4.9(e) for example) is disguised (as in Figure 4.8(e)). Further, if such biased error estimates are used for data weighting, for example in main field modelling (Langel et al, 1982; Backus et al, 1987), then observatories most affected by disturbance fields will be underweighted, introducing a bias into the field model.

4.5   Summary and Conclusions

In this chapter a new method has been developed specifically for the analysis of the time–dependence of the geomagnetic field at individual locations. It is specific in that it evaluates the validity of a particular, though widely assumed, hypothesis — that of linear SV. The algorithm considers all possible partitions of a give time–series and determines the statistically strongest piecewise quadratic model which gives an adequate fit to the data, while being optimal in the sense of a trade off between fit to the data and number of parameters required. Transition dates from one quadratic segment to the next are self selecting. The method was tested on synthetic data. The algorithm was then applied to a large geomagnetic annual means data set, corrected for the cumulative effects of time–dependent external magnetic fields.

The first conclusion from the analysis is that the time–series of geomagnetic annual means considered can be well represented by piecewise quadratic models. Although this has not been compared against other methods such as stochastic time–series models (see eg. Chatfield, 1984) the time–scales over which the quadratic parameterisation is valid have been assessed semi–objectively and the fit to the data shown to be adequate. In total approximately 93% of the annual means were parameterised by a quadratic segment. The typical length of a segment, or period of linear SV, was found to be about 10 years. This may not be typical of SV in general since of the 119 observatories analysed only about 40% were operating before 1950 and of these only 11 operated before 1900. Consideration of the results from these observatories alone, however, indicates that even for time–series of 80+ years the typical segment length is only marginally greater. The weighted residuals are very well fitted by a standard normal distribution while the unweighted residuals are more Cauchy, though it has been shown that this may be due to European bias. Residuals to data not corrected for external field effects have significantly higher variance and show distinct abnormality and could lead to bias for weighting procedures in deriving field models.

Having shown that for the majority of geomagnetic time–series the dominant characteristic is a piecewise quadratic time-dependence, the interesting hypothesis can be made that such segments be interpreted as the asymptotic output of the electromagnetic mantle filter, with an input which is a third order impulse in the geomagnetic field at the core–mantle boundary. If this is the case then one would expect to be able to detect some global synchronicity in the transition dates from one segment to the next. This hypothesis will now be investigated.

Chapter 5

Geomagnetic jerks of 1970, 1978 and 1983

5.1 Introduction

The primary aim of this Chapter is to assess whether the jerk of 1970 and supposed jerks of 1978 and 1983 discussed in Chapter 1 are worldwide and whether each event occurs at the same time in different locations. As the data analysed in Chapter 4 were adjusted to remove the effects of external fields and as the results of that chapter are to be used here such changes in field behaviour will (by default) be considered to be of internal origin. Having argued that they are simultaneous and global in extent, their spatial distribution will be mapped using a technique which has already been developed and used successfully by others for mapping the field and its changes.

5.2 Global, simultaneous geomagnetic jerks

In Chapter 4 time–series of annual means corrected for the effects of external fields for field components X, Y and Z for 119 observatories were analysed. It was shown that the majority of these series can be adequately represented by a succession of quadratic functions of time. The typical duration of such quadratics (segments) was found to be of the order of 10 years, and they represent periods in which the secular acceleration (SA) can be considered constant. If one such period follows closely after another or

they overlap then the field component being represented could be considered to have experienced an impulse (within the resolution of the analysis (approximately 3 years)) in its third time derivative. Such an event will be termed a *virtual impulse* or VI. An intersection or overlap of the two quadratics shows that data in, or close to, this transition period can be equally well parameterised by either quadratic (within the limits of the data noise). The date at which the first derivatives of the quadratics are equal is the date at which the VI occurred and will be termed the *virtual impulse epoch* or VIE. Such VIs in the observed field may be the surface expression of an impulse in the third time–derivative of the field at the CMB as seen through a partially conducting mantle. Alternatively the VI may occur at a particular date, not as the result of some single global "event" at the CMB, but merely by chance as a consequence of the piecewise quadratic representation of the idiosyncratic behaviour of the field at a particular location. If one accepts the latter hypothesis then an even distribution of VIs in time would be expected. However in the case of a large scale CMB impulse one would expect VIs at different observatories to occur at about the same time.

To investigate this point, plots showing the number of VIs occurring in each year are presented in Figures 5.1 to 5.4. The plots show relative VI frequency (RVIF) — the number of VIs which occur in a given year normalised by the number of observatories operating (times 3 if all components are considered together) for at least 5 years before and after that year. Figure 5.1(a) shows that considering all components from all observatories together, the distribution of VIs in time is uneven. It would appear that for the post 1950 period the dates 1969, 1978 and 1983 are the most prominent for the occurence of VIs. The peak at 1969 is interpreted as being associated with the widely investigated jerk at that time and those at 1978 and 1983 to be associated with similar events (see Chapter 1). These RVIF peaks will therefore be referred to as jerks for the sake of lucidity. In the interpretation of these plots the width of a peak (ie. the number of successive years with a high RVIF) is important, as well as its height. For example, Figure 5.1(a) shows that between 1968 and 1971 47% of all field components experienced a VI, whereas 19% have a VI during the years 1963 to 1966. However the primary purpose of these plots is qualitative rather than statistical. It is also important to note that prior to 1957/58 (the International Geophysical Year when a lot of obser-

vatories were established) the number of observatories contributing to each histogram drops very sharply (Figure 5.5) and so the RVIF is much less reliable.

In this earlier part of the century there is a slight concentration of VIs in the late 1940s, a date conjectured by Golovkov *et al* (1989) as a jerk epoch; however, only 40 of the observatories analysed were operating at that time. There are also some large RVIF peaks prior to 1920 but fewer than 20 observatories contribute in this period making an interpretation of these peaks as being globally significant less reliable. Figures 5.1(b)-(d) shows the RVIF for all observatories separated by field component. In the X component the 1969 jerk appears to reach a maximum at 1971/1972 and in general is spread over a longer period than in the Y component, for which the maximum RVIF is reached in 1969 as it is for Z. The 1978 jerk is almost absent from X but in Y is as clear as the 1969 event. For Z, 1965 and 1978 seem to be as significant as 1969 with an apparent jerk in 1983 which is also present in X but not in Y.

Several studies have highlighted the prominence of the 1969 jerk in the Y component in Europe (eg. Courtillot *et al*, 1978; Backus & Hough, 1985; Gavoret *et al*, 1986), which might suggest this jerk is a regional feature of the secular variation (SV) rather than being worldwide in extent. Figure 5.2 compares RVIF for the (37) European and (82) non–European observatories in the study. "Europe" here means the 37 observatories represented in Figure 5.7(b). Comparison of Figures 5.2(a.i) and 5.2(a.ii) shows that the jerks are not confined to Europe. The apparently smaller proportion of field components affected in Figure 5.2(a.ii) may simply result from some regions being unaffected by the jerk whereas in others it may be as strong as in Europe. The 1969 event is represented in the Y component at the majority of European observatories in either 1969 or 1970 while in the X component it clearly occurs later and over a longer period. The 1983 event is very pronounced in the Z component in Europe, with Z at half the observatories being affected in 1983 alone. Four other geographic sub–regions are considered in Figures 5.3 and 5.4. The smaller number of observatories in the sub–regions "the Americas" (18), "East Asia" (20) and the southern hemisphere (22) makes the histograms less reliable and jerks harder to define, and jerks would probably not have been identified from these sub–plots alone. However the 1970, 1978 and 1983 jerks are all apparent in both the Americas and East Asia although each jerk appears strongest in different components
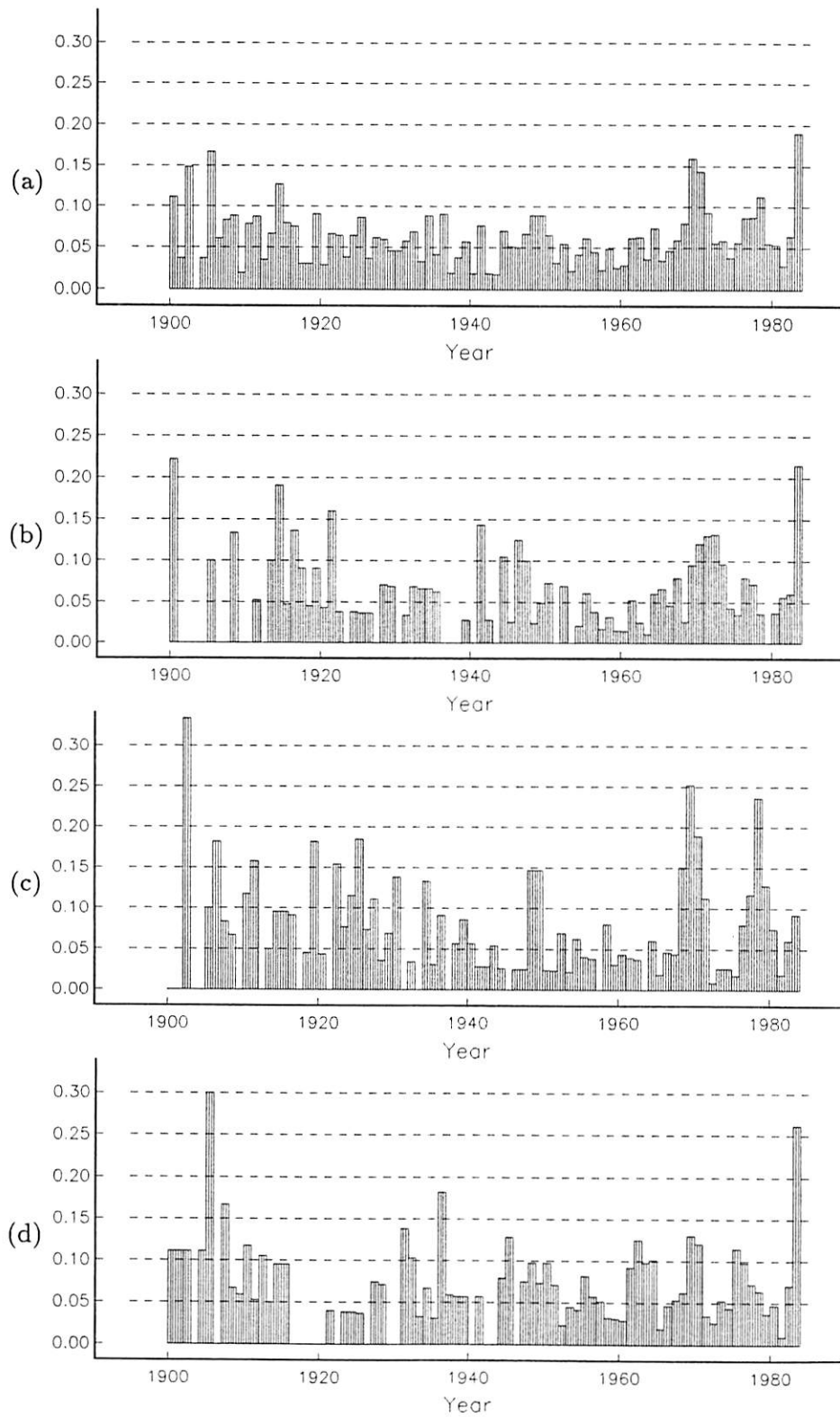
Figure 5.1: RVIF for all 119 observatories analysed. Plots are (a) for all components, (b), (c), (d), for X, Y and Z components respectively.
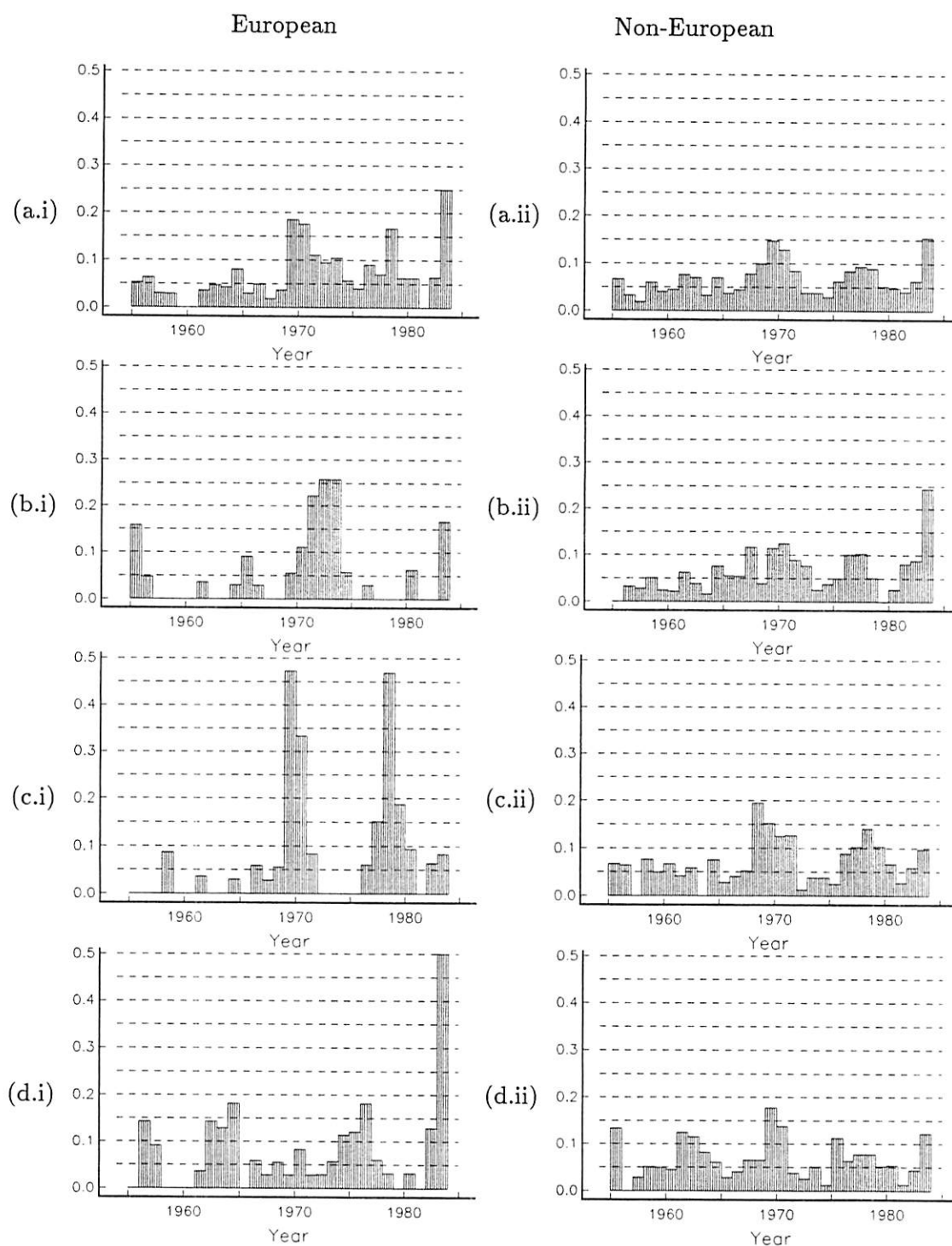
Figure 5.2: RVIF for European (i) and non–European (ii) observatories. Plots are (a) for all components, (b), (c), (d), for X, Y and Z components respectively.

96
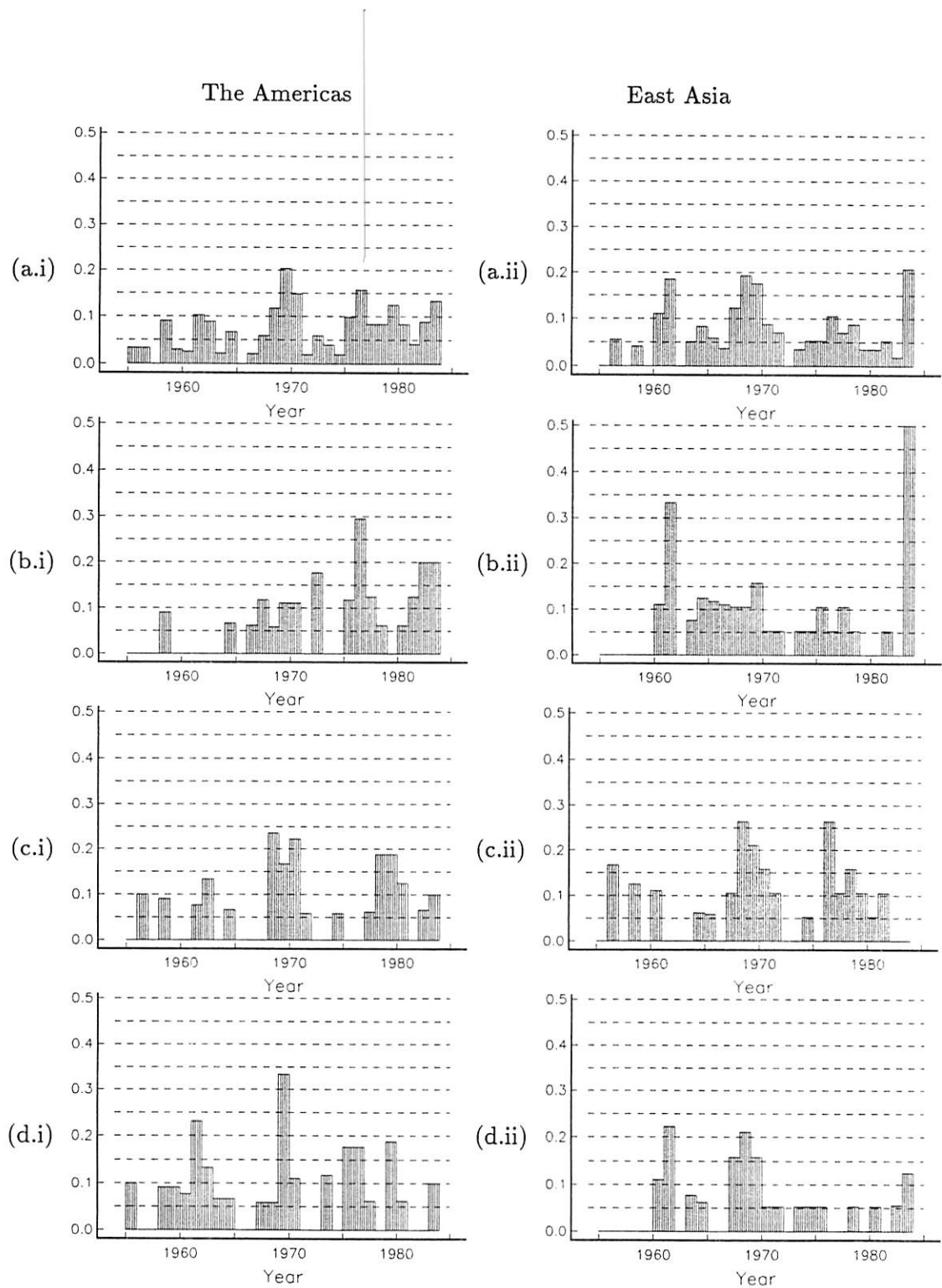
Figure 5.3: RVIF for (i) observatories in north and south America (total 18) and (ii) East Asian observatories (total 20). Plots are (a) for all components, (b), (c), (d), for X, Y and Z components respectively.
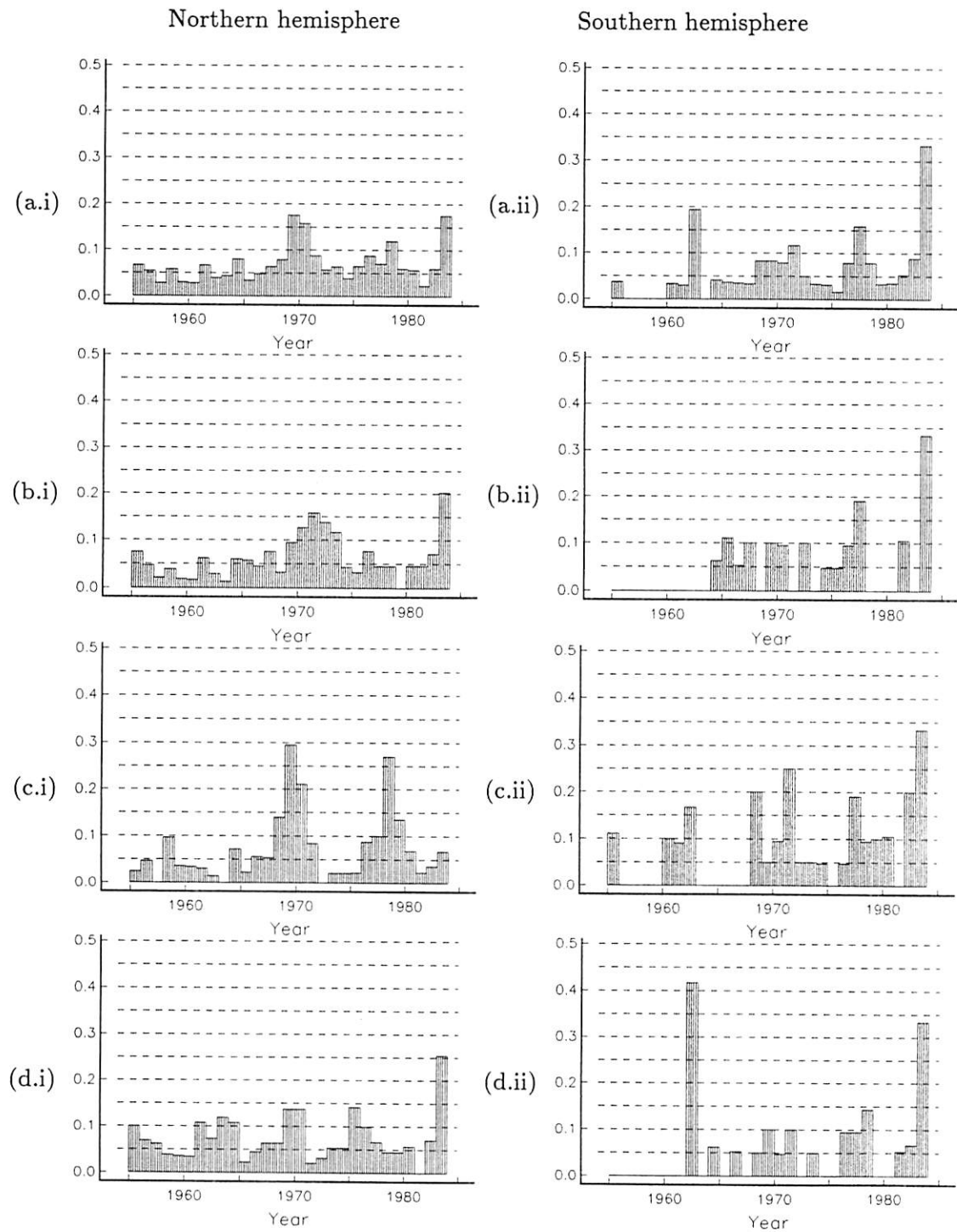
Figure 5.4: RVIF for (i) northern hemisphere observatories (total 97) and (ii) southern hemisphere observatories. Plots are (a) for all components, (b), (c), (d), for X, Y and Z components respectively.
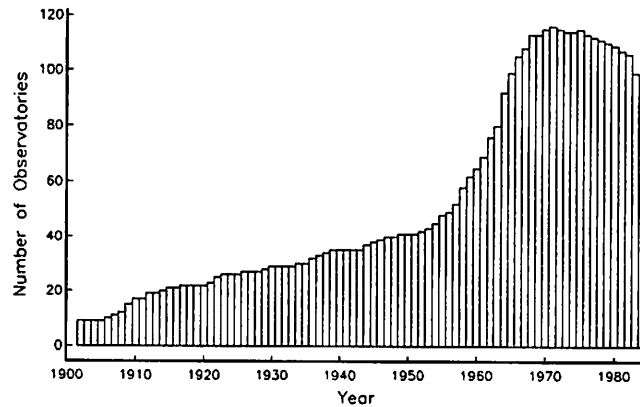
Figure 5.5: Number of observatories with time–series extending at least five years before and after the given date.

in each region. Ducruix *et al* (1980) claimed the 1970 event was absent in observatory records from southern hemisphere observatories but Figure 5.4 indicates that this is not entirely true. There is also an apparent change in the Z component in 1962 which appears to be confined to the southern hemisphere. It is interesting to note that rapid changes in the SV in 1983/84 in Southern Africa have been noticed recently (Kotzé *et al*, 1991) and South Georgia (Dowson *et al*, 1988).

5.3 Models of the main field, secular variation and secular acceleration

In the last section it was argued that changes in the time–dependence of the field of global significance have occurred around 1970 and 1978, and possibly 1983. In this section, reliable spherical harmonic (SH) models of these phenomena are derived under the assumption that they arise from an impulse of finite power in the third time derivative of the field (third order impulse) at the core–mantle boundary (CMB). Under this hypothesis, the resulting change in the field at the Earth's surface has a quadratic time–dependence which is only approached asymptotically as a result of the smoothing effects of the electromagnetic mantle filter (Backus, 1983).

It was shown in Chapter 4 that at most observatories the time–dependence of the field can be reasonably approximated by quadratics between such jerk events and so a

quadratic time–dependence will be adopted for the main field (MF) as a whole. The epochs 1965.5, 1974.5, 1981.5 and 1986.5 (corresponding to minima in the RVIF histogram of Figure 5.1(a)) will be assumed to be dates at which the global SA is at its most stable either following or prior to a jerk and at which, therefore, a quadratic time–dependence is most valid for the main field. For brevity such a date will be referred to as *stable secular acceleration date*, or SSAD. Time–dependent SH models for the MF will be derived for these epochs (SSAD models) and will be used to derive spatial models of the jerks of 1970, 1978 and 1983 (jerk models).

5.3.1 Stochastic inversion

In the following it will be assumed that the field variations being represented are of purely internal origin, external fields having been largely removed as described earlier. It will also be assumed that all observatories involved are at sea-level and that the Earth is spherical of radius $r_S = 6371.2km$ and that the core is also spherical with radius $r_C = 3485km$. The time–dependent magnetic field $\mathbf{B}$ can be represented by the gradient of a scalar potential V using

$$\mathbf{B} = \begin{pmatrix} -X \\ +Y \\ -Z \end{pmatrix} = -\nabla V \tag{5.1}$$

which in turn can be expanded as a spherical harmonic series

$$V(r, \theta, \phi; t) = r_s \sum_{n=1}^{N} \sum_{m=0}^{n} \left\{ [g_n^m(t) \cos(m\phi) + h_n^m(t) \sin(m\phi)] \left(\frac{r_s}{r}\right)^{n+1} \right\} P_n^m(\theta) \tag{5.2}$$

where P_n^m are Schmidt quasi–normalised associated Legendre functions. N must be infinite to fully represent an arbitrary potential however only a finite number of coefficients can be estimated from a finite data set. Let each SH coefficient g_n^m of a SSAD model have quadratic time–dependence given by

$$g_n^m(t) = a_{ng}^m[t - t_1]^2 + b_{ng}^m[t - t_1] + c_{ng}^m \tag{5.3}$$

and similarily for $h_n^m(t)$, where t_1 is an arbitrary reference epoch. The data, X, Y, Z and their time–dependence can be related to the model parameters via (5.1), (5.3) and the derivatives of (5.2) with respect to r, θ and ϕ. For finite vectors $\mathbf{d}$ and $\mathbf{m}$ of n_d data and p model parameters respectively this relationship can be succinctly expressed as

$$d = Gm + e, \tag{5.4}$$

where G is known as the *equations of condition matrix* and e is the vector of errors or more exactly the discrepancy between the data and the model estimate of the data. The method of *least squares* has traditionally been used to find the "best–fitting" model estimate by minimising the sum of squares of the residuals. The least squares solution is given by

$$\hat{m} = (G^T G)^{-1} G^T d. \tag{5.5}$$

Finding a solution involves an arbitrary truncation of the field at some fixed and finite value of N, which is equivalent to requiring that all harmonics of degree $n > N$ are identically zero.

An alternative method known as *stochastic inversion* (SI) (introduced to geomagnetic field modelling in a series of papers by D. Gubbins and J. Bloxham during the mid 1980s (Gubbins, 1983; Gubbins, 1984; Gubbins and Bloxham, 1985) hereafter referred to as GFA1, GFA2 and GFA3 respectively) allows more general prior information to be introduced. This is achieved by the specification of a covariance matrix C_m for the model parameters and the solution is then

$$\hat{m} = (G^T C_e^{-1} G + C_m^{-1})^{-1} G^T C_e^{-1} d \tag{5.6}$$

where C_e is the covariance matrix for the data. This solution minimises the quantity $e^T C_e^{-1} e + \hat{m}^T C_m^{-1} \hat{m}$, where e is the vector of residuals. The solution is equivalent to that of simple least squares if $C_m^{-1} = 0$, the zero matrix and $C_e^{-1} = I$, the identity matrix. It is equivalent to a *damped least squares* solution if C_m is a scalar multiple of the identity matrix.

5.3.2 Data

Consider a SSAD t_2 for which a quadratic time–dependent model of the field is required. The model must be valid for epoch t_2 and therefore any observatory field components with an acceptable quadratic model segment (see Chapter 4) in which t_2 falls will provide an estimate of the time–dependence of that component to be used as data for the model. Let the coefficients of the relevant segment for the ith observatory field component be

c, b and a with errors, of estimated variance δc^2, δb^2 and δa^2, which are independent by the forced orthogonality of the quadratics in Chapter 4. Recall from equation (4.2) that the estimate of the field component from this segment is given by

$$\hat{u}(t) = a((t - \bar{t})^2 - \bar{t^2}) + b(t - \bar{t}) + c \tag{5.7}$$

where $\bar{t}$ is the mean epoch for the segment and $\bar{t^2}$ is the mean square epoch for the segment. Although valid for epoch t_2, the segment must be defined with respect to some common reference epoch t_1. To do this express $\hat{u}$ as

$$\hat{u}(t) = a'(t - t_1)^2 + b'(t - t_1) + c' \tag{5.8}$$

and hence

$$\left. \begin{array}{l} a' = a \\ b' = 2at_{\mathrm{d}} + b \\ c' = a(t_{\mathrm{d}}^2 - \bar{t^2}) + bt_{\mathrm{d}} + c \end{array} \right\} \tag{5.9}$$

where $t_{\mathrm{d}} = t_1 - \bar{t}$.

Rather than using the diagonal elements of the segment parameter covariance matrix $\hat{\sigma}_{\mathrm{s}}^2 \mathbf{G}_{\mathrm{s}}^T \mathbf{G}_{\mathrm{s}}$ as δc^2, δb^2 and δa^2 (where the subscript s indicates that the $\hat{\sigma}$ and $\mathbf{G}$ are from estimating the segment coefficients in the OPRA analysis) a slight modification is introduced and $(\rho_0 \sigma_{\mathrm{p}})^2 \mathbf{G}_{\mathrm{s}}^T \mathbf{G}_{\mathrm{s}}$ is used instead, where ρ_0 is the value of the excess standard deviation which gave an optimal segment model for this component and σ_{p} is the prior value for the component's standard deviation used in the OPRA analysis. The value $(\rho_0 \sigma_{\mathrm{p}})$ probably gives a less biased estimate of the standard deviation of the data than $\hat{\sigma}$ as it is derived from all the segments for a component rather than a single segment. In practice this correction was found to have a very minor effect on the results of the inversions.

The short spatial wavelength field associated with crustal magnetisation will contribute to c and hence c'. This is corrected for here by subtracting crustal anomaly values. The primary source of these corrections is Bloxham *et al* (1989) who computed the anomaly values by comparison of observatory annual means with a model derived from data from the satellite Magsat at epoch 1980. For observatories for which no such anomaly value was available, values from GFA3 were used and, failing that, values from

Langel *et al* (1982) were used. For observatories at Changchun, Wuhan, Guangzhou and Lanzhou, for which no correction was available, the variance of c was increased by $(300nT)^2$, $(350nT)^2$, $(500nT)^2$ for the X, Y and Z components respectively, these values being representative of the mean squared crustal anomaly (Benton *et al*, 1987). At all other observatories, δc^2 was increased by $(50nT)^2$ to allow for error in the crustal anomaly value.

The error estimates for the a and b coefficients from Chapter 4 were found to be consistently very optimistic. Figures 5.6(a)-(d) show examples of first differences of the data plotted with one of the fitted model segments, together with the same segment with its a coefficient ((a) and (c)) and b coefficient ((b) and (d)) perturbed by *ten* times their estimated errors. It is clear, particularly for the longer segment, that using the original estimated errors would be unrealistic and so for the present purpose the estimated variance is increased by a factor of 100. Note in Figures 5.6(a) and (b) the small (approximately $2nT$ r.m.s) systematic variation, which may well be the unmodelled contribution from the solar cycle modulation of the S_q.

Data for the inversions consisted of the results from the 119 observatories analysed in Chapter 4, and their geographical distribution is shown in Figure 5.7. Codes, names, locations and period of operation of these observatories are given in Tables 4.1 and 4.2. For each of the four SSADs identified, the segments for each observatory field component "active" at that date were selected and reduced to the common reference epochs 1970.0, 1978.0 and 1983.0. This meant a total of 6 inversions were necessary which could then be used to derive models of the 3 jerks. If segments overlapped at a SSAD, the transition date from one segment to the next was defined as in §4.2.4. Not all data were spanned by a segment in the OPRA analysis and so not all field components at each observatory provided data for the inversion. Plots of the selected segments against data (first differences again) were visually inspected to ensure they adequately represented the time–dependence of the field at that epoch. For example, in some cases the SSAD fell at the very extremity of a segment, and the behaviour of the field at that epoch was not entirely clear. The number of components contributing to each of the models, (pre and post 1970, pre and post 1978, pre and post 1983), were 299, 316, 316, 285, 285, 222 respectively. The start and end years of the quadratic segments used are given for each
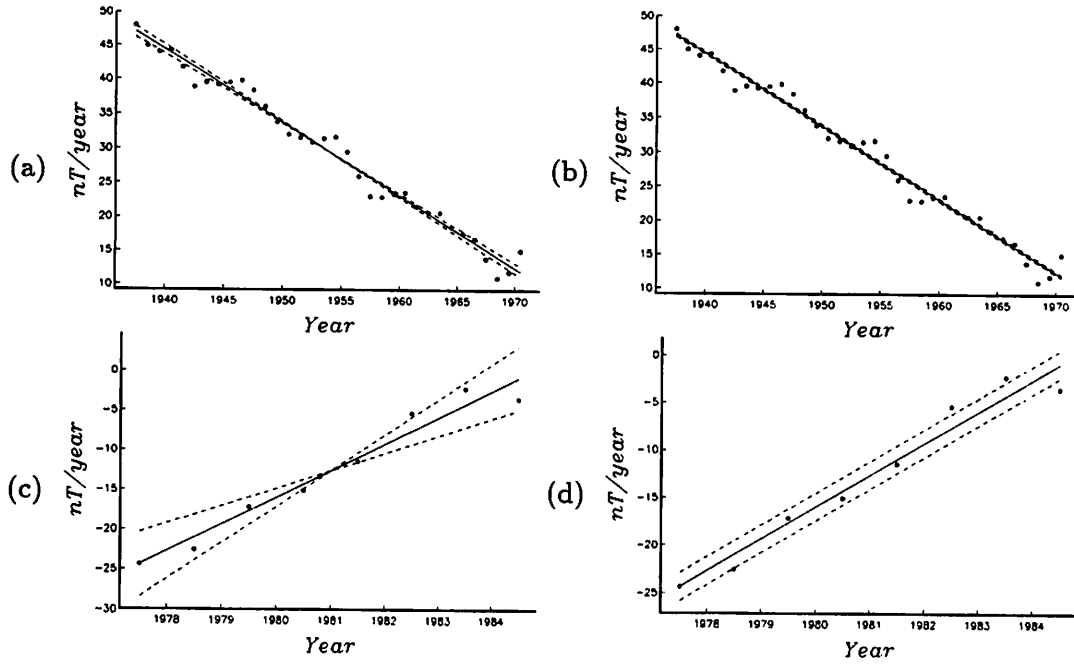
Figure 5.6: Examples of first time–derivative of model segments perturbed by errors. Solid line is from the model segment, while dashed lines are from the segment with slope (a coefficient) and offset (b coefficient) perturbed by 10 times the estimated error from Chapter 4. (a) and (b) are for Eskdalemuir ($\dot{Y}$ component) while (c) and (d) are for Honolulu ($\dot{X}$ component). Note the apparent (unmodelled) solar cycle effect at Eskdalemuir.

of the 6 models in Table A.1 in the appendix. The resulting models will henceforth be referred to as models PR1970, PO1970, PR1978, PO1978, PR1983 and PO1983. Note that models PO1970 and PR1978 are derived from the same data set, as are PO1978 and PR1983. The difference between them is that PR1970 and PO1970 have their time-dependence defined w.r.t. reference epoch 1970.0, PR1978 and PO1978 w.r.t reference epoch 1978.0 and PR1983 and PO1983 w.r.t. reference epoch 1983.0, which means that the data covariance matrices, which will be discussed next, are all different.

5.3.3 Structure of the data covariance matrix

The reduction of the quadratic coefficients to a common reference epoch introduces correlations between the estimates of their standard errors and hence the data covariance matrix C_e for the problem is non-diagonal. Thus a simultaneous inversion for all coefficients is necessary. As this matrix is of dimension $n_d \times n_d$ inverting it could be
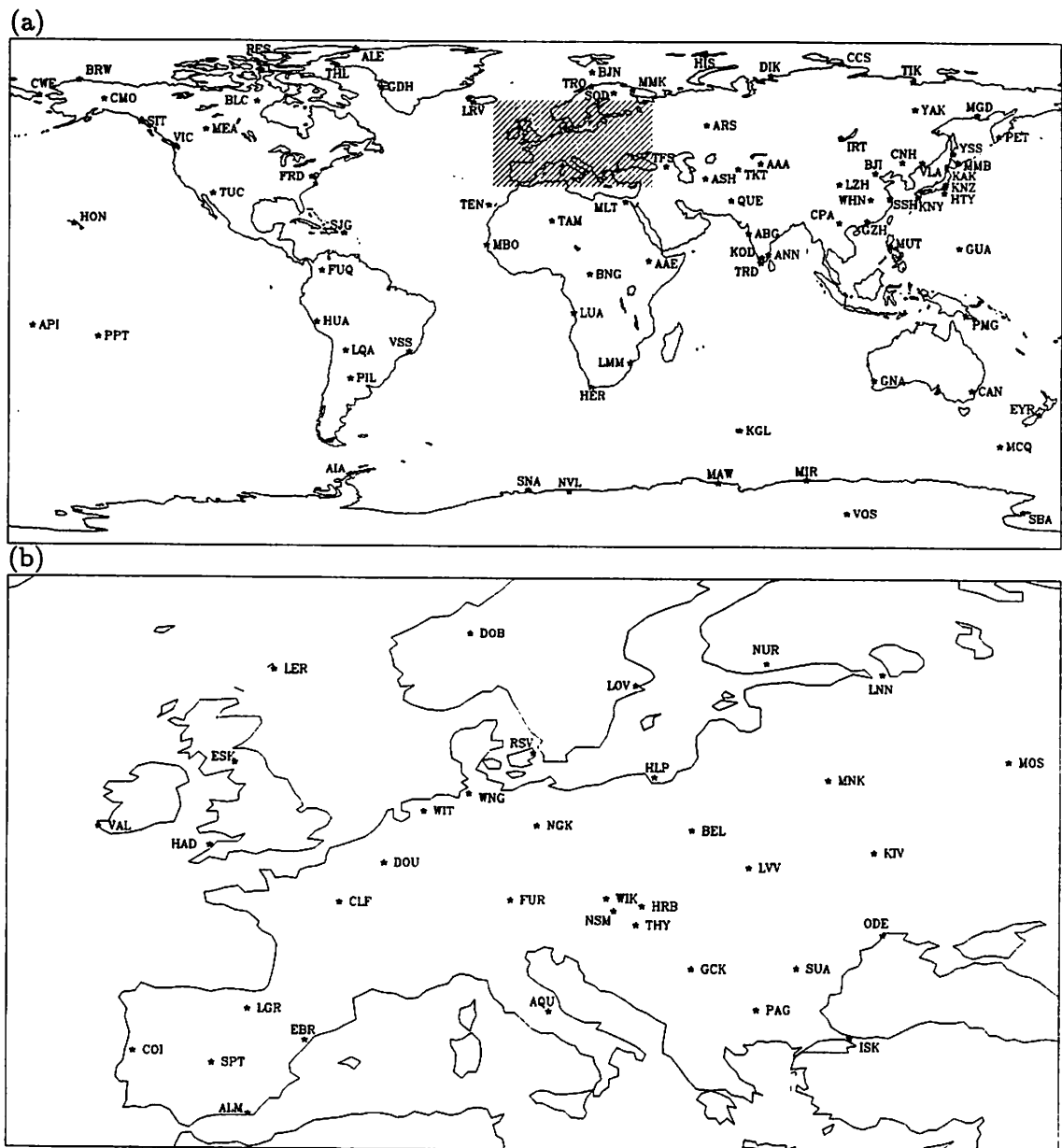
Figure 5.7: Distribution of observatories used in the stochastic inversions and for which OPRA analysis (Chapter 4) was performed. Star indicates observatory location and the IAGA code of the observatory is shown close by. (a) Worldwide, excluding "Europe" (shaded). Latitude shown is from 90° south to 85° north. (b) "European" observatories (Latitude 35° to 65° North; Longitude 15° west to 40° east). Projections are cylindrical equidistant.

formidable; however, by ordering the data as

$$(c'_1, b'_1, a'_1, \ldots, c'_K, b'_K, a'_K)$$

the covariance matrix is of the form

$$\begin{pmatrix} \mathbf{C}_1 & \cdots & 0 & \cdots & 0 \\ \vdots & \ddots & & & \vdots \\ 0 & & \mathbf{C}_i & & 0 \\ \vdots & & & \ddots & \vdots \\ 0 & \cdots & 0 & \cdots & \mathbf{C}_K \end{pmatrix} \qquad (5.10)$$

where the $\mathbf{C}_i$ are 3×3 submatrices, one for each of the K observatory field components analysed (hence $n_d = 3K$). $\mathbf{C}_e^{-1}$ is then of form (5.10) with $\mathbf{C}_i^{-1}$ in place of the $\mathbf{C}_i$. Dropping the subscript i, each covariance submatrix is of form

$$\begin{pmatrix} (t_d^2 - \bar{t}^2)^2 \delta a^2 + t_d^2 \delta b^2 + \delta c^2 & 2t_d(t_d^2 - \bar{t}^2)\delta a^2 + t_d \delta b^2 & (t_d^2 - \bar{t}^2)\delta a^2 \\ 2t_d(t_d^2 - \bar{t}^2)\delta a^2 + t_d \delta b^2 & 4t_d^2 \delta a^2 + \delta b^2 & 2t_d \delta a^2 \\ (t_d^2 - \bar{t}^2)\delta a^2 & 2t_d \delta a^2 & \delta a^2 \end{pmatrix}. \quad (5.11)$$

5.3.4 Parameter covariance matrix: model norms

For the remainder of §5.3 MF, SV and SA will be used to refer to the time–dependence defined by coefficients c_{np}^m, b_{np}^m and a_{np}^m respectively ($p = g, h$) for lucidity, even though at $t = t_1$ the secular acceleration (SA) is defined by $2a_{np}^m$. In choosing the form of prior information, it is clearly preferrable to make a choice which has some physical interpretation rather than, for example, the arbitrary and premature truncation of the field in simple least squares. The quantity $\dot{m}^T \mathbf{C}_m^{-1} \dot{m}$ defines a *norm* of $\dot{m}$. The solution (5.6) has the property that, for a given *residual norm* $e^T C_e^{-1} e$, the model norm is a minimum. The key is to choose $\mathbf{C}_m$ such that $\dot{m}^T \mathbf{C}_m^{-1} \dot{m}$ has a physical interpretation. GFA1 introduced the *uniform variance norm*, which in essence encodes the information that the field originates in the core rather than just somewhere within the Earth, and the *minimum energy norm* which corresponds to minimising the mean squared radial field at the CMB. GFA3 considered two further norms: the *finite Ohmic heating norm* and the *dissipation norm*. The former requires that the Ohmic heating in the core be

finite and is the only one of the four norms which is rigorous whilst the latter minimises an estimate of the effects of diffusion and is the strongest constraint.

The latter two norms can be used in connection with the MF but cannot be applied justifiably to its time derivatives. Here the dissipation norm is used for the main field, following Bloxham *et al* (1989). The uniform variance norm was introduced in the analysis of SV in GFA2 and is used here for the SV and SA as it is intuitively attractive. In specifying the prior information, the spherical harmonics are assumed independent so that C_m is diagonal. For the dissipation norm the variance of an nth degree harmonic is

$$\lambda_1^{-1} \left(\frac{r_c}{r_s} \right)^{2n} \frac{(2n+1)}{(n+1)^2 n^4} \tag{5.12}$$

and for the uniform variance norm

$$\lambda_j^{-1} \left(\frac{r_c}{r_s} \right)^{2n+4} \frac{1}{(n+1)^2}, \qquad j = 2,3 \tag{5.13}$$

where λ_1, λ_2 and λ_3 are *damping parameters* for MF, SV and SA respectively. As the damping parameters are increased the implied prior variance for the model coefficients is decreased (the prior information is imposed more strongly) and the residual norm will increase.

5.3.5 Results

Substitution of the model coefficients back into equations (5.1) to (5.3) allows the MF predicted by the model to be plotted for a specified epoch. Differentiation with respect to time allows the SV and SA to be plotted (although of course SA is constant for each model). Figure 5.8(a), (b) and (c) show the Z component of MF for epochs 1965.5, 1974.5 and 1986.5. In common with other maps of the radial flux at the CMB (eg. Bloxham *et al*, 1989), these maps show some important features of the field including areas of "reversed" flux in both hemispheres, undulation of the magnetic equator and concentration of flux in 4 "lobes" at approximately 120° longitude east and west with equatorial symmetry. There appear to be no significant changes in these main field maps over the relatively short time period investigated here, probably due to the rather low spatial resolution (see below and Figure 5.14) which drops off sharply at around

spherical harmonic degree 9 for the main field. Secular acceleration for epochs 1965.5, 1974.5 and 1981.5 is shown in Figures 5.9 to 5.11, for each of the components $\ddot{X}$, $\ddot{Y}$ and $\ddot{Z}$. These are plotted at the Earth's surface since the uniform variance norm does not ensure convergent error estimates at the CMB. Downward continuation of the SA and SV, under the insulating mantle approximation, is less appropriate than for the main field as the effects of a weakly conducting mantle are expected to be greater for the higher time derivatives of the field (Benton & Whaler, 1983).

Damping

The non-diagonal nature of the data covariance matrix adds a slight complication to the exploration of the damping parameter space as, for example, altering λ_1 (which determines the part of the model norm relating to the c coefficients) will also affect the values of the a and b coefficients determined. This effect was investigated for all 6 models and an example is shown in Figure 5.12. These *trade-off curves* show how as damping is increased the model norm (and hence model complexity) is reduced at the expense of increased residual norm. Here the log of the *partial model norms* was plotted against approximate misfit $((e^T C_e^{-1} e / n_d)^{\frac{1}{2}})$. (The partial model norm is defined here as that part of $\hat{m}^T C_m^{-1} \hat{m}$ arising from the SA, SV and MF separately and with the damping parameter omitted from C_m^{-1}.) It is clear that the damping parameters can be varied independently for all practical purposes. Therefore to explore the parameter space each damping parameter was varied in turn while the others were held constant. This is illustrated in Figure 5.13. The trade–off curves were then used to choose the value of damping parameters for the final models, the upper end of the "knee" being preferred. The same damping parameters $\lambda_1 = 10^{-12}$, $\lambda_2 = 10^{-6}$ and $\lambda_3 = 10^{-3}$ were chosen for all 6 models following the Bayesian philosophy (Bloxham al, 1989) that the prior assumptions about the variance of the model coefficients should not change from one epoch to the next. This is certainly justifiable for λ_1 as the physics of the core should not change from one epoch to the next, however, for the uniform variance norm it could be argued that for epochs with significantly less data (ie. model PO1983) the variance of the coefficients should be expected to be higher.
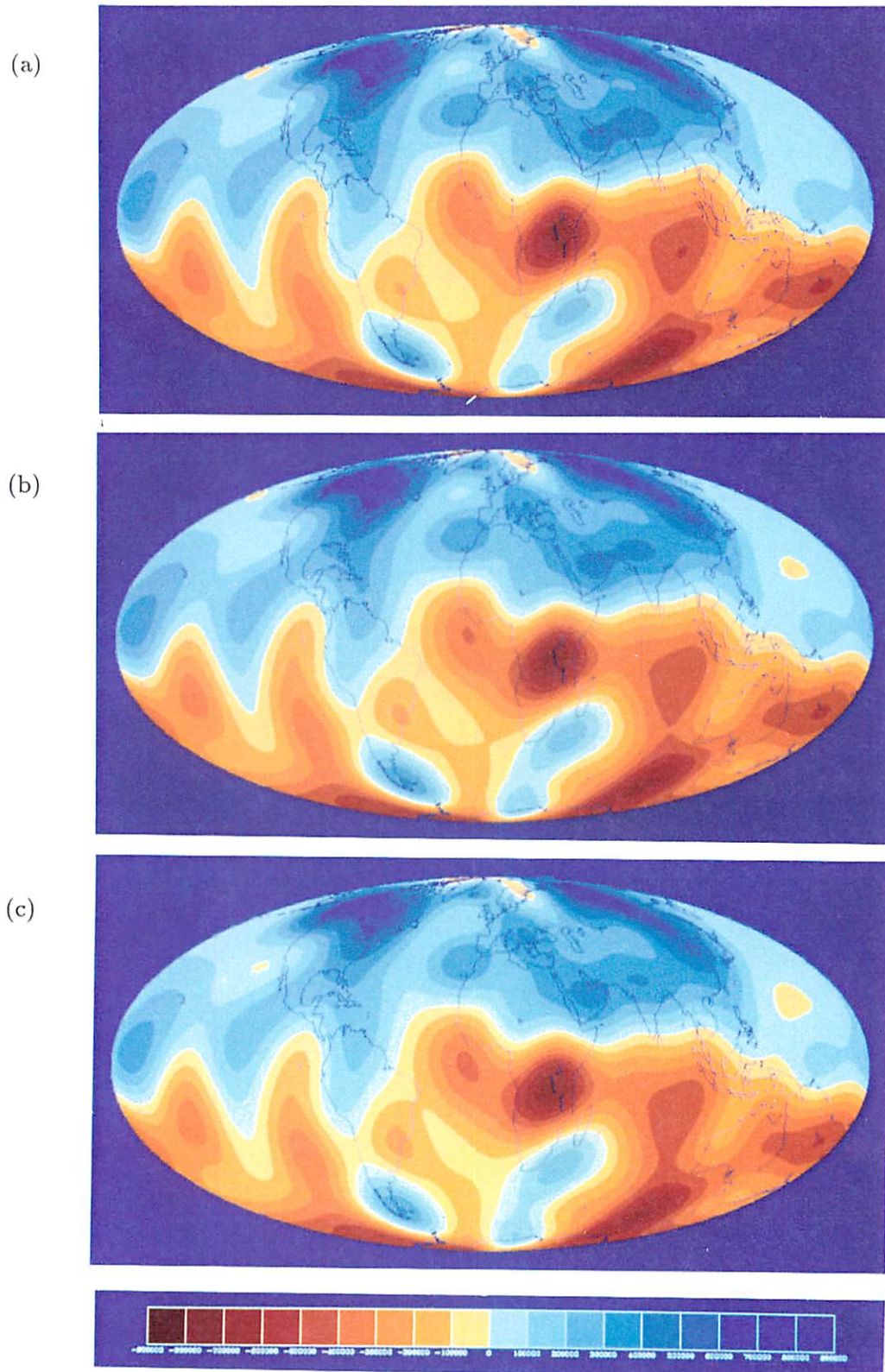
Figure 5.8: Z component of the magnetic field at the CMB for epochs (a) 1965.5, (b) 1974.5 and (c) 1986.5 derived from models PR1970, PR1978 and PO1983 respectively. Scale is from $-9 \times 10^5 nT$ to $9 \times 10^5 nT$ and the projection is Mollweide.
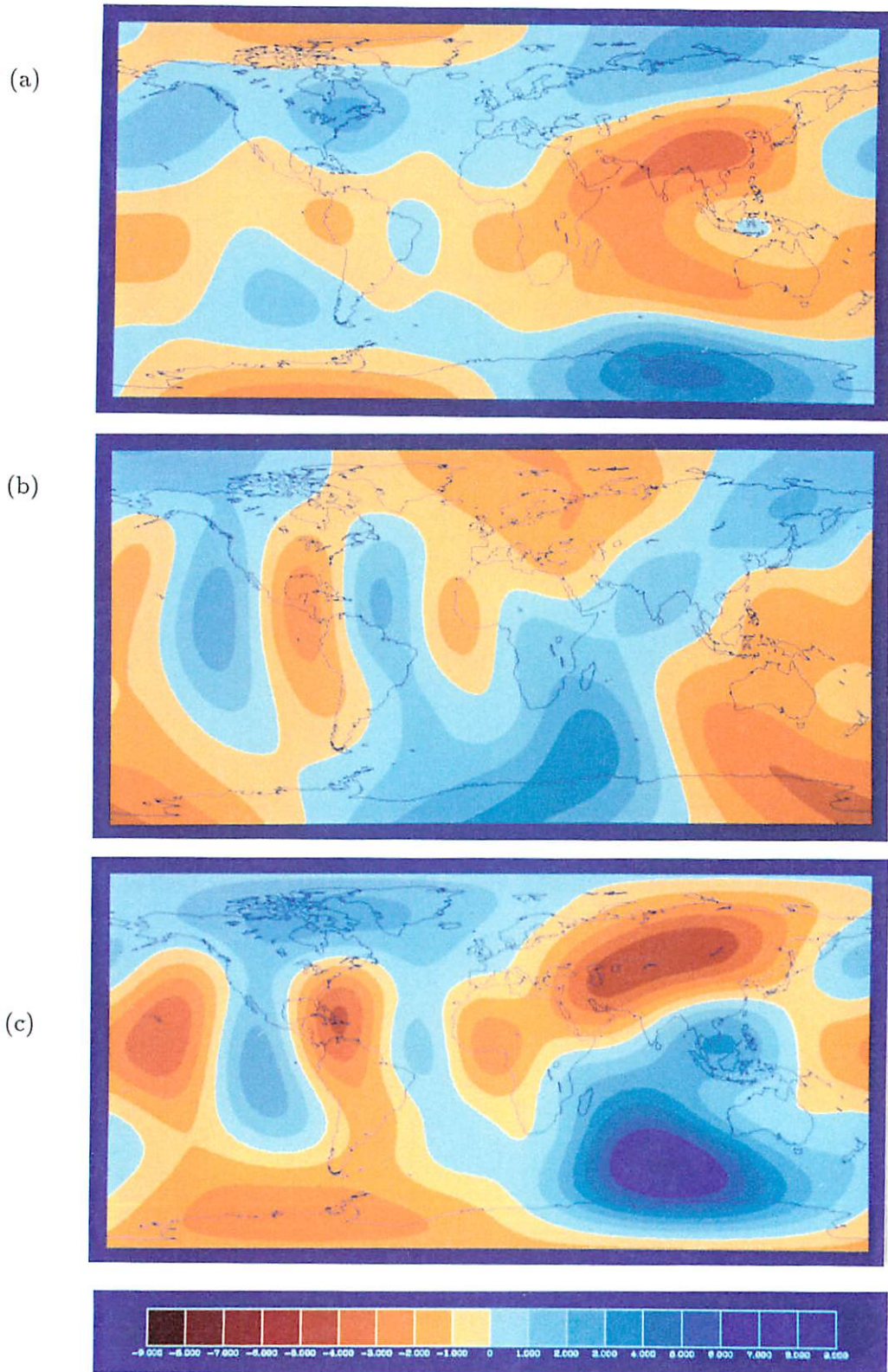
Figure 5.9: Components (a) $\ddot{X}$, (b) $\ddot{Y}$ and (c) $\ddot{Z}$ of secular acceleration for epoch 1965.5 from model PR1970. Scale is from $-9nT/yr^2$ to $9nT/yr^2$ for all components. Projection is cylindrical equidistant.
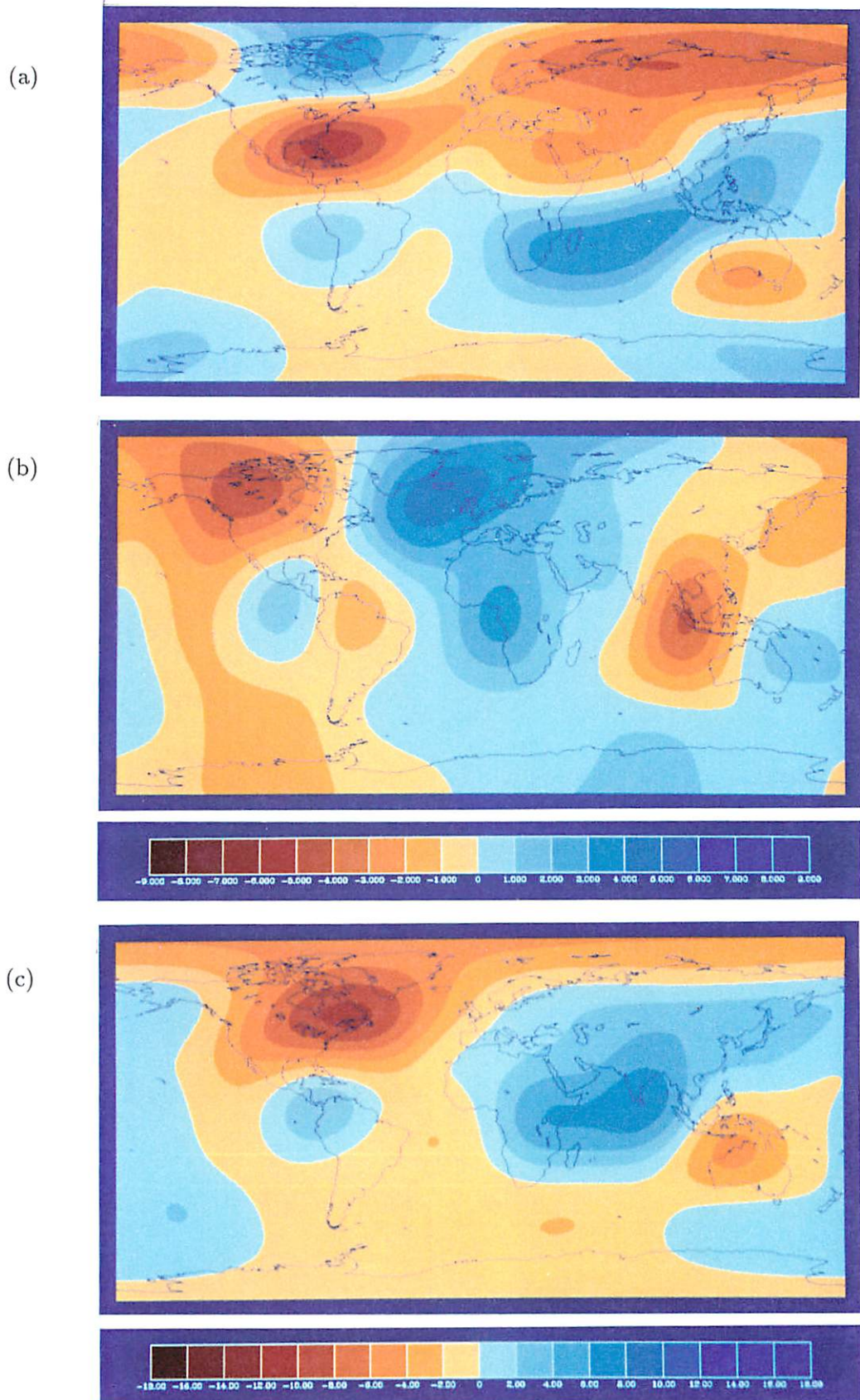
Figure 5.10: Components (a) $\ddot{X}$, (b) $\ddot{Y}$ and (c) $\ddot{Z}$ of secular acceleration for epoch 1974.5 from model PR1978. Scales are from $-9nT/yr^2$ to $9nT/yr^2$ for $\ddot{X}$ and $\ddot{Y}$ and $-18nT/yr^2$ to $18nT/yr^2$ for $\ddot{Z}$. Projection is cylindrical equidistant.
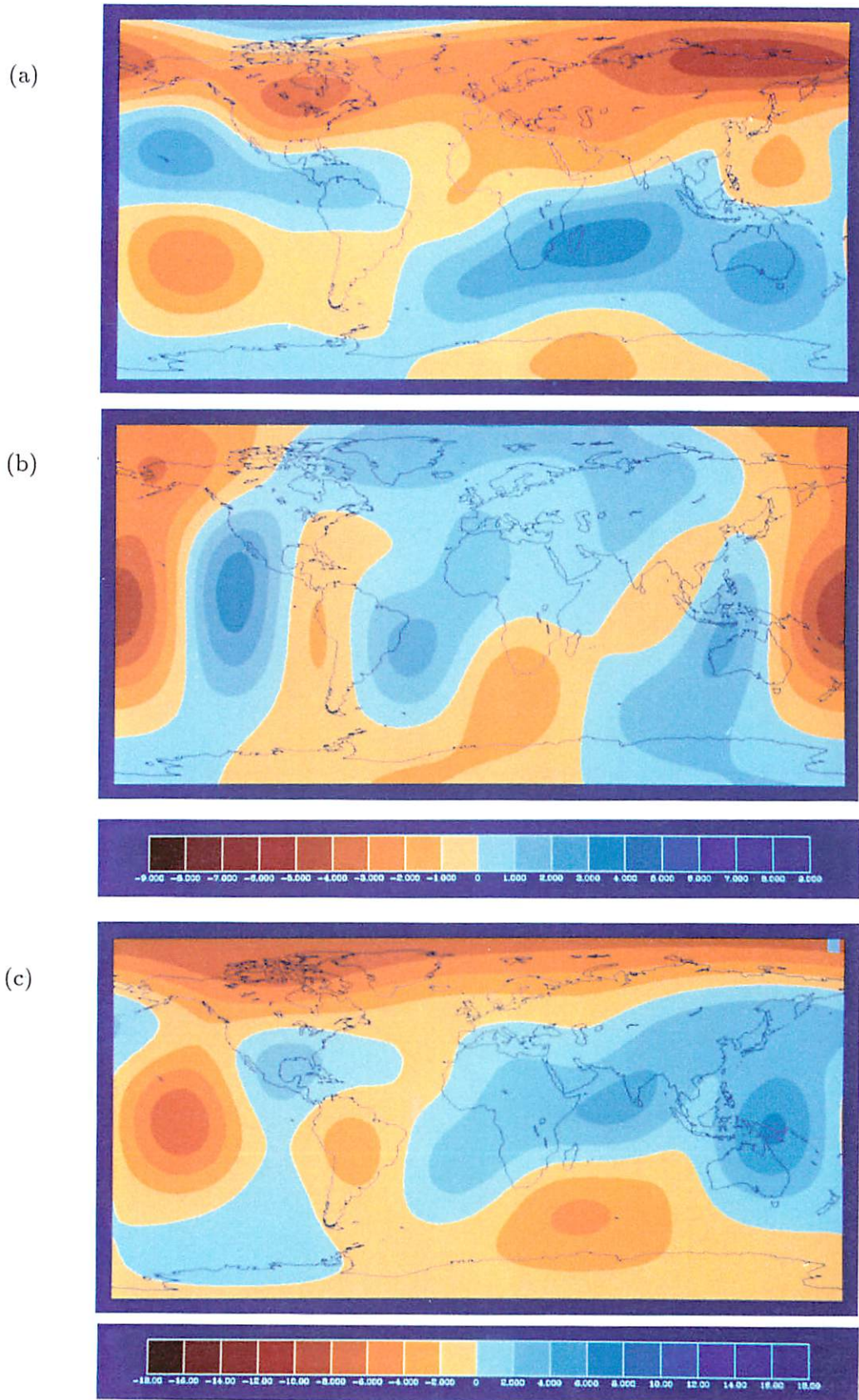
Figure 5.11: Components (a) $\ddot{X}$, (b) $\ddot{Y}$ and (c) $\ddot{Z}$ of secular acceleration for epoch 1981.5 from model PR1983. Scales are from $-9nT/yr^2$ to $+9nT/yr^2$ for $\ddot{X}$ and $\ddot{Y}$ and $-18nT/yr^2$ to $+18nT/yr^2$ for $\ddot{Z}$. Projection is cylindrical equidistant.

Resolution and convergence

The resolution matrix **R** defines the relationship between the model estimate and the true model and is given by

$$\mathbf{R} = (\mathbf{G}^T\mathbf{C}_e^{-1}\mathbf{G} + \mathbf{C}_m^{-1})^{-1}(\mathbf{G}^T\mathbf{C}_e^{-1}\mathbf{G}). \tag{5.14}$$

The diagonal elements of **R** give an indication as to what degree the model coefficients are well determined and these are plotted for each of the models in Figure 5.14. All models were determined using a truncation at degree $N = 14$. To check that this was not too low, the truncation level was gradually increased keeping the damping fixed. Any changes in the models arising were found to be insignificant, with a typical field power (Lowes, 1966) of magnitude $10^{-2}(nT)^2$, $10^{-6}(nT/yr)^2$ and $10^{-9}(nT/(yr)^2)^2$ for the MF, SV and SA respectively at degree 14. The trace of **R** (sum of diagonal elements) gives the effective number of degrees of freedom of the model and can be evaluated separately for the MF, SV and SA.

The statistics of the six inversions are given in Table 5.1.

Fit to the annual means

To assess how well the models fit the original annual means in comparison to other models, residuals to the constant secular acceleration models and to a time–dependent model of the magnetic field for the period 1840 to 1990 (Bloxham & Jackson, 1990; to be referred to here as the BJ2 model) were computed. The results of this comparison are summarised in Table 5.2. It is apparent that over the time periods for which the constant secular acceleration models are expected to be valid, the BJ2 model gives a slightly better fit to the data though the difference is marginal. For the shortest time period (1979.5 – 1983.5) the spline model gives a poorer fit. The BJ2 was based on a much larger data set than used here, including both satellite and survey data in addition to observatory data, as well as being greatly over–parameterised (A. Jackson, personal communication, 1991), and this may account for the slightly better fit. Figure 5.15 shows a plot of mean residuals to both the BJ2 model and model PR1970 calculated for the years 1961.5 to 1977.5 (thus taking model PR1970 beyond its expected range of validity). To eliminate the dominant effect of unmodelled short wavelength crustal field,

Table 5.1: Statistics of the stable secular acceleration models. Trace and model norm are as defined in §5.3.5, while n_d is the number of data. The misfit is defined as $(e^T C_e^{-1} e/(n_d - \text{Trace}(R)))^{1/2}$. Misfit, trace and n_d are all dimensionless.

	Misfit	Trace			Model norm			n_d
		MF	SV	SA	MF	SV	SA	
Units	—	—	—	—	$10^{13}(nT)^2$	$10^7(nT/yr)^2$	$10^4(nT/yr^2)^2$	—
PR1970	0.93	97.9	72.4	52.1	7.54	5.40	3.59	894
PO1970	0.89	102.6	75.1	49.0	8.01	4.91	4.25	945
PR1978	0.89	102.7	75.7	47.9	8.09	5.26	4.16	945
PO1978	0.85	100.6	72.8	43.1	8.45	4.38	2.33	852
PR1983	0.86	100.5	72.0	43.8	8.54	4.16	2.37	852
PO1983	0.69	85.8	58.6	32.8	6.51	2.58	1.16	663
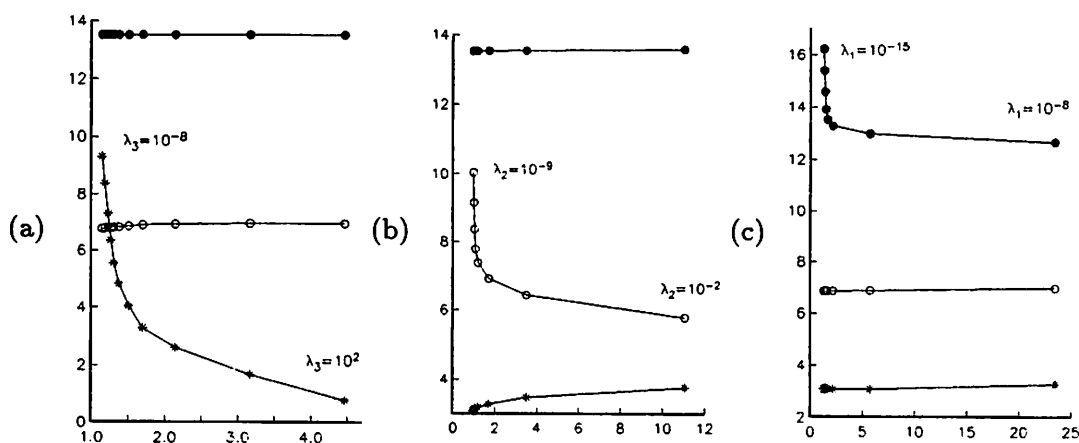
Figure 5.12: Trade–off curves for model PR1970 showing how the damping parameters λ_1, λ_2 and λ_3 can be varied (almost) independently (see §5.3.4 and §5.3.5). Points are for actual values relating to MF ($\bullet$), SV (o) and SA ($*$) for different values of damping parameters and curves are linearly interpolated. Abscissæ are approximate misfit $(e^T C_e^{-1} e/n_d)^{1/2}$ whilst ordinates are log of partial model norm for the MF, SV and SA separately.

(a) is for $\lambda_1 = 10^{-11}$, $\lambda_2 = 10^{-4}$ and $\lambda_3 = 10^{-8}$ to $\lambda_3 = 10^2$ increasing by factors of 10

(b) is for $\lambda_1 = 10^{-11}$, $\lambda_3 = 10^{-1}$ and $\lambda_2 = 10^{-9}$ to $\lambda_2 = 10^{-2}$ increasing by factors of 10

(c) is for $\lambda_2 = 10^{-4}$, $\lambda_3 = 10^{-1}$ and $\lambda_1 = 10^{-15}$ to $\lambda_1 = 10^{-8}$ increasing by factors of 10.
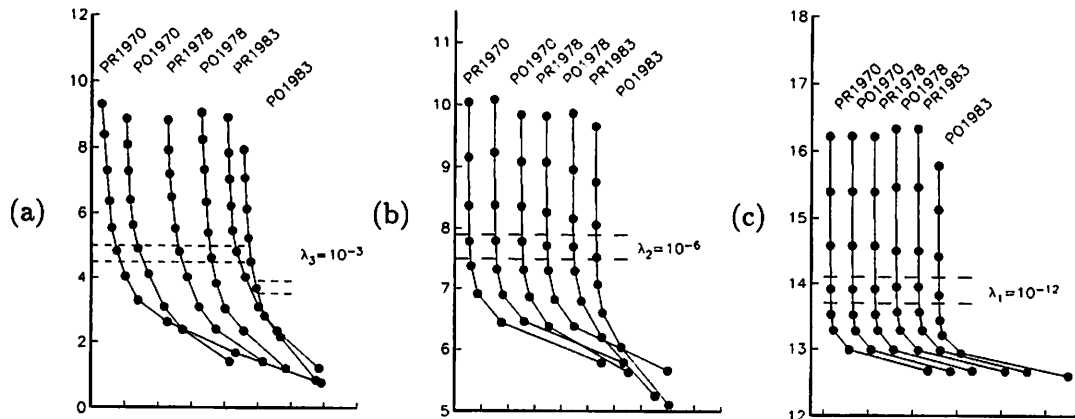
Figure 5.13: Trade–off curves for the SA, SV and MF for all 6 models. Curves have been horizontally offset for clarity, hence the horizontal scales are omitted Dashed lines bound the points (indicated by •) corresponding to the values of damping parameter chosen for the final models ($\lambda_1 = 10^{-12}$, $\lambda_2 = 10^{-6}$ and $\lambda_3 = 10^{-3}$). (a) shows the partial model norm for the SA for a range of values of λ_3, (b) is for the SV for a range of values of λ_2 and (c) is for the MF for a range of values of λ_1 with, in each case, the other two damping parameters held constant. Damping parameters change by factors of 10 from one point to th next.

the mean residual for the period 1961.5 to 1969.5 for each observatory was subtracted from the residuals before forming the mean for all observatories. It can be seen that model PR1970 gives a good fit to the data prior to 1970 (although there is some evidence of a systematic error in the X component) but breaks down quite rapidly after this date. The spline model continues to fit the data well throughout the whole time period.

5.3.6 A note on computational efficiency and accuracy

All computations were performed using double precision arithmetic in FORTRAN 77 on a Sun Sparc–station. The most time–consuming operation in the inversion procedure is forming the *normal equations matrix* $G^T C_e^{-1} G$. Although this need only be computed once, the linear system involving $(G^T C_e^{-1} G + C_m^{-1})^{-1}$ must be solved anew for each choice of damping parameters. Three different algorithms were used for the matrix inversion. The routine F01ABF of the Numerical Algorithms Group Limited (NAG, 1988) uses Cholesky decomposition with iterative refinement (eg. Press *et al*, 1989) to compute the inverse of a positive definite symmetric matrix to full machine precision and
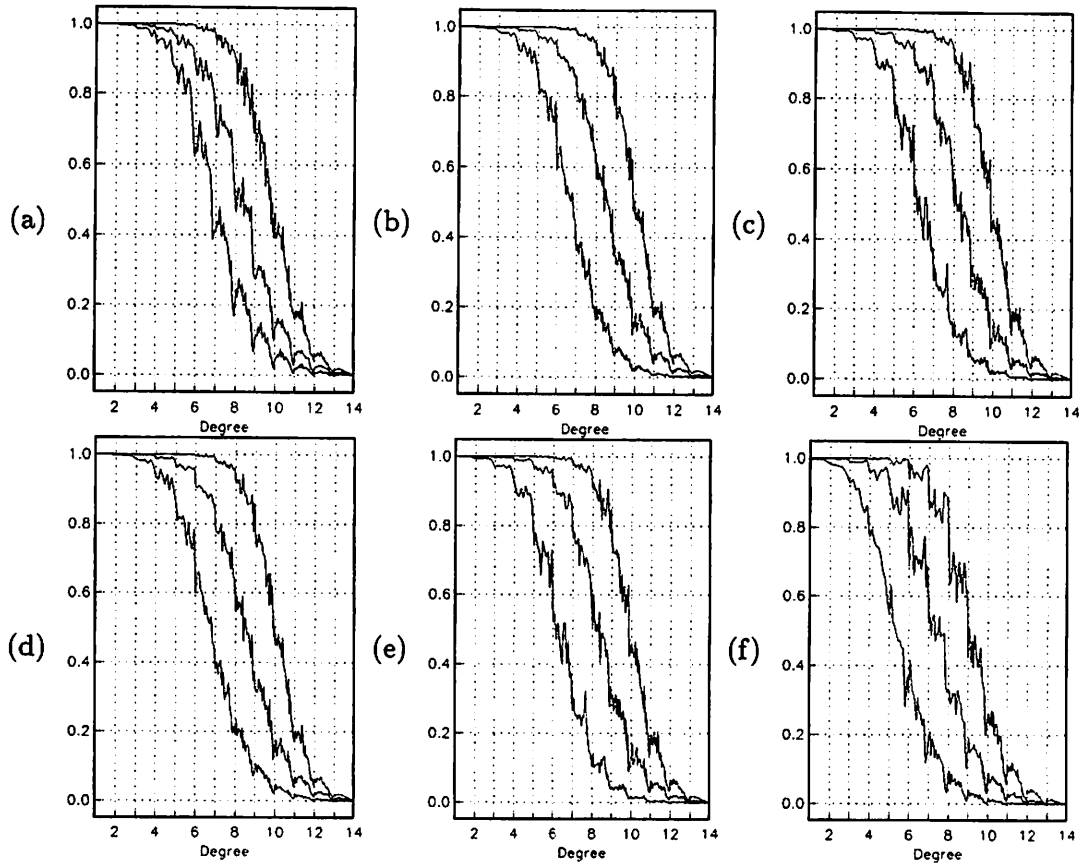
Figure 5.14: Plots of diagonal elements of the resolution (equation 5.14) against harmonic degree for models (a) PR1970 (b) PR1978 (c) PR1983 (d) PO1970 (e) PO1978 and (f) PO1983. The different curves in each plot are for the three types of spherical harmonic coefficient a_{np}^m (leftmost), b_{np}^m (centre) and c_{np}^m (rightmost) from equations (5.2) and (5.3) where p is either g or h and the ordering of elements is increasing harmonic order within harmonic degree.

was used as a standard against which other routines could be checked. The drawback of this routine is that it is very slow which is an important consideration when exploring the parameter space. Therefore two other routines were tried: a Cholesky decomposition routine based on the method of Lawson & Hanson (1974, p123) and the NAG routine F01AAF which calculates the approximate inverse of a real matrix using Crout's method. For a model of maximum degree 14 (672 parameters) the times taken to solve the linear system of equations were 16920, 1940 and 572 seconds respectively on a Sun Sparc 2 workstation running at $33MHz$. Mean absolute differences between elements of the inverse matrices computed by different methods were found to be 5×10^{-13} for the

Table 5.2: Comparison of the residuals to the annual means used in this study to (1) the constant secular acceleration models and (2) model BJ2 (see §5.3.5) for four time periods. Figures given are the r.m.s. residual for all observatories, though with respect to the mean residual for each observatory. Ratios are the mean of the r.m.s. residual to the spline model divided by the r.m.s. residual to the constant secular acceleration model, for each observatory. Units are nT.

Model	Span	X r.m.s.		Y r.m.s.		Z r.m.s.		Ratios		
		(1)	(2)	(1)	(2)	(1)	(2)	X	Y	Z
PR1970	1961.5–1970.5	4.81	4.44	4.01	3.31	7.72	6.15	0.99	0.83	0.79
PO1970	1971.5–1978.5	4.50	3.01	3.55	3.12	5.72	4.01	0.70	0.82	0.91
PO1978	1979.5–1983.5	8.07	8.15	13.48	13.69	9.73	9.50	1.14	1.13	0.91
PO1983	1984.5–1990.5	4.40	3.74	3.54	2.98	6.59	4.93	0.92	0.86	0.95
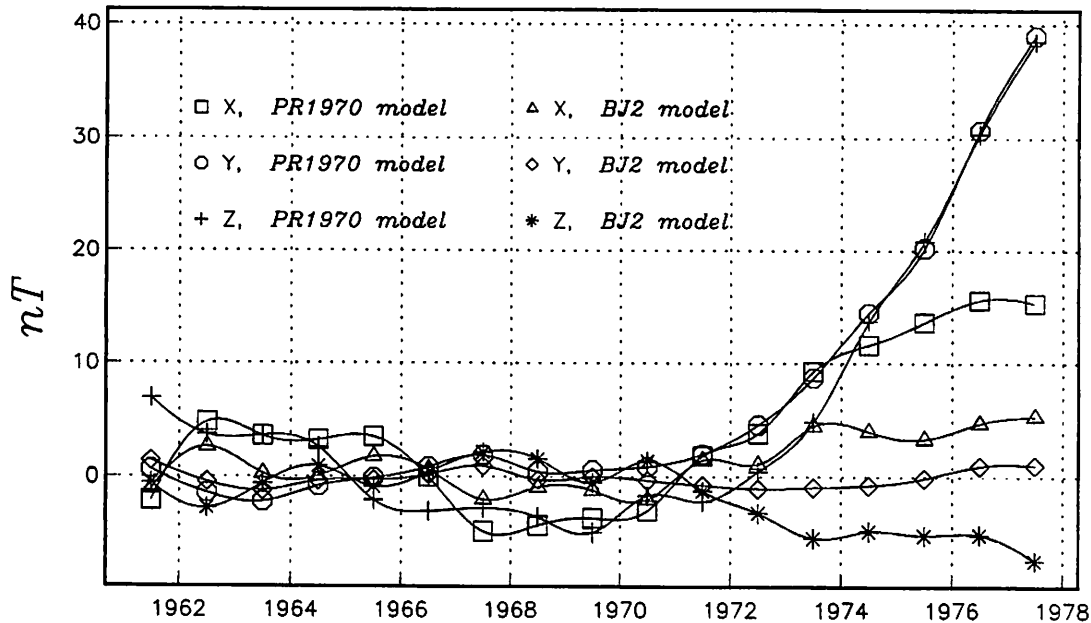
Figure 5.15: Mean residuals (corrected for time–independent crustal bias as described in §5.3.5) to the PR1970 model and the time–dependent field model BJ2.

Lawson & Hanson method versus F01ABF (close to machine precision) and 2×10^{-11} for F01AAF versus F01ABF. The field models resulting from the use of F01AAF were found to have identical coefficients to at least 7 significant digits, which is sufficient to parameterise the Earth's magnetic field accurately using observatory data. This algorithm was therefore used in computing the models presented here.

5.4 Models of the geomagnetic jerks of 1969, 1978 and 1983.

The change in SA for each of the 3 jerk epochs can now be simply calculated as the difference between the SA predicted by the pre and post jerk models. The covariance matrix for the jerk is obtained by the sum of 4 times the covariance matrices for the pre and post jerk models. All 3 components of the step change in secular acceleration are plotted for the 1970, 1978 and 1983 jerks in Figures 5.16 to 5.18.

Estimated errors on jerk values

The reliability of these plots can be assessed to some extent by plotting the half width of the 99% confidence region, $t_{0.995} \sqrt{(\mathbf{a}^T \hat{\sigma}^2 (\mathbf{G}^T \mathbf{C}_e^{-1} \mathbf{G} + \mathbf{C}_m^{-1})^{-1} \mathbf{a})}$, where $t_{0.995}$ is the Student's t statistic on the appropriate number of degrees of freedom (taken as the trace of the part of the resolution matrix associated with the SA (hence $t_{0.995} \approx 2.6$)). $\mathbf{a}$ is a single equation of condition which depends on postion. This is shown for each component of the 1970 jerk in Figure 5.19 and the maximum and minimum values for each field component for the 1970 jerk is given in Table 5.3. These represent the variability in the model response arising from poor observatory distribution and data

Table 5.3: Uncertainty estimates (given as half widths of 99% confidence region) for each component of the 1970 jerk. Units are (nT/yr^2)

Component	Minimum half width	Maximum half width
X	0.005	0.110
Y	0.012	0.102
Z	0.009	0.173

errors. An additional error, due to the truncation of the spatial expansion (5.2) has also been assessed according to the method of GFA1. For the radial component of the 1970 jerk this was found to be $11.5 \times 10^{-8}(nT/yr^2)$. For the SA for each model the truncation error was found to be consistently of the order 10^{-8} and so is clearly negligible. It is clear that the total uncertainty is less than the contour intervals in Figures 5.16 to 5.18 and so their reliability is reasonably assured.

5.5 Discussion.

The 1970 jerk

The 1970 jerk has been quite widely investigated previously (refer to the review in Chapter 1) and plotted by Malin et al (1983) (and by Kerridge & Barraclough (1985) using the same models). Figure 5.16 shows that the change in secular acceleration associated with the 1970 jerk consists of several foci which seem to occur particularly, although by no means exclusively, at high latitudes. Features present in Figures 8, 9 and 10 of Malin et al (1983) are in some cases double the amplitude of the corresponding features in Figure 5.16, 5.17 and 5.18. In particular their Figure 10 shows a focus with maximum intensity $-19nT/yr^2$ in the $\ddot{Z}$ component over the east Indian Ocean which is only $-10nT/yr^2$ in Figure 5.16(c). Similarily they show a focus in the $\ddot{Z}$ component which reaches $+11nT/yr^2$ over the Galapagos Islands, an area with virtually no observatory data coverage, which is non-existent in Figure 5.16(c). Although based on a similar number of data, their analysis was derived from main field models arbitrarily truncated at degree 6 which is likely to have introduced errors into the coefficients through aliasing from shorter wavelength features of the field (see eg. Whaler & Gubbins (1981)). These were then successively first differenced to yield a model of the change in secular acceleration associated with the 1970 jerk which was then truncated at degree 4.

Table 5.4 gives the spatial power spectra of secular acceleration change of the 1970, 1978 and 1983 jerks computed here, as well as those for the 1970 jerk as computed by other authors. Not surprisingly, from the similarity of the jerk maps, the spatial power spectrum of the 1970 jerk is qualitatively similar to that of Malin et al (1983), being dominated by degree 2 harmonics. This is also the case for the power of the jerk model
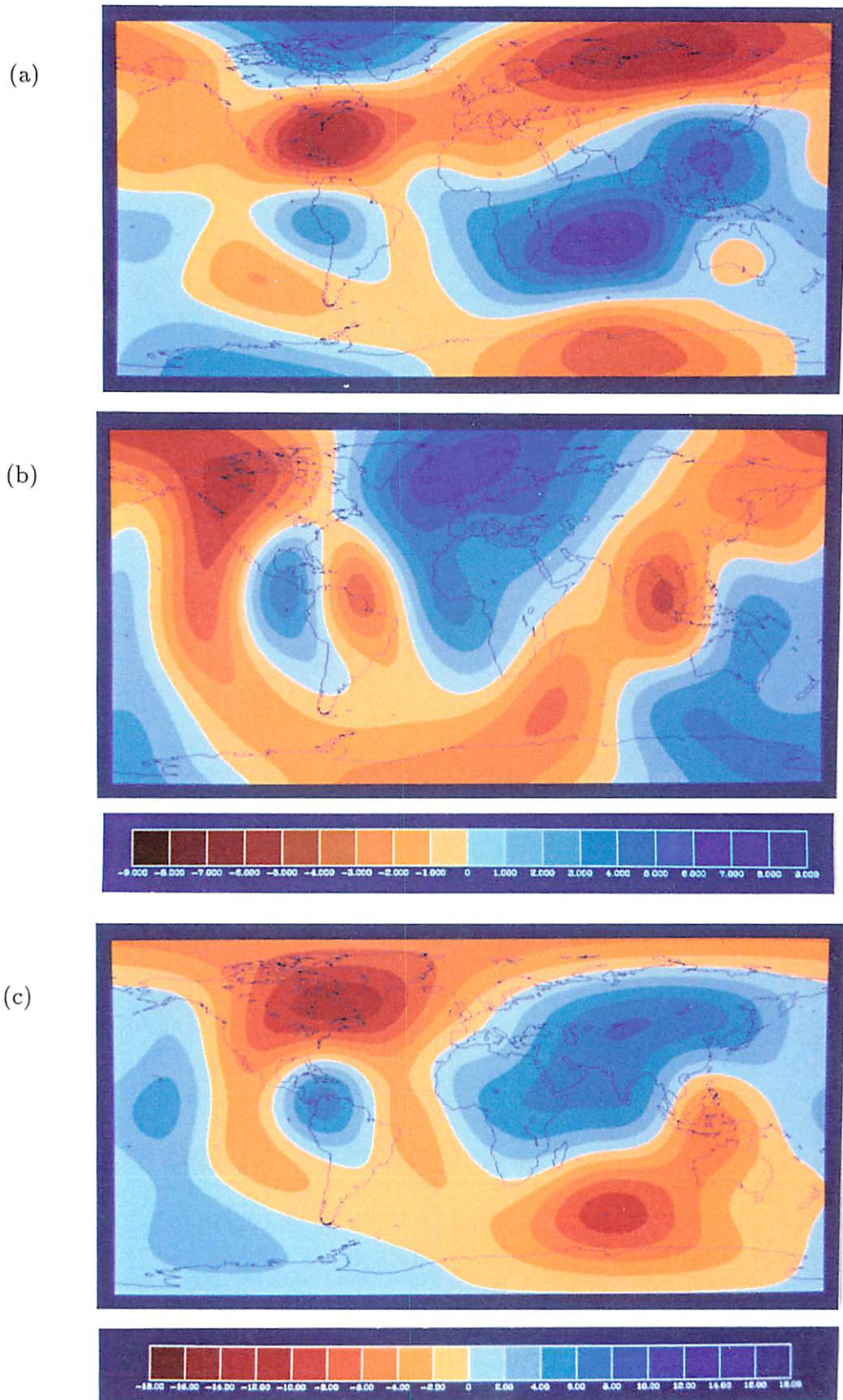
Figure 5.16: Change in the (a) $\ddot{X}$, (b) $\ddot{Y}$ and (c) $\ddot{Z}$ components of secular acceleration associated with the 1970 jerk. Scales are $-9nT/yr^2$ to $+9nT/yr^2$ for $\ddot{X}$ and $\ddot{Y}$ and $-18nT/yr^2$ to $+18nT/yr^2$ for $\ddot{Z}$. Projection is cylindrical equidistant.
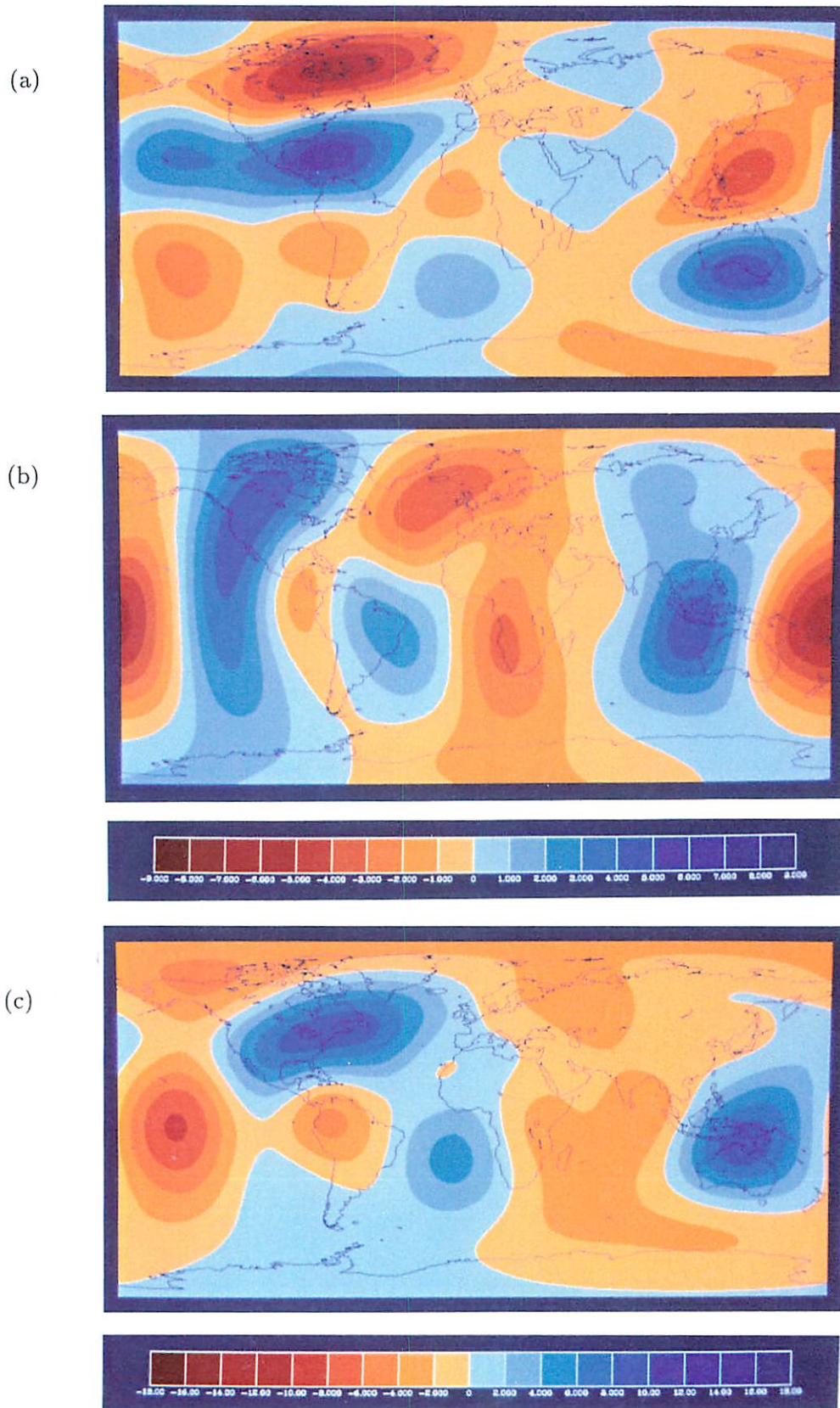
Figure 5.17: Change in the (a) $\ddot{X}$, (b) $\ddot{Y}$ and (c) $\ddot{Z}$ components of secular acceleration associated with the 1978 jerk. Scales are $-9nT/yr^2$ to $+9nT/yr^2$ for $\ddot{X}$ and $\ddot{Y}$ and $-18nT/yr^2$ to $+18nT/yr^2$ for $\ddot{Z}$. Projection is cylindrical equidistant.
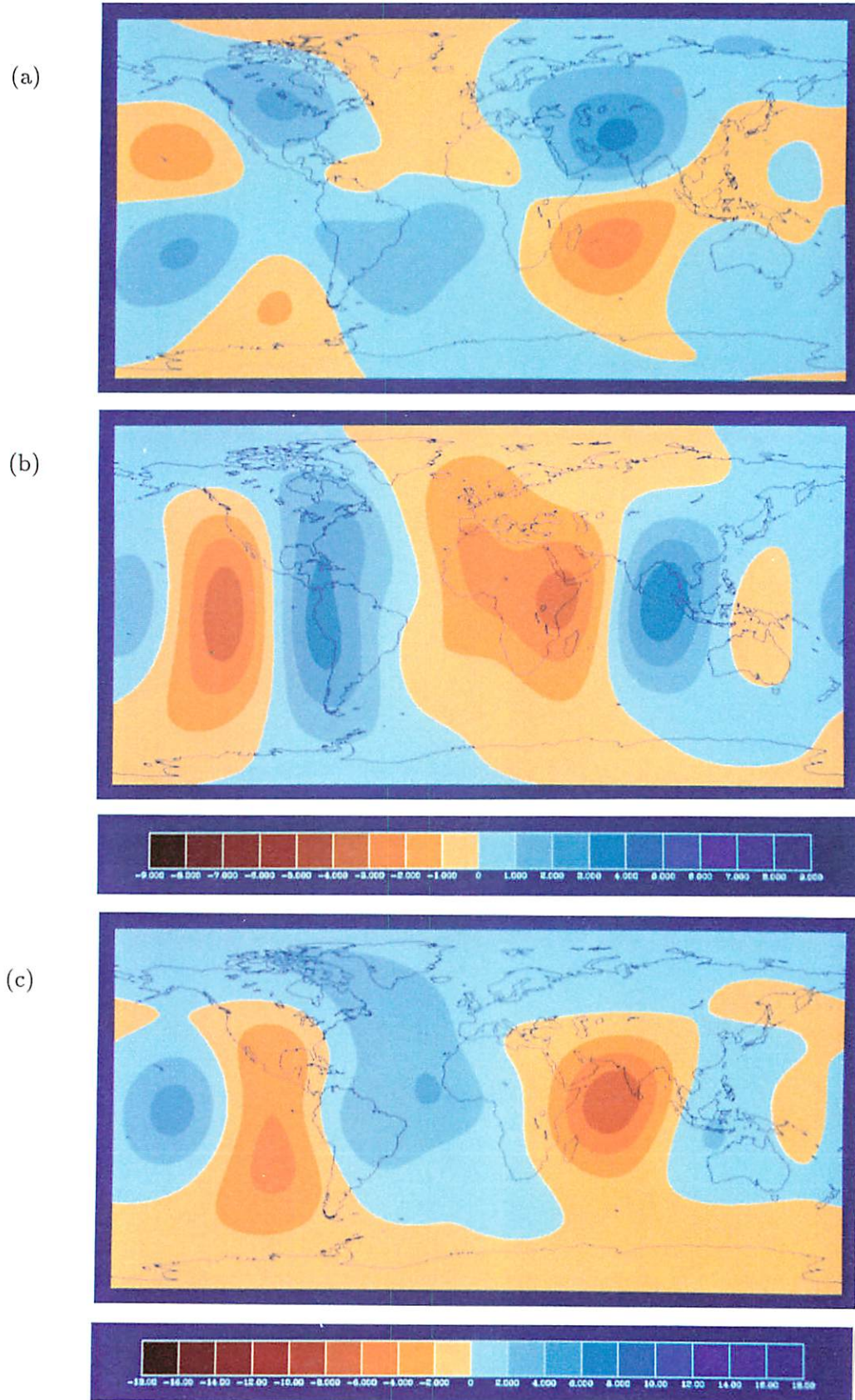
Figure 5.18: Change in the (a) $\ddot{X}$, (b) $\ddot{Y}$ and (c) $\ddot{Z}$ components of secular acceleration associated with the 1983 jerk. Scales are $-9nT/yr^2$ to $+9nT/yr^2$ for $\ddot{X}$ and $\ddot{Y}$ and $-18nT/yr^2$ to $+18nT/yr^2$ for $\ddot{Z}$. Projection is cylindrical equidistant.
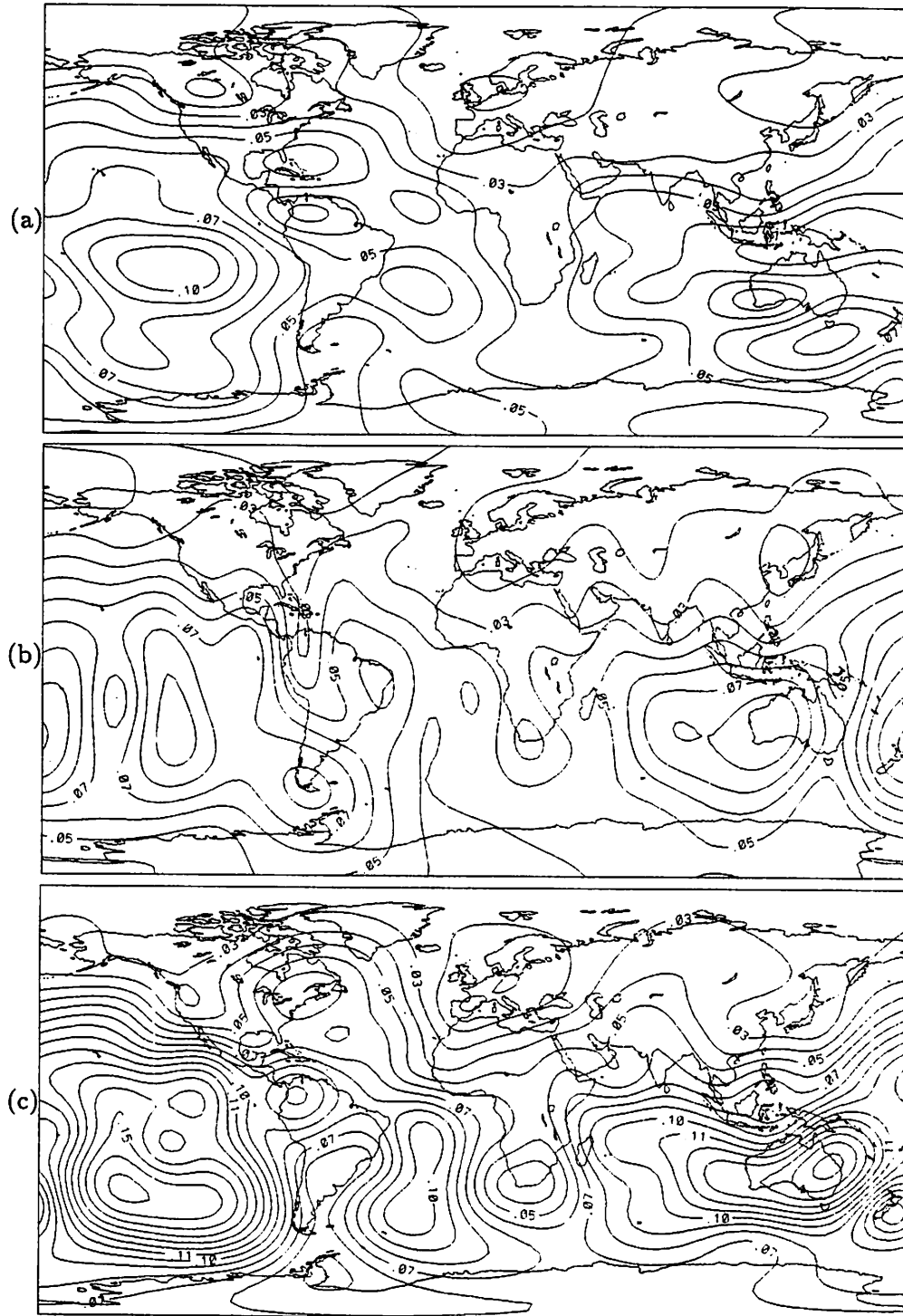
Figure 5.19: 99% Confidence region half width for the change in secular acceleration associated with the 1970 jerk (see Figure 5.16) for (a) the X component (b) the Y component and (c) the Z component. Cylindrical equidistant projection. Latitude goes from -90 to +90 degrees. Contour intervals are $0.01 nT/yr^2$ for all components. Projection is cylindrical equidistant.

computed in GFA2 which used stochastic inversion to compute the secular variation from which the jerk model was derived. The jerk model of Malin & Hodder (1982) differs in that it is dominated by the degree 3 harmonics although they did not publish all the coefficients and so a full spectrum cannot be computed here. Their model was based on a smaller data set and was also derived using a least squares fit to a truncated series of spherical harmonics.

The 1978 and 1983 jerks

The regional features of the 1978 jerk (Figure 5.17) are of comparable amplitude to those of the 1970 jerk although the overall power is about two thirds that of the 1970 jerk (Table 5.4). There also appears to be an anti-correlation between certain regional features of the 1970 and 1978 jerks, in particular over North, Central and South America, south-east Asia and in Europe (at least in the Y component). Assuming the jerks are independent the correlation coefficient between the jerk fields,

Table 5.4: Power spectra of the change in secular acceleration associated with the jerks of 1970, 1978 and 1983. Error estimates were computed using linear propagation (see equation (2.2)) of the diagonal elements of the covariance matrices. Column headed GFA2 is computed from coefficients in Gubbins (1984). Column M1 contains the results of Malin *et al* (1983) for which no error estimates were available. M2 is computed from Malin & Hodder (1982) (not all coefficients available). GFA2, M1 and M2 are all for the 1970 jerk.

Degree	Impulse power $((nT)^2(yr)^{-6})$					
	GFA2	M1	M2	1970	1978	1983
1	4.04	7.1	14.07±2.05	0.98±0.32	0.15±0.15	0.62±0.41
2	19.83	43.9	22.89±2.44	13.49±1.10	6.07±0.99	3.64±1.04
3	13.12	22.6	32.04±2.19	5.93±0.65	5.73±0.75	1.80±0.61
4	5.40	8.6	13.47±1.34	2.33±0.35	2.72±0.41	1.48±0.44
5	2.16	7.2	—	1.78±0.26	1.54±0.23	0.33±0.12
6	1.33	5.5	—	0.85±0.11	0.62±0.10	0.13±0.05
7	—	—	—	0.12±0.02	0.12±0.03	0.02±0.01
8	—	—	—	0.03±0.01	0.01±0.00	0.00±0.00
Total (to degree 14)	45.88	94.9	82.47±4.09	25.53±1.40	16.98±1.34	8.03±1.35

$$C = \frac{\int_\Omega \dot{\mathbf{B}}_{1970} \cdot \dot{\mathbf{B}}_{1978} d\Omega}{\left\{ \int_\Omega \dot{\mathbf{B}}_{1970} \cdot \dot{\mathbf{B}}_{1970} d\Omega \int_\Omega \dot{\mathbf{B}}_{1978} \cdot \dot{\mathbf{B}}_{1978} d\Omega \right\}^{\frac{1}{2}}} \tag{5.15}$$

which can be approximated by

$$\hat{C} = \frac{\sum_{n=1}^{N}(n+1)\sum_{m=0}^{n}(\dddot{g}_{n1970}^{m}\dddot{g}_{n1978}^{m} + \dddot{h}_{n1970}^{m}\dddot{h}_{n1978}^{m})}{\left\{ \left[\sum_{n=1}^{N}(n+1)\sum_{m=0}^{n}(\dddot{g}_{n1970}^{m}\dddot{g}_{n1970}^{m})\right]\left[\sum_{n=1}^{N}(n+1)\sum_{m=0}^{n}(\dddot{h}_{n1978}^{m}\dddot{h}_{n1978}^{m})\right] \right\}^{\frac{1}{2}}} \tag{5.16}$$

was calculated, where $\dddot{}$ denotes the step change in secular acceleration at the epoch indicated and $\int_\Omega d\Omega$ denotes integration over the Earth's surface. For the 1970 and 1978 jerks, $\hat{C} = -0.466$ which, assuming the jerks to be independent and the number of degrees of freedom n_f to be equal to the trace of the resolution matrix for the secular acceleration models, (≈ 50) has a 1.2×10^{-3} probability of occurring by chance using a two-tailed Student's t test. The quantity $t = \hat{C}\sqrt{\frac{n_f - 2}{1 - \hat{C}^2}}$ is taken as the sample t statistic (Kendall & Stuart, 1961). Of course the assumption of the independence of the jerks is flawed since they share the same data for the intervening period.

The 1983 jerk has an overall power half that of the 1978 event and its features are typically half the amplitude of those of the other jerks. Its correlation coefficient with the 1978 jerk is 0.04 and with the 1970 jerk is -0.21, which has a probability of approximately 0.15 of occurring by chance. As more data accumulate, through more observatories reporting data to the world data centres, a more thorough analysis of the apparent 1983 jerk should be possible but this preliminary investigation suggests that it is of much less significance than those of 1970 and 1978.

5.6 Conclusions.

The method of stochastic inversion has been used to determine models of the main field with a quadratic time–dependence for the epochs 1965.5, 1974.5, 1981.5 and 1986.5. These have been used to produce reliable models of the secular acceleration at these epochs and of the change in secular acceleration associated with the jerks of 1970, 1978 and 1983. It is believed that the resulting maps of the spatial distribution of the jerk of 1970 eliminate some spurious features that were present in previous maps and give a more realistic estimate of the strength of the supposed impulse. Another jerk occurring at about 1978, the spatial distribution of which has not previously been investigated,

has been shown to be of comparable power to that of 1970 and appears to be anti-correlated with it. The 1983 jerk is much weaker than the others and does not appear to be similar in its distribution. All three events, however, are of comparable strength to the secular acceleration itself. As the external field model AVDF91 is believed to remove the most significant contribution to the annual means from external sources it has been confirmed that the 1970 jerk, and now the 1978 and 1983 jerks, are real features of the field originating in the core. By comparison with the fit to the data of the BJ2 time–dependent field model, it has been shown that a sequence of field models with quadratic time–dependence is as effective at representing the observatory data. This leads to the hypothesis that the evolution of the core field on the decade time–scale could be adequately modelled by periods of constant secular acceleration punctuated by impulses in the third time–derivative. Whether the observed morphology of the jerks is consistent with an impulse in the third time–derivative of the field at the CMB will be addressed in Chapter 7.

Chapter 6

Geomagnetism and the rotation of the Earth

6.1 Introduction

In this chapter, supposed correlations between geomagnetic variations and one of the few other measurable geophysical parameters indicative of core dynamics, the rate of Earth rotation, are investigated. The observed period of the Earth's rotation, or "length of day" (LOD) is known to vary on a range of time–scales. More precisely, what is actually observable is the period of rotation of the crust and mantle. Of these observed variations, by far the largest are the so called "decade fluctuations", which are of the order of a few milli–seconds occurring over a period of 10 years or so. By conservation of angular momentum (AM), changes in the length of day must be accompanied by changes in the rotation rate of the core, atmosphere or oceans, or a change in the moment of inertia of the mantle and crust (including oceans and ice caps). Changes on shorter time–scales up to a year or two can for the most part be explained by changes in the angular momentum of the atmosphere and the mean bulk displacement of the oceans associated with the so called El Niño events (Lambeck, 1980; Mörner, 1989). Although a change in moment of inertia is favoured by certain authors (Mörner, 1989) to explain the decade fluctuations also, it is more widely accepted that changes in the rotation rate of the core are more plausible (Rochester, 1984; Hide, 1986). The question of how the necessary exchange
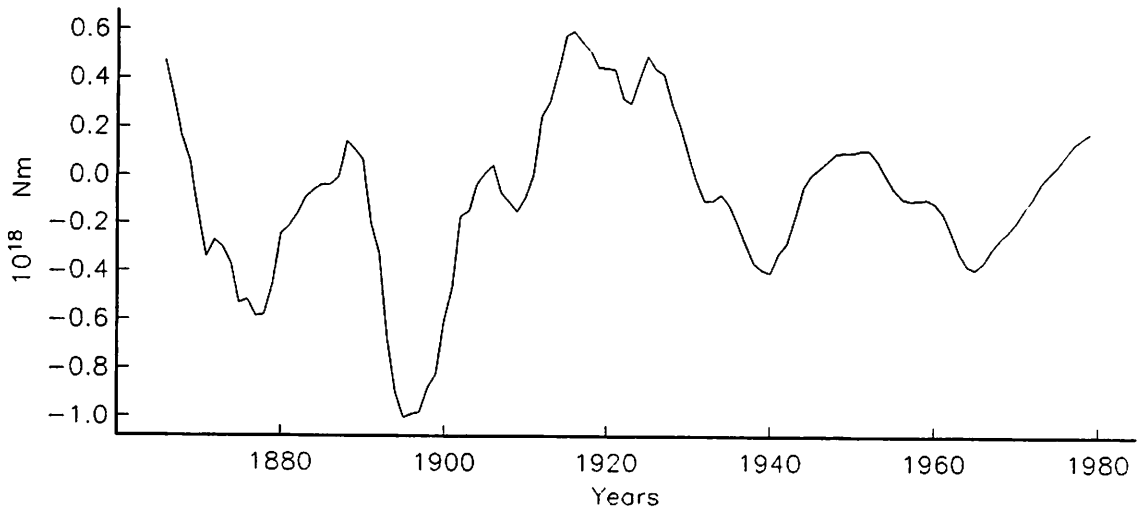
Figure 6.1: Torque that must act on the mantle to explain the decade fluctautions in the length of day based on the data of Morrison (1979) and McCarthy & Babcock (1986) (see §6.4.1).

of angular momentum between core and mantle occurs however, is still the subject of much current research (see eg. Aldridge *et al*, 1990). The primary objective here will be to consider the viability of electromagnetic (EM) coupling, in which electromagnetic forces exert a torque on the mantle (and the core necessarily), as a mechanism for the exchange of AM between the core and the mantle. Time–dependent EM torques will be computed using recent models of the geomagnetic field and flow at the top of the core and compared with the torque inferred from changes in Earth rotation. The torque that would be required to act on the the mantle to explain the decade fluctuations inferred from astronomical observations is shown in Figure 6.1.

6.2 Electromagnetic core–mantle coupling.

The broad scenario of the EM coupling mechanism is that with the core rotating more slowly than the mantle, as evidenced by the gradual westward drift of the magnetic field with respect to the Earth's surface (Bullard *et al*, 1950), the velocity disparity at the core–mantle boundary (CMB) gives rise to induced fields in the conducting mantle. Torques associated with these fields are believed to retard the rotation of the mantle (Rochester, 1960). Toroidal fields generated by convection in deeper, more rapidly ro-

tating regions of the core are believed to "leak" into the mantle giving rise to torques which counterbalance the retarding torque (eg. Stix & Roberts, 1984). Bullard *et al* (1950) considered the role of electromagnetic coupling associated with the axial dipole but dismissed it as an insufficient mediator in the exchange of angular momentum between core and mantle. However Rochester (1960) showed that the mantle torque is significantly increased by the inclusion of the effects of the non–dipole field and is of a sufficient order of magnitude to account for the decade fluctuations. Roden (1963) modified Rochester's 1960 uniformly conducting lower mantle model to a three-layer model and concluded that the order of magnitude of the EM torque is sufficient to account for the irregular fluctuations in LOD — most efficiently if high conductivity is concentrated toward the CMB. Stix & Roberts (1984) appear to have been the first to attempt to evaluate a time–dependent EM torque (see also Paulus & Stix, 1986). Using main field and secular variation (SV) models (truncated at spherical harmonic degree and orders 5 and 6) of Hodder (1981) as an approximation to the poloidal field at the CMB the torque associated with poloidal and toroidal fields induced in the mantle by advection of the main field was computed for a series of epochs this century. They concluded that the induced toroidal (field) torque exceeds the induced poloidal (field) torque by at least an order of magnitude. They also found the mean EM torque to be negative and 2 orders of magnitude larger than the mean LOD torque while the fluctuations of the torque are of a comparable order of magnitude to those related to the LOD. The spherically symmetric conductivity distribution they used was of the form

$$\sigma = \sigma_0 \left(\frac{r_c}{r} \right)^{\alpha} \tag{6.1}$$

where r is the radius, r_c is the radius of the CMB (assumed spherical) and σ_0 is the conductivity of the mantle at the CMB, in common with (eg.) McDonald (1957), Alldredge (1977b) and Stix (1982). Stix & Roberts (1984) arbitrarily chose $\alpha = 30$ and $\sigma_0 = 3000 Sm^{-1}$. Their results failed to show any close correspondence between the time–dependence of the computed and observed torques. This may in part be due to poorly determined and (perhaps) overly simplistic (zonal) models of core fluid velocity (which they determined using a simple SV misfit minimisation method) as well as the enhancement of errors in the field and SV models by downward continuation from the

surface to the CMB. However, more recent work has shown significant agreement between the LOD torque and the EM torque and will be discussed later (Paulus, 1986; Paulus & Stix, 1989).

6.2.1 A thin conducting layer at the base of the mantle.

The following formulation for the electromagnetic torque associated with a thin conducting layer was first suggested and outlined by Professor F. Busse to whom I am indebted. The expanded algebra and all the numerical formulation and computations however are my own work.

The result of some recent experiments in high pressure mineral physics suggest that the base of the mantle may consist of a highly reactive zone (Jeanloz, 1990), possibly the most chemically active region of the Earth (Jeanloz, 1991), in which the conductivity is extremely high, possibly even comparable to that of the core itself (Li & Jeanloz, 1987). Stevenson (1990) suggests that there may be infiltration of liquid iron into the mantle at the CMB interface which would significantly affect the conductivity of the lowermost mantle. It is thought that this may correspond in part with the seismologically distinct D'' layer at the base of the mantle, which is of the order $200km$ to $300km$ thick. In light of these ideas, it is interesting to consider what effect such a layer would have on the electro–magnetic interaction between the core and the mantle. Therefore, as a working model it is assumed that the mantle is an insulator except in a conducting layer, next to the CMB, of thickness δ. Magnetic diffusivity in the core is neglected.

In the following, let subscripts C and M relate to quantities in the core and in the conducting layer at the base of the mantle respectively. The boundary condition for the electric field at the CMB, assumed spherical of radius $r_C = 3485km$, reduces to

$$-\mathbf{r} \times ((\nabla \times \mathbf{r}\psi) \times \mathbf{B_C}) \quad = \quad \mathbf{r} \times (\eta_M \nabla \times \mathbf{B_M}) \tag{6.2}$$

where ψ is the toroidal stream function for the flow at the top of the core, η_M is the magnetic diffusivity of the conducting layer and $\mathbf{r}$ is a radially outward vector of length r. Poloidal and toroidal decompositions of $\mathbf{B_C}$ and $\mathbf{B_M}$,

$$\mathbf{B_M} \quad = \quad \nabla \times (\nabla \times \mathbf{r}S_M) + \nabla \times \mathbf{r}T_M \tag{6.3}$$

$$\mathbf{B_C} = \nabla \times (\nabla \times \mathbf{r} S_{\mathrm{C}}) + \nabla \times \mathbf{r} T_{\mathrm{C}} \tag{6.4}$$

(where S and T are poloidal and toroidal scalars respectively) can be substituted into (6.2), and $\mathbf{r}.\nabla\times$ applied to give

$$\eta_{\mathrm{M}} \mathbf{r}.\nabla \times (\mathbf{r} \times \nabla \times \nabla \times (\mathbf{r} T_{\mathrm{M}})) + \eta_{\mathrm{M}} \mathbf{r}.\nabla \times (\mathbf{r} \times \nabla \times \nabla \times \nabla \times (\mathbf{r} S_{\mathrm{M}}))$$

$$= -\mathbf{r}.\nabla \times [\mathbf{r} \times [(\nabla \times (\mathbf{r}\psi)) \times (\nabla \times \nabla \times (\mathbf{r} S_{\mathrm{C}}))] + \mathbf{r} \times [(\nabla \times (\mathbf{r}\psi)) \times (\nabla \times (\mathbf{r} T_{\mathrm{C}}))]] \tag{6.5}$$

at $r = r_{\mathrm{C}}$. As the toroidal field does not extend beyond the conducting region and is therefore not directly observable, it will be assumed that the only toroidal field present in the conducting layer is that generated by advection of the poloidal field by the toroidal flow at the top of the core.

It can be shown that

$$\mathbf{r} \times [(\nabla \times (\mathbf{r}\psi)) \times (\nabla \times (\mathbf{r} T_{\mathrm{C}}))] = 0 \tag{6.6}$$

(as toroidal flow does not advect toroidal field) which eliminates the second term in the RHS of (6.5). Also

$$\eta_{\mathrm{M}} \mathbf{r}.\nabla \times (\mathbf{r} \times \nabla \times \nabla \times (\mathbf{r} T_{\mathrm{M}})) = -\eta_{\mathrm{M}} \frac{\partial}{\partial r} (r L^2 T_{\mathrm{M}}), \tag{6.7}$$

$$-\mathbf{r}.\nabla \times (\mathbf{r} \times ((\nabla \times (\mathbf{r}\psi)) \times (\nabla \times \nabla \times (\mathbf{r} C_{\mathrm{M}})))) = r^2 \nabla_{\mathrm{H}}.(\nabla_{\mathrm{H}}\psi L^2 S_{\mathrm{C}}) \tag{6.8}$$

and

$$\eta_{\mathrm{M}} \mathbf{r}.\nabla \times (\mathbf{r} \times \nabla \times \nabla \times \nabla \times (\mathbf{r} S_{\mathrm{M}}) = 0 \tag{6.9}$$

where ∇_{H} is the horizontal part of the gradient operator and L^2 is related to the horizontal part of the Laplacian by $L^2 = -r^2 \nabla_{\mathrm{H}}^2$. Since $L^2 S_{\mathrm{M}} = L^2 S_{\mathrm{C}}$ (by continuity of the radial poloidal field across the boundary), equation (6.5) reduces to

$$\eta_{\mathrm{M}} \frac{\partial}{\partial r} (r L^2 T_{\mathrm{M}}) = -r^2 \nabla_{\mathrm{H}}.(\nabla_{\mathrm{H}}\psi L^2 S_{\mathrm{M}}) \tag{6.10}$$

at $r = r_{\mathrm{C}}$. To solve for T_{M} within the layer, expand the radial dependence of T_{M} in a Taylor series about $r = r_{\mathrm{C}}$ giving

$$T_{\mathrm{M}}(r) \approx T_{\mathrm{M}}(r_{\mathrm{C}}) + \frac{\partial T_{\mathrm{M}}}{\partial r}\bigg|_{r=r_{\mathrm{C}}} (r - r_{\mathrm{C}}) + \mathrm{O}(\delta^2) \tag{6.11}$$

This linear approximation is reasonable if $\delta \ll r_C$, and will be adopted henceforth. At the upper boundary of the conducting layer, at $r = r_C + \delta$, the toroidal field must vanish and hence, using (6.11),

$$0 = T_M(r_C + \delta) = T_M(r_C) + \left. \frac{\partial T_M}{\partial r} \right|_{r=r_C} (r_C + \delta - r_C)$$

$$\Rightarrow T_M(r_C) = - \left. \frac{\partial T_M}{\partial r} \right|_{r=r_C} \delta \tag{6.12}$$

Substitution of (6.12) into (6.11) followed by application of the L^2 operator leads to

$$L^2 T_M = - \left. \frac{\partial (L^2 T_M)}{\partial r} \right|_{r=r_C} \delta + \left. \frac{\partial (L^2 T_M)}{\partial r} \right|_{r=r_C} (r - r_C) \tag{6.13}$$

Finally, expanding the r derivative in (6.10) and substituting into (6.13) results in

$$L^2 T_M = (r - \delta - r_C) \left[-\frac{1}{\eta_M} G - \frac{L^2 T_M}{r_C} \right]_{r=r_C} \tag{6.14}$$

where

$$G = \left[r \nabla_H \cdot (\nabla_H \psi L^2 S_M) \right]_{r=r_C} \tag{6.15}$$

Since $|r - r_C - \delta| \le \delta$ and $\frac{\delta}{r_C} \ll 1$, a reasonable approximation to equation (6.14) is

$$L^2 T_M = -(r - r_C - \delta) \frac{G}{\eta_M} \tag{6.16}$$

which is the final approximate solution for the toroidal field in the conducting layer.

6.2.2 Formulation of the torque integral.

The torque Γ about the Earth's rotational axis (in the unit direction $\hat{k}$) can be expressed as

$$\mu \Gamma = \int \int \int_V (\hat{k} \times r) \cdot [(\nabla \times B) \times B] dV \tag{6.17}$$

where V is the volume of the conducting region of the mantle and μ the permeability, taken as that of free space. Thus, in the case of the thin layer under consideration here, the axial torque arising from the induced toroidal field can be written as (see for example Gubbins & Roberts, 1987, p62; Rochester, 1960)

$$\Gamma = \frac{\delta}{\eta_M \mu} \int \int_\Omega \left(\frac{\partial (L^{-2} G)}{\partial \theta} L^2 S_M \right)\Bigg|_{r=c} \sin \theta d\Omega \tag{6.18}$$

where $\int \int_\Omega d\Omega$ denotes integration over the core–mantle boundary. Let

$$\sum_{n_i,m_i}$$

denote the double summation

$$\sum_{n_i=1}^{N_i} \sum_{m_i=-n_i}^{+n_i}$$

Initially, assume N_i is infinite; later, finite values will need to be adopted for numerical computation. Expand G, ψ and S_M (at $r = r_C$) as series of fully normalised complex spherical harmonics Y_n^m:

$$G = \sum_{n_1,m_1} G_{n_1}^{m_1} Y_{n_1}^{m_1}. \qquad (6.19)$$

$$\psi = \sum_{n_2,m_2} \psi_{n_2}^{m_2} Y_{n_2}^{m_2}, \qquad (6.20)$$

and

$$S_M = r_C \sum_{n_3,m_3} S_{n_3}^{m_3} Y_{n_3}^{m_3}. \qquad (6.21)$$

Y_n^m are related to the Schmidt quasi–normalised associated Legendre functions P_n^m by

$$Y_n^m = \left(\frac{2n+1}{4\pi}\right)^{\frac{1}{2}} e^{im\phi} P_n^m, \qquad m \geq 0 \qquad (6.22)$$

which satisfy the orthogonality relation

$$\langle Y_n^m (Y_p^q)^* \rangle = 1 \qquad (6.23)$$

when $n = p$ and $m = q$, where $\langle . \rangle$ denotes integration over the unit sphere and $*$ denotes complex conjugate. Also define $Y_n^{-m} = (-1)^m (Y_n^m)^*$ (see eg. Winch, 1974; Jackson & Bloxham, 1991; Phinney & Burridge, 1973). Substitution of (6.19), (6.20) and (6.21) into equation (6.15) results in

$$\sum_{n_1,m_1} G_{n_1}^{m_1} Y_{n_1}^{m_1} = r_C^2 \sum_{n_2,m_2} \sum_{n_3,m_3} \psi_{n_2}^{m_2} S_{n_3}^{m_3} \nabla_H (\nabla_H Y_{n_2}^{m_2} L^2 Y_{n_3}^{m_3}) \qquad (6.24)$$

Multiplication by $(Y_{n_1}^{m_1})^*$ followed by integration over the unit sphere results in

$$G_{n_1}^{m_1} = r_C^2 \sum_{n_2,m_2} \sum_{n_3,m_3} \psi_{n_2}^{m_2} S_{n_3}^{m_3} \langle \nabla_H (\nabla_H Y_{n_2}^{m_2} L^2 Y_{n_3}^{m_3})(Y_{n_1}^{m_1})^* \rangle \qquad (6.25)$$

by virtue of the orthogonality relation (6.23). Now,

$$\nabla_H.(\nabla_H Y_{n_2}^{m_2} L^2 Y_{n_3}^{m_3}) = n_3(n_3+1)[(\nabla_H Y_{n_2}^{m_2}).(\nabla_H Y_{n_3}^{m_3}) - \frac{1}{r^2}n_2(n_2+1)Y_{n_2}^{m_2}Y_{n_3}^{m_3}] \quad (6.26)$$

which reduces equation (6.25) to

$$G_{n_1}^{m_1} = r_c^2 \sum_{n_2,m_2} \sum_{n_3,m_3} \psi_{n_2}^{m_2} S_{n_3}^{m_3} \langle n_3(n_3+1) \left[((\nabla_H Y_{n_2}^{m_2}).(\nabla_H Y_{n_3}^{m_3}))(Y_{n_1}^{m_1})^* \right.$$
$$\left. -\frac{1}{r_c^2}n_2(n_2+1)(Y_{n_1}^{m_1})^* Y_{n_2}^{m_2} Y_{n_3}^{m_3} \right] \rangle \quad (6.27)$$

Use of the identity (which may be demonstrated using integration by parts)

$$\langle (Y_{n_1}^{m_1})^*(\nabla_H Y_{n_2}^{m_2}).(\nabla_H Y_{n_3}^{m_3}) \rangle \equiv \frac{1}{2r^2}[n_2(n_2+1) + n_3(n_3+1) - n_1(n_1+1)]G_T \quad (6.28)$$

where G_T is the Gaunt integral $\langle (Y_{n_1}^{m_1})^* Y_{n_2}^{m_2} Y_{n_3}^{m_3} \rangle$ (see eg. Winch, 1974), results in the simpler form

$$G_{n_1}^{m_1} = \frac{1}{2} \sum_{n_2,m_2} \sum_{n_3,m_3} \psi_{n_2}^{m_2} S_{n_3}^{m_3} n_3(n_3+1)[n_3(n_3+1) - n_1(n_1+1) - n_2(n_2+1)]G_T. \quad (6.29)$$

Thus G can be evaluated given ψ and S_M. The torque can now be expressed in a form in which it may readily be evaluated numerically. Noting that

$$\sin\theta \frac{\partial Y_n^m}{\partial \theta} = n \left[\frac{(n+m+1)(n-m+1)}{(2n+1)(2n+3)} \right]^{\frac{1}{2}} Y_{n+1}^m$$
$$-(n+1) \left[\frac{(n+m)(n-m)}{(2n+1)(2n-1)} \right]^{\frac{1}{2}} Y_{n-1}^m \quad (6.30)$$

(eg. Chapman & Bartels, 1940) and $L^2 Y_n^m = n(n+1)Y_n^m$, substitution of (6.19) and (6.21) into (6.18) gives

$$\Gamma = \frac{\delta}{\eta_M \mu} \int \int_\Omega \sum_{n_1,m_1} \left\{ n_1 \left[\frac{(n_1+m_1+1)(n_1-m_1+1)}{(2n_1+1)(2n_1+3)} \right]^{\frac{1}{2}} Y_{n_1+1}^{m_1} \right.$$
$$\left. -(n_1+1) \left[\frac{(n_1+m_1)(n_1-m_1)}{(2n_1+1)(2n_1-1)} \right]^{\frac{1}{2}} Y_{n_1-1}^{m_1} \right\} G_{n_1}^{m_1} \frac{1}{n_1(n_1+1)}$$
$$\times c \sum_{n_3,m_3} \{ n_3(n_3+1)Y_{n_3}^{m_3} S_{n_3}^{m_3} \} \, d\Omega \quad (6.31)$$

Again utilising the orthogonality of the spherical harmonics, this expression finally reduces to

$$\Gamma = \delta\sigma_M r_c^2 \sum_{n_3,m_3} S_{n_3}^{m_3} n_3(n_3+1) \left\{ \frac{1}{n_3} G_{n_3-1}^{-m_3} \left[\frac{(n_3-m_3)(n_3+m_3)}{(2n_3-1)(2n_3+1)} \right]^{\frac{1}{2}} \right.$$

$$-\frac{1}{(n_3+1)}G^{-m_3}_{n_3+1}\left[\frac{(n_3+m_3+1)(n_3-m_3+1)}{(2n_3+3)(2n_3+1)}\right]^{\frac{1}{2}}\Bigg\} \tag{6.32}$$

where $\sigma_M = (\eta_M\mu)^{-1}$ is the conductivity of the layer and $G^{m_3}_0 = 0$ for all m_3. Note that the torque is directly proportional to the conductance of the layer ($\delta\sigma_M$).

To evaluate the electromagnetic torque, recent results from geomagnetic field modelling and core flow calculation will be used. In such work it is common practice to assume that the mantle is an insulator and so for the purpose of defining the poloidal field at the CMB and the flow at the top of the core this assumption will be temporarily adopted. The complex spherical harmonic coefficients for the poloidal scalar at the CMB can be related to the real Schmidt quasi–normalised cosine/sine coefficients g^m_n and h^m_n for the geomagnetic field potential at the surface by

$$S^{m_3}_{n_3} = \left(\frac{r_s}{r_c}\right)^{n_3+2}\frac{1}{n_3}\left(\frac{4\pi}{2n_3+1}\right)^{\frac{1}{2}}\times\begin{cases}\frac{1}{2}(g^{m_3}_{n_3}-ih^{m_3}_{n_3}) & m_3 > 0 \\ g^0_{n_3} & m_3 = 0 \\ \frac{1}{2}(-1)^{m_3}(g^{-m_3}_{n_3}+ih^{-m_3}_{n_3}) & m_3 < 0\end{cases} \tag{6.33}$$

where r_s is the radius of the Earth's surface. Similarily the complex flow coefficients are related to the real Schmidt flow coefficients $_ct^m_n$ and $_st^m_n$ (cosine/sine) at the CMB by

$$\psi^{m_2}_{n_2} = \left(\frac{4\pi}{2n_2+1}\right)^{\frac{1}{2}}\times\begin{cases}\frac{1}{2}(_ct^{m_2}_{n_2}-i_st^{m_2}_{n_2}) & m_2 > 0 \\ _ct^0_{n_2} & m_2 = 0 \\ \frac{1}{2}(-1)^{m_2}(_ct^{-m_2}_{n_2}+i_st^{-m_2}_{n_2}) & m_2 < 0\end{cases} \tag{6.34}$$

Numerical implementation

The above scheme was implemented in double precision FORTRAN77 with the Gaunt integrals computed in terms of the Wigner 3–j coefficients (see eg. Edmonds, 1957). As expression (6.15) for G is identical (within a factor $r_c(l+1)$) to the expression for the potential of the secular variation produced by advection by a poloidal flow with defining scalar ψ (Whaler, 1986), it was possible to verify the coefficients of G (equation (6.19)) against independently developed and verified code (K. A. Whaler, personal communication, 1991). The torques were also verified using a single precision implementation of the scalar spherical transform method, closely related to the vector spherical transform method of Lloyd & Gubbins (1990) (D. Gubbins, personal communication, 1991). This

gave 6 significant figure agreement for the coefficients of G and 5 significant figures for the torques.

6.2.3 Field and flow at the core–mantle boundary

For the magnetic field in the torque calculation single epoch "snap–shots" of the geomagnetic field at the Earth's surface were taken from an unpublished time–dependent model of J. Bloxham and A. Jackson for the period 1840 to 1980 (to be referred to here as BJ1). This was derived by a very similar method to that of Bloxham & Jackson (1991b) (Jackson, personal commmunication, 1991) with a temporal representation in B–splines. This gives a much improved temporal fit over earlier time–dependent models (Bloxham, 1987; Bloxham & Jackson, 1989) and eliminates end effects (A. Jackson, personal communication, 1991). The stochastic inversion method used also ensures spatial convergence of the field at the CMB which represents a significant improvement over more traditional methods, for example those involving an arbitrary truncation of the spherical harmonic expansion. Previous attempts to calculate the time dependent electro–magnetic torque (Stix & Roberts, 1984; Paulus & Stix, 1986), have used field models which are inappropriate for downward continuation.

For the evaluation of the torque, estimates of the toroidal part of the flow at the top of the core are required. The problem of inferring the flow at the top of the core from the secular variation has been the focus of much research in recent years. In such work it is usually assumed that the conductivity of the core is sufficiently high that diffusion in the core can be neglected and so field lines are effectively frozen in to the liquid and act as a tracer; this is commonly known as the *frozen–flux hypothesis* (Roberts & Scott, 1965). The inherent non–uniqueness of the problem (Backus, 1968) can at least be partially surmounted through the imposition of prior physical assumptions concerning the flow. The most commonly investigated of these — steady flow, geostrophic flow and toroidal flow (Voorhies & Backus, 1985; Voorhies, 1986; Whaler, 1991; Jackson & Bloxham, 1991; LeMouël, 1984; Lloyd & Gubbins, 1990) have led to improved determinations of the flows. A suite of flow models derived under the assumption of tangential geostrophy were used here (Jackson & Bloxham, 1990). Although the models include toroidal, poloidal and shear coefficients, only the toroidal coefficients are required here. The flows

were of maximum degree and order 14 and were available for epochs 1900 to 1980 at 5 year intervals.

6.3 Results

Calculations were carried out using a layer of conductance $10^8 S$, which could for example be a layer of thickness $\delta = 100 km$ thick with a conductivity of $\sigma_M = 1000 Sm^{-1}$. By virtue of the particular formulation used here the torque depends linearly on the conductance $\delta \sigma_M$. These results are shown in Figure 6.2 which also shows how the time dependent torque converges with increasing harmonic degree of flow included. It can be seen that the torque is well converged by about degree 3 or 4 for the flow. The computed torque shows a significant increasing trend as well as fluctuations (Figure 6.2(a)).

6.4 Discussion

6.4.1 Astronomical observations of Earth rotation.

From astronomically inferred variations in the period of the Earth's rotation, Morrison (1979) found that $10^{18} Nm$ can be considered as an approximate upper bound on the torque acting upon the mantle associated with the decade fluctuations. A thorough analysis of occultation data was performed, resulting in a time–series of values of ΔT, the deviation of the instantaneous period of rotation from its mean or excess length of day, for the period 1860 to 1978. This can then be scaled to give $\Delta \theta$, the sidereal displacement angle of the Greenwich meridian. The associated torque can then be calculated from the second time derivative of this quantity. Morrison evaluated this as the second derivative of a quadratic fitted to his data over an 11 year window. This has been repeated here though using the estimated data errors to perform a weighted quadratic fit. This modification was found to make almost no difference to the resulting curves although it allowed errors based on the weighted misfit to be derived. Morrison's data were first supplemented by post–1978 data from McCarthy & Babcock (1986), whose results for the excess length of day essentially reproduce those of Morrison (1979) and Stephenson & Morrison (1984) prior to this date. However, for consistency in the weighted fit, the
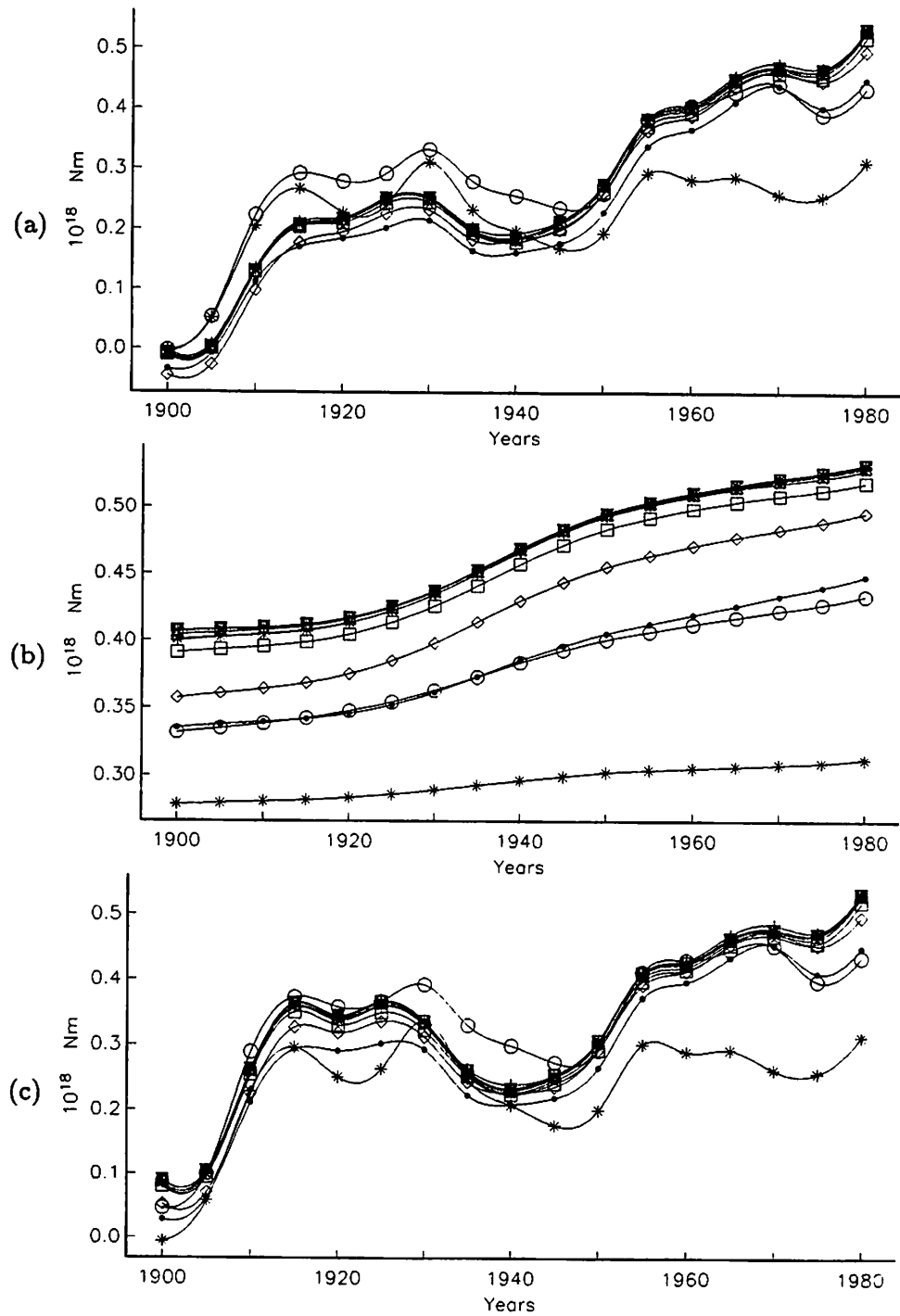
Figure 6.2: Time–dependent torque based on toroidal part of Jackson & Bloxham (1990) geostrophic flows and field models derived from spline model BJ1 (see §6.2.3) for epochs 1900 to 1980 at 5 year intervals using (a) field and flow models for each epoch, (b) field models from each epoch and flow model for 1980, (c) field model for 1980 and flow models for each epoch. Curves are interpolated using splines. In each plot, different symbols are for increasing maximum degree of the flows included in the torque calculation. (maximum degrees 1–4 are $*$, $\circ$, $\bullet$ and $\diamond$ respectively.) Torque units are $10^{18}Nm$.

errors of Morrison (1979) are used rather than those of McCarthy & Babcock. The resulting LOD torque is shown in Figure 6.1.

6.4.2 The case for electromagnetic coupling.

The visual agreement between the EM torque (Figure 6.2(a)) using the full toroidal part of the geostrophic flows and the LOD torque (Figure 6.1) is poor, even allowing for the significant linear trend in the former. As the fluctuations in the torque arise primarily from the time–dependence of the flow, this disagreement may arise from ambiguity in the flow models. To test this, consider the significant increase in the computed torque over the period 1950 to 1980 (Figure 6.2(a)). Now consider the plots of the toroidal part of the geostrophic flows for epochs 1950, 1965 and 1980 (Figure 6.3). The main feature that develops in these flows over the period 1950 to 1980 is the increase in predominantly non–zonal flow beneath Siberia, Central Asia and the Arctic Sea north of Alaska, and so it is likely that this part of the flow is responsible for the changes in the EM torque over this period. However these areas correspond to regions in which the geostrophic constraint does not completely resolve the non-uniqueness of the velocities (see eg. Backus & LeMouël, 1986; Jackson & Bloxham, 1991). Such regions account for som 41% of the core surface (Bloxham & Jackson, 1991a). As these features of the flow are primarily non–zonal, the torques were recomputed, again for a layer of conductance $10^8 S$, this time using only the zonal toroidal coefficients of the geostrophic flows. Simultaneous fits to the EM torques by a linear trend plus a scalar multiple of the LOD torques for the period 1945–1978 (Figure 6.4(a)) and 1861–1978 (Figure 6.4(b)) for phase shifts between the EM torque and the LOD torque ranging from -30 to +20 years were performed. (There were insufficient EM torques to do this just for the post–1955 era of atomic timescale and proton magnetometers.) In both cases the optimal fit was found for a 6 year lag of the EM torque after the LOD torque. For the former period the fit of the EM torques lies mostly within the 1 standard error limits of the LOD data, but for both cases the fit is reasonable for the whole 1894–1974 period. The statistics are given in Table 6.1.

The agreement between the EM and LOD torques in Figure 6.4 suggests that EM coupling may be an important mechanism by which angular momentum is transferred

0.5℃ℇ+02
ΜΑΧΙΜΥΜ ΛΕCΤΟR   km/yr
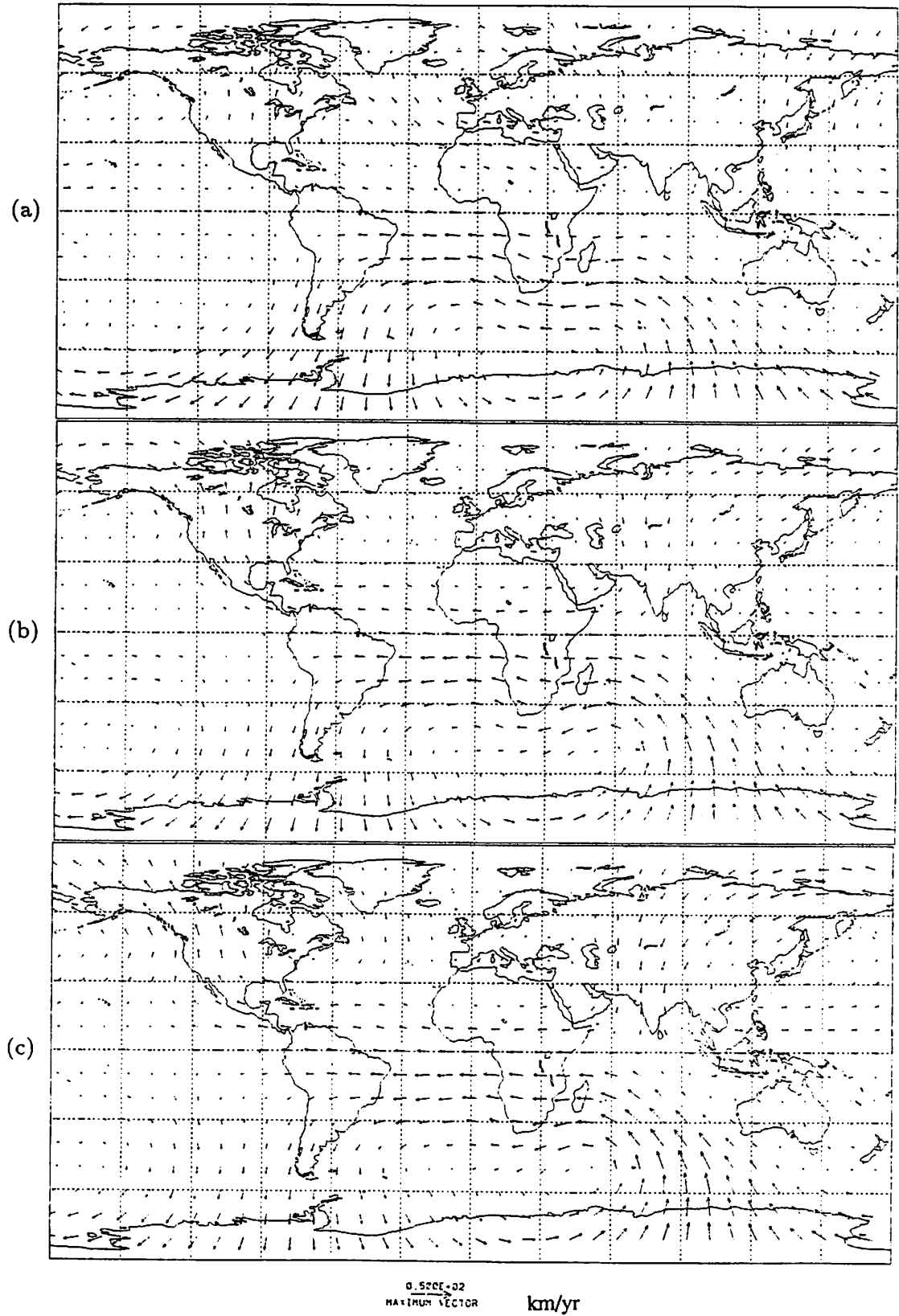
Figure 6.3: Toroidal part of the geostrophic flows of Jackson & Bloxham (1990) for epochs (a) 1950, (b) 1965, (c) 1980. Grid spacing is 30°. Note the marked increase in flow beneath Siberia, Central Asia and Arctic Canada from 1950 to 1980.
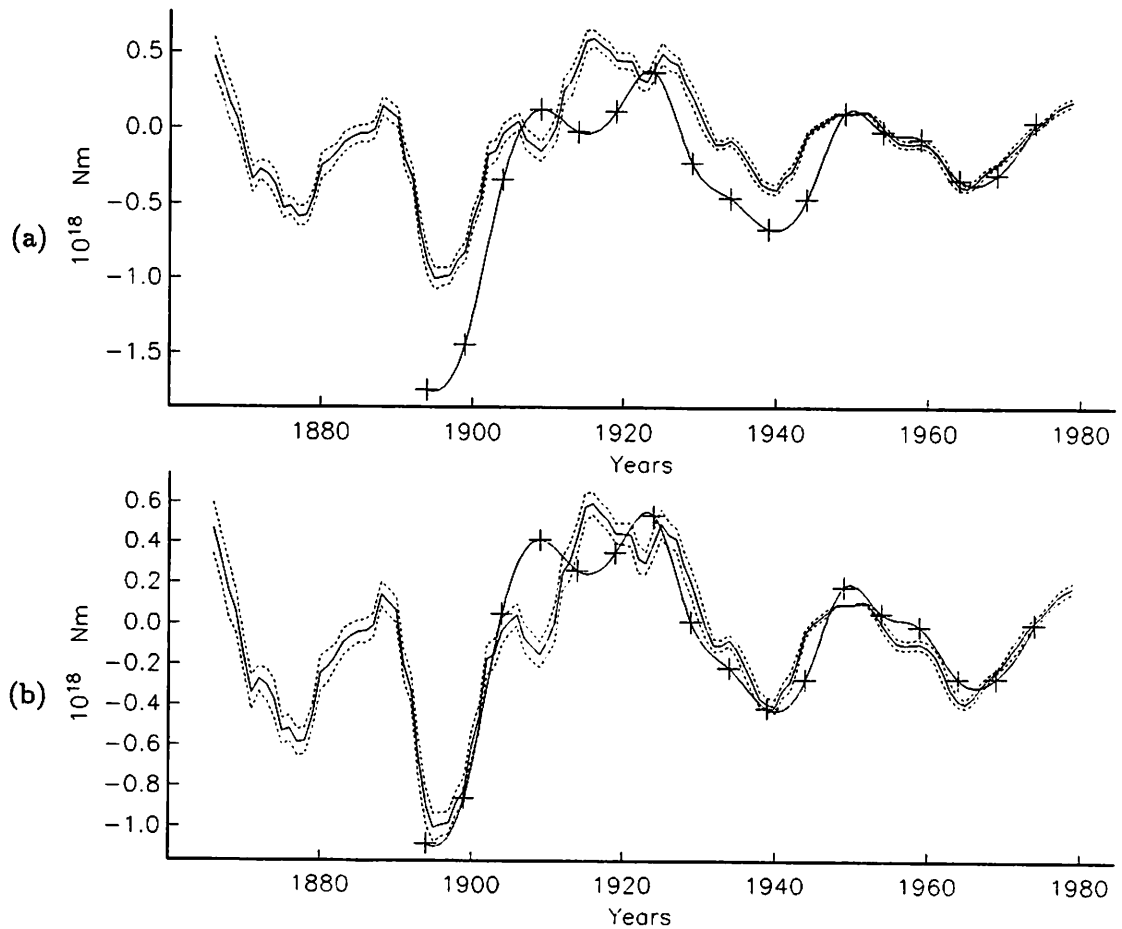
Figure 6.4: Time–dependent electromagnetic torque based on zonal toroidal part of geostrophic flows (see §6.2.3) all taken to degree and order 14. Electromagnetic torque has been scaled, linearly detrended, offset and phase shifted by -6 years. Its values are marked by + and interpolated with cubic-splines. Comparison is with the torque required to explain the decade fluctuations in the LOD (solid line with 1 standard error envelope (dashed lines)) as derived from the data of Morrison (1979) (1861–1978) and McCarthy & Babcock (1986) (1979–1984) (see §6.4.2). Detrending etc. computed for the time periods (a) 1945–1978 and (b) 1894–1978 (see §6.3). Torque units are $10^{18}Nm$.

between core and mantle. The scale factor required to make the decade fluctuations in the torques agree implies a layer at the base of the mantle of conductance $(6.67 \pm 0.88) \times 10^{8}Sm^{-1}$ when the torques are compared over the period 1894 to 1974. The implications of this for the conductivity of the lower mantle will be considered in Chapter 7. The offset and trend need some explanation. Stix & Roberts (1984) found their EM torque to

Table 6.1: Results of a simultaneous least squares fit of the EM torques from zonal flows to the LOD torques plus a linear trend, for (n) epochs (a) $1945,\ldots,1980$ and (b) $1900,\ldots,1980$ with the EM torques phase shifted by -6 years. When the EM torque for a layer of conductance $10^8 Sm^{-1}$ is multiplied by the scale factor, and the trend and offset removed, the result fits the LOD torque with the indicated misfit over the n epochs. (See Figure 6.4.)

	n	Misfit	Scale factor	Offset	Trend
Units	—	$10^{18} Nm$	—	$10^{18} Nm$	$10^{18} Nm/yr$
(a)	6	0.007	7.88±1.22	1.36±0.28	0.014±0.004
(b)	17	0.030	6.67±0.88	0.76±0.14	0.017±0.003

have a mean value of $-1.5 \times 10^{18} Nm$ and suggested that in reality this may be balanced by the couple due to "leakage" of toroidal flux from the core into the mantle, which has not been accounted for in the present work. This argument rests on the supposition that the toroidal field in the core is generated by motions of the deeper core with a longer characteristic time–scale than the free stream at the top of the core. The presence of the significant trend amounting to $\sim 0.7 \times 10^{18} Nm$ in 50 years is a little more surprising. This may well result from the rather bold assumption used earlier that the poloidal field at the Earth's surface may be downward continued to the base of the mantle assuming the mantle to be insulating. This crude approximation could perhaps be refined and would be worth future investigation. Paulus & Stix (1989) used the Fourier transform method to solve the induction equation for the magnetic field in the mantle and arrived at a torque (using zonal flows) which gave good agreement (with no trend) with the LOD torque though requiring a -18 year phase shift for the EM torque. Their Figure 5 is reproduced in Figure 6.5. They used a power law conductivity distribution of the form (6.1) with $\sigma_0 = 600 Sm^{-1}$ and $\alpha = 0.5$, a rather "flat" conductivity distribution.

6.4.3 Alternative coupling mechanisms

In addition to EM coupling, "topographic" coupling, arising from pressure forces acting on departures from spherical (or more precisely ellipsoidal) symmetry on the CMB, and "viscous" coupling arising from viscous forces acting between core and mantle are commonly considered as agents of angular momentum transfer. The latter mechanism
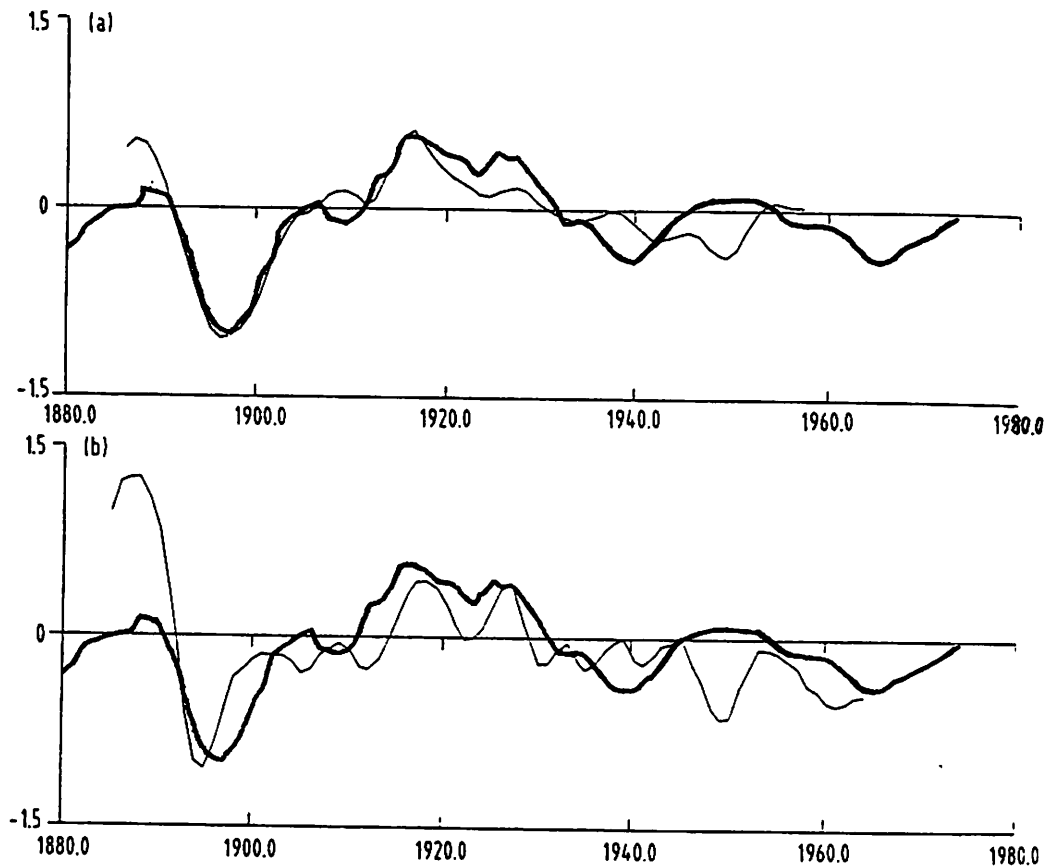
Figure 6.5: The torque required to account for the length of day fluctuations (Morrison, 1979; dark curves) and the EM torque of Paulus & Stix (1989) shifted 18 years into the past. Units are $10^{18}Nm$. EM torques were calculated using field coefficients supplied to these authors by (a) D. R. Barraclough and (b) R. A. Langel. (Personal communications.) Reproduced from Paulus & Stix (1989)

is usually considered to be too weak, in the case of the Earth, to account for the observations and most investigations have concentrated on the former (eg. Hide, 1989; R. Hide in Aldridge *et al*, 1990). Topographic coupling has excited much recent interest with the emergence of seismological evidence for significant CMB topography ranging from about $10km$ peak to trough amplitude (Morelli & Dziewonski, 1987) to $20km$ peak to trough (Creager & Jordan, 1986). Although Jault & LeMouël (1989) consider that topographic coupling is a good candidate mechanism they also conclude that it may be difficult to compute even given more precise knowledge of the CMB topography and flow at the top of the core. Using large scale features of the flow and topography alone, Jault & LeMouël (1989) found the topographic torque to be 2 orders of magnitude too large to be compatible with LOD fluctuations using the topography model of Morelli & Dziewonski (1987) and also concluded that smaller scale features would contribute significantly to the torque. There is however significant uncertainty as to the true magnitude of the CMB topography: Neuberg & Wahr (1991) have, for example, recently argued that such topography may be limited to 2–$3km$ on lateral length scales up to $400km$. Furthermore Gwinn *et al* (1986) showed that the deviation from hydrostatic equilibrium can be represented by a P_2^0 harmonic with a peak to trough amplitude of $490 \pm 110m$, which is an order of magnitude smaller than that of Morrelli & Dziewonski (1987).

6.4.4 Angular momentum budget.

Besides the question of the coupling mechanism between core and mantle, the total angular momentum (AM) of the core–mantle system must be preserved. Vestine & Kahle (1968) found that by assuming that the exchange of AM is restricted to the upper $200km$ of the core, reasonable agreement between the observed drift of the eccentric dipole and that inferred from the LOD fluctuations could be obtained. It was found that the observed eccentric dipole drift lags that inferred from LOD by about 5 years (see Figure 6.6), in agreement with the lag found here. Jault *et al* (1988) recently derived a simple expression for the changes in the AM of the core using estimated surficial velocity fields computed under the assumption that the flow is tangentially geostrophic and the core is a perfect conductor. They found some agreement between the changes
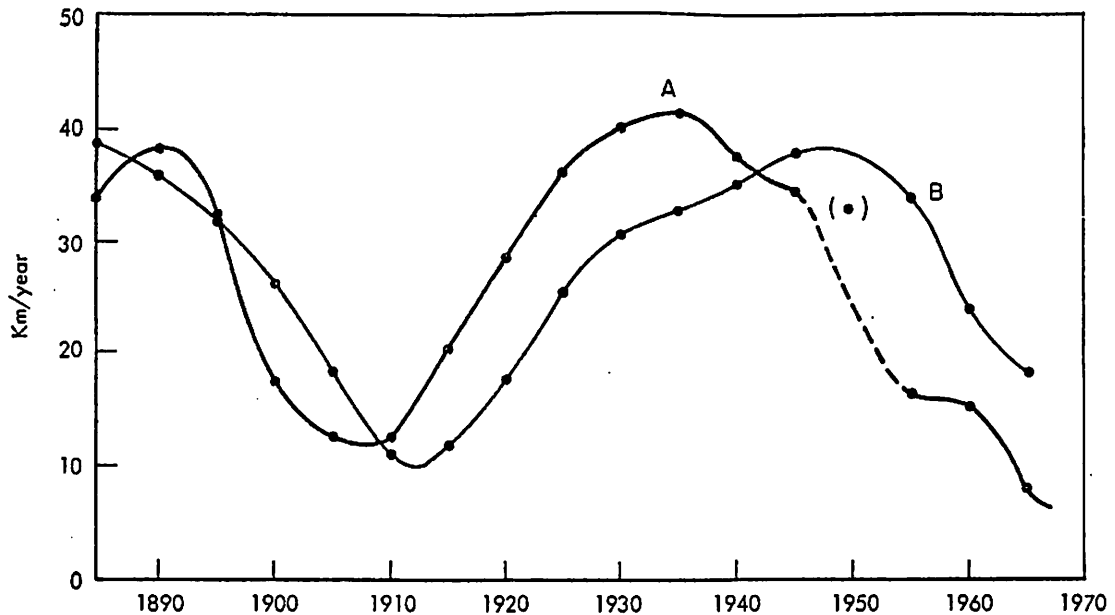
Figure 6.6: Westward drift velocity at the surface of the Earth from A, change in angular momentum of outer 200km layer of core necessary to balance LOD change, and B, observed eccentric dipole motion. Figure 4 of Vestine & Kahle (1968).

LOD over the period 1969–1985 although the AM is a rather smooth function of time over this period. Jault et al (1988) also claim reasonable agreement prior to 1970 but do not show it. They also find no lag between the geomagnetically and LOD inferred AM. This computation was also made by Jackson (1989), using geostrophic flows he derived independently, for the whole of the 20th century, who found qualitative agreement with LOD fluctuations with a lag of geomagnetically inferred changes between 5 and 25 years after LOD changes (Jackson's (1989) Figure 6.14). More recently, Jackson & Bloxham (1990) and Jackson et al (1991) find reasonable agreement though are unable to determine whether geomagnetically predicted LOD leads or lags the actual LOD.

6.5 Conclusions

It has been demonstrated that, assuming the existence of a thin conducting layer at the base of the mantle, the electromagnetic torque associated with induced toroidal fields

6.5   Conclusions

It has been demonstrated that, assuming the existence of a thin conducting layer at the base of the mantle, the electromagnetic torque associated with induced toroidal fields arising from advection of poloidal field by toroidal core flow can be calculated. When computed for a series of epochs this century for a layer of approximate conductance $6.7 \pm 0.9 \times 10^8 S$, the resulting time–dependent torque agrees well over an 80 year period with that inferred from fluctuations in the length of day. The electromagnetic and length of day torques are out of phase by 6 years with the former lagging behind the latter. On the assumption that the electromagnetic torque is solely responsible for the decade fluctuations, useful constraints can be placed on the conductivity distribution in the lower mantle as will be seen in Chapter 7.

Chapter 7

The electrical conductivity of the lower mantle

7.1 Introduction

As was pointed out in Chapter 1 our understanding of the (electrical) conductivity of the mantle and its lower regions in particular (below about $1000km$ or so) is very poor. The purpose of this chapter is to review *briefly*, current knowledge (primarily from geomagnetic evidence) of lower mantle conductivity and to advance some suggestions and supporting evidence pertinent to the conductivity distribution. In particular the implications of the work in Chapters 5 and 6 will be discussed. For the most part, conductivity distributions with spherical symmetry will be considered, as even with this approximation our knowledge is imprecise and we are some way from being able to discern lateral heterogeneities in the lower mantle, although their possible existence will be briefly investigated and discussed.

Unlike upper mantle conductivity, discussed in Chapter 3, that of the lower mantle is beyond the reach of induction studies based on externally induced field variations, with a limit of around $1000km$ depth being the norm (see eg. Parkinson & Hutton, 1989), although Achache *et al* (1981) used data in the period range 4 days to 11 years to obtain conductivity estimates down to $2000km$. Instead, estimates have relied primarily, though not exclusively, upon consideration of the propagation of the secular variation through

the mantle. Recent experiments in mineral physics at high temperatures and pressures for example (see eg. Knittle & Jeanloz, 1991) suggest that the base of the mantle could have an electrical conductivity as high as the core itself (currently accepted to be of the order $5 \times 10^5 Sm^{-1}$ (Melchior, 1986)).

McDonald (1957) used a conductivity distribution of the form

$$\sigma(r) = \sigma_0 \left(\frac{r_c}{r}\right)^\alpha \tag{7.1}$$

(as per equation (6.1)) where $r_c = 3485 km$ is the radius of the core. McDonald concluded $\sigma_0 = 223 Sm^{-1}$ and $\alpha = 5.1$ as a best estimate for this profile based on the assumption that the time–averaged spatial spectrum of the magnetic field at the core–mantle boundary (CMB) is white. This form of conductivity distribution has been used by many authors since, primarily it seems for mathematical convenience. Table 7.1 summarises a selection of these models. Alldredge (1977b) derived a conductivity profile with $\alpha = 25$ and $\sigma_0 = 10^5 Sm^{-1}$, a value 3 orders of magnitude higher than McDonald's estimate. Alldredge's main reason for choosing these particular parameters out of several combinations that could have explained his results equally well was the requirement that

Table 7.1: Summary of the various lower mantle electrical conductivity distributions considered in this chapter.
(Abbreviations: SV, secular variation; EM, electromagnetic; CM, core–mantle; MHD, magnetohydrodynamic.)

Power law profile					
Authors	$r_{min}(km)$	$r_{max}(km)$	$\sigma_0(Sm^{-1})$	α	Method
Alldredge (1977b)	3485	5371	100000	25.0	15/25 year waves
Backus (1983)	3485	5731	3000	11.3	1969/70 jerk
Courtillot et al (1984)	3485	5731	1000	19.0	1969/70 jerk
Kolomiytseva (1972)	3485	6371	710000	30.0	60 year wave
McDonald (1957)	3485	5671	223	5.1	SV spectrum
Paulus & Stix (1989)	3485	5485	600	0.5	EM CM coupling
Stix & Roberts (1984)	3485	5485	3000	30.0	EM CM coupling
Slab/Layered profile					
Achache et al (1980)	3485	5485	100	—	1969/70 jerk
Currie (1968)	3485	5485	200	—	MHD turbulence
Ducruix et al (1980)	3485	3871	100	—	1969/70 jerk
	3871	4871	30	—	
	4871	5871	1	—	

the profile match that of Banks (1969) for the upper mantle at about $1000km$. However there is no clear physical reason why such a functional form should pertain to any particular part of the mantle let alone the whole of the mantle below $600km$. Based on the assumption that all observed geomagnetic variations with periods less than 13 years originate externally to the Earth, Alldredge took advantage of apparent periodicities of 15 and 25 years (Alldredge, 1977a) to derive his conductivity distribution by assuming these originate in the core with equal amplitude. This bold assumption is as arbitrary as the "white field spectrum" assumption of McDonald (1957) which Alldredge (1977b) roundly criticises. Alldredge's (1976, 1977a,b) methods of analysis and conclusions were themselves criticised (McLeod, 1982; Courtillot & LeMouël, 1979) thus casting some doubt on Alldredge's conductivity estimates. Kolomiytseva (1972) had previously concluded however that $\alpha = 30$ and $\sigma_0 = 7.1 \times 10^5 Sm^{-1}$ which is similar to the profile favoured by Alldredge. Kolomiytseva considered the phase of an apparent induced 60 year variation from the core and also concluded that a large jump in the conductivity at the CMB is inconsistent with the observations.

Ducruix et al (1980), Achache et al (1980) and Currie (1968), all considered mean conductivities for the lower $1500km$ to $2000km$ of the mantle. Currie (1968) estimated the mean conductivity of the lower $2000km$ of the mantle to be $200Sm^{-1}$ after making assumptions about the spatial spectrum of the magnetic field at the CMB based on simple theories of magnetohydrodynamic turbulence. The former authors noted the apparent rapidity of the 1969/70 jerk and assuming it was impulsive in nature estimated a mean conductivity of between $60Sm^{-1}$ and $150Sm^{-1}$. A (typical) value of $100Sm^{-1}$ for Achache et al (1980) will be used in further discussions. Ducruix et al (1980) considered a more refined, three layer model to be likely. The estimates of Achache et al (1980) and Ducruix et al (1980) were based on a rather simple infinite plane layer "slab" formalism of Runcorn (1955). Courtillot et al (1984) used Backus's (1983) mantle filter theory (see §7.4.1) to interpret the 1969/70 jerk and reached a qualitatively similar profile to that of Backus (loc. cit.). Paulus & Stix (1989) solved the induction equation in Fourier space and found that a rather "flat" conductivity distribution gave the electromagnetic (EM) torque closest to the torque that must act on the mantle to explain the decade fluctuations in the length of day (LOD). The profile quoted in Table 7.1 for Stix &

Roberts (1984) is one they assumed rather than determined, although they did find EM torques of an appropriate order of magnitude for the decade fluctuations.

Although there is a variation of several orders of magnitude in the estimates of the conductivity at the base of the mantle, what most of the models in Table 7.1 have in common is a rapid drop–off of conductivity with distance from the CMB and hence a concentration of conductance towards the CMB. This has important implications for electromagnetic core–mantle coupling (and *vice versa*) which will now be discussed.

7.2 Electromagnetic core–mantle coupling

It was shown in Chapter 6 that the torque acting on the mantle as a result of the advection of poloidal field by the zonal toroidal part of particular models of core surface motions correlates very closely with the LOD torque. Morever, if as a working hypothesis it is assumed that the electromagnetic coupling is the sole agent of angular momentum transfer between core and mantle, the correlation places important constraints on the conductance of the lower mantle. In Chapter 6 it was seen that if the conducting material is concentrated in a homogeneous thin layer just above the CMB then this must have a conductance of approximately $(6.7 \pm 0.9) \times 10^8 S$ (a weighted mean of the two values in Table 6.1). Approximating this by the conductance range $10^8 S$ to $10^9 S$ (the margin for error has been widened to allow for the trend effect discussed in §6.4.2), the compatibility of the various conductivity distributions discussed so far with the LOD fluctuations can be assessed. Consider the extent to which the conductance associated with each conductivity model is concentrated within different distances of the core–mantle boundary (Figure 7.1). Assume that this approximate "equivalent thin layer" conductance must be in the range $10^8 S$ to $10^9 S$. The horizontal bars in Figure 7.1 mark this conductance range at 3 radii: $3785 km$, $4085 km$ and $4685 km$ corresponding to layers of thickness $300 km$, $600 km$ and $1200 km$ respectively. Now consider which of the models do and do not have a conductance of the appropriate order of magnitude to sustain the necessary torque, ie. which conductance profiles intersect the horizontal bars.

Firstly, the model of Ducruix *et al* (1980) is at least half an order of magnitude too small to explain the LOD fluctuations, whilst the models of Alldredge (1977b) and
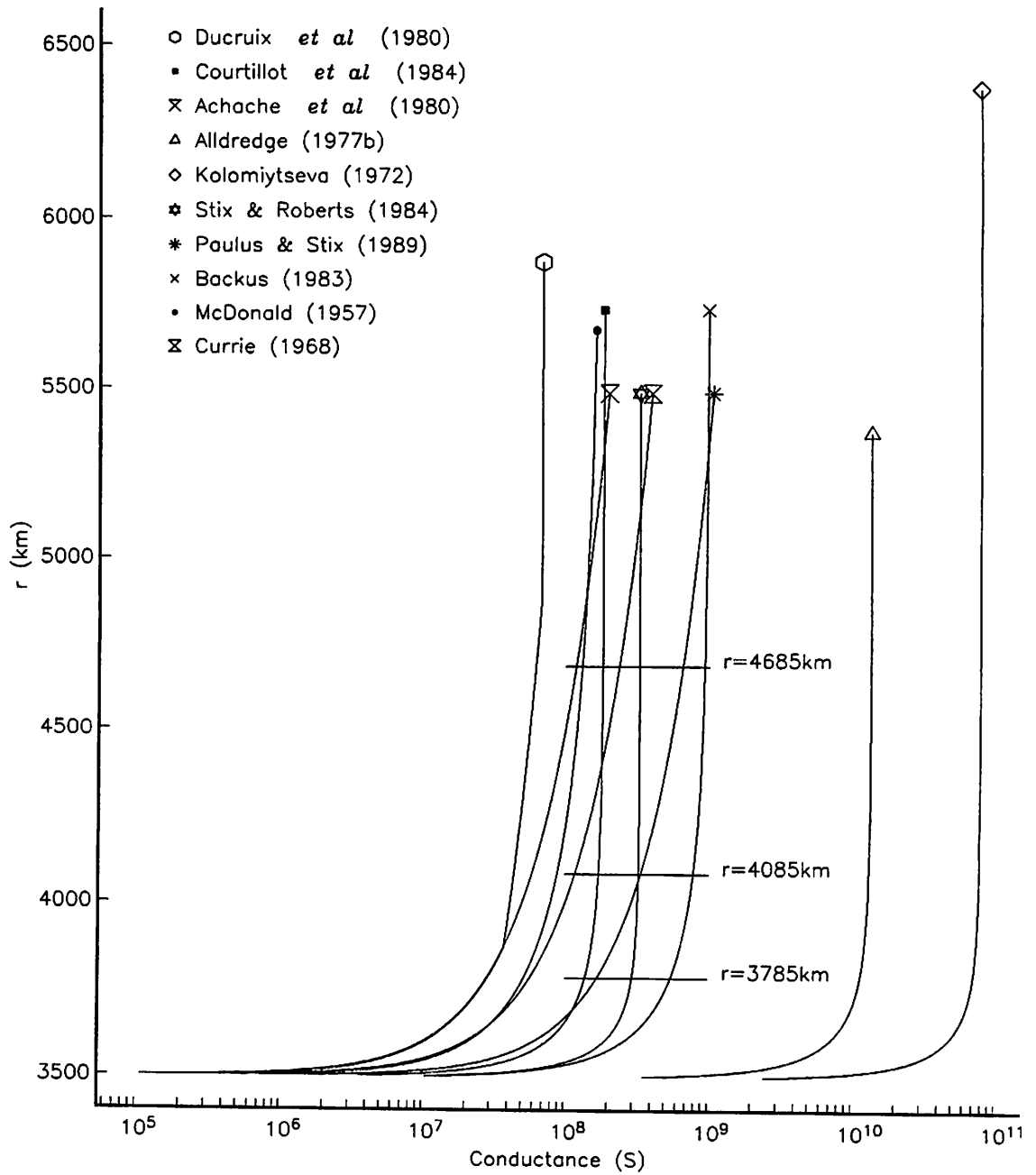
Figure 7.1: Integrated conductivity (conductance) for the radius intervals $[r_c, r]$ ($r_c = 3485km$) from 10 different published profiles of lower mantle electrical conductivity (summarised in Table 7.1 and described in §7.1). Horizontal bars mark the conductance range $10^8 S$–$10^9 S$. Curves are terminated at their upper radius of validity by their key symbol.

Table 7.2: Conductivity models from §7.1 for which the lower δkm has a sufficient conductance to produce EM torques to account for the decade fluctuations in the LOD. Figures given are the percentage of the conductance of the whole model which is contained in the layer.

Models	$\delta = 300$ (%)	$\delta = 600$ (%)	$\delta = 1200$ (%)	Total Conductance $10^8 S$
Backus (1983)*	56	80	96	9.8
Courtillot et al (1984)*	76	94	99	1.8
McDonald (1957)	32	55	81	1.6
Paulus & Stix (1989)*	16	32	62	10.6
Stix & Roberts (1984)*	90	99	100	3.3
Achache et al (1980)	14	30	60	2.0
Currie (1968)	14	30	60	4.0

Kolomiytseva (1972) have conductances within $500km$ of the CMB that are 2 to 3 orders of magnitude too large to be consistent with the required torques. This leaves 7 models which could conceivably be approximated by thin layer models and the concentration of conductance in the three layers for these 7 is summarised in Table 7.2. Those of Achache et al (1980) and McDonald (1957) however, are only just adequate (Figure 7.1) and only if the layer thickness is $1200km$ which is pushing the linearised Taylor expansion approximation for the induced toroidal field in Chapter 6 to the limit. Coming down further to a $300km$ thick layer, the model of Currie (1968) is also excluded, which leaves four candidate models indicated by a * in Table 7.2. The Paulus & Stix (1989) profile is particularily flat and would require the full $1200km$ thickness to account for the torque (see Table 7.2). The models of Stix & Roberts (1984) and Courtillot et al (1984) have most of the conductivity concentrated in the first $300km$ but the conductivities would need to be increased by factors of about 3 and 5 respectively. Backus (1983) has the most appropriate conductance of all the models and the equivalent layer would need to be about $600km$ thick. It is not surprising, looking back at Table 7.1, to find that these last 3 models are all qualitatively similar: a conductivity of a few thousand Sm^{-1} at the base of the mantle with a rapid drop-off away from the CMB.

7.3 Locating the core–mantle boundary geomagnetically

Hide (1978) proposed a method by which the electrically conducting core of a planet can be located from external magnetic measurements. Hide applied the method to the Earth and determined a radius (to be referred to here as the "electromagnetic core–mantle boundary" or ECMB) which agreed within 2% of the seismologically determined radius of $3485 \pm 5km$. Hide argued that by assuming the frozen–flux hypothesis and that the mantle is an insulator, the total absolute magnetic flux (or *pole strength*) through the CMB (Ω) (assumed spherical and of radius r) given by

$$\mathcal{N}_r = \int_\Omega |B_r| d\Omega \tag{7.2}$$

has to be time–independent. Hide & Malin (1981) used the definitive field model of Barraclough *et al* (1978) for 1965.0 and calculated $\mathcal{N}_r$ for 1964.5 and 1965.5, using the secular variation coefficients to extrapolate the main field coefficients backwards and forwards in time, and placed the ECMB at $r = 3233 \pm 361km$. They sought the radius at which $\dot{\mathcal{N}}_r$ (where the dot denotes differentiation w.r.t time) is zero, for various truncations of the field. Their "mean" ECMB radius is arrived at by using radii at which $\dot{\mathcal{N}}_r$ reaches a local minimum and only at truncations 3, 4 and 5 do any of their curves actually reach zero and none of these for a radius greater then $3200km$ (their Figure 1).

Voorhies & Benton (1982) and Voorhies (1984) suggest that field models separated by at least 10–20 years ought to be used in the determination of the ECMB radius. Voorhies (1984) calculated the change in $\mathcal{N}_r$ computed for each of several models relative to a reference Magsat model for epoch 1980 as a function of r. All the models were based on spherical harmonic expansions of the field truncated at maximum degrees ranging from 6 to 9. The mean estimate of the ECMB radius from 44 determinations was $3506 \pm 301km$ whilst an "appropriate subset" of these gave $3489 \pm 35km$. Voorhies (1984) also noted a significant decrease in $\mathcal{N}_r$ at $r = 3485km$ from 1600 to the end of the 19th century using models of Barraclough (1974) but concluded that there was no significant change during the present century. These observations were based on field models truncated severely at degree 4. It is not clear how accurate these determinations really are: for example Voorhies's $\mathcal{N}_r$ for $r = 3485km$ at 1980 up to degree 4 is $5.4GWb$ less than that of Bloxham *et al* (1989) who used a model up to degree 14 derived using stochastic

inversion. Benton & Voorhies (1987) found no significant change in $\mathcal{N}_r$ over the period 1945 to 1985 using Definitive Geomagnetic Reference Field models.

The question of the ECMB radius will now be briefly considered using the model of Bloxham & Jackson (1990) (kindly supplied by A. Jackson and which will be referred to as BJ2) as it is felt that this is one of the most reliable representations of the time–dependent geomagnetic field at the CMB currently available. This model is based on a temporal expansion in cubic B–splines and is valid for the period 1840-1990. The determination of the radius r for which the difference between $\mathcal{N}_r$ for two epochs is zero, as used by Hide & Malin (1981) and Voorhies (1984), depends on the assumption that $\mathcal{N}_r$ varies linearly in the intervening period. This is certainly not true of the geomagnetic field itself except as a crude approxiamation over short periods of time and is therefore unlikely to be true of a non–linear functional of the field such as $\mathcal{N}_r$. Bloxham *et al* (1989) noted slight evidence of an increase in $\mathcal{N}_r$ for $r = 3485km$ over this century though they pointed out that the scatter is large and the increase inconclusive. However their models were derived individually for a sequence of epochs whereas model BJ2 was derived by a simultaneous inversion for both spatial and temporal dependence and is therefore more temporally homogeneous. The pole strength is plotted as a function of time for $r = 3400km, \ldots, 4300km$ in $100km$ steps in Figure 7.2. It is immediately apparent from this that over a 150 year period, $\mathcal{N}_r$ computed at $r = 3500km$ (the $15km$ difference being negligible) is definitely not constant and that the depth $3800km$ is a more convincing location for the ECMB. This is somewhat surprising as it is contrary to all previous magnetic determinations of the core radius. However it is, to my knowledge, the first use of a fully time–dependent field model over such a long period for this purpose and is therefore believed to give a more consistent representation of the time–dependent pole strength. The significant vascillations in $\mathcal{N}_r$ even at $r = 3800km$ indicate why methods depending on the difference between pole strengths at two arbitrary epochs being zero may not work.

This lack of constancy for the pole strength over the CMB could arise for several reasons. Firstly, the effects of diffusion are now believed by some authors to be significant (Bloxham & Gubbins, 1985, 1986) on the decade time scale by consideration of flux through patches on the CMB bounded by null-flux curves. Secondly, Hide & Malin (1981)
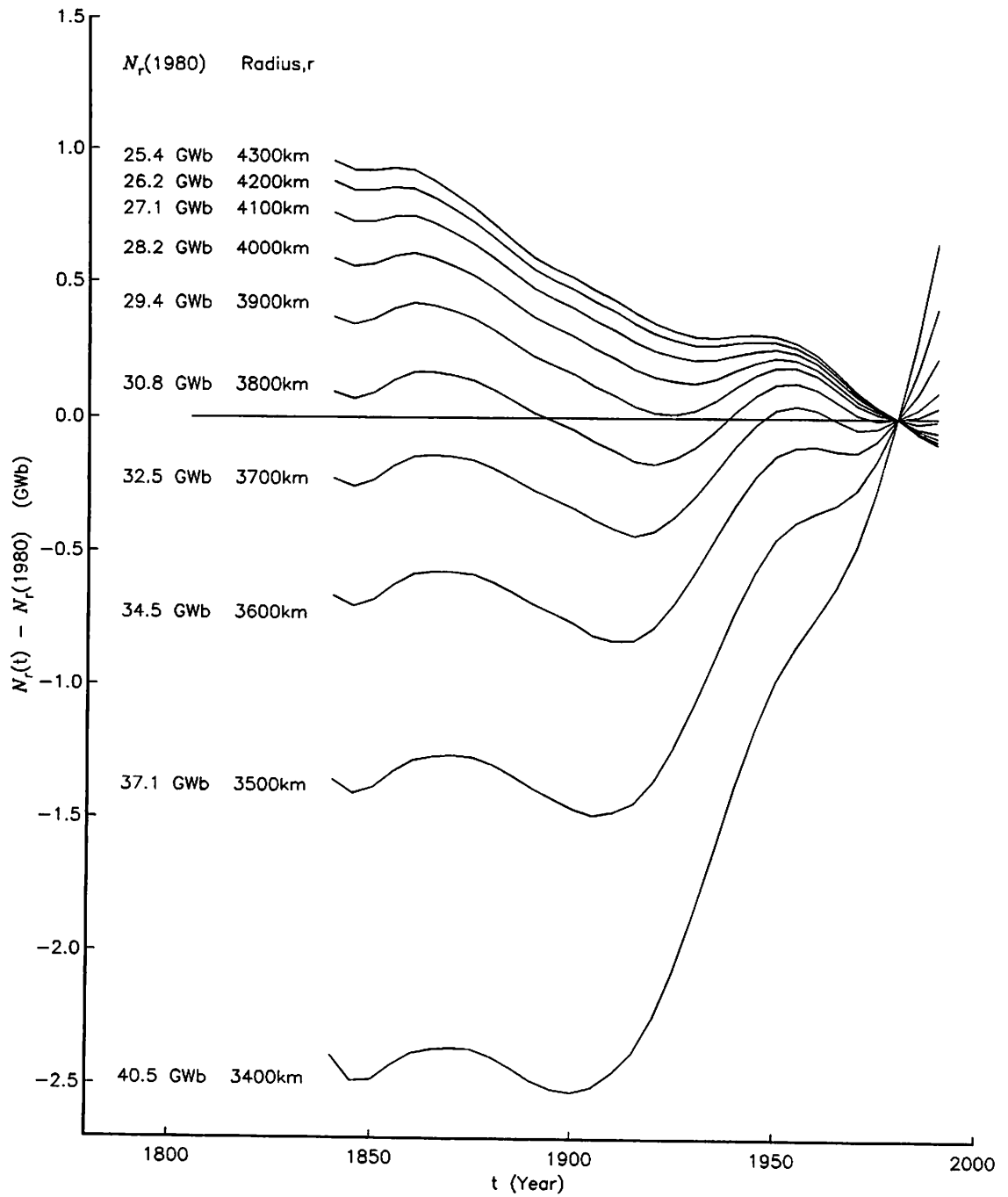
Figure 7.2: Integrals of the unsigned radial magnetic flux ($\mathcal{N}_r$) through spherical surfaces of radius $r = 3400km$ to $r = 4300km$. Values are plotted relative to the 1980 value for each radius. Values for 1980 are given on the left of the curves. See §7.3 for details.

believe that imperfect knowledge of **B** and its rate of change are the main sources of uncertainty in $\mathcal{N}_r$. Thirdly, and more importantly in the context of the present chapter, the conductivity in the mantle immediately above the CMB may be significantly non-zero. If the conductivity there is sufficiently high then one of Hide's (1978) conditions for the constancy of the pole strength breaks down. The second of these hypotheses cannot be tested here as covariance estimates for the BJ2 model coefficients were not available. However Gubbins & Bloxham (1985) estimated errors for the flux over the northern hemisphere "patch" of around $30MWb$, which might suggest an error of around $0.050GWb$ for $\mathcal{N}_r$. Voorhies (1984) typically estimates the error in $\mathcal{N}_r$ at $r = 3485km$ to be of the order $0.2GWb$ which the changes in $\mathcal{N}_r$ over the 150 years in Figure 7.2 for $r = 3500km$ exceed by an order of magnitude. Fluctuations in $\mathcal{N}_r$ at $r = 3800km$ are of approximate amplitude $0.2GWb$. Differentiation between the first and last hypotheses may not be possible: the tests for diffusion (eg. Bloxham & Gubbins, 1986) depend implicitly on prior knowledge of the core radius. (This is also true of all field models based on the norms commonly used in geomagnetic stochastic inversion including BJ2 (eg. Gubbins, 1983; Gubbins & Bloxham, 1985 and Bloxham & Jackson, 1990).) It seems possible however that the changes in the pole strength arise from the presence of a highly conducting layer at the bottom of the mantle which ends rather abruptly at $r = 3800km$. If this is the case then it could bring results attributing changes in flux integrals to the action of diffusion in the core into question.

7.4 Geomagnetic impulses and mantle conductivity.

The initial identification of geomagnetic jerks as secular variation originating within the core with a short characteristic time–scale (Courtillot *et al*, 1978) produced a particular flurry of interest in the topic of lower mantle conductivity. The recognition of the 1970 jerk's global character allowed Malin & Hodder (1982) to argue, fairly convincingly, that the jerk originated within the Earth's core. This was seen as strong evidence that signals coming from beneath the mantle with a characteristic time–scale shorter than Currie's (1967) "cutoff" period of 4 years are observable at the Earth's surface. Whilst Alldredge (1975, 1977b, 1984) vociferously refuted a core origin for signals with such a short time–

scale, others (eg. Ducruix *et al*, 1980; Achache *et al*, 1980; Backus, 1982,1983; Courtillot *et al*, 1984) took their observation as a stimulus to re–evaluate mantle conductivity estimates and the theory of propagation of magnetic signals through the mantle. Achache *et al* (1980) estimated the mean conductivity of the lower mantle to be between $60Sm^{-1}$ and $150Sm^{-1}$ using the theory of Runcorn (1955), values significantly lower than most previous estimates and insufficient to explain supposed correlations between jerks and changes in the LOD (Le Mouël & Courtillot, 1981) by electromagnetic coupling. On the contrary, Backus (1983) argued that the apparent timescale of the 1969 jerk is not inconsistent with a conductivity as high as $3000Sm^{-1}$ at the base of the mantle provided the conductivity drops off rapidly away from the CMB. The quantitative interpretation of the jerk results of Chapter 5 will now be considered in the context of Backus's (1983) theory.

7.4.1 Geomagnetic jerks: the core impulse hypothesis

In Backus's (1983) formalism for investigating the way in which geomagnetic impulses are propagated through the mantle, conductivity σ is assumed to be a function of radius alone. Backus showed that the mantle would act as a filter on each spherical harmonic of degree n of the impulse and that the two most useful time constants of the filter are the zero frequency delay time $\tau_1(n)$ and the smoothing time $\sigma_2(n)$. Backus further showed that these time constants could be related to the mantle conductivity by the linear and quadratic functionals

$$\lambda \tau_1(n) = \mu_0 \int_{rc}^{rs} r\sigma(r) \left[1 - \left(\frac{r_c}{r} \right)^{\lambda} \right] dr \tag{7.3}$$

$$\lambda^2 (\sigma_2(n))^2 = \mu_0^2 \int_{rc}^{rs} \int_{rc}^{rs} rs\sigma(r)\sigma(s) \left[\left(min \left\{ \left(\frac{s}{r} \right), \left(\frac{r}{s} \right) \right\} \right)^{\frac{\lambda}{2}} - \left(\frac{r_c^2}{rs} \right)^{\frac{\lambda}{2}} \right]^2 drds \tag{7.4}$$

where r_s is the radius of the Earth's surface, $\lambda = 2n+1$ and *min* indicates the minimum of the arguments. Backus further showed that for an impulse in the third time derivative of a field harmonic (third order impulse) the output $f(t)$ of the mantle filter asymptotically approaches a quadratic $f_\infty(t)$. (Refer to Figure 7.3 reproduced from Figure 1 of Backus (1983).) If the quadratic time–dependence of each harmonic coefficient of the asymptotic behaviour of the field at the Earth's surface before and after the impulse can

be determined then both the amplitude of the impulse (equal to the resulting asymptotic change in the second time derivative of the field discussed in Chapter 5), the *centroid date* or *emergence time* $t_f = t_0 + \tau_1$ (where t_0 is the date the impulse occurred at the CMB presumed independent of n) and the smoothing time σ_2 for each harmonic degree and order can all be determined. The asymptotic response of the mantle filter to the third order impulse is a quadratic which can simply be estimated by the difference of the asymptotic field behaviour after and before the impulse. Note that $f_\infty(t_f)$ need not be zero. Thus in determining the asymptotic behaviour of the field before and after the jerk the quadratics should not be constrained to be equal at the centroid date. No such constraint was imposed on the field models with quadratic time dependence derived in
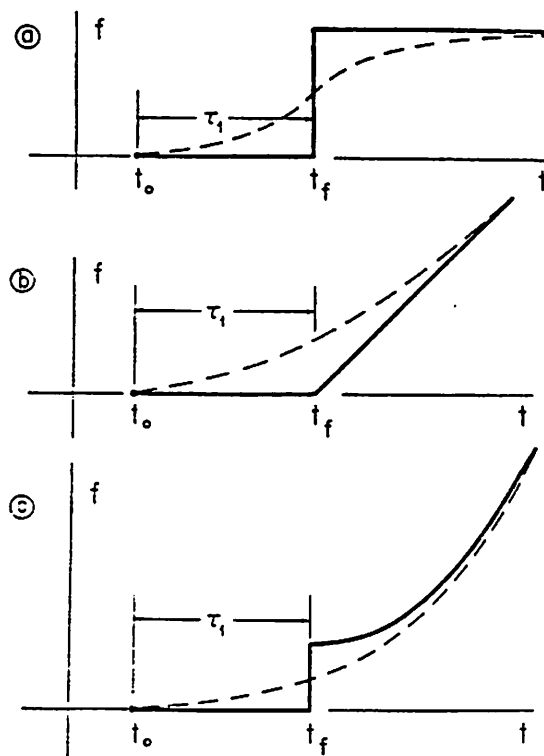
Figure 7.3: The input to the mantle filter is an impulse at $t = t_0$ in the (a) first (b) second and (c) third time derivative and the output is $f(t)$ (shown as a dashed line). The apparent delay time is τ_1, the centroid date is t_f and the output asymptotically approaches a polynomial of order 0, 1 and 2 respectively (bold line). Figure 1 from Backus (1983).

Chapter 5 and so these can be used as models of the asymptotic behaviour of the field before and after the jerks of 1970, 1978 and 1983. Discontinuity does not imply that the field itself is discontinuous at t_f only that its asymptotic time–dependence before and after the impulse is (which is only a valid representation of the field for $|t - t_f| > \sigma_2$ anyway). Note that to estimate τ_1 some other means must be used for estimating the epoch t_0 at which the impulse originated on the CMB. Backus also pointed out that the field at particular locations can appear to change more rapidly than the smoothing time on account of *mode mixing* (between harmonic degrees). The timescale of the jerks certainly appears to be of the order of 1 or 2 years at many observatories.

As the mantle filter constants τ_1 and σ_2 and hence the *impulse constants* t_f and σ_2 depend on harmonic degree but not harmonic order, Backus *et al* (1987) were able to quantitatively test the *core impulse hypothesis* that:

(1) the conductivity of the mantle is a function of radius alone and

(2) before passing through the mantle the jerk was an impulse in the third time derivative of the field.

Backus *et al* (1987) concluded that the jerk of 1969/70 is *not* consistent with this hypothesis. Their impulse constants and associated statistics for the core impulse hypothesis (their Table 2) are reproduced in Table 7.3. Only the centroid dates for degrees 2 and 3 are rejected as not self–consistent with 99% certainty although this is a rather less strict interpretation than that of Backus *et al* (1987). Most of the χ^2 statistics are quite high and only one of the smoothing times is significantly non–zero.

7.4.2 Impulse constants from the 1970, 1978 and 1983 jerks

If the asymptotic output from the mantle filter has quadratic time–dependence

$$f_\infty(t) = a_n^m t^2 + b_n^m t + c_n^m \tag{7.5}$$

then the impulse constants for this harmonic can be determined from

$$t_f = -\frac{b_n^m}{2a_n^m} \tag{7.6}$$

and

$$\sigma_2^2 = \frac{c_n^m}{a_n^m} - (t_f)^2 \tag{7.7}$$

Table 7.3: Mean impulse constants of Backus *et al* (1987) for harmonic degrees $n = 1, \ldots, 7$. χ^2 statistics are for the hypothesis that the $(2n + 1)$ values of τ_1 and σ_2^2 for each harmonic degree n are equal. If these exceed χ_C^2 values then this hypothesis, and hence the core impulse hypothesis (see §7.4.1) must be rejected (with 99% certainty on $2n$ degrees of freedom). $\delta\hat{\tau}_1(l)$ and $\delta\hat{\sigma}_2^2(l)$ are the estimated errors.

n	$t_0 + \hat{\tau}_1(n) \pm \delta\hat{\tau}_1(n)$	$\chi^2_{\hat{\tau}_1(n)}$	$\hat{\sigma}_2^2(n) \pm \delta\hat{\sigma}_2^2(n)$	$\chi^2_{\hat{\sigma}_2^2(n)}$	χ_C^2
1	1968.87±0.33	2.38	1.51±0.42	7.04	9.21
2	1970.06±0.14	28.47	-0.39±0.31	11.59	13.28
3	1969.08±0.24	33.80	-0.04±0.35	3.16	16.81
4	1969.22±0.36	14.07	0.07±0.32	13.46	20.09
5	1969.51±0.59	2.99	-0.07±0.30	6.67	23.21
6	1969.36±0.55	10.68	0.05±0.27	10.28	26.22
7	1968.80±0.74	4.40	0.05±0.26	6.71	29.14

(Backus *et al*, 1987). The impulse constants t_f and σ_2 were computed for the jerks of 1970, 1978 and 1983 using models PR1970, PO1970, PR1978, PO1978, PR1983 and PO1983 (Chapter 5). These are presented in Table 7.4 (together with the appropriate statistics for testing the core impulse hypothesis calculated by the method given in Backus *et al* (1987)). Only harmonic degrees 1-6 are presented bearing in mind the resolution curves for the secular acceleration (Figure 5.14). It is immediately clear from the χ^2 statistics that the core impulse hypothesis must be rejected at all three epochs. This means that either the events do not originate in the core, a possibility that seems increasingly unlikely in light of the earlier chapters of this thesis, the events were not impulsive (in the third time derivative), or significant lateral conductivity heterogeneity exists in the mantle. The second possibility has to be true to some extent—any physical process takes a finite time; the important question is whether or not the characteristic timescale of the jerks is short compared to the characteristic timescale of other features of the global secular variation. In Chapter 4 it was argued that the typical time between virtual impulses is of the order of 10 years and so this could be taken as a characteristic time-scale of SV. The observed changes in SV associated with jerks however seem to occur within an interval of a year or two. Such evidence certainly suggests that the change in field at the CMB associated with jerks is probably quite well described by

Table 7.4: Mean impulse constants for harmonic degrees $n = 1, \ldots, 6$ from the (a) 1970 jerk (b) 1978 jerk and (c) 1983 jerk from the models presented in Chapter 5. χ^2 statistics are for the hypothesis that the $(2n + 1)$ values of τ_1 and σ_2^2 for each harmonic degree are equal to the mean. If these exceed the χ_C^2 values then this hypothesis, and hence the core impulse hypothesis (see §7.4.1) must be rejected (with 99% certainty on $2n$ degrees of freedom). For an explanation of the computation of these quantities see §7.4.2.

	n	$t_0 + \hat{\tau}_1(n) \pm \delta\hat{\tau}_1(n)$	$\chi^2_{\hat{\tau}_1(n)}$	$\hat{\sigma}_2^2(n) \pm \delta\hat{\sigma}_2^2(n)$	$\chi^2_{\sigma_2^2(n)}$	χ_C^2
(a)	1	1970.12±0.07	1890	-38.80±2.15	1335	9.21
	2	1968.76±0.02	2241	9.11±0.71	3797	13.28
	3	1969.84±0.02	3488	-37.25±0.81	6210	16.81
	4	1970.15±0.03	1169	-73.56±1.46	1453	20.09
	5	1968.01±0.04	742	-2.40±2.29	1774	23.21
	6	1970.00±0.06	3564	3.69±2.97	4487	26.22
(b)	1	1976.99±0.17	853	58.39±5.03	1091	9.21
	2	1976.97±0.02	329	-17.22±0.79	3002	13.28
	3	1977.16±0.02	2694	-29.65±0.96	9030	16.81
	4	1977.53±0.03	260	-107.97±1.22	9400	20.09
	5	1977.01±0.04	1383	-0.89±1.37	9403	23.21
	6	1977.26±0.05	628	127.62±3.17	5570	26.22
(c)	1	1980.53±0.12	537	126.35±9.62	2246	9.21
	2	1983.56±0.05	1968	-40.26±2.01	4530	13.28
	3	1981.30±0.07	205	-35.62±2.23	1201	16.81
	4	1984.81±0.08	1234	-81.65±3.23	538	20.09
	5	1982.57±0.18	1055	-418.10±20.98	1539	23.21
	6	1984.67±0.20	527	112.17±10.55	1287	26.22

a third order impulse as a first approximation. Therefore the possibility of significant lateral heterogeneity in mantle conductivity seems much more likely as an explanation for the gross inconsistency of the jerk models with the core impulse hypothesis. The extreme scatter in the smoothing parameters in Table 7.4 is probably due to their reciprocal dependence (equation (7.7)) on the a_n^m coefficients which are relatively poorly determined compared to c_n^m and some of which are therefore suppressed by the stochastic inversion procedure. The enormous χ^2 statistics may arise from the inability of the standard errors, which are believed by some (eg. Langel et al, 1989) to be significantly underestimated by stochastic inversion, to account for the scatter within each harmonic degree.

7.5 Propagation times

Although the emergence time t_f for each harmonic degree can be determined directly from the geomagnetic data, the delay time τ_1 cannot. For this some independent estimate of the impulse date at the core mantle boundary t_0 is necessary. Chapter 6 highlighted a possible direct link between the geomagnetic field and Earth rotation and the observed phase difference (6 years) is certainly suggestive of a mean delay associated with the propagation of poloidal field through the mantle. It will be assumed here that a change in the gross angular momentum of the outer core leads immediately to a change in the angular momentum of the mantle. Even disregarding the possible role of EM coupling between the core and mantle, any phase difference between other geomagnetic and LOD parameters may be indicative of the propagation time. Backus (1983) has hypothesised a step–like change in the axial angular acceleration of the Earth around 1956 as possibly heralding the occurrence of the geomagnetic impulse which became apparent at the Earth's surface around 1969. This implies a propagation time of ~ 13 years for changes in the magnetic field to reach the surface. Le Mouël *et al* (1981) point to an apparent correlation between declination and the Earth's rotation rate, with magnetic variation *leading* those of the rotation rate by some 10 years rather than lagging behind. This correlation is further supported with the addition of more recent data by Gire & LeMouël (1986) who also discuss the physical mechanisms proposed by LeMouël & Courtillot (1982) to explain the core–mantle couple and the phase of the correlation. Contrary to their findings, however, Vestine & Kahle (1968) found a good correlation between westward drift inferred from the angular momentum (AM) of the top 200km of the core consistent with the LOD observations and the drift of the eccentric dipole with the latter lagging 5 years behind the former variations (see §6.4.4 and Figure 6.6). This too suggests a typical time of around 5 years for changes in the poloidal magnetic field at the CMB to reach the surface on the assumption that exchange of AM is between the mantle and the upper layers of the core as opposed to deeper regions. In Figure 6.4 there is a sharp "elbow" in the LOD torque at around 1964 which could be associated with the 1970 jerk, the most powerful of the three jerks investigated in Chapter 5, which would also suggest a 6 year delay time. There are however no other sharp changes in

the LOD torque at 1972 and 1977 associated with the 1978 and 1983 jerks.

The evidence considered so far in this chapter has been pointing toward particular distributions of conductivity with a concentration of conductance toward the CMB. The impulse delay and smoothing times calculated according to equations (7.3) and (7.4) for the models examined in §7.1 and §7.2 are presented in Table 7.5 together with two thin homogeneous layer models of the appropriate conductance to explain the LOD fluctuations. The 3 published models highlighted earlier as being most compatible with the LOD data are marked by an asterisk. Bearing in mind the earlier comment that the conductivities of Stix & Roberts (1984) and Courtillot et al (1984) would have to be increased by factors of 3 and 5 respectively to account for the LOD fluctuations, the delay times of the 5 LOD compatible models in Table 7.5 are all of the correct order of magnitude to account for the phase lag between the torques. However all these monotonic conductivity profiles lead to delay and smoothing times which decrease distinctly with harmonic degree, a feature not apparent from the jerk data either in Tables 7.3 or 7.4. The delay times for the 1970 and 1978 jerks in particular are not suggestive of any systematic dispersion among different harmonics. The L1 model (a homogeneous $300km$ conducting layer) shows the least dispersion of the five. All the models have smoothing times of about 0.6 or more of the delay time, thus a delay time of around 6 years would also imply a smoothing time of several years which is not compatible with the observed characteristic time–scale of jerks. Therefore to explain the apparent rapidity of the jerks as seen in the data, significant mode mixing would have to occur in many different regions which seems unlikely. Backus also showed that certain consistency conditions relating τ_1 and σ_2 must hold but as σ_2^2 is so poorly determined these are not useful here. It may be that a simultaneous analysis of all 3 jerks could be performed to yield more reliable estimates of the mantle filter constants as these should be time–invariant.

7.6   Conclusions.

Several strands of evidence highlighted above have led toward the idea that the lower part of the mantle, perhaps the bottom $300km$ or so, consists of a region of high conductivity.

Firstly a number of previously published models of lower mantle conductivity have been compared, most of which show a significant concentration of conductance toward the CMB. If these are approximated by thin homogeneous layers at the base of the mantle, then only a few of them appear to be compatible with the LOD fluctuations if EM forces are the sole mechanism of core–mantle coupling. The method of Hide (1978) for locating the CMB with geomagnetic measurements has failed to give agreement with

Table 7.5: Impulse delay and smoothing times derived using equations (7.3) and (7.4) for the 10 published models already discussed and two homogeneous layer models of conductance 6.7×10^8 and thickness $300km$ (L1) and $600km$ (L2). Models marked * are compatible with the electromagnetic coupling results.

Delay times $\tau_1(n)$ (years)						
n	1	2	3	4	5	6
Backus (1983)*	12.26	10.62	9.36	8.36	7.55	6.88
Courtillot *et al* (1984)*	1.42	1.29	1.18	1.09	1.02	0.95
Stix & Roberts (1984)*	1.67	1.57	1.48	1.40	1.33	1.26
L1 (300km)*	3.96	3.76	3.57	3.39	3.23	3.08
L2 (600km)*	7.54	6.84	6.24	5.71	5.26	4.86
Achache *et al* (1980)	6.03	4.75	3.86	3.23	2.77	2.41
Alldredge (1977b)	80.85	75.08	70.08	65.70	61.84	58.41
Currie (1968)	12.05	9.49	7.73	6.47	5.53	4.82
Ducruix *et al* (1980)	1.17	0.99	0.85	0.74	0.66	0.59
Kolomiytseva (1972)	395.58	371.61	350.39	331.45	314.46	299.12
McDonald (1957)	3.44	2.81	2.36	2.02	1.77	1.57
Paulus & Stix (1989)	31.01	24.51	20.02	16.79	14.40	12.57
Smoothing times $\sigma_2(n)$ (years)						
Backus (1983)*	8.20	6.79	5.73	4.92	4.29	3.78
Courtillot *et al* (1984)*	0.96	0.85	0.76	0.68	0.62	0.57
Stix & Roberts (1984)*	1.15	1.06	0.98	0.91	0.85	0.80
L1 (300km)*	3.20	2.99	2.82	2.65	2.49	2.35
L2 (600km)*	6.03	5.35	4.76	4.26	3.83	3.45
Achache *et al* (1980)	4.62	3.40	2.59	2.03	1.63	1.34
Alldredge (1977b)	55.16	50.19	45.94	42.26	39.05	36.25
Currie (1968)	9.24	6.81	5.18	4.05	3.25	2.67
Ducruix *et al* (1980)	0.83	0.66	0.54	0.45	0.38	0.32
Kolomiytseva (1972)	271.07	250.35	232.18	216.16	201.92	189.20
McDonald (1957)	2.40	1.83	1.44	1.16	0.96	0.80
Paulus & Stix (1989)	23.57	17.41	13.28	10.42	8.38	6.89

the CMB radius known from seismology. One reason for this could be a sharp drop in conductivity at around 300km above the CMB. The impulse propagation characteristics of such conductivity models seem to be incompatible with the mantle filter constants derived from the observed jerks of 1970, 1978 and 1983, whilst internal inconsistencies among the mantle filter constants point to the presence of significant lateral heterogeneity in the lower mantle conductivity. The preferred model is a $300km$ thick layer of $\sim$ $2500Sm^{-1}$ conductivity at the base of the mantle. A final note of caution: to quote such figures conveys an unwarranted sense of certainty; the main conclusion from the foregoing discussion ought to be that our knowledge of lower mantle conductivity is still very sketchy. The geomagnetic evidence certainly appears to point to the concentration of mantle conductance in the $200km$ to $300km$ thick D'' layer which is believed from seismology to be highly heterogeneous (see eg. Anderson, 1989).

Chapter 8

Concluding remarks

8.1 Summary

The research described in this thesis has been directed at enhancing our understanding of the ways in which the Earth's magnetic field changes on the month to decade time-scales. In particular the phenomena known as geomagnetic jerks have been investigated. In light of previous arguments about the internal or external nature of the 1969/70 jerk, special attention has been paid to assessing the extent to which geomagnetic fields of external origin contribute to time–averaged observatory data. Using monthly means of the aa index as a temporal basis function the (dimensionless) spatial morphology of the associated relative amplitude function has been shown to be dominated by spherical harmonics representing a dipole aligned with though of opposite polarity to the Earth's main tilted dipole field. Seasonal fluctuations in the field have been analysed also, revealing that the annual variation is dominated by degree 2 harmonics and the biannual variation by degree 1 and degree 2 in approximately equal measure. The results have been found to be consistent with an insulating mantle to a depth of about $600km$ or $700km$ and a uniform conductance of between $0.1Sm^{-1}$ and $1Sm^{-1}$ below this.

The resulting simple model for the external and induced disturbance fields can be used to eliminate what is believed to be the most significant time–dependent field of non–core origin on this time–scale. Quantitative analysis of the resulting improved representation of the core field using the optimised piecewise regression algorithm developed in Chapter 4 has revealed semi–objectively three approximate dates, 1970, 1978

and 1983, at which the field appears to have undergone rather abrupt changes in its behaviour. As most of the major effect of external fields is believed to have been removed these events are believed to be of internal origin. The analysis has also shown that the time–dependence of the geomagnetic field at individual sites can be approximated well by piecewise quadratic functions, the typical duration of which has been found to be approximately 10 years. Removal of disturbance field effects has been shown to reduce residual variance to such quadratics by about 50% to 70%.

Spherical harmonic models of the field with a quadratic time–dependence have been prepared for epochs 1965.5, 1974.5, 1981.5 and 1986.5. The technique of stochastic inversion, applied simultaneously to estimates of the time–dependence of each field component at each observatory, has been used. Based on such estimates from about 100 observatories in each case, the resolution of these models extends to about degrees 9, 7 and 6 for the main field, secular variation and secular acceleration respectively. The models are all truncated at degree 14 but convergence of the models was achieved well before this value. These models have allowed the jump in secular acceleration ("jerk field") associated with the jerks of 1970, 1978 and 1983 to be mapped. The spatial distribution for the 1969/70 jerk has been found to be in broad agreement with previously published results, though the models are believed to be the most reliable jerk models yet produced. All 3 events have been shown clearly to be worldwide in extent. The strength of the 1978 jerk, as measured by the mean squared value of the jerk field, has been found to be $16.98 \pm 1.34 (nT/yr^2)^2$ which is significantly smaller than the $25.53 \pm 1.40 (nT/yr^2)^2$ found for the 1970 jerk. There is also some evidence of an anti–correlation between the two. The 1983 jerk has been found to be weaker still with a mean squared value of $8.03 \pm 1.35 (nT/yr^2)^2$. These events are thought to be reasonably well represented by "step" changes in the secular acceleration of 1 or 2 years duration. However the jerks seem to be inconsistent with the core impulse hypothesis: that the jerk was impulsive at the CMB and mantle conductivity is a function of radius alone. Failure of this hypothesis is believed to be due primarily to lateral heterogeneity of the conductivity though this belief is subjective. The jerk emergence times have been shown to vary significantly with harmonic degree although it is believed the error estimates may be overly optimistic (see Chapter 7).

The relationship between the geomagnetic field and Earth rotation has been investigated by evaluation of the electromagnetic torque that would act on the mantle if the base of the mantle consists of a thin, homogeneous, conducting layer. The torque has been computed for epochs 1900 to 1980 at 5 year intervals using recent models of the field and flow. The resulting time–dependence of the torque has been found to arise almost entirely from the time–dependence of the flow and certain features of the torque were shown to correspond to primarily non–zonal core flow in regions where the non–uniqueness of these flows is unresolved. Therefore a time–dependent torque has been computed using only the zonal terms of the flow. This preferred torque shows good agreement with the torque required to explain the decade fluctuations in the length of day and results in a best estimate of $6.7 \pm 0.9 \times 10^8 S$ for the conductance of such a layer. However a linear trend in the computed torque remains to be explained and it is believed this may arise from an over–simplistic downward continuation of the poloidal field to the base of the mantle. Various pieces of evidence relating to mantle conductivity have been drawn together in Chapter 7 and the conclusion reached that the base of the mantle may consist of a (thin) region of high conductivity.

8.2 Conclusions and future work

8.2.1 External and induced fields

The method developed in Chapters 2 and 3 to separate the external, induced and core fields offers a novel alternative to the application of more traditional time–series analysis techniques such as low, high and band–pass filtering which arbitrarily assume a distinction of the external and induced fields from the core field in the frequency domain. It has been shown that the method can successfully separate the external and induced fields from the core field by making prior assumptions about their time–dependence, which have then been further separated into parts of external and internal (induced) origin.

There are certainly short–comings in the method— for example the cubic time–dependence assumed for the core field is rather simple leading to a "sliding window" method which is clumsy though effective. It was also confirmed, after disturbance effects were removed from monthly means, that solar cycle modulations of the annual

(and perhaps biannual) periodicities can be large and so the estimates obtained for the amplitudes of these periodicities are probably averages over one or more solar cycles. A more sophisticated model could be developed in which the core field over a whole time-series is expanded in B-splines and the annual and biannual fluctuations allowed to vary with some solar cycle related function, perhaps a sequence of half sine waves of length 11 years as a crude approximation, or the smoothed sunspot number time-series. There probably is no "solar cycle variation" as such in the geomagnetic field — merely a solar cycle modulation of several geomagnetic phenomena.

The origins of the annual and biannual variations could certainly be tested more specifically; the large quantity of hourly means available on the National Geophysical Data Centre optical disk data base could be used for a systematic investigation of the ionospheric daily variation and its modulation on biannual, annual and solar cycle time-scales, as well as changes in character between quiet and disturbed times. At least one model of the S_q (solar quiet) field for a solar minimum year already exists (Campbell, 1989) and could be used to partially correct monthly and annual means for ionospheric effects. Better determinations of magnetic fields related to geo-solar interactions should allow improvements in our knowledge of the conductivity of the upper mantle, as well as better representations of the core field.

8.2.2   The time–dependent magnetic field and core flows

The investigation of the time-dependence of the core field can be approached from two opposing directions; firstly by considering these changes statistically, (as in Chapter 4) and secondly from the physical standpoint.

In the statistical/observational approach (effectively a "mapping" philosophy) the question is essentially reduced to one of how best the temporal and spatial dependence of the field can be summarised most concisely without loss of information. The application of the method of stochastic inversion to large data sets to determine over–parameterised models (eg. Bloxham & Jackson, 1991b) runs the inherent risk of over-fitting the data. Appropriate spatial norms for this method have been developed based on the physics of the geomagnetic field (as discussed in Chapter 5) but the choice of norm for the temporal expansion remains rather arbitrary — for example minimisation of the second

time–derivative of the field (Bloxham & Jackson, 1989). Although such time–dependent models give a good representation of changes in the field, the models derived in Chapter 5 appear to give a comparable fit to the data on the time–scale of a decade or so. These models were based on the assumption that all time–derivatives higher than the second are zero and therefore have a much simpler parameterisation, though of course this constraint is as arbitrary as minimisation of the second derivative. The models developed in Chapter 5 were intended to quantify the quadratic time–dependence of the field at specific epochs with no continuity constraints between such models. More general time–dependent models such as that of Bloxham & Jackson (1991b) provide a continuous representation of the field over long time spans and will therefore have wider applicability. The simultaneous inversion for main field and secular variation from original data is probably preferable as in principle it allows models of the secular variation and higher time–derivatives with convergent error estimates at the core–mantle boundary to be obtained.

From the physical standpoint the ability of inferred core flows to reproduce the observed secular variation is of key importance. Research in this field has gone beyond the simple question of whether or not flow models can account for the secular variation to questions of how accurately this can be done, and which constraints imposed on the flows are most compatible with the data. The use of models of secular variation for such investigations introduces an extra step in which statistical uncertainty can mar the results; proper assessment of flow models is most likely to be best served by relating flows directly to the data. This is particularily important in the case of apparently rapid features of the secular variation such as geomagnetic jerks. The assumption implicit in most investigations of flow at the top of the core is that of frozen–flux, ie. that diffusion in the core is negligible. As spatial resolution and temporal extent of geomagnetic data sets improve, hopefully with the introduction of more vector magnetic satellites with a significant lifespan and extension of the permanent magnetic observatory network, an understanding of diffusion in the dynamics of the core and how it can be incorporated in the determination of flow models will become increasingly important.

The method of piecewise regression analysis of time–series developed in Chapter 4 has applications beyond geomagnetism and probably beyond geophysics. The adapta-

tion of the method of Kent *et al* (1983) from principal components to regression analysis was relatively straightforward and could easily be modified further for other parameterisations of other data series. (For the picking of stratigraphic horizons in well–log data for example.) Although rather computer intensive, the algorithm can offer a useful method for the objective interpretation of noisy data where the underlying model is believed to be only piecewise continuous.

8.2.3 Mantle conductivity

As pointed out in Chapter 7 changes in the pole–strength computed at the core–mantle boundary suggest a possible failure of the frozen–flux hypothesis but could perhaps be attributable to the presence of a highly conducting region at the base of the mantle. The presence of such a layer could have profound implications for our understanding of the geomagnetic field and hence the dynamics of the core. If the conductivity is as high as the few thousand Sm^{-1} in the lowest few hundred kilometres of the mantle as has been suggested here then there could be a higher contrast in conductivity at the top of such a layer than at the core–mantle boundary itself. The forward problem of understanding the effects of such a layer on the magnetic field leaving the core needs to be carefully considered if we wish to accurately downward continue the observed field to the core mantle boundary. This could be especially important if significant heterogeneities in the conductivity at the base of the mantle exist as seems increasingly likely. However the hope of determining such a conductivity distribution from geomagnetic evidence alone seems slim. Even if lateral heterogeneity was on a large enough scale to be within the resolution of geomagnetic data we are faced with the ever present "blind deconvolution problem" of an unknown input to an unknown filter. However if such heterogeneities are as small as $100km$ as has been suggested elsewhere (Jeanloz, 1991) then even the forward modelling problem may have to be treated by a statistical averaging method. Indeed it has been suggested that apart from the dipole term, the geomagnetic field coefficients have the characteristics of a random process for each harmonic degree (Hulot & LeMouël, 1991). If the mantle is largely insulating apart from the metallic alloy products of a vigorous reaction between perovskite and liquid iron (Knittle & Jeanloz, 1991) then presumably some solid state diffusive equilibrium must be reached creating a boundary

layer at the base of the mantle. The radial variation of conductivity within such a layer does not appear to have been considered yet in the literature. The question of how and by what mechanism such highly conductive reaction products may be distributed within such a layer needs further investigation. For example recent work on Earth nutation forced by electromagnetic coupling (Buffet *et al*, 1990) has suggested the existence of a highly conducting layer at the base of the mantle, of similar conductance to that preferred in Chapter 7 though 2 orders of magnitude thinner. Stevenson (1990) has suggested that permeation of liquid iron from the core into the mantle may occur depending on the extent of CMB topography, which would have a significant effect on mean conductivity there, although the extent of such permeation is believed by some to be minor (Poirier & LeMouël, 1991).

8.2.4 Endpiece

The presence of highly electrically conducting regions at the base of the mantle is expected to lead to a significant interaction between the core and the mantle. As well as coupling arising from toroidal field induced in the conducting regions, toroidal field from the core may "leak" into the mantle giving rise to further torques. If torques strong enough to accelerate and decelerate the mantle arise from a thin conducting region then the stresses acting within such a region must be very large and the implications of this need consideration. If the conductivity is highly heterogeneous then advection of the magnetic field past such regions could lead to local intensification of the field (Jeanloz, 1990). Such locking of flux, perhaps over the time–scales of the core flow (several years say if the conductivity is sufficiently high), could lead to the accumulation of magnetic energy in a manner analogous to flux ropes in sunspots (see eg. Barnes & Sturrock, 1972). Concentration of flux could then lead to a catastrophic release of magnetic energy resulting in a sudden change in the geomagnetic field, such as a jerk (as suggested by Backus & Hough, 1985), on a time–scale shorter than that of core–flows.

Clearly such ideas are wildly speculative but there seems little doubt that jerks, and the sudden changes in the secular acceleration that characterise them, are a real phenomenon originating in the interior of the Earth. As it is now widely believed that the secular variation of the geomagnetic field arises primarily from flow in the upper part

of the core (see eg. Gubbins, 1991) such phenomena are likely to be associated with such flows also. However the time–scale of changes in the secular variation associated with such phenomena is so short, even compared to that of the flow, that they may well arise from some interaction of the magnetic field with the overlying mantle. The evidence presented in Chapter 6 pointing to electromagnetic core–mantle coupling as being significant implies that it may not be possible to treat the core and mantle as independently in geomagnetism as has often been the case. A burgeoning of research into core-mantle interactions is resulting from improved data sets and methods in geomagnetism and seismology. Recent research into pole paths during geomagnetic reversals point to significant heterogeneity of the lower mantle and control by the mantle of reversal transitions. Mineral physics experiments point to the lower mantle as possibly the most chemically active and heterogeneous zone of the Earth. If our understanding of the deep Earth, its magnetic field and the interaction between the core and mantle is to be significantly advanced these apparently disparate subjects will have to be skillfully blended to lead to a better understanding of the dynamics of the Earth and ultimately other planets.

References

Achache, J., Courtillot, V., Ducruix, J., LeMouël, J. L., 1980. The late 1960's secular variation impulse: constraints on deep mantle conductivity, *Phys. Earth. Planet. Inter.*, **23**, 72–75.

Achache, J., LeMouël, J.-L., Courtillot, V., 1981. Long period geomagnetic variations and mantle conductivity: an inversion using Bailey's method, *Geophys. J. R. Astron. Soc.*, **65**, 579–601.

Akaike, H., 1973. Information Theory and an extension of the maximum likelihood principle, in *Proceedings of the 2nd International Symposium on Information Theory*, eds. Petrov and Czaki, p267–281.

Aldridge, K. D., Bloxham, J., Dehant, V., Gubbins, D., Hide, R., Hinderer, J., Hutcheson, K., Jault, D., Jones, C. A., Legros, H., LeMouël, J. L., Lloyd, D., Wahr, J. M., Whaler, K. A., Zhang, K., 1990. Core–Mantle interactions, *Surveys in Geophysics*, **11**, 329–353.

Alldredge, L. R., 1975. A hypothesis for the source of impulses in geomagnetic secular variations, *J. Geophys. Res.*, **80**, 1571–1578.

Alldredge, L. R., 1976. Effects of solar activity on annual means of gemagnetic field components, *J. Geophys. Res.*, **81**, 2990–2996.

Alldredge, L. R., 1977a. Geomagnetic variations with periods from 13 to 30 years, *J. Geomagn. Geoelectr.*, **29**, 123–235.

Alldredge, L. R., 1977b. Deep mantle conductivity, *J. Geophys. Res.*, **82**, 5427–5431.

Alldredge, L. R., 1979. Commentaire sur: "Sur une accélération récente de la variation séculaire du champ magnétique terrestre" de Vincent Courtillot, Joël Ducruix et Jean-Louis Le Mouël, *C. R. Hebd. Sceances Acad. Sci. Ser. B*, **289**, 169–171.

Alldredge, L. R., 1984. A Discussion of Impulses and Jerks in the geomagnetic field, *J. Geophys. Res.*, **89**, 4403–4412.

Alldredge, L. R., Stearns, C. O., Sugiura, M., 1979. Solar cycle variations in geomagnetic external spherical harmonic coefficients, *J. Geomagn. Geoelectr.*, **31**, 495–508.

Anderson, D. L., 1989. Theory of the Earth, Blackwell Scientific Publications, London.

Arfken, G, 1985. Mathematical methods for physicists, Academic Press, Inc., London, *third edition, international edition.*

Backus, G. E., 1968. Kinematics of geomagnetic secular variation in a perfectly conducting core, *Phil. Trans. R. Soc. London*, **A263**, 239-266.

Backus, G. E., 1982. The electric field produced in the mantle by the dynamo in the core, *Phys. Earth. Planet. Inter.*, **28**, 191-214.

Backus, G. E., 1983. Application of mantle filter theory to the magnetic jerk of 1969, *Geophys. J. R. Astron. Soc.*, **74**, 713-746.

Backus, G. E., Estes, R. H., Chinn, D., Langel, R. A., 1987. Comparing the jerk with other global models of the geomagnetic field from 1960 to 1978, *J. Geophys. Res.*, **92**, 3615-3622.

Backus, G. E., Hough, S., 1985. Some models of the geomagnetic field in western Europe from 1960-1980, *Phys. Earth. Planet. Inter.*, **39**, 243-254.

Backus, G. E., Le Mouël, J.-L., 1986. The region on the core-mantle boundary where a geostrophic velocity field can be determined from frozen-flux geomagnetic data, *Geophys. J. R. Astron. Soc.*, **85**, 617-628.

Banks, R. J., 1969. Geomagnetic variations and the conductivity of the upper mantle, *Geophys. J. R. Astron. Soc.*, **17**, 457-487.

Banks, R. J., 1972. The overall conductivity distribution of the Earth, *J. Geomagn. Geoelectr.*, **24**, 337-351.

Barnes, C. W., Sturrock, P. A., 1972. Force-free magnetic-field structures and their role on solar flare activity, *Astrophys. Jou.*, **174**, 659-670.

Barraclough, D. R., 1974. Spherical harmonic analysis of the geomagnetic field for eight epochs between 1600 and 1910, *Geophys. J. R. Astron. Soc.*, **36**, 497-513.

Barraclough, D. R., 1978. Spherical harmonic models of the geomagnetic field, *Geomagnetic Bulletin 8*, HMSO Stationery Office, London.

Barraclough, D. R., 1981. The 1980 geomagnetic reference field, *Nature*, **294**, 14-15.

Barraclough, D. R., Harwood, J. M., Leaton, B. R., Malin S. R. C., 1975. A model of the geomagnetic field at 1975, *Geophys. J. R. Astron. Soc.*, **43**, 645-649.

Barraclough, D. R., Harwood, J. M., Leaton, B. R., Malin S. R. C., 1978. A definitive model of the geomagentic field and its secular variation for 1965 I: derivation of the

model and comparison with the IGRF, *Geophys. J. R. Astron. Soc.*, **55**, 111–121.

Barraclough, D. R., Clark, T. D. G., Cowley, S. W. H., Gubbins, D., Hibberd, F. H., Hide, R., Kerridge, D. J., Lowes, F. J., Malin, S. R. C., Murphy, T., Rishbeth, H., Runcorn, S. K., Soffel, H. C., Stewart, D. N., Stuart, W. F., Whaler, K. A., Winch, D. E., 1992. 150 years of magnetic observatories: recent researches on world data, *Surveys in Geophysics*, **13**, 47–88.

Benton, E. R., Estes, R. H., Langel, R. A., 1987. Geomagnetic field modeling incorporating constraints from frozen–flux geomagnetism, *Phys. Earth. Planet. Inter.*, **48**, 241–264.

Benton, E. R., Voorhies, C. V., 1987. Testing recent geomagnetic field models via magnetic flux conservation at the core–mantle boundary, *Phys. Earth. Planet. Inter.*, **48**, 350–357.

Benton, E. R., Whaler, K. A., 1983. Rapid diffusion of the poloidal geomagnetic field through the weakly conducting mantle: a perturbation solution, *Geophys. J. R. Astron. Soc.*, **75**, 77–100.

Bloxham, J., 1987. Simultaneous stochastic inversion for geomagnetic main field and secular variation 1. A large scale inverse problem, *J. Geophys. Res.*, **92**, 11597–11608.

Bloxham, J., Gubbins, D., 1985. The secular variation of the Earth's magnetic field, *Nature*, **317**, 777–781.

Bloxham, J., Gubbins, D., 1986. Geomagnetic field analysis IV: testing the frozen–flux hypothesis, *Geophys. J. R. Astron. Soc.*, **84**, 139–152.

Bloxham, J., Gubbins, D., Jackson, A., 1989. Geomagnetic secular variation, *Phil. Trans. Roy. Soc. Lon.*, **329**, 415–502.

Bloxham, J., Jackson, A., 1989. Simultaneous stochastic inversion for geomagnetic main field and secular variation 2. 1820–1980, *J. Geophys. Res.*, **94**, 15753–15769.

Bloxham, J., Jackson, A., 1990. The secular variation of the Earth's magnetic field, in Reversals, secular variation and dynamo theory, *SEDI Symposium Abstracts*, Sante Fe, New Mexico, 1990.

Bloxham, J., Jackson, A., 1991a. Fluid flow near the surface of Earth's outer core, *Reviews of Geophysics*, **29**, 97–120.

Bloxham, J., Jackson, A., 1991b. Time–dependent mapping of the magnetic field at the

core–mantle boundary, preprint submitted to *J. Geophys. Res.*.

Buffet, B. A., Herring, T. A., Mathews, P. M., Shapiro, I. I., 1990. Anomalous dissipation in the Earth's forced nutation: inferences on electrical conductivity at the core–mantle boundary, *Trans. Am. Geophys. Union*, **71**, **17**, p496.

Bullard, E. C., Freedman, C., Gellman, H., Nixon, J., 1950. The westward drift of the Earth's magnetic field, *Phil. Trans. R. Soc. London*, **A243**, 67–92.

Campbell, W. H., 1980. Secular, annual and semiannual changes in the baseline level of the Earth's magnetic field at North American locations, *J. Geophys. Res.*, **85**, 6557–6571.

Campbell, W. H., 1982. Annual and semi–annual changes of the quiet daily variations S_q in the geomagnetic field at North American locations, *J. Geophys. Res.*, **87**, 785–796.

Campbell, W. H., 1987. Some effects of quiet geomagnetic field changes upon values used for main field modeling, *Phys. Earth. Planet. Inter.*, **48**, 193–199.

Campbell, W. H., 1989. Global quiet day field variation model WDCA/SQ1, *EOS*, **70**, 66–74.

Campbell, W. H., Matsushita, S., 1982. S_q currents: a comparison of quiet and active year behaviour, *J. Geophys. Res.*, **87**, 5305–5308.

Chapman, S., 1919. Solar and lunar diurnal variations of terrestrial magnetism, *Phil. Trans. R. Soc. London*, **A218**, 1–118.

Chapman, S., Bartels, J., 1940. Geomagnetism, Oxford University Press, two volumes.

Chatfield, C., 1984. The Analysis of Time Series: An Introduction, Chapman and Hall, London, (third edition).

Courtillot, V., Ducruix, J., LeMouël, J. L., 1978. Sur une accélération récente de la variation séculaire du champ magnétique terrestre, C. R. Hebd. sceances Acad. Sci. Ser. D, **287**, 1095–1098.

Courtillot, V., LeMouël, J. L., 1976a. On the long period variations of the Earth's magnetic field from 2 months to 20 years, *J. Geophys. Res.*, **81**, 2941–2950.

Courtillot, V., LeMouël, J. L., 1976b. Time variations of the Earth's magnetic field with a period longer than two months, *Phys. Earth. Planet. Inter.*, **12**, 237–240.

Courtillot, V., LeMouël, J. L., 1979. Comment on "Deep Mantle Conductivity" by L. R. Alldredge, *J. Geophys. Res.*, **84**, 4785–4793.

Courtillot, V., LeMouël, J. L., 1984. Geomagnetic secular variation impulses, *Nature*, **311**, 709–716

Courtillot, V., LeMouël, J. L., Ducruix, J., 1984. On Backus' mantle filter theory and the 1969 geomagnetic impulse, *Geophys. J. R. Astron. Soc.*, **78**, 619–625.

Cox, A., Doell, R. R., 1964. Long period variations of the geomagnetic field, *Bull. Seismol. Soc. Amer.*, **54**, 2243–2270.

Creager, K. C., Jordan, T.H., 1986. Aspherical structure of the core–mantle boundary from PKP travel–times, *Geophys. Res. Lett.*, **13**, 1497–1500.

Currie, R. G., 1966. The geomagnetic spectrum – 40 days to 5.5 years, *J. Geophys. Res.*, **71**, 4579–4598.

Currie, R. G., 1967. Magnetic shielding properties of the Earth's mantle, *J. Geophys. Res.*, **72**, 2623–2633.

Currie, R. G., 1968. Geomagnetic spectrum of internal origin and lower mantle conductivity, *J. Geophys. Res.*, **73**, 2779–2786.

Dowson, M. J., Buckingham, J. P., Simmons, D. A., 1988. Notes on geomagnetic repeat measurements at Grytviken, April 1987, *Br. Antarct. Surv. Bull.*, **71**, 49–52.

Ducruix, J., Courtillot, V., LeMouël, J. L., 1980. The late 1960s secular variation impulse, the 11 year magnetic variation and the electrical conductivity of the deep mantle, *Geophys. J. R. Astron. Soc.*, **61**, 73–94.

Edmonds, A., R., 1957. Angular momentum in quantum mechanics, Princeton University Press, Princeton, New Jersey.

Gavoret, J., Gibert, D., Menveille, M., LeMouël, J. L., 1986. Long term variations of the external and internal components of the Earth's magnetic field, *J. Geophys. Res.*, **91**, 4787–4796.

Gilbert, W., 1600. De Magnete, Gilbert Club revised English translation, Chiswick Press, London.

Gire, C., Le Mouël, J.-L., 1986. Flow in the fluid core and Earth's rotation, in *Earth rotation: solved and unsolved problems*, Cazenave, A., (ed.), NATO ASI Series C: Vol 187, p241–258.

Gire, C., Le Mouël, J.-L., 1990. Tangentially geostrophic flow at the core–mantle boundary compatible with the observed geomagnetic secular variation: the large scale com-

ponent of the flow, *Phys. Earth. Planet. Inter.*, **59**, 259–287.

Godivier, R., 1982. Observations Magnetiques, Bangui No.3, République centrafricaine de 1972 à 1981, Office de la Récherche Scientifique et Technique Outre–mer.

Golovkov, V. P., Zvereva, T. I., Simonyan, A. O., 1989. Common feature and differences between "jerks" of 1947, 1958 and 1969, *Geophys. Astrophys. Fluid Dyn.*, **49**, 81–96.

Gubbins, D., 1983. Geomagnetic field analysis I: Stochastic inversion, *Geophys. J. R. Astron. Soc.*, **73**, 641–652.

Gubbins, D., 1984. Geomagnetic field analysis —II. Secular variation consistent with a perfectly conducting core, *Geophys. J. R. Astron. Soc.*, **77**, 753–766.

Gubbins, D., 1991. Dynamics of the secular variation, *Phys. Earth. Planet. Inter.*, **68**, 170–182.

Gubbins, D., Bloxham, J., 1985. Geomagnetic field analysis —III. Magnetic fields on the core–mantle boundary, *Geophys. J. R. Astron. Soc.*, **80**, 695–713.

Gubbins, D., Roberts, P., H., 1987. Magnetohydrodynamics of the Earth's core, in *Geomagnetism Volume 2*, ed. Jacobs, J., A., Academic press, London.

Gubbins, D., Tomlinson, L., 1986. Secular variation from monthly means from Apia and Amberley magnetic observatories, *Geophys. J. R. Astron. Soc.*, **86**, 603–616.

Gwinn, C. R., Herring, T. A., Shapiro, I. I., 1986. Geodesy by radio interferometry: studies of forced nutations of the Earth 2. Interpretation, *J. Geophys. Res.*, **91**, 4755–4765.

Hald, A., 1952. Statistical Theory with Engineering Applications, John Wiley & Sons, Canada.

Harwood, J. M., Malin, S. R. C., 1977. Sunspot cycle influence on the geomagnetic field, *Geophys. J. R. Astron. Soc.*, **50**, 605–619.

Hide , R., 1978. How to locate the electrically conducting fluid core of a planet from external magnetic observations, *Nature*, **271**, 640–641.

Hide, R., 1986. Presidential address– The Earth's differential rotation, *Q. Jl R. astron. Soc.*, **278**, 3-14.

Hide, R., Malin, S. R. C., 1981. On the determination of the size of the Earth's core from observations of the geomagnetic secular variation, *Proc. Roy. Soc. London*, **A374**, 15–33.

Hide, R., 1989. Fluctuations in the Earth's rotation and the topography of the core–mantle interface, *Phil. Trans. R. Soc. London*, **A328**, 351–363.

Hodder, B. M., 1981. Geomagnetic secular variation since 1901, *Geophys. J. R. Astron. Soc.*, **65**, 763–776.

Hulot, G., Le Mouël, J.-L., 1991. Statistical properties of the core field, *AGU 1991 Fall meeting abstracts*, abstract GP32A-3.

Ince, E., L., 1956. Ordinary differential equations, Dover publications.

Jackson, A., 1989. The Earth's magnetic field at the core mantle boundary, *Ph.D. Thesis*, Univeristy of Cambridge.

Jackson, A., Bloxham, J., 1990. Angular momentum in the core-mantle system, *Eos: Transactions of the American Geophysical Union*, **71**, No.43, Abtract GP21B-11.

Jackson, A., Bloxham, J., 1991. Mapping the fluid flow and shear near the core surface using the radial and horizontal components of the magnetic field, *Geophys. J. Int.*, **105**, 199–212.

Jackson, A. Bloxham, J., Gubbins, D., 1991. Time–dependent flow at the core surface and conservation of angular momentum in the coupled core–mantle system, *Geophysical Monograph series: Proceedings of IUGG Symposium U6—"Dynamics of the Earth's Deep Interior"*, Vienna, (preprint).

Jackson, J. D., 1975. Classical Electrodynamics, Second Edition, John Wiley and Sons, New York.

Jackson, J. E., 1991. A user's guide to principal components, John Wiley & Sons, Inc, New York.

Jacobs, J.A., (ed.), 1987a. Geomagnetism Volume 1, Academic Press, London.

Jacobs, J.A., (ed.), 1987b. Geomagnetism Volume 2, Academic Press, London.

Jacobs, J. A., (ed.), 1989. Geomagnetism Volume 3, Academic Press, London.

Jacobs, J. A., (ed.), 1991. Geomagnetism Volume 4, Academic Press, London.

Jady, R. A., 1975. Electromagnetic induction in the mantle by aperiodic variations, *Geophys. J. R. Astron. Soc.*, **40**, 67–83.

Jady, R. A., Paterson, G., A., Whaler, K. A., 1983. Inversion of electromagnetic induction problem using Parkers' algorithms with both precise and practical data, *Geophys. J. R. Astron. Soc.*, **75**, 125–142.

Jault, D., Gire, C., Le Mouël, J.-L., 1988. Westward drift, core motions and exchanges of angular momentum between core and mantle, *Nature*, **333**, 353-356

Jault, D., LeMouël, J.-L., 1989. The topographic torque associated with a tangentially geostrophic motion at the core surface and inferences on the flow inside the core, *Geophys. Astrophys. Fluid Dyn.*, **48**, 273-296.

Jeanloz, R., 1990. The nature of the Earth's core, *Ann. Rev. Earth Planet. Sci.*, **18**, 357-386.

Jeanloz, R., 1991. Nature and processes of the deep mantle and core, abstract from session U1, program and abstracts, IUGG Vienna, 1991.

Jones, A. G., 1980. Report on the COPROD study, Paper read at the Fifth workshop on electromagnetic induction in the Earth and Moon, Istanbul.

Kellog, O. D., 1953. Foundations of Potential Theory, Dover Publications, New York.

Kendall, M. G., Stuart, A., 1961. The Advanced Theory of Statistics, Volume 2, Charles Griffin & Company Limited, London.

Kent, J. T., Briden, J. C., Mardia K.V., 1983. Linear and planar structure in ordered multivariate date as applied to progressive demagnetization of palaeomagnetic remanence, *Geophys. J. R. Astron. Soc.*, **75**, 593-621.

Kerridge, D. J., Barraclough, D. R., 1985. Evidence for geomagnetic jerks from 1931 to 1971, *Phys. Earth. Planet. Inter.*, **39**, 228-236.

Knittle, E., Jeanloz, R., 1991. Earth's core-mantle boundary: results of experiments at high pressures and temperatures, *Science*, **251**, 1438-1443.

Kolomiytseva, G. I., 1972. Distribution of electrical conductivity in the mantle of the Earth, according to data on secular geomagnetic variations, *Geomagn. Aeron.*, **12**, 1082-1085; English trans. 938-941.

Kotzé, P. B., Kühn, G. J., Scheepers, G. L. M., 1991. Abrupt secular variation change in the southern African region in 1984, *IUGG, Vienna, abstracts*, session GAM 1.1.

Lambeck, K., 1980. The Earth's variable rotation, Cambridge University Press.

Langel, R., A., 1987. The Main Geomagnetic Field, Chapter 4 in *Geomagnetism, Volume 1*, ed. Jacobs, J., A.

Langel, R. A., Benson, B. J., Orem., R. M., 1991. The Magsat Bibliography, NASA Technical memorandum 100776, National Aeronautics and Space Administration, Wash-

ington D.C.

Langel, R. A., Estes, R. H., 1985. Large scale, near field, magnetic fields from external sources and the corresponding induced internal field, *J. Geophys. Res.*, **90**, 2487-2494.

Langel, R. A., Estes, R. H., Mead, G. D., 1982. Some new methods in geomagnetic field modeling applied to the 1960-1980 epoch, *J. Geomagn. Geoelectr.*, **34**, 327-349.

Langel, R. A., Kerridge, D. J., Barraclough, D. R., Malin, S. R. C ., 1986. Geomagnetic temporal change: 1903-1982, a spline representation, *J. Geomagn. Geoelectr.*, **38**, 573-597.

Langel, R. A., Estes, R. H., Sabaka, T. J., 1989. Uncertainty estimates in geomagnetic field modeling, *J. Geophys. Res.*, **94**, 12281-12299.

Lawson, C. L., Hanson, R. J., 1974. Solving least squares problems, Prentice Hall, Englewood Cliffs, N. J.

Le Mouël, J.-L., 1984, Outer core geostrophic flow and secular variation of Earth's magnetic field, *Nature*, **311**, 734-735.

Le Mouël, J.-L., Courtillot, V., 1981. Core motions, electromagnetic core–mantle coupling and variations in the Earth's rotation: new constraints from geomagnetic secular variation impulses, *Phys. Earth. Planet. Inter.*, **24**, 236-241.

Le Mouël, J.-L., Courtillot, V., 1982. On the outer layers of the core and geomagnetic secular variation, *J. Geophys. Res.*, **87**, 4103-4108.

Le Mouël, J.-L., Ducruix, J., Duyen, C. H., 1982. The worldwide character of the 1969-1970 impulse of secular acceleration rate, *Phys. Earth. Planet. Inter.*, **28**, 337-350.

Le Mouël, J.-L., Madden, T., R., Ducruix, J., Courtillot, V.,1981. Decade fluctuations in geomagnetic westward drift and Earth rotation, *Nature*, **290**, p763-765.

Li, X., Jeanloz, R., 1987. Electrical conductivity of $(Mg,Fe)SiO_3$ perovskite and a perovskite dominated assemblage at lower mantle conditions, *Geophys. Res. Lett.*, **14**, 1075-1078.

Linhart H., Zucchini W., 1986. Model selection, John Wiley & Sons, New York.

Lloyd, D., Gubbins, D., 1990. Toroidal fluid motion at the top of the Earth's core, *Geophys. J. Int.*, **100**, 455-467.

Lowes, F., J., 1966. Mean square values on the sphere of spherical harmonic vector fields, *J. Geophys. Res.*, **71**, 2179.

Lowes, F., J., 1974. Spatial power spectrum of the main geomagnetic field, and extrapolation to the core, *Geophys. J. R. Astron. Soc.*, **36**, 717–730.

Malin, S. R. C., 1969. Geomagnetic secular variation and its changes 1942.5 to 1962.5, *Geophys. J. R. Astron. Soc.*, **17**, 415–441.

Malin, S. R. C., Clark, A. D., 1974. Geomagnetic secular variation 1962.5 to 1967.5, *Geophys. J. R. Astron. Soc.*, **36**, 11–20.

Malin, S. R. C., Hodder, B. M., 1982. Was the 1970 geomagnetic jerk of internal or external origin? *Nature*, **296**, 726–728.

Malin, S. R. C., Hodder, B. M., Barraclough, D. R., 1983. Geomagnetic secular variation: a jerk in 1970, *Ebro Observatory Mem. Pub.*, **14**, 239-256.

Malin S. R. C., Isikara, A. M., 1976. Annual variation of the geomagnetic field, *Geophys. J. R. Astron. Soc.*, **47**, 445–457.

Matsushita, S., Campbell, W. H., (eds.), 1967. Physics of Geomagnetic Phenomena, Academic Press, (two volumes).

Mayaud P. N., 1980. Derivation, meaning and use of geomagnetic indices, American Geophysical Union, Washington D.C.

McCarthy, D. D., Babcock, A. K., 1986. The length of day since 1656, *Phys. Earth. Planet. Inter.*, **44**, 281–292.

McDonald, K. L., 1957. Penetration of the geomagnetic field through a mantle of variable conductivity, *J. Geophys. Res.*, **62**, 117–141.

McLeod, M. G., 1982. A note on secular variation of the geomagnetic field, *Phys. Earth. Planet. Inter.*, **29**, 119–134.

McLeod, M. G., 1989a. Geomagnetic jerks and secular variation, preprint.

McLeod, M. G., 1989b. Geomagnetic jerks and secular variation, *Abstract, AGU Fall meeting*.

Melchior, P., 1986. The Physics of the Earth's Core: an introduction, Pergamon Press, Oxford.

Montgomery, D., C., Peck, E. A., Introduction to Linear Regression Analysis, John Wiley & Sons, Canada, 1982.

Mörner, N.-A., 1989. Changes in the Earth's rotation on an El Niño to century basis, in *Geomagnetism and Palaemagnetism*, F.J. Lowes, 45–53.

Morelli, A., Dziewonski, A. M., 1987. Topography of the core–mantle boundary and lateral heterogeneity of the liquid core, *Nature*, **325**, 678–683.

Morrison, L. V., 1979. Re–determination of the decade fluctuations in the rotation of the Earth in the period 1861–1978, *Geophys. J. R. Astron. Soc.*, **58**, 349–360.

Murtagh, F., Heck, A., 1987. Multivariate Data Analysis, Reidel, Netherlands.

National Geophysical Data Centre, (1987). Selected geomagnetic and other solar–terrestrial physics data of NOAA and NASA, (optical disc NGDC01), NGDC, 325 Broadway, Boulder, Colorado 80303, USA.

Neuberg, J., Wahr, J., 1991. Detailed investigation of a spot on the core–mantle boundary using digital PcP data, *Phys. Earth. Planet. Inter.*, **68**, 132–143.

Nevenlinna, H., Sucksdorff, C., 1981. Impulse in global geomagnetic "secular variation", 1977–1979, *J. Geophys.*, **50**, 68–69.

Numerical Algorithms Group Limited, 1988. NAG Manual Mk. 13 Volume 4, Numerical Algorithms Group Limited, Oxford, 1988, ISBN1–85206–040–9.

Oldenburg, D. W., 1983. Funnel functions in linear and non–linear appraisal, *J. Geophys. Res.*, **88**, 7387–7398.

Parker, E. N., 1979. Cosmical Magnetic Fields, their origin and their activity, Oxford University Press, Oxford.

Parkinson, W. D., 1983. Introduction to Geomagnetism, Scottish Academic Press.

Parkinson, W. D., Hutton, V. R. S., 1989. The Electrical Conductivity of the Earth, in *Geomagnetism, Volume 3*, ed. Jacobs, J. A., Academic Press, 1989.

Paulus, M., 1986. Elektromagnetische Kern–Mantel Kopplung, Diploma thesis, University of Freiburg.

Paulus, M., Stix, M., 1986. Electromagnetic core–mantle coupling, in *Earth rotation: solved and unsolved problems*, Cazenave, A., (ed.), NATO ASI Series C: Vol 187, 259–267.

Paulus, M., Stix, M., 1989. Electromagnetic core–mantle coupling: the Fourier method for the solution of the induction equation, *Geophys. Astrophys. Fluid Dyn.*, **47**, 237–249.

Phinney, R. A., Burridge, R., 1973. Representation of the elasto–gravitational excitation of a spherical Earth model by generalized spherical harmonics, *Geophys. J. R. Astron.*

Soc., **34**, 451–487.

Poirier, J. P., Le Mouël, J.-L., 1991. Does "infiltration" of the core into the lower mantle affect the geomagnetic secular variation?, *AGU 1991 Fall meeting program and abstracts*, abstract GP32A-2.

Preisendorfer, R. W., 1988. Principal component analysis in meteorology and oceanography, posthumously compiled and edited by Mobley, C. D., Elsevier, Oxford.

Press, W. H., Flannery, B. P., Teukolsky, S. A., Vetterling, W. T., Numerical Recipes: the Art of Scientific Computing, Cambridge University Press, Cambridge, 1989.

Roberts, P. H., Scott, S., 1965. On the analysis of secular variation, 1 A hydromagnetic constraint: theory, *J. Geomagn. Geoelectr.*, **17**, 137–151.

Rochester, M., G., 1960. Geomagnetic westward drift and irregularities in the Earth's rotation, *Phil. Trans. Roy. Soc. Lon.*, **A252**, 531–555.

Rochester, M., G., 1984. Causes of fluctuations in the rotation of the Earth, *Phil. Trans. Roy. Soc. Lon.*, **A313**, 95–105.

Roden, R. B., 1963. Electromagnetic core–mantle coupling, *Geophys. J. R. Astron. Soc.*, **7**, 361–374.

Runcorn, S. K., 1955. The electrical conductivity of the Earth's mantle, *Trans. Am. Geophys. Un.*, **36**, 191–198.

Schot, S. H., 1978. Jerk: the time rate of change of acceleration, *Am. J. Phys.*, **46**, 1090–1094.

Schultz, A., Larsen, J. C., 1987. On the electrical conductivity of the mid–mantle — I. Calculation of equivalent scalar magnetotelluric response functions, *Geophys. J. R. Astron. Soc.*, **88**, 733–761.

Schuster, A., 1889. The diurnal variation of Terrestrial magnetism, *Phil. Trans. R. Soc. London*, **A180**, 467–518.

Simmons, D. A, 1986. Geomagnetic repeat measurements at Grytviken, November 1984, *Br. Antarct. Surv. Bull.*, **71**, 69–72.

Smith, Donald, R., 1974. Variational Methods in Optimization, Prentice Hall.

Stacey, F. D., MacQueen, H. W., Smylie, D. E., Rochester, M. G., Conley, D., 1978. Geomagnetic secular variation and lower mantle electrical conductivity, *Trans. Am. Geophys. Un.*, (abstract), **59**, 1027.

Stephenson, F. R., Morrison, L. V., 1984. Long–term changes in the rotation of the Earth: 700 B.C. to A.D. 1980, *Phil. Trans. R. Soc. London*, **A313**, 47–70.

Stevenson, D., 1990. The core–mantle permeable membrane, *Eos: Transactions of the American Geophysical Union*, **71**, **No.43**, Abstract GP21B-1.

Stewart, D. N., Whaler, K. A., 1992. Geomagnetic disturbance fields: an analysis of monthly means, *Geophys. J. Int.*, **108**, 215–223.

Stix, M., 1982. On Electromagnetic core-mantle coupling, *Geophys. Astrophys. Fluid Dyn.*, **21**, 303–313.

Stix, M., Roberts, P. H., 1984. Time–dependent electromagnetic core–mantle coupling, *Phys. Earth. Planet. Inter.*, **36**, 49–60.

Vestine, E. H., Kahle, A. B., 1968. The westward drift and geomagnetic secular change, *Geophys. J. R. Astron. Soc.*, **15**, 29–37.

Voorhies, C. V., 1984. Magnetic location of the Earth's core–mantle boundary and estimates of the adjacent fluid motion, *PhD thesis*, Faculty of the Graduate School of the University of Colorado, Department of Astrophysical, Planetary and Atmospheric Sciences.

Voorhies, C. V., 1986. Steady flows at the top of Earth's core derived from geomagnetic field models, *J. Geophys. Res.*, **91**, 12444–12466.

Voorhies, C. V., Backus, G. E., 1985. Steady flows at the top of the core from geomagnetic field models: The steady motions theorem, *Geophys. Astrophys. Fluid Dyn.*, **32**, 163–173.

Voorhies, C. V., Benton, E. R., 1982. Pole strength of the Earth from MAGSAT and magnetic determination of the core radius, *Geophys. Res. Lett.*, **9**, 258–261.

Walker, G. B., O'Dea, P. L., 1952. Geomagnetic secular–change impulses, *Eos Trans. AGU*, **33**, 797–800.

Weber, A. M., Roberts, E. B., 1951. The 1950 world isogonic chart, *J. Geophys. Res.*, **56**, 81–84.

Weidelt, P., 1972. The Inverse Problem of Geomagnetic Induction, 257–289 in *Zeischrift für Geophysik, 1972, Band 38*, Physica–Verlag, Würzburg.

Weidelt, P., 1985. Construction of conductance bounds from magnetotelluric impedences, *J. Geophys.*, **57**, 191–206.

Whaler, K. A., 1986. Geomagnetic evidence for fluid upwelling at the core–mantle boundary, *Geophys. J. R. Astron. Soc.*, **86**, 563–588.

Whaler, K. A., 1987. A new method for analysing geomagnetic impulses, *Phys. Earth. Planet. Inter.*, **48**, 221-240.

Whaler, K. A., 1990. A steady velocity field at the top of the Earth's core in the frozen–flux approximation — errata and further comments, *Geophys. J. Int.*, **102**, 507–509.

Whaler, K. A., 1991. Properties of steady flows at the core–mantle boundary in the frozen–flux approximation, *Phys. Earth. Planet. Inter.*, **68**, 144–155.

Whaler, K. A., Clarke, S. O., 1988. A steady velocity field at the top of the Earth's core in the frozen flux approximation., *Geophys. J.*, **94**, 143-155.

Whaler, K. A., Gubbins, D., 1981. Spherical harmonic analysis of the geomagnetic field: an example of a linear inverse problem, *Geophys. J. R. Astron. Soc.*, **65**, 645–693.

Winch, D. E., 1974. Evaluation of geomagnetic dynamo integrals, *J. Geomagn. Geoelectr.*, **26**, 87–94.

Wonnacott, T., H., Wonnacott, R., J., 1981. Regression: A Second Course in Statistics, John Wiley & Sons, Canada.

Yukutake, T., Cain, J., 1979. Solar cycle variations of the first degree spherical harmonic components of the geomagnetic field, *J. Geomagn. Geoelectr.*, **31**, 509–544.

Appendix A

Summary of data used in field models

Table A.1: Start and end years of the segments (see Chapter 4) which define the quadratic time–dependence used as data in the stochastic inversions of Chapter 5, resulting in time–dependent field models PR1970, PO1970, PR1978, PO1978, PR1983 and PO1983.

IAGA code	Component	PR1970	PO1970/PR1978	PO1978/PR1983	PO1983
AAA	X	—	1967.5–1986.5	1967.5–1986.5	—
AAA	Y	—	1967.5–1986.5	1967.5–1986.5	—
AAA	Z	—	1970.5–1976.5	1974.5–1988.5	1974.5–1988.5
AAE	X	1958.5–1972.5	1971.5–1979.5	1977.5–1982.5	1984.5–1989.5
AAE	Y	1958.5–1963.5	1961.5–1982.5	1961.5–1982.5	1983.5–1989.5
AAE	Z	1958.5–1966.5	1968.5–1984.5	1968.5–1984.5	1982.5–1988.5
ABG	X	1944.5–1960.5	1963.5–1985.5	1963.5–1985.5	1983.5–1988.5
ABG	Y	1966.5–1971.5	1970.5–1988.5	1970.5–1988.5	—
ABG	Z	1947.5–1970.5	1968.5–1983.5	1968.5–1983.5	1983.5–1989.5
AIA	X	1957.6–1984.5	1957.6–1984.5	1957.6–1984.5	—
AIA	Y	1957.6–1973.5	1971.5–1979.5	1978.5–1984.5	—
AIA	Z	1957.6–1979.5	1957.6–1979.5	1978.5–1983.5	—
ALE	X	1962.5–1970.5	1968.5–1977.5	1975.5–1985.5	1983.5–1988.5
ALE	Y	1962.5–1969.5	1969.5–1974.5	—	—
ALE	Z	1961.9–1973.5	1974.5–1980.5	1974.5–1980.5	1983.5–1988.5
ALM	X	1956.5–1968.5	1972.5–1985.5	1972.5–1985.5	1983.5–1989.5
ALM	Y	1956.5–1966.5	1964.5–1984.5	1964.5–1984.5	1982.5–1989.5
ALM	Z	1955.5–1978.5	—	1976.5–1989.5	1976.5–1989.5
ANN	X	1960.5–1972.5	1971.5–1976.5	—	1977.5–1988.5
ANN	Y	1962.5–1975.5	1962.5–1975.5	—	1979.5–1988.5
ANN	Z	1962.5–1970.5	1969.5–1985.5	1969.5–1985.5	1983.5–1988.5
API	X	1969.5–1974.5	1969.5–1974.5	1978.5–1984.5	—
API	Y	1958.5–1972.5	1970.5–1977.5	1975.5–1983.5	1981.5–1988.5
API	Z	—	1974.5–1986.5	1974.5–1986.5	1984.5–1989.5
AQU	X	1964.5–1970.5	1968.5–1989.5	1968.5–1989.5	1968.5–1989.5
AQU	Y	1961.5–1969.5	1968.5–1979.5	1978.5–1983.5	1981.5–1989.5
AQU	Z	1962.5–1989.5	1962.5–1989.5	1962.5–1989.5	1962.5–1989.5
ARS	X	1926.5–1966.5	1971.5–1986.5	1971.5–1986.5	—
ARS	Y	1951.5–1974.5	1972.5–1980.5	—	—
ARS	Z	1949.5–1971.5	1969.5–1978.5	1976.5–1984.5	—
ASH	X	1959.5–1986.5	1959.5–1986.5	1959.5–1986.5	1984.5–1989.5
ASH	Y	1959.5–1989.5	1959.5–1989.5	1959.5–1989.5	—
ASH	Z	1963.5–1970.5	1968.5–1977.5	1975.5–1989.5	1975.5–1989.5

Table A.1: Continued...

IAGA code	Component	PR1970	PO1970/PR1978	PO1978/PR1983	PO1983
BEL	X	—	1969.5–1984.5	1969.5–1984.5	1983.5–1989.5
BEL	Y	—	1967.5–1981.5	1982.5–1987.5	1982.5–1987.5
BEL	Z	—	1960.5–1979.5	1980.5–1985.5	1984.5–1989.5
BJI	X	1957.5–1970.5	—	1968.5–1988.5	1983.5–1988.5
BJI	Y	1959.5–1971.5	1969.5–1980.5	1978.5–1983.5	1983.5–1988.5
BJI	Z	1959.5–1972.5	1971.5–1988.5	1971.5–1988.5	1971.5–1988.5
BJN	X	1951.5–1967.5	1967.5–1990.5	1967.5–1990.5	1967.5–1990.5
BJN	Y	1951.5–1972.5	1971.5–1980.5	1978.5–1987.5	1985.5–1990.5
BJN	Z	1956.5–1964.5	1971.5–1985.5	1971.5–1985.5	1984.5–1989.5
BLC	X	1957.5–1982.5	1957.5–1982.5	—	1980.5–1988.5
BLC	Y	1951.6–1970.5	1968.5–1981.5	—	1984.5–1989.5
BLC	Z	1962.5–1969.5	1967.5–1980.5	1967.5–1980.5	—
BNG	X	1955.5–1967.5	1965.5–1988.5	1965.5–1988.5	1965.5–1988.5
BNG	Y	1955.5–1971.5	1970.5–1977.5	1977.5–1983.5	1981.5–1988.5
BNG	Z	1955.5–1970.5	1968.5–1988.5	1968.5–1988.5	1968.5–1988.5
BRW	X	1963.4–1972.5	1971.5–1985.5	1971.5–1985.5	1983.5–1989.5
BRW	Y	1963.4–1970.5	1968.5–1989.5	1968.5–1989.5	1968.5–1989.5
BRW	Z	1963.4–1976.5	—	1973.5–1986.5	1984.5–1989.5
CAN	X	1941.5–1970.5	1970.5–1976.5	1974.5–1987.5	1974.5–1987.5
CAN	Y	1947.5–1972.5	1970.5–1980.5	1979.5–1984.5	—
CAN	Z	1953.5–1974.5	1973.5–1979.5	1977.5–1987.5	—
CCS	X	1954.5–1971.5	1969.5–1980.5	1978.5–1989.5	1978.5–1989.5
CCS	Y	1951.5–1989.5	1951.5–1989.5	—	1951.5–1989.5
CCS	Z	1954.5–1974.5	1972.5–1987.5	1972.5–1987.5	—
CLF	X	1912.5–1977.5	1975.5–1980.5	1975.5–1980.5	—
CLF	Y	1921.5–1967.5	1967.5–1981.5	1981.5–1986.5	—
CLF	Z	1964.5–1969.5	1967.5–1984.5	1967.5–1984.5	—
CMO	X	—	1968.5–1983.5	1968.5–1983.5	—
CMO	Y	1961.5–1970.5	1968.5–1985.5	1968.5–1985.5	1983.5–1988.5
CMO	Z	1961.5–1979.5	1961.5–1979.5	1979.5–1985.5	—
CNH	X	1959.5–1970.5	1968.5–1973.5	1972.5–1988.5	1972.5–1988.5
CNH	Y	1957.5–1969.5	1967.5–1982.5	1980.5–1985.5	1983.5–1988.5
CNH	Z	1957.5–1970.5	1968.5–1974.5	1972.5–1988.5	1972.5–1988.5
COI	X	—	1966.5–1989.5	1966.5–1989.5	1966.5–1989.5
COI	Y	1948.5–1970.5	1968.5–1979.5	1980.5–1989.5	1980.5–1989.5
COI	Z	1952.5–1984.5	1952.5–1984.5	1952.5–1984.5	1983.5–1988.5
CPA	X	1955.5–1975.5	1955.5–1975.5	—	—
CPA	Y	1962.5–1969.5	1969.5–1980.5	—	—
CPA	Z	1955.5–1979.5	1955.5–1979.5	—	—
CWE	X	1956.5–1977.5	1956.5–1977.5	—	—
CWE	Y	1960.5–1967.5	1969.5–1989.5	1969.5–1989.5	1969.5–1989.5
CWE	Z	—	1966.5–1980.5	1978.5–1985.5	1983.5–1989.5
DIK	X	1954.5–1972.5	1971.5–1986.5	1971.5–1986.5	1984.5–1989.5
DIK	Y	1949.5–1963.5	1964.5–1988.5	1964.5–1988.5	—
DIK	Z	1957.5–1967.5	1965.5–1975.5	1973.5–1984.5	1984.5–1989.5
DOB	X	—	1969.5–1986.5	1969.5–1986.5	1984.5–1989.5
DOB	Y	1952.5–1969.5	1967.5–1979.5	1977.5–1984.5	1977.5–1984.5
DOB	Z	1959.5–1974.5	1972.5–1985.5	1972.5–1985.5	—
DOU	X	1962.5–1972.5	1970.5–1988.5	1970.5–1988.5	1970.5–1988.5
DOU	Y	1956.5–1970.5	1968.5–1979.5	1981.5–1987.5	1981.5–1987.5
DOU	Z	1961.5–1975.5	1973.5–1984.5	1973.5–1984.5	1982.5–1988.5
EBR	X	—	—	—	—
EBR	Y	1951.5–1969.5	1967.5–1980.5	—	—
EBR	Z	1955.5–1980.5	1955.5–1980.5	—	—
ESK	X	1948.5–1972.5	1970.5–1988.5	1970.5–1988.5	1970.5–1988.5
ESK	Y	1936.5–1971.5	1969.5–1979.5	1980.5–1988.5	1980.5–1988.5
ESK	Z	1961.5–1970.5	1968.5–1984.5	1968.5–1984.5	1983.5–1989.5
EYR	X	1940.5–1973.5	1971.5–1976.5	1980.5–1985.5	—
EYR	Y	1957.5–1973.5	1971.5–1978.5	1976.5–1986.5	1984.5–1989.5
EYR	Z	1942.5–1965.5	1965.5–1989.5	1965.5–1989.5	1965.5–1989.5
FRD	X	1945.5–1968.5	1968.5–1979.5	1977.5–1989.5	1977.5–1989.5
FRD	Y	1959.5–1981.5	1959.5–1981.5	1959.5–1981.5	1981.5–1988.5
FRD	Z	1946.5–1972.5	1971.5–1976.5	1974.5–1989.5	1974.5–1989.5
FUQ	X	1955.5–1978.5	1955.5–1978.5	1976.5–1981.4	—
FUQ	Y	1954.9–1982.5	1954.9–1982.5	1954.9–1982.5	—
FUQ	Z	1957.5–1969.5	1968.5–1974.5	1972.5–1981.4	—
FUR	X	1939.5–1969.5	1967.5–1989.5	1967.5–1989.5	1967.5–1989.5
FUR	Y	1943.5–1971.5	1969.5–1980.5	—	1981.5–1989.5
FUR	Z	1954.5–1963.5	1961.5–1978.5	1976.5–1983.5	1981.5–1989.5
GCK	X	1962.5–1971.5	1969.5–1985.5	1969.5–1985.5	1983.5–1988.5
GCK	Y	1959.5–1970.5	1969.5–1979.5	—	1980.5–1989.5
GCK	Z	—	—	—	—
GDH	X	1951.5–1968.5	1966.5–1978.5	1976.5–1986.5	1984.5–1989.5
GDH	Y	1937.5–1967.5	1965.5–1989.5	1965.5–1989.5	1965.5–1989.5
GDH	Z	1962.5–1970.5	1968.5–1982.5	—	—
GNA	X	1955.5–1976.5	1955.5–1978.5	1976.5–1988.5	1976.5–1988.5
GNA	Y	1960.5–1974.5	1972.5–1978.5	1979.5–1988.5	1979.5–1988.5
GNA	Z	1953.5–1971.5	1969.5–1978.5	1976.5–1988.5	1976.5–1988.5
GUA	X	—	1968.5–1980.5	1978.5–1986.5	1984.5–1989.5
GUA	Y	1959.5–1968.5	1971.5–1978.5	1976.5–1989.5	1976.5–1989.5
GUA	Z	1958.5–1967.5	1969.5–1979.5	1977.5–1984.5	1982.5–1987.5
GZH	X	1959.5–1970.5	1968.5–1977.5	1975.5–1986.5	1975.5–1986.5
GZH	Y	1964.5–1970.5	1968.5–1981.5	—	1979.5–1988.5
GZH	Z	1958.5–1988.5	1958.5–1988.5	1958.5–1988.5	1958.5–1988.5
HAD	X	1948.5–1971.5	1969.5–1989.5	1969.5–1989.5	1969.5–1989.5
HAD	Y	1933.5–1970.5	1968.5–1979.5	1978.5–1983.5	1982.5–1989.5
HAD	Z	1961.5–1971.5	1969.5–1979.5	1981.5–1989.5	1981.5–1989.5

Table A.1: Continued...

IAGA code	Component	PR1970	PO1970/PR1978	PO1978/PR1983	PO1983
HER	X	1946.5-1967.5	1965.5-1988.5	1965.5-1988.5	—
HER	Y	1954.5-1979.5	1954.5-1979.5	1977.5-1989.5	1977.5-1989.5
HER	Z	1962.5-1984.5	1962.5-1984.5	1962.5-1984.5	—
HIS	X	1959.5-1966.5		1966.5-1989.5	1966.5-1989.5
HIS	Y	1951.5-1973.5	—	—	
HIS	Z	—	—	1973.5-1987.5	—
HLP	X	1955.5-1971.5	1969.5-1984.5	1969.5-1984.5	1983.5-1988.5
HLP	Y	1957.5-1969.5	1968.5-1980.5	1979.5-1984.5	1984.5-1989.5
HLP	Z	1957.5-1963.5	1961.5-1978.5	1976.5-1983.5	1981.5-1989.5
HON	X	—	1967.5-1978.5	1976.5-1985.5	1983.5-1989.5
HON	Y	1959.5-1967.5	1966.5-1976.5	1975.5-1984.5	1982.5-1987.5
HON	Z	1962.5-1967.5	1965.5-1978.5	1976.5-1986.5	1984.5-1989.5
HRB	X	1965.5-1970.5	1969.5-1988.5	1969.5-1988.5	—
HRB	Y	1950.5-1970.5	1969.5-1979.5	1978.5-1984.5	1982.5-1989.5
HRB	Z	1950.5-1975.5	—	—	—
HTY	X	—	—	—	—
HTY	Y	—	—	—	—
HTY	Z	—	—	—	—
HUA	X	1953.5-1967.5	1965.5-1980.5	1978.5-1987.5	—
HUA	Y	1958.5-1972.5	1970.5-1983.5	1970.5-1983.5	1981.5-1986.5
HUA	Z	1959.5-1968.5	1966.5-1978.5	1976.5-1988.5	1976.5-1988.5
IRT	X	1960.5-1967.5	1967.5-1989.5	1967.5-1989.5	1967.5-1989.5
IRT	Y	1957.5-1973.5	1972.5-1984.5	1972.5-1984.5	1984.5-1989.5
IRT	Z	1942.5-1970.5	1968.5-1989.5	1968.5-1989.5	1968.5-1989.5
ISK	X	1951.5-1977.5	—	—	—
ISK	Y	1947.5-1971.5	1970.5-1977.5	—	—
ISK	Z	1948.5-1972.5	—	—	—
KAK	X	1959.5-1966.5	1964.5-1977.5	1976.5-1989.5	1976.5-1989.5
KAK	Y	1955.5-1967.5	1968.5-1979.5	1977.5-1987.5	1977.5-1987.5
KAK	Z	1960.5-1974.5	1972.5-1989.5	1972.5-1989.5	1972.5-1989.5
KGL	X	1960.5-1984.5	1960.5-1984.5	1960.5-1984.5	—
KGL	Y	1959.5-1969.5	1968.5-1974.5	1972.5-1987.5	1972.5-1987.5
KGL	Z	1961.5-1972.5	1970.5-1979.5	1977.5-1983.5	1981.5-1987.5
KIV	X	1958.5-1974.5	1973.5-1986.5	1973.5-1986.5	1984.5-1989.5
KIV	Y	1958.5-1970.5	1969.5-1979.5	1977.5-1989.5	1977.5-1989.5
KIV	Z	1959.5-1964.5	1964.5-1979.5	1977.5-1982.5	1983.5-1989.5
KNY	X	1959.5-1965.5	1964.5-1978.5	1976.5-1982.5	1982.5-1987.5
KNY	Y	1966.5-1971.5	1969.5-1978.5	1976.5-1989.5	1976.5-1989.5
KNY	Z	—	1966.5-1979.5	1978.5-1983.5	1981.5-1987.5
KNZ	X	—	1964.5-1975.5	1973.5-1986.5	1973.5-1986.5
KNZ	Y	1961.5-1966.5	1968.5-1978.5	1976.5-1987.5	1976.5-1987.5
KNZ	Z	—	1968.5-1988.5	1968.5-1988.5	1968.5-1988.5
KOD	X	1959.5-1972.5	1973.5-1982.5	1973.5-1982.5	1980.5-1988.5
KOD	Y	1964.5-1971.5	—	—	—
KOD	Z	1960.5-1970.5	1971.5-1976.5	1977.5-1985.5	1983.5-1988.5
LER	X	1953.5-1971.5	1969.5-1988.5	1969.5-1988.5	—
LER	Y	1935.5-1971.5	1969.5-1978.5	1976.5-1989.5	1976.5-1989.5
LER	Z	1959.5-1971.5	1969.5-1985.5	1969.5-1985.5	1984.5-1989.5
LGR	X	—	1970.5-1976.5	—	—
LGR	Y	1958.5-1970.5	1971.5-1976.5	—	—
LGR	Z	1963.5-1969.5	1969.5-1976.5	—	—
LMM	X	1963.5-1972.5	1970.5-1987.2	1970.5-1987.2	1970.5-1987.2
LMM	Y	1959.6-1974.5	1973.5-1979.5	1980.5-1985.5	—
LMM	Z	—	1964.5-1979.5	1978.5-1983.5	—
LNN	X	—	1970.5-1987.5	1970.5-1987.5	—
LNN	Y	1962.5-1970.5	1968.5-1980.5	1978.5-1983.5	—
LNN	Z	1951.5-1968.5	1968.5-1973.5	1973.5-1985.5	—
LOV	X	1947.5-1975.5	1974.5-1986.5	1974.5-1986.5	—
LOV	Y	1945.5-1971.5	1969.5-1980.5	—	—
LOV	Z	1954.5-1962.5	1972.5-1985.5	1972.5-1985.5	1984.5-1989.5
LQA	X	—	—	—	—
LQA	Y	—	—	—	—
LQA	Z	—	—	—	—
LRV	X	1957.8-1975.5	1957.8-1975.5	1973.5-1986.5	1984.5-1989.5
LRV	Y	1958.5-1969.5	1968.5-1979.5	1979.5-1986.5	1979.5-1986.5
LRV	Z	1961.5-1970.5	1969.5-1983.5	—	1984.5-1989.5
LUA	X	1957.8-1974.5	1975.5-1985.5	1975.5-1985.5	—
LUA	Y	1960.5-1975.5	1960.5-1975.5	1975.5-1982.5	—
LUA	Z	1957.8-1966.5	1964.5-1985.5	1964.5-1985.5	—
LVV	X	1963.5-1973.5	1971.5-1981.5	1971.5-1981.5	1979.5-1989.5
LVV	Y	1957.5-1971.5	1969.5-1977.5	1977.5-1983.5	1982.5-1989.5
LVV	Z	1961.5-1979.5	1961.5-1979.5	1977.5-1982.5	1982.5-1989.5
LZH	X	1961.5-1968.5	1966.5-1986.5	1966.5-1986.5	—
LZH	Y	1959.5-1969.5	1970.5-1977.5	1977.5-1987.5	—
LZH	Z	1961.5-1971.5	1970.5-1988.5	1970.5-1988.5	—
MAW	X	1957.5-1970.5	1969.5-1987.5	1969.5-1987.5	1969.5-1987.5
MAW	Y	1958.5-1971.5	1969.5-1984.5	1969.5-1984.5	
MAW	Z	1955.8-1973.5	1971.5-1987.5	1971.5-1987.5	1971.5-1987.5
MBO	X	1952.6-1967.5	—	—	—
MBO	Y	1961.5-1967.5	1965.5-1987.5	1965.5-1987.5	—
MBO	Z	1955.5-1984.5	1955.5-1984.5	1955.5-1984.5	—
MCQ	X	1951.2-1969.5	1972.5-1977.5	1977.5-1988.5	1977.5-1988.5
MCQ	Y	1951.2-1974.5	1972.5-1977.5	1976.5-1981.5	1982.5-1988.5
MCQ	Z	1962.5-1970.5	1971.5-1980.5	1978.5-1988.5	1978.5-1988.5
MEA	X	1916.8-1978.5	1916.8-1978.5	1976.5-1982.5	1981.5-1986.5
MEA	Y	1920.5-1972.5	1970.5-1979.5	1980.5-1986.5	1980.5-1986.5
MEA	Z	1962.5-1967.5	1965.5-1989.5	1965.5-1989.5	1965.5-1989.5

Table A.1: Continued...

IAGA code	Component	PR1970	PO1970/PR1978	PO1978/PR1983	PO1983
MGD	X	1967.5-1972.5	1970.5-1986.5	1970.5-1986.5	1984.5-1989.5
MGD	Y	1960.5-1969.5	1969.5-1979.5	1977.5-1982.5	1980.5-1987.5
MGD	Z	1961.5-1968.5	1966.5-1989.5	1966.5-1989.5	1966.5-1989.5
MIR	X	1957.5-1975.5	1973.5-1988.5	1973.5-1988.5	1973.5-1988.5
MIR	Y	1956.5-1973.5	1971.5-1985.5	1971.5-1985.5	1983.5-1988.5
MIR	Z	1956.5-1967.5	1965.5-1988.5	1965.5-1988.5	1965.5-1988.5
MLT	X	1929.5-1980.5	—	—	—
MLT	Y	1941.5-1972.5	—	—	—
MLT	Z	1933.5-1979.5	—	—	—
MMB	X	1962.5-1967.5	1965.5-1975.5	1973.5-1986.5	1984.5-1989.5
MMB	Y	1959.5-1971.5	1969.5-1979.5	1979.5-1986.5	1984.5-1989.5
MMB	Z	1963.5-1969.5	1968.5-1973.5	1971.5-1989.5	1971.5-1989.5
MMK	X	1958.6-1971.5	1971.5-1984.5	1971.5-1984.5	—
MMK	Y	1959.5-1970.5	1968.5-1982.5	1980.5-1985.5	—
MMK	Z	1961.5-1975.5	—	1976.5-1983.5	—
MNK	X	1962.5-1972.5	1970.5-1981.5	1979.5-1986.5	—
MNK	Y	1964.5-1969.5	1967.5-1980.5	1978.5-1983.5	1983.5-1988.5
MNK	Z	—	1963.5-1978.5	1976.5-1985.5	1983.5-1988.5
MOS	X	1947.5-1975.5	1973.5-1988.5	1973.5-1988.5	—
MOS	Y	1962.5-1971.5	1971.5-1980.5	—	1981.5-1989.5
MOS	Z	1954.5-1968.5	1966.5-1978.5	1976.5-1984.5	1981.5-1988.5
MUT	X	1952.5-1966.5	1964.5-1982.5	—	—
MUT	Y	1953.5-1983.5	1953.5-1983.5	—	—
MUT	Z	1951.5-1974.5	—	1976.5-1987.5	—
NGK	X	1946.5-1971.5	1969.5-1986.5	1969.5-1986.5	1984.5-1989.5
NGK	Y	1943.5-1971.5	1969.5-1980.5	—	—
NGK	Z	1960.5-1979.5	1960.5-1979.5	—	1979.5-1989.5
NSM	X	1961.5-1970.5	1968.5-1986.5	1968.5-1986.5	1984.5-1989.5
NSM	Y	1961.5-1967.5	1965.5-1981.5	1981.5-1987.5	1981.5-1987.5
NSM	Z	—	1963.5-1978.5	1976.5-1982.5	1980.5-1989.5
NUR	X	1953.5-1973.5	1971.5-1987.5	1971.5-1987.5	—
NUR	Y	1953.5-1967.5	1968.5-1979.5	1977.5-1989.5	1977.5-1989.5
NUR	Z	1958.5-1964.5	1962.5-1976.5	1974.5-1984.5	1982.5-1989.5
NVL	X	—	—	—	—
NVL	Y	1962.5-1975.5	1973.5-1987.5	—	—
NVL	Z	1961.5-1987.5	1961.5-1987.5	—	—
ODE	X	1953.5-1974.5	1973.5-1986.5	1973.5-1986.5	1984.5-1989.5
ODE	Y	1951.5-1971.5	1969.5-1979.5	1977.5-1982.5	1981.5-1989.5
ODE	Z	1950.5-1968.5	1966.5-1978.5	1976.5-1985.5	1983.5-1989.5
PAG	X	1961.5-1967.5	1970.5-1981.5	1970.5-1981.5	—
PAG	Y	1953.5-1972.5	1970.5-1979.5	1977.5-1982.5	—
PAG	Z	1948.5-1972.5	1970.5-1975.5	1976.5-1981.5	—
PET	X	—	1969.5-1986.5	1969.5-1986.5	1969.5-1986.5
PET	Y	—	1969.5-1976.5	1975.5-1981.5	1982.5-1987.5
PET	Z	—	1969.5-1983.5	1969.5-1983.5	1982.5-1988.5
PIL	X	1926.5-1954.5	1962.5-1978.5	1976.5-1983.5	1983.5-1988.5
PIL	Y	1942.5-1966.5	1969.5-1981.5	1969.5-1981.5	—
PIL	Z	—	1956.5-1986.5	1956.5-1986.5	—
PMG	X	1964.5-1970.5	—	1974.5-1985.5	1983.5-1988.5
PMG	Y	1961.5-1968.5	1966.5-1981.5	1979.5-1988.5	1979.5-1988.5
PMG	Z	1959.5-1967.5	1968.5-1976.5	1974.5-1988.5	—
PPT	X	—	1969.5-1977.5	1975.5-1986.5	—
PPT	Y	—	1970.5-1984.5	1970.5-1984.5	1982.5-1988.5
PPT	Z	—	1968.5-1978.5	1976.5-1984.5	1982.5-1988.5
QUE	X	1953.9-1987.5	1953.9-1987.5	1953.9-1987.5	—
QUE	Y	1958.5-1968.5	—	—	—
QUE	Z	1953.9-1974.5	—	—	—
RES	X	1954.5-1968.5	1966.5-1978.5	1976.5-1984.5	1982.5-1989.5
RES	Y	1960.5-1969.5	1967.5-1977.5	1977.5-1989.5	1977.5-1989.5
RES	Z	1958.5-1974.5	1974.5-1987.5	1974.5-1987.5	1974.5-1987.5
RSV	X	1950.5-1975.5	1973.5-1978.5	—	—
RSV	Y	1944.5-1971.5	1969.5-1980.5	—	—
RSV	Z	1960.5-1976.5	1960.5-1976.5	—	—
SBA	X	—	1964.5-1989.5	1964.5-1989.5	1964.5-1989.5
SBA	Y	—	1966.5-1989.5	1966.5-1989.5	1966.5-1989.5
SBA	Z	—	1966.5-1989.5	1966.5-1989.5	1966.5-1989.5
SIT	X	1962.5-1972.5	1970.5-1981.5	1979.5-1985.5	1983.5-1988.5
SIT	Y	1961.5-1969.5	1969.5-1980.5	1978.5-1985.5	1983.5-1989.5
SIT	Z	1959.5-1976.5	—	1977.5-1987.5	1977.5-1987.5
SJG	X	—	1965.5-1979.5	1977.5-1987.5	—
SJG	Y	1963.5-1969.5	1967.5-1980.5	1978.5-1989.5	1978.5-1989.5
SJG	Z	1955.5-1971.5	1969.5-1982.5	1969.5-1982.5	1980.5-1987.5
SNA	X	1960.5-1989.5	—	—	—
SNA	Y	1960.5-1978.5	—	—	—
SNA	Z	1960.5-1989.5	—	—	—
SOD	X	1963.5-1968.5	1968.5-1987.5	1968.5-1987.5	1968.5-1987.5
SOD	Y	1947.5-1972.5	1970.5-1980.5	—	—
SOD	Z	1954.5-1966.5	—	1974.5-1984.5	—
SPT	X	1953.5-1966.5	1968.5-1988.5	1968.5-1988.5	1968.5-1988.5
SPT	Y	1948.5-1971.5	1969.5-1979.5	—	1980.5-1988.5
SPT	Z	1947.5-1985.5	1947.5-1985.5	—	—
SSH	X	1944.5-1966.5	1964.5-1981.5	1979.5-1984.5	1983.5-1988.5
SSH	Y	1956.5-1969.5	1967.5-1981.5	1980.5-1986.5	—
SSH	Z	1952.5-1967.5	1965.5-1988.5	1965.5-1988.5	—

Table A.1: Continued...

IAGA code	Component	PR1970	PO1970/PR1978	PO1978/PR1983	PO1983
SUA	X	—	—	1971.5-1982.5	1984.5-1989.5
SUA	Y	1960.5-1969.5	1967.5-1982.5	1967.5-1982.5	1980.5-1988.5
SUA	Z	—	1961.5-1989.5	1961.5-1989.5	1961.5-1989.5
TAM	X	—	—	—	—
TAM	Y	—	—	—	—
TAM	Z	—	—	—	—
TEN	X	—	1960.5-1988.5	1960.5-1988.5	1960.5-1988.5
TEN	Y	—	1964.5-1985.5	—	—
TEN	Z	—	—	—	—
TFS	X	1961.5-1966.5	1970.5-1983.5	1970.5-1983.5	1981.5-1987.5
TFS	Y	1962.5-1970.5	1971.5-1977.5	1977.5-1989.5	1977.5-1989.5
TFS	Z	1948.5-1972.5	1970.5-1979.5	—	1981.5-1989.5
THL	X	1956.5-1971.5	1969.5-1977.5	1975.5-1985.5	1983.5-1988.5
THL	Y	1957.5-1979.5	1957.5-1979.5	1978.5-1986.5	1978.5-1988.5
THL	Z	1957.5-1974.5	1972.5-1981.5	1979.5-1987.5	1979.5-1987.5
THY	X	1955.5-1974.5	1972.5-1978.5	1978.5-1987.5	—
THY	Y	1955.5-1972.5	1970.5-1978.5	1976.5-1989.5	1976.5-1989.5
THY	Z	1961.5-1989.5	1961.5-1989.5	1961.5-1989.5	—
TIK	X	1961.5-1971.5	1967.5-1977.5	1976.5-1986.5	1984.5-1989.5
TIK	Y	1949.5-1964.5	1964.5-1979.5	1977.5-1987.5	1977.5-1987.5
TIK	Z	1956.5-1989.5	1956.5-1989.5	1956.5-1989.5	1956.5-1989.5
TKT	X	1960.5-1968.5	1970.5-1984.5	1970.5-1984.5	1982.5-1989.5
TKT	Y	1964.5-1969.5	1968.5-1987.5	1968.5-1987.5	1968.5-1987.5
TKT	Z	1947.5-1971.5	1969.5-1979.5	1978.5-1983.5	—
TRD	X	1965.5-1970.5	1969.5-1978.5	—	—
TRD	Y	—	1966.5-1980.5	1966.5-1980.5	1982.5-1989.5
TRD	Z	1957.9-1972.5	1970.5-1981.5	1979.5-1985.5	1983.5-1989.5
TRO	X	1958.5-1967.5	1972.5-1986.5	1972.5-1986.5	1984.5-1989.5
TRO	Y	1958.5-1968.5	1967.5-1979.5	1977.5-1982.5	1981.5-1990.5
TRO	Z	1931.5-1965.5	1965.5-1990.5	1965.5-1990.5	1965.5-1990.5
TUC	X	—	1967.5-1980.5	—	—
TUC	Y	1956.5-1964.5	1963.5-1978.5	1976.5-1985.5	—
TUC	Z	1961.5-1967.5	1965.5-1981.5	1979.5-1984.5	—
VAL	X	—	1969.5-1988.5	1969.5-1988.5	1969.5-1988.5
VAL	Y	1951.5-1969.5	1967.5-1979.5	1984.5-1989.5	1984.5-1989.5
VAL	Z	—	1965.5-1985.5	1965.5-1985.5	—
VIC	X	—	1968.5-1981.5	—	1980.5-1989.5
VIC	Y	1961.5-1968.5	1968.5-1980.5	1979.5-1984.5	1984.5-1989.5
VIC	Z	1960.5-1970.5	1968.5-1989.5	1968.5-1989.5	1968.5-1989.5
VLA	X	1958.5-1988.5	1958.5-1988.5	1958.5-1988.5	—
VLA	Y	1958.5-1968.5	1966.5-1981.5	—	—
VLA	Z	1959.5-1970.5	1968.5-1988.5	1968.5-1988.5	1968.5-1988.5
VOS	X	—	—	—	—
VOS	Y	—	—	—	—
VOS	Z	—	—	—	—
VSS	X	1954.5-1971.5	1970.5-1981.5	1970.5-1981.5	1982.5-1988.5
VSS	Y	1962.5-1972.5	—	1976.5-1987.5	1976.5-1987.5
VSS	Z	1958.5-1979.5	1958.5-1979.5	1977.5-1984.5	1982.5-1987.5
WHN	X	1960.5-1967.5	1965.5-1977.5	—	1983.5-1988.5
WHN	Y	1961.5-1972.5	1971.5-1976.5	1976.5-1981.5	1980.5-1988.5
WHN	Z	1963.5-1968.5	1966.5-1988.5	1966.5-1988.5	1966.5-1988.5
WIK	X	1946.5-1966.5	1969.5-1986.5	1969.5-1986.5	1984.5-1989.5
WIK	Y	1945.5-1970.5	1968.5-1980.5	1978.5-1989.5	1978.5-1989.5
WIK	Z	—	1961.5-1979.5	1977.5-1983.5	1983.5-1989.5
WIT	X	1951.5-1971.5	1969.5-1986.5	1969.5-1986.5	1969.5-1986.5
WIT	Y	1959.5-1970.5	1969.5-1979.5	1980.5-1987.5	1980.5-1987.5
WIT	Z	1961.5-1972.5	1973.5-1981.5	1973.5-1981.5	1982.5-1987.5
WNG	X	1946.5-1971.5	1969.5-1987.5	1969.5-1987.5	1969.5-1987.5
WNG	Y	1960.5-1970.5	1969.5-1978.5	1978.5-1989.5	1978.5-1989.5
WNG	Z	1960.5-1975.5	1973.5-1984.5	1973.5-1984.5	1983.5-1989.5
YAK	X	1963.5-1972.5	1970.5-1986.5	1970.5-1986.5	1970.5-1986.5
YAK	Y	1949.5-1970.5	1968.5-1979.5	1977.5-1983.5	—
YAK	Z	1950.5-1966.5	1966.5-1979.5	1977.5-1987.5	—
YSS	X	1961.5-1989.5	1961.5-1989.5	1961.5-1989.5	—
YSS	Y	1950.5-1969.5	1967.5-1983.5	1967.5-1983.5	—
YSS	Z	1950.5-1963.5	1964.5-1983.5	1964.5-1983.5	—